UNCLASSIFIED
SECURITY CLASSIFICATION OF THIS PAGE (When Data Entered)

REPORT DOCUMENTATION PAGE		READ INSTRUCTIONS BEFORE COMPLETING FORM
1. REPORT NUMBER AFFDL-TR-75-100	2. GOVT ACCESSION NO.	3. RECIPIENT'S CATALOG NUMBER
4. TITLE (and Subtitle) SMALL DISTURBANCE TRANSONIC FLOWS ABOUT OSCILLATING AIRFOILS AND PLANAR WINGS		5. TYPE OF REPORT & PERIOD COVERED Final Report June 1974 - June 1975
		6. PERFORMING ORG. REPORT NUMBER SAI-76-543-LA
7. AUTHOR(s) R. M. Traci E. D. Albano J. L. Farr, Jr.		8. CONTRACT OR GRANT NUMBER(s) F33615-74-C-3094
9. PERFORMING ORGANIZATION NAME AND ADDRESS Science Applications, Inc. 101 Continental Building, Suite 310 El Segundo, California 90245		10. PROGRAM ELEMENT, PROJECT, TASK AREA & WORK UNIT NUMBERS Project 1370 Task 137004
11. CONTROLLING OFFICE NAME AND ADDRESS Air Force Flight Dynamics Laboratory Aerospace Dynamics Branch, FYS Wright-Patterson AFB, Ohio 45433		12. REPORT DATE August 1975
		13. NUMBER OF PAGES 165
14. MONITORING AGENCY NAME & ADDRESS(if different from Controlling Office) Air Force Flight Dynamics Laboratory (same as above)		15. SECURITY CLASS. (of this report) Unclassified
		15a. DECLASSIFICATION/DOWNGRADING SCHEDULE

16. DISTRIBUTION STATEMENT (of this Report)

Distribution limited to U.S. Government agencies only, test and evaluation, statement applied August 1975. Other requests for this document must be referred to AF Flight Dynamics Laboratory (FY), Wright-Patterson AFB, Ohio 45433.

17. DISTRIBUTION STATEMENT (of the abstract entered in Block 20, if different from Report)

N/A

[redacted]

18. SUPPLEMENTARY NOTES

N/A

19. KEY WORDS (Continue on reverse side if necessary and identify by block number)

Unsteady Aerodynamics	Flutter
Transonic Flow	Small Disturbance Theory
Oscillating Airfoils	Relaxation Methods

20. ABSTRACT (Continue on reverse side if necessary and identify by block number)

A theory and numerical solution method are presented for the problem of two or three dimensional flow about thin wings undergoing harmonic oscillations. The theory is based on a treatment of the unsteady flow as a small perturbation on the nonlinear steady flow. The coupled governing equations for the steady and unsteady perturbation potentials are of mixed elliptic/hyperbolic type and are solved using the mixed differencing line relaxation

DD FORM 1 JAN 73 1473 EDITION OF 1 NOV 65 IS OBSOLETE

UNCLASSIFIED
SECURITY CLASSIFICATION OF THIS PAGE (When Data Entered)

technique of Murman and Cole. The theory and solution method have been generalized to treat subsonic or supersonic freestream flows, solid or porous wall effects and three dimensional flow about planar wings. Calculations demonstrating each of these capabilities are presented.

Accuracy of the method for realistic steady and unsteady flows is examined by comparison to more exact numerical results and experimental data. The comparison indicates that the present method provides a useful and efficient inviscid solution. Quantitative differences between the present results and experimental data are attributed primarily to viscous effects, pointing out the importance of such effects for transonic flows.

The method is used to calculate the two dimensional unsteady flow about two airfoils (NACA 64A006 and 64A410) undergoing rigid body oscillations in the transonic Mach number range (0.8 to 1.2) at low reduced frequencies (0 to 0.2). The entire matrix of calculations for one airfoil (∿ 110 cases) required approximately 1.25 hours of CDC 7600 time indicating the practical utility of the method. Results of a transonic flutter analysis, using the unsteady aerodynamic coefficients so generated, are also presented.

FOREWORD

[redacted]

This report was prepared by the Los Angeles Division of Science Applications, Incorporated, Los Angeles, California for the Vehicle Dynamics Division of the Air Force Flight Dynamics Laboratory, Wright-Patterson Air Force Base, Ohio. The research was conducted under Project 1370, "Dynamic Problems in Flight Vehicles," Task 137004, "Design Analysis," Contract F33615-74-C-3094. James J. Olsen and later Lt. William L. Holman of AFFDL/FYS were the Air Force task engineers.

R. M. Traci was the principal investigator for the study. J. L. Farr, Jr. contributed to the development for the numerical solution method and developed the necessary computer programs. Consultant E. D. Albano contributed to and guided the research.

The authors submitted this report in July 1975 for publication as an AFFDL technical report to cover research performed from June 1974 through June 1975.

Other reports prepared and submitted under the aforementioned contract are: AFFDL-TR-74-37, "Small Disturbance Transonic Flows about Oscillating Airfoils," AFFDL-TR-74-135, "Computer Programs for Calculating Small Disturbance Transonic Flows about Oscillating Airfoils," and AFFDL-TR-75-103, "Computer Programs for Calculating Small Disturbance Transonic Flows about Oscillating Planar Wings."

TABLE OF CONTENTS

[redacted]

LIST OF ILLUSTRATIONS

LIST OF ILLUSTRATIONS (CON'T)

LIST OF ILLUSTRATIONS (CON'T)

LIST OF ILLUSTRATIONS (CON'T)

LIST OF ILLUSTRATIONS (CON'T)

LIST OF ILLUSTRATIONS (CON'T)

LIST OF ILLUSTRATIONS (CON'T)

1.0 INTRODUCTION

A basic reason for studying unsteady flows is the prediction of the effect of unsteady aerodynamic forces on a flight vehicle. The transonic speed regime is particularly important in this respect for the same physical reason that drag and other steady forces are generally higher than in subsonic or supersonic speed regimes. Another characteristic of transonic flows is the potentially large phase lag between boundary motion and induced unsteady pressures. These effects tend to increase the likelihood of aeroelastic instabilities, so that transonic speeds are most critical for aircraft flutter. There is a clear and present need for accurate and efficient predictive techniques for unsteady transonic airloads. This need motivated the investigation of the perturbation method for transonic flows about oscillating airfoils presented in this and a previous report.[1] The present report contains a potpourri of analyses, numerical tests and calculated results which generalize, verify and exercise the method introduced in Reference 1. By way of introduction, the following description of the nature of unsteady transonic flows and the past and present attempts at describing the inherently nonlinear processes is presented.

The physical mechanism underlying the build-up of pressure amplitudes and phase lags has been described by Landahl[2] by considering the propagation of a low-frequency acoustic disturbance. The upstream-facing portion of the disturbance (the "receding wave") travels at a rate which is essentially the difference between freestream speed and the sound speed. In a transonic flow, this speed is so slow that acoustic disturbances may interact and build up to a finite amplitude. In order to describe the phenomena, the steady or low frequency unsteady equations must necessarily be nonlinear, thereby providing the essential difficulty in the analysis of transonic flow. It has been pointed out by Rott[3], Landahl[4] and others, however, that the unsteady equations may be linearized and uncoupled from the mean steady flow for high frequency disturbances near Mach 1. These so-called "sonic theories" have been developed for both two and three dimensional wings by a number of investigators[3,4,5]. Many of these classical studies of the high frequency equation are summarized in Landahl's monograph[4]. It is often the case, however, that the nonlinear low frequency regime is of greater practical importance for aircraft flutter. Fortunately, a linear system can be recovered for low frequency transonic flow, as demonstrated by Landahl[4], by expanding the unsteady flow as a small perturbation about the nonuniform steady flow. The linear equation remains quite formidable since various coefficients are functions of the nonlinear steady flow so that numerical solution procedures, of which the present work is one, are indicated.

Analytical or semi-analytical approaches to the solution of the unsteady flow, based on this linearization about the steady flow, have recently been presented. Stahara and Spreiter[6] and Isogai[7] have applied the "local linearization" method, developed for steady, near sonic flows, to the nonuniform unsteady system. The approach is promising but its aplication to general supercritical flows is questionable.

Of more practical interest for general applications are the numerical approaches which have become highly developed for steady flows in recent years. Two basic finite difference techniques have been used; known generally as time dependent methods and relaxation methods. The time dependent methods solve the complete set of conservation equations or the unsteady full potential equation by forward differencing in time. This approach has been applied to the calculation of steady flows as the steady limit of the time dependent solution. The method can handle mixed flows and shocks within the accuracy of the finite difference mesh[8]. Time dependent calculations of flows about two dimensional airfoils oscillating at supercritical Mach numbers have been reported by Magnus and Yoshihara[9] and Beam and Warming[10]. Such calculations are very important as they involve no inherent limiting assumption but they are quite expensive computer timewise. Ballhaus and Lomax[11] have presented time accurate solutions of the low frequency unsteady small disturbance potential equation. Recent applications of the method[12] indicate that it could be a very efficient approach to the oscillating airfoil problem.

Another promising technique for both steady and unsteady flows, which must be considered in a separate classification, is the finite element method. The method has been applied to the oscillating airfoil problem by Bratanow and Ecer[13] for compressible flow and recently by Chan and Brashears[14] for transonic flows.

The other class of numerical techniques, which have received wide application to steady transonic flows[15,16], are the relaxation methods. Ehlers[17] and the present authors[1] have reported the application of relaxation methods to unsteady transonic flows about harmonically oscillating airfoils. Both methods are apparently similar except that the work presented here concentrates in a consistent manner, from formulation through results, on the low frequency regime. In the approach, the flow is considered as a small perturbation on the steady flow which results in a pair of boundary value problems for the steady and first order unsteady perturbation potentials. The equation for the steady flow is just the nonlinear small disturbance potential equation. The first order unsteady equation is linear, and for the harmonic boundary disturbances considered, its reduced wave equation form is of mixed elliptic/hyperbolic type depending upon the nature of the steady solution. Both steady and unsteady equations are solved by the mixed differencing line relaxation procedure first introduced for steady flows by Murman and Cole[10].

Since the approach and numerical solution procedure have been reported in detail in the previous report[1], they are but summarized in Section 2.0, with the addition of certain generalizations to the basic method presented in that report. These generalizations and extentions to treat higher order frequency effects, supersonic freestream flows, wind tunnel wall effects and three dimensional planar wing flows are presented in Section 3.0, along with illustrative results. Section 4.0 presents additional work concerning the accuracy, convergence, and stability of the method. An attempt at verifying the accuracy of the method for airfoils with practical shape and unsteady amplitudes is presented in Section 5.0, with comparisons of the present results to those of an "exact" numerical method[9] and experimental data[18,19]. Detailed calculated results for a NACA 64AC06 and 64A410 airfoil oscillating in pitch, plunge and control surface rotation in the Mach number range 0.8 to 1.2 and reduced frequency range 0 to 0.2 are presented in Section 6.0. Mean airfoil angle of attack and wind tunnel wall effects are briefly studied and the results presented in that section. The results for unsteady aerodynamic coefficients are used in a three degree of freedom flutter analysis and the results are discussed in Section 7.0. Finally, Section 8.0 summarizes study results and comments on the current state of development of the method.

2.0 FORMULATION AND SOLUTION PROCEDURE

Small disturbance theory is the principal analytical tool for all speed ranges and has become increasingly important in the transonic speed range in recent years. The general theory including the unsteady small perturbation approach used in this work is summarized in Section 2.1. Generalizations of the basic method, described in detail previously[1,20] to include higher frequency effects and an extension of the method to three dimensional planar flows are included in the summary. The required numerical solution methods for the steady and unsteady systems are described in Section 2.2

2.1 Small Perturbation Approach to Unsteady Transonic Flow

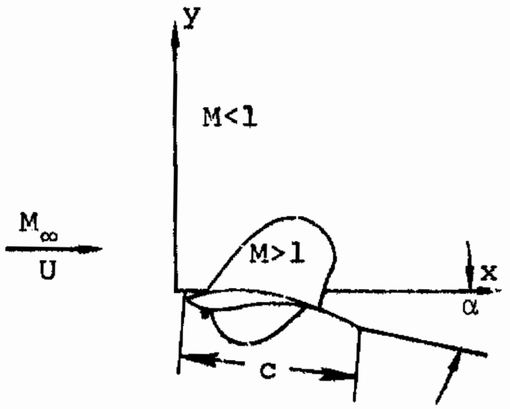

FIGURE 1. SCHEMATIC OF AIRFOIL GEOMETRY AND TRANSONIC FLOWFIELD

The problem of interest is the flow about an airfoil (two dimensional) or planar wing (three dimensional) oscillating with various flexible or rigid body degrees of freedom in the transonic speed range. The airfoil geometry, flowfield schematic and coordinate definition are given in Figure 1 above. Rectangular coordinates (x,y,z) are fixed to the airfoil leading edge with origin at the wing root and U, M_∞, a_∞ are the freestream velocity, Mach number and sound speed respectively. The airfoil has a thickness ratio δ, which is the airfoil maximum thickness divided by its chord c, an angle of attack α and a semi-span b. The assumption is made that $\delta << 1$

and α is of the same order of magnitude as δ. Also, the oscillatory motion of the airfoil is assumed to be described by a small non-dimensional displacement $\varepsilon << \delta$ and a reduced frequency $k=\omega c/U$ based on airfoil chord where ω is the frequency of oscillation.

Assuming inviscid, isentropic flow, the problem can be reduced to the solution of a single equation for a velocity potential plus the tangency boundary condition on the airfoil surface. As is well known, the derivation of a small disturbance theory for transonic flows requires a singular perturbation approach. The following scaling is thereby introduced:

$$\tilde{x} = \frac{x}{c}, \quad \tilde{y} = [(1+\gamma)\delta M_\infty^2]^{1/3} \frac{y}{c} \qquad \tilde{z} = [(1+\gamma)\delta M_\infty^2]^{1/3} \frac{z}{c}$$

$$\tilde{t} = \frac{[(1+\gamma)\delta M_\infty^2]^{2/3}}{M_\infty^2} \frac{U}{c} t \tag{1}$$

and the total potential is expanded about the uniform flow:

$$\psi = Uc\tilde{x} + \frac{\delta^{2/3} Uc}{[(1+\gamma)M_\infty^2]^{1/3}} \tilde{\phi}(\tilde{x},\tilde{y},\tilde{z},\tilde{t}) + \ldots \tag{2}$$

Retaining all terms of leading order in the total potential equation and boundary conditions results in the following form for the unsteady small disturbance system.

$$(K-\tilde{\phi}_{\tilde{x}})\tilde{\phi}_{\tilde{x}\tilde{x}} + \tilde{\phi}_{\tilde{y}\tilde{y}} + \tilde{\phi}_{\tilde{z}\tilde{z}} = 2\tilde{\phi}_{\tilde{x}\tilde{t}} + \underline{\frac{k}{\Omega}\tilde{\phi}_{\tilde{t}\tilde{t}}} \tag{3}$$

where the transonic similarity parameters are:

$$K = \frac{(1-M_\infty^2)}{[(1+\gamma)\delta M_\infty^2]^{2/3}}, \qquad \Omega = \frac{M_\infty^2}{[(1+\gamma)\delta M_\infty^2]^{2/3}} k$$

with boundary conditions:

$$\tilde{\phi}_{\tilde{y}} = \left(\frac{\partial}{\partial \tilde{x}} + \underline{\frac{k}{\Omega}\frac{\partial}{\partial \tilde{t}}}\right) f_{u,\ell}\ (\tilde{x},\tilde{z},\tilde{t}) \tag{4}$$

$$\text{on } \tilde{y} = \pm 0 \ \begin{cases} 0 \le \tilde{x} \le 1 \\ 0 \le \tilde{z} \le b \end{cases}$$

$$\left[\tilde{\phi}_{\tilde{x}} + \underline{\frac{k}{\Omega}\ \tilde{\phi}_{\tilde{t}}}\right] = 0, \text{ on } \tilde{y}=0 \ \begin{cases} \tilde{x} > 1 \\ 0 \le \tilde{z} \le b \end{cases} \tag{5}$$

$$\tilde{\phi}^2_{\tilde{x}} + \tilde{\phi}^2_{\tilde{y}} + \tilde{\phi}^2_{\tilde{z}} \to 0 \text{ as } \tilde{x}^2+\tilde{y}^2+\tilde{z}^2 \to \infty \tag{6}$$

where $f_{u,\ell}$ is the unsteady airfoil shape function (Equation (7) below) on the upper and lower surfaces respectively, and where [] denotes a jump in the enclosed quantity between $y = 0^-$ and 0^+. It is noted that the airfoil tangency boundary condition (Equation 4) and the Kutta condition (Equation 5) are applied in the small disturbance manner on $y = 0$.

The system of Equations 3-6 provides a formulation of the unsteady airfoil problem in the non-linear domain, which includes flowfields with shocks. Certain terms in the above system are underlined as they may be omitted for a low frequency $[k \sim 0(\delta^{2/3})]$ approximation. This approximation is in fact used in most of the work presented in this report. The treatment of higher frequency effects (use of underlined terms), necessary for oscillations in plunge for example, is examined in Section 3.1 with some comment as to the effect on the accuracy of the theory.

The low frequency approximation results in significant numerical advantage when solved by a time dependent technique as pointed out recently by Ballhaus and Lomax[11]. Such approaches to the solution of the above system have yet to be fully exploited for the unsteady aerodynamics problem.

The approach presented herein for solving the non-linear system given above (Equations 3-6) is to expand the perturbation potential function in terms of the unsteady boundary disturbance $\varepsilon \ll 1$. From this point on all tildas (∿) will be dropped with the understanding that all variables are scaled variables. Harmonic boundary disturbances are explicitly treated:

$$f(x,z,t) = f_o(x,z) + \varepsilon f_\varepsilon(x,z)e^{i\Omega t} \qquad (7)$$

and the perturbation potential is expanded as follows:

$$\phi(x,y,z,t) = \phi^0(x,y,z) + \varepsilon\,\phi^1(x,y,z)e^{i\Omega t} + \qquad (8)$$

Substituting this into the perturbation potential equation plus boundary conditions and combining terms results in the following pair of boundary value problems for ϕ^0 and ϕ^1 respectively. (In the following text, the superscript has been dropped from ϕ^1.)

$$\left.\begin{array}{l}
(K-\phi^0_x)\phi^0_{xx} + \phi^0_{yy} + \phi^0_{zz} = 0 \\[2ex]
\phi^0_y = f'_o(x,z), \quad \text{on } y = \pm 0 \quad \begin{cases} 0 \le x \le 1 \\ 0 \le z \le b \end{cases} \\[3ex]
[\phi^0_x] = 0, \quad \text{on } y = 0 \quad \begin{cases} x > 1 \\ 0 \le z \le b \end{cases} \\[3ex]
(\phi^0_x)^2 + (\phi^0_y)^2 + (\phi^0_z)^2 \to 0 \quad \text{as } x^2+y^2+z^2 \to \infty
\end{array}\right\} \qquad (9)$$

and

$$\left.\begin{array}{l}
(K-\phi^0_x)\phi_{xx} + \phi_{yy} + \phi_{zz} - (\phi^0_{xx} + 2i\Omega)\phi_x + \underline{k\Omega\phi} = 0 \\[2ex]
\phi_y = f'_\varepsilon + \underline{ikf_\varepsilon}, \quad \text{on } y = \pm 0 \quad \begin{cases} 0 \le x \le 1 \\ 0 \le z \le b \end{cases} \\[3ex]
[\phi_x + \underline{ik\phi}] = 0, \quad \text{on } y = 0 \quad \begin{cases} x > 1 \\ 0 \le z \le b \end{cases} \\[3ex]
(\phi_x)^2 + (\phi_y)^2 + (\phi_z)^2 \to 0, \quad \text{as } x^2+y^2+z^2 \to \infty
\end{array}\right\} \qquad (10)$$

System 9 is recognized as the usual formulation for steady transonic flow and system 10 is the formulation for the unsteady perturbation thereof. It is noted that the governing equation for ϕ is linear but of the same mixed elliptic/hyperbolic type as the steady solution. It is also noted that ϕ is in general complex thereby permitting phase shifts between field quantities and the boundary disturbance. As before, underlined terms in system 10 are neglected for a consistent low frequency approximation. Also for two dimensional airfoil sections, the z dependence on all quantities and the ϕ_{zz} terms in the equations are neglected.

The main physical quantities of interest are the pressure coefficient and airfoil force coefficients. The pressure coefficient, defined in the usual manner, is given by:

$$C_p = \frac{\delta^{2/3}}{[(1+\gamma)M_\infty^2]^{1/3}} \left(\bar{C}_p^0 + \epsilon \bar{C}_p e^{i\Omega t}\right) \qquad (11)$$

where the steady and unsteady scaled pressure coefficients are given to leading order in the small disturbance approximation by:

$$\bar{C}_p^0 = -2\phi_x^0, \qquad \bar{C}_p = -2(\phi_x + \underline{ik\phi}) \qquad (12)$$

The formulations of the boundary value problems are essentially complete with the exception of the practical matter of setting the boundary conditions away from the airfoil, which depends on the particular problem; subsonic or supersonic free field, wind tunnel wall etc. Asymptotic far field solutions to Equations 10 have been developed for two dimensional subsonic or supersonic free air or wind tunnel flows and for three dimensional subsonic flow. These solutions are described in Section 3.0 as they apply to the various generalizations of the method and are summarized for completeness in Appendix A.

2.2 Finite Difference Solution Method

The numerical solution procedure for the boundary value problems for the steady and unsteady perturbation potential, is based on the mixed differencing, line relaxation procedure developed by Murman, Cole and Krupp[15,16]. They pointed out the essential ingredient for the success of relaxation procedures for the steady transonic potential equation. The key to the approach is to account for the local nature of the flow (elliptic in subsonic regions, hyperbolic is supersonic regions) in the finite difference approximation to the governing equations. The solution method used in the present work for the steady perturbation potential, ϕ^0, is patterned after the method for general lifting airfoils developed by Krupp[16]. Extensions of this method for steady flows, to treat supersonic freestream flows, wind tunnel wall effects and three dimensional flows are presented in Section 3.0. The version of this technique implemented for the two dimensional unsteady perturbation is described here. Generalizations of the unsteady solution method are likewise presented in Section 3.0.

The linearity of the governing equation for ϕ would suggest that many of the powerful techniques of classical analysis could be applied. The equation is seriously complicated, however, by the fact that various coefficients are functions of the nonlinear steady potential, for which the only general solution methods are numerical. In view of this complication and the success of the mixed differencing relaxation procedure for the steady potential equation of similar type, it was decided to use this same method to develop unsteady solutions.

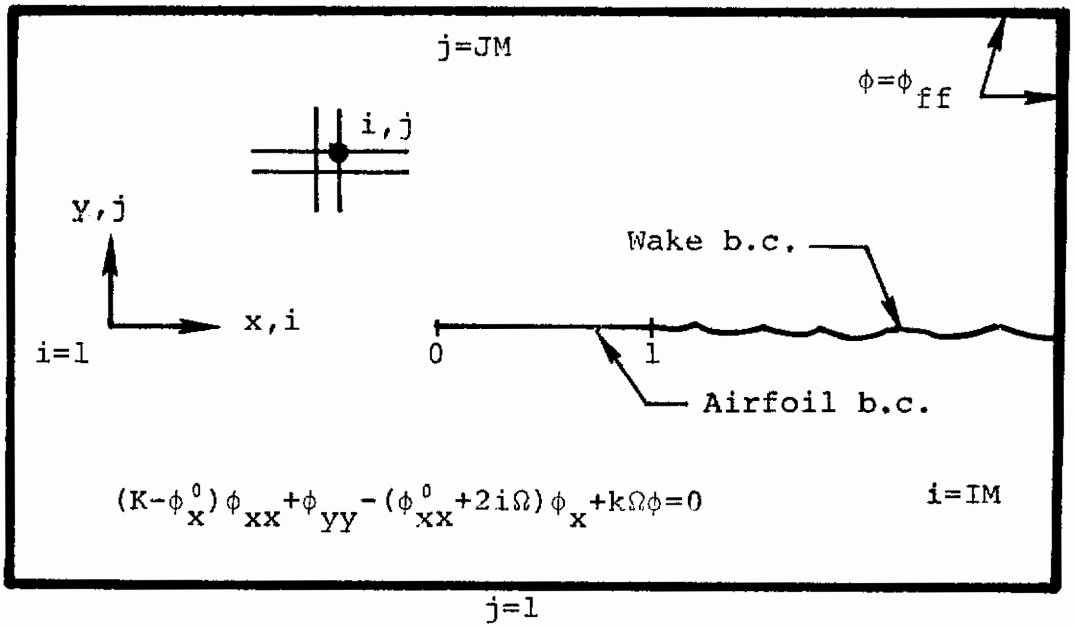

FIGURE 2. SCHEMATIC OF NUMERICAL SOLUTION DOMAIN

Consider the boundary value problem for the unsteady transonic potential, with numerical solution domain indicated schematically in Figure 2. In the numerical scheme, a rectangular mesh with general grid line spacing is overlayed on the solution field in physical x, y coordinates. Uneven grid spacing makes it possible to concentrate grid points near the airfoil slit and in regions where rapid changes in the potential or its derivative (wing leading edge, shocks, etc.) are expected and to expand the grid in a regular manner out to the boundaries of the mesh. The required solution for ϕ^0, which does not depend on ϕ, is solved independently on the same or a more refined grid and the resulting solution stored on magnetic tape. The converged solution so obtained is then used in the solution process for the corresponding ϕ. This approach has the benefit that ϕ^0 need not be regenerated for each unsteady boundary disturbance or reduced frequency of interest.

The local nature of the equation at each grid point is determined by the corresponding value of $(K-\phi_x^0)_{i,j} = V_{i,j}$ at the same grid point. Then if $K-\phi_x^0 > 0$ (elliptic) the x derivatives of ϕ are center differenced and if $K-\phi_x^0 < 0$ (hyperbolic) the x derivatives are backward differenced. Near the sonic line at so-called "parabolic points," the center difference form for the x derivatives of ϕ are used. The finite difference approximation to the unsteady potential equation are thus summarized as follows:

$\underline{V_{i,j} > 0, \text{ elliptic}}$

$$V_{i,j}(\phi_{xx})^E_{i,j} + (\phi_{yy})^E_{i,j} - [2i\Omega + (\phi^0_{xx})^E_{i,j}]\ (\phi_x)^E_{i,j} + \underline{k\Omega\phi} = 0 \tag{13}$$

$\underline{V_{i,j} < 0, \text{ hyperbolic}}$

$$V^H_{i,j}(\phi_{xx})^H_{i,j} + (\phi_{yy})^E_{i,j} - [2i\Omega + (\phi^0_{xx})^H_{i,j}]\ (\phi_x)^H_{i,j} + \underline{k\Omega\phi} = 0 \tag{14}$$

$\underline{V_{i,j} < 0,\ V_{i-1,j} > 0,\ \text{parabolic}}$

$$V_{i,j}(\phi_{xx})^{H}_{i,j} + (\phi_{yy})^{E}_{i,j} \qquad \text{(15}$$

$$-[2i\Omega+(\phi^{0}_{xx})^{H}_{i,j}]\ (\phi_{x})^{H}_{i,j} + \underline{k\Omega\phi} = 0$$

Where $V_{i,j}$, $V^{H}_{i,j}$ and the elliptic (superscript E) and hyperbolic (superscript H) difference forms are centered or backward differenced in the usual manner.

Using the above forms, the finite difference equations are set up for each column (x = constant) in the grid. Appropriate finite difference approximations are made for the body boundary condition, Kutta condition and farfield boundary to effectively close the system of equations. The resulting sequence of linear algebraic equations is solved by Gaussian elimination. After each column is solved, it is relaxed with a variable relaxation factor, depending on the local nature of the solution. This process is repeated for each column in turn, sweeping the grid from left to right until the change in ϕ for all grid points during one grid sweep is less than some arbitrary small amount. Iteration is also required on the unknown airfoil circulation which is always over-relaxed and which is updated along with the farfield at regular intervals. A grid-halving routine has been implemented with considerable improvement in the efficiency of the method. Complete details of the differencing and treatment of body boundary condition, Kutta conditions and farfield boundary conditions are presented in References 1 and 20.

3.0 GENERALIZATIONS OF THE METHOD

One of the main goals of the research reported here was to generalize and extend the method and solution procedure to treat higher frequency effects, supersonic freestream flows, wind tunnel wall effects and three-dimensional planar wing flows. Pertinent studies relating to these developments are summarized in this section and typical calculated results are presented. In particular, the development and implementation of boundary conditions required for the treatment of supersonic freestream flows, wind tunnel flows and three dimensional subsonic flows are discussed in this section and summarized in Appendix A.

3.1 Higher Order Frequency Effects

The previous formulation of the unsteady flow problem was restricted to low reduced frequencies $k \sim O(\delta^{2/3})$ and as a result did not include the effect of plunge (or the so-called "piston pressure" component) since this is a second order ($O(k)$) effect at low frequencies. As summarized in Section 2, the formulation can be generalized to include higher frequency effects and therefore explicitly treat the effect of plunging motion on all unsteady modes. Since all previous results as well as the unsteady results (for pitch and control surface motion) presented in this report used the consistent low frequency formulation, it is important to examine the effect of the high frequency terms on the results for reduced frequencies up to $k = .2$.

The generalization to the formulation is accomplished by retaining the ψ_{tt} term in the full potential equation as well as the unsteady terms in the airfoil boundary condition and definition of pressure coefficient. There is some question about the validity of the resulting small disturbance equation (Equation 3) for general frequencies but it is accepted by most authors as the lowest order unsteady small disturbance equation. Before proceeding with the linearized unsteady perturbation analysis and the comparison of the low frequency to the generalized results, it is instructive to examine the governing equation in some detail to point out the essential difference between the low frequency approximation and the present more general formulation.

3.1.1 Characteristic Analysis of Governing Equation

The governing equation is classified as a quasi-linear equation of hyperbolic type with the non-linearity concentrated in the coefficient $(K-\phi_x^0)$ of the ϕ_{xx} term. This coefficient is essentially the deviation of the local flow velocity from sonic-velocity and for the purposes of the following analysis let $K-\phi_x^0 = V$. For any point (x,y) in the two dimensional physical plane the equation can be linearized in the usual manner and is written as follows:

$$V\,\phi_{xx} + \phi_{yy} - 2\,\phi_{xt} - \frac{k}{\Omega}\,\phi_{tt} = 0 \tag{16}$$

It is noted that tildes have been dropped from all variables with the understanding that they are scaled variables. The hyperbolic nature of the equation as well as the essence of the low frequency approximation can be made apparent by examining the "Monge cones" associated with the equation at a point. Introducing the following transformation:

$$\begin{aligned} \xi &= x \\ \eta &= \sqrt{|V|}\,y \\ \tau &= Vt + x \end{aligned} \tag{17}$$

the canonical form of Eq. (16) becomes:

$$\phi_{\xi\xi} + \phi_{\eta\eta} - \mu\,\phi_{\tau\tau} = 0 \tag{18}$$

where

$$\mu = 1 + \frac{k}{\Omega}\,V$$

The characteristic lines in the (x,t) plane are given by the section of the Monge cone in the (ξ,η) plane which from Eq. (18) are:

$$\tau \pm \sqrt{|\mu|}\ \xi = \text{constant}$$

or in x,t coordinates:

$$t = \frac{1}{V}\,(1 \pm \sqrt{|\mu|})x = \text{constant} \qquad (19)$$

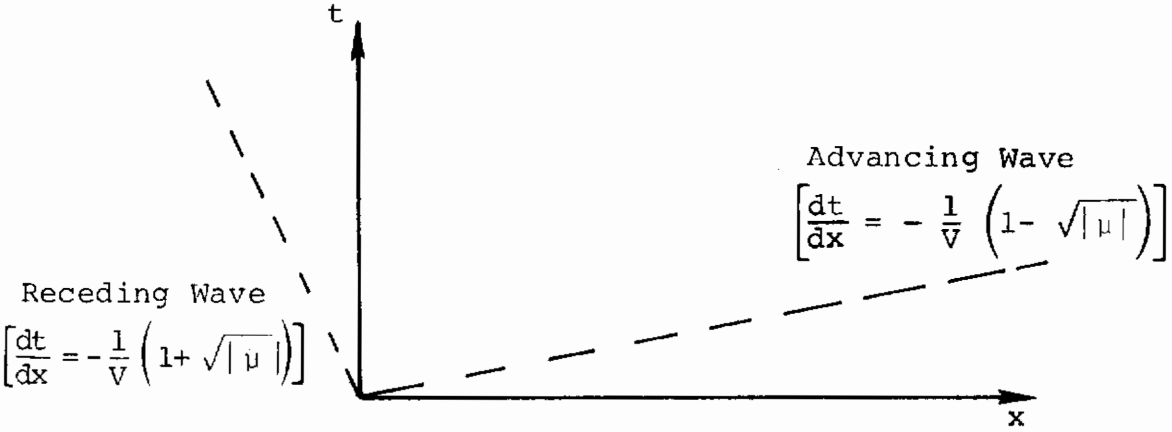

FIGURE 3. CHARACTERISTICS OF SMALL DISTURBANCE POTENTIAL EQUATION

The two families of characteristics at a subsonic $(V > 0)$ point are shown in Figure 3. They physically represent the locus of the wavefronts for the upstream facing or "receding" wave and the downstream facing or advancing wave. The slope of each curve is the inverse of the wave speed in scaled coordinates. It is noted that in the low frequency approximation $\mu = 1$ so that the slope of the downstream characteristic is 0 and the advancing wave speed is infinite. Thus this approximation effectively neglects the effect of the advancing wave;

the physical assumption being that the advancing waves move rapidly away from the airfoil and therefore have a negligible effect on the flow as compared to the receding wave which remains in the neighborhood of the airfoil. It is noted that near a shock or compression through sonic velocity, $V \overset{\sim}{>} 0$ and the slope of the upstream characteristic → ∞ so that receding waves from downstream of the sonic point accumulate at the sonic point and can build up to large amplitude disturbances. This phenomenon is responsible for the inherent nonlinearity of transonic flow as described by Landahl[2].

As the reduced frequency increases, μ becomes appreciably greater than one so that the slope of the downstream characteristic increases away from zero and the corresponding advancing wave speed decreases. Thus the advancing wave becomes more important as the frequency increases, and could in fact become equally important as the receding wave for reduced frequencies of order 1. The generalized theory presented here includes the receding wave and would therefore account for such higher frequency effects.

One final note before leaving the characteristic analysis concerns the genesis of the so-called "sonic theories". It is noted that for very high frequencies ($\mu \to \infty$) and for local Mach number everywhere very close to sonic $1-M_\infty \to 0$ or $V \to 0$ the upstream and downstream characteristics and in fact the Monge cone coalesces to a single vertical line. In this case the upstream or downstream communication through the ϕ_{xx} term becomes negligible so that the governing equation reduces to the linear equation:

$$\phi_{yy} - 2\,\phi_{xt} - \frac{k}{\Omega}\,\phi_{tt} = 0 \tag{20}$$

which for harmonic disturbances has a reduced wave equation form:

$$\phi_{yy} - 2\,\phi_{x} - \frac{k}{\Omega}\,\phi = 0 \tag{21}$$

The equation is parabolic and can be solved by classical methods leading to the theories valid for high frequency sonic flow.

3.1.2 Unsteady Perturbation Analysis

The development of the linearized unsteady perturbation for the general unsteady small disturbance system proceeds in the same manner as described in detail for the low frequency system in previous work[1] and as summarized in Section 2. The resulting system of equations (Eq. 10) varies from the low frequency theory by way of the addition of frequency dependent terms in the governing equation, body boundary condition and wake condition. The treatment of these terms in the finite difference solution method is straightforward and they have been added to the computer programs developed in the study as an option thereby facilitating the comparison of the low frequency formulation to the present formulation. Some comments are contained in this section concerning the implementation of these various changes to the method.

The governing equation for the unsteady perturbation potential requires but the addition of the $k\Omega\phi$ term which includes the advancing wave in the formulation. The term is included in the finite difference equations in the obvious manner. Of greater practical importance to the results of airfoil pressures at low frequencies are the addition of unsteady terms to the body boundary and wake condition and to the definition for pressure coefficients. This is because these terms directly affect the flow near the airfoil whereas the modification to the field equation indirectly affects the flow about the airfoil. For example, the new body boundary condition is:

$$\phi_y = \frac{\partial f_\varepsilon}{\partial x} + \underline{ikf_\varepsilon} \tag{22}$$

It is noted that the low frequency approximation neglects the effect of boundary motion on the downwash including only the effect of the quasi-steady change in airfoil slope. As noted earlier, the pure plunging mode ($f_\varepsilon = -1$) results in the null solution ($\phi \equiv 0$) for the low frequency formulation but is included in the present formulation. It is expected that the addition of the plunge motion to the downwash at the wing will have its greatest effect on the out of phase component ($\mathrm{Im}\phi$) of the solution and should therefore affect the phase of the resulting airfoil pressures. Based on the general form of the body boundary conditions and definition of pressure coefficient (below) it is expected that this effect will be of $O(k)$.

The other change in the formulation involves addition of the unsteady term to the equation for the small disturbance pressure and the resulting effect that this has on the wake condition. The equation for the unsteady component of the scaled pressure coefficient is:

$$\bar{C}_p = -2(\phi_x + \underline{ik\phi}) \tag{23}$$

Again, for low frequencies, the primary effect of the generalized formulation will be on the out of phase ($\mathrm{Im}\ C_p$) component of the pressure.

The Kutta condition requires that the jump in pressure at, and downstream of, the airfoil trailing edge be zero:

$$\Big[\phi_x + ik\phi\Big]_{0-}^{0+} = \Delta\phi_x + ik\ \Delta\phi = 0 \tag{24}$$

$$\text{on } y = 0,\ x \geq 1$$

where $\Delta\phi$ is the jump in potential across the wake. Eq. (24) can be solved explicitly to give:

$$\Delta\phi = \Delta\phi_{te}\ e^{ik(x-1)} \tag{25}$$

$$y = 0,\ x \geq 1$$

where $\Delta\phi_{te}$ is the jump in potential at the trailing edge equal to the airfoil circulation. It is recalled that in the low frequency approximation $\Delta\phi \equiv \Delta\phi_{te}$ so that this generalization involves an oscillatory change in phase of the wake jump condition due to the downstream facing wave.

The generalized forms for the body boundary condition (Eq. 22) wake condition (Eq. 25) and pressure coefficient (Eq. 23) are incorporated into the finite difference equations in an analogous fashion to the low frequency version discussed in detail in Reference 1 and they need not be repeated here. The finite difference solution method also proceeds in the same manner and the comparison calculations presented in the next section indicate that the generalizations described here have little if any effect on convergence or other numerical details of the scheme.

3.1.3 Results for the Generalized Formulation

Results are presented in this report using the low frequency approximation for various unsteady modes of oscillation and for reduced frequencies up to $k = .2$. It is appropriate to verify the accuracy of these results in light of the higher order frequency effects discussed above. To this end, calculations have been performed for a flat plate oscillating in pitch in a subsonic stream and for a NACA 64A410 airfoil oscillating in pitch and plunge at a supercritical Mach number. Results for the low frequency formulation are compared to the modified formulation and to results of alternate formulations.

Results for the flat plate airfoil oscillating in pitch $[(f_\varepsilon' = -1 - ik(x - x_p)]$ at $M_\infty = .7$ and a reduced frequency $k = .2$ are presented in Figure 4. Distributions of the Real and Imaginary parts of the jump in pressure coefficient across the airfoil per unit angle of attack are shown. The results calculated by the present method in its approximate low frequency and generalized form are compared to the corresponding results calculated by the doublet-lattice method[21]. The calculations are for perturbations about a uniform ($\phi^0 \equiv 0$) mean flow and the generalized results should compare within numerical error to the doublet-lattice results. Indeed, as shown in the figure, the results of the high frequency formulation compare within a few percent to the doublet-lattice solution. It should be pointed out that the present method used 26 finite difference points on the airfoil and the doublet-lattice method used 25 chordwise boxes so that they are being compared on the same basis in terms of numerical definition. Results using the low frequency approximation are also shown in Figure 4 and they indicate the expected effect of the high frequency terms on the out of phase component (Imaginary part) of the solution.

The corresponding results for a NACA 64A410 airfoil with a mean angle of attack of 2^o oscillating in pitch about the leading edge at k = .2 are shown in Figures 5 and 6. Figure 5 presents the unsteady component of lift as a function of angle of attack (or time) and Figure 6 gives the perturbed pressure coefficient distribution over the airfoil. In Figure 5 the results of the low frequency and generalized frequency formulation are compared to the "exact" numerical results of Magnus and Yoshihara[9] (see Section 5 for more details). Note that for an integrated quantity such as lift the higher order frequency effects produce but a slight change in magnitude and phase. It is noted that both formulations compare surprisingly well with the Magnus and Yoshihara results. The comparison of pressure distributions in Figure 6 shows the slight effect of the high frequency terms on the in-phase component and a somewhat larger effect on the out of phase component; similar to the result for the fully subsonic flow. As an aside, a comparison of Figures 4 and 6 show the large transonic flow effect for an airfoil with a practical thickness, camber and mean angle of attack. The comparison with the Magnus and Yoshihara results given here and in Section 5 show that the present theory, in either its low frequency approximate form or its general frequency form, model these nonuniform flow effects. These strong transonic flow effects are likewise shown in Figure 7 which presents results calculated using the present method for the same NACA 64A410 oscillating in uniform plunge at k = .2. A comparison of the perturbation pressures due to pitch and plunge in Figures 6 and 7, respectively show that for low frequencies, pressures and forces due to plunge are, in magnitude, approximately 20 percent of the pressure and forces due to pitch. This is consistent with the estimate of higher order frequency effects which indicate that such effects are O(k).

In summary, the generalizations of the low frequency theory to include higher frequency effects, necessary for the treatment of plunge oscillations, would seem to give an accurate representation of such effects. The comparisons presented here show that these effects are O(k) in the low frequency regime so that the generalized formulation should be used for all unsteady modes for reduced frequencies as large as k = .2. Since the high frequency terms do not seem to degrade the efficiency, convergence or stability of the numerical solution method, the generalized formulation presented here would seem to be recommended over the previous low frequency formulation.

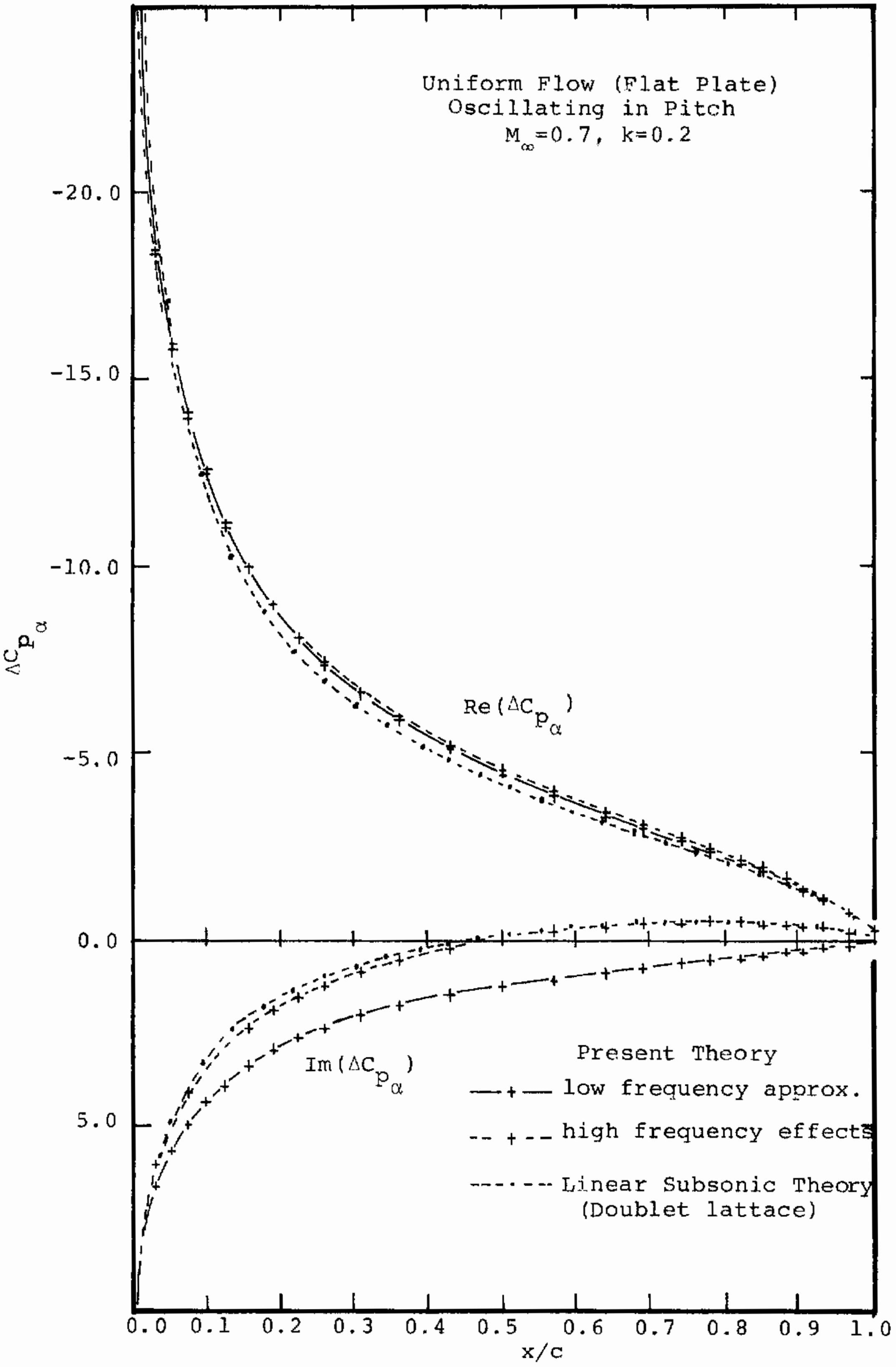

FIGURE 4. JUMP IN UNSTEADY AIRFOIL PRESSURE COEFFICIENT DUE TO OSCILLATION IN PITCH

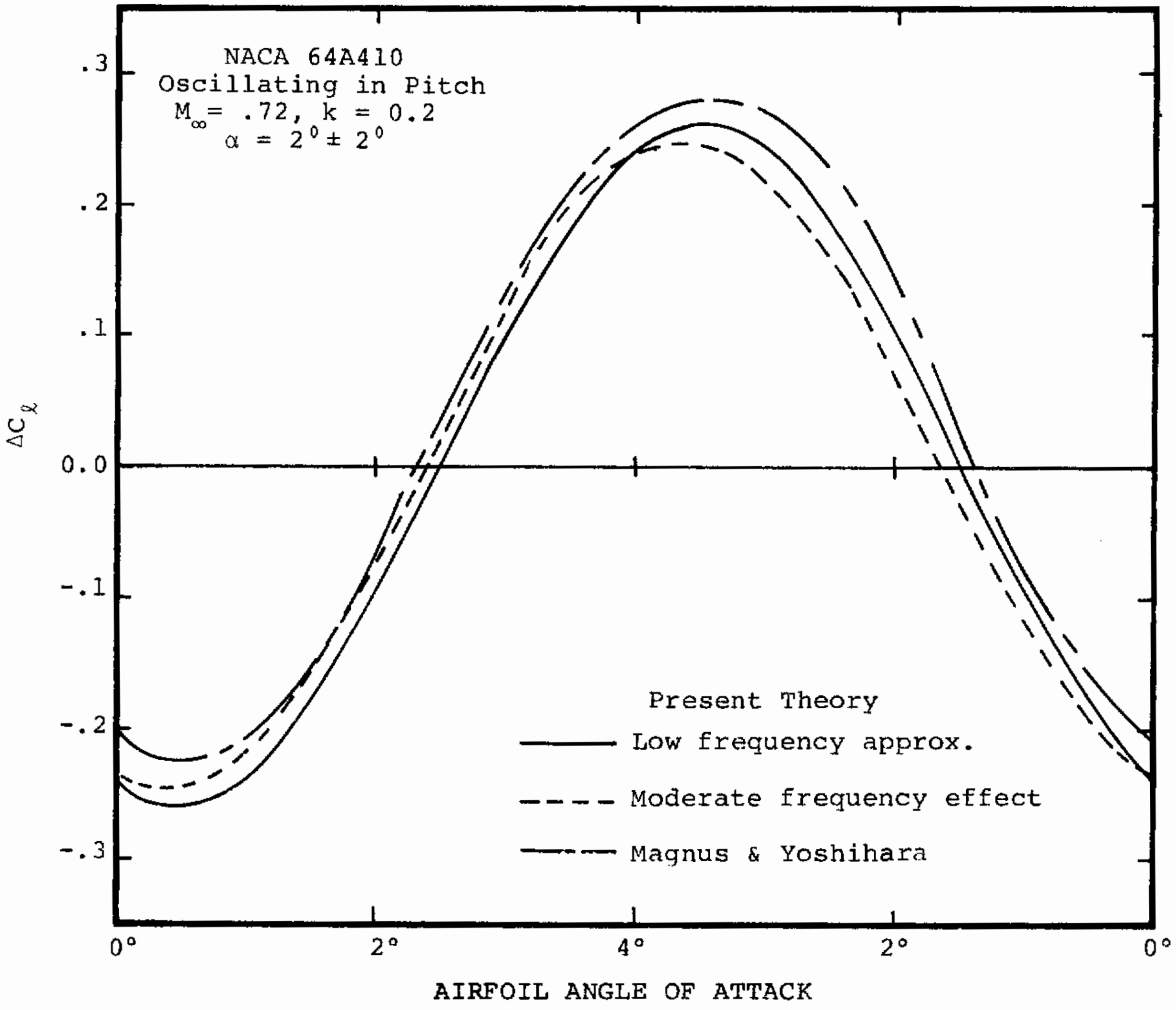

FIGURE 5. UNSTEADY LIFT PERTURBATION FOR NACA 64A410 AT M = .72, REDUCED FREQUENCY = 0.2

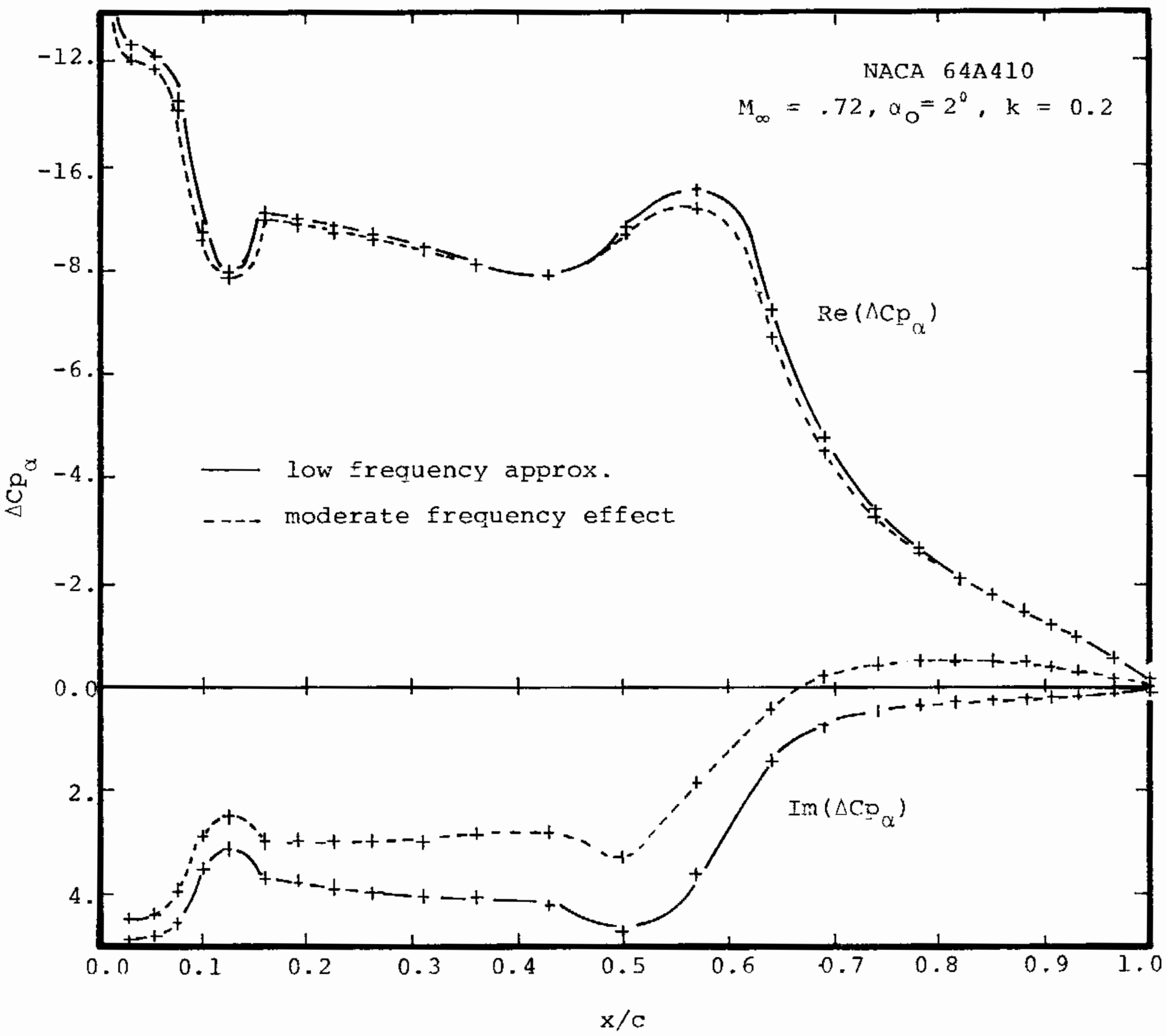

FIGURE 6. JUMP IN UNSTEADY AIRFOIL PRESSURE COEFFICIENT DUE TO OSCILLATION IN PITCH

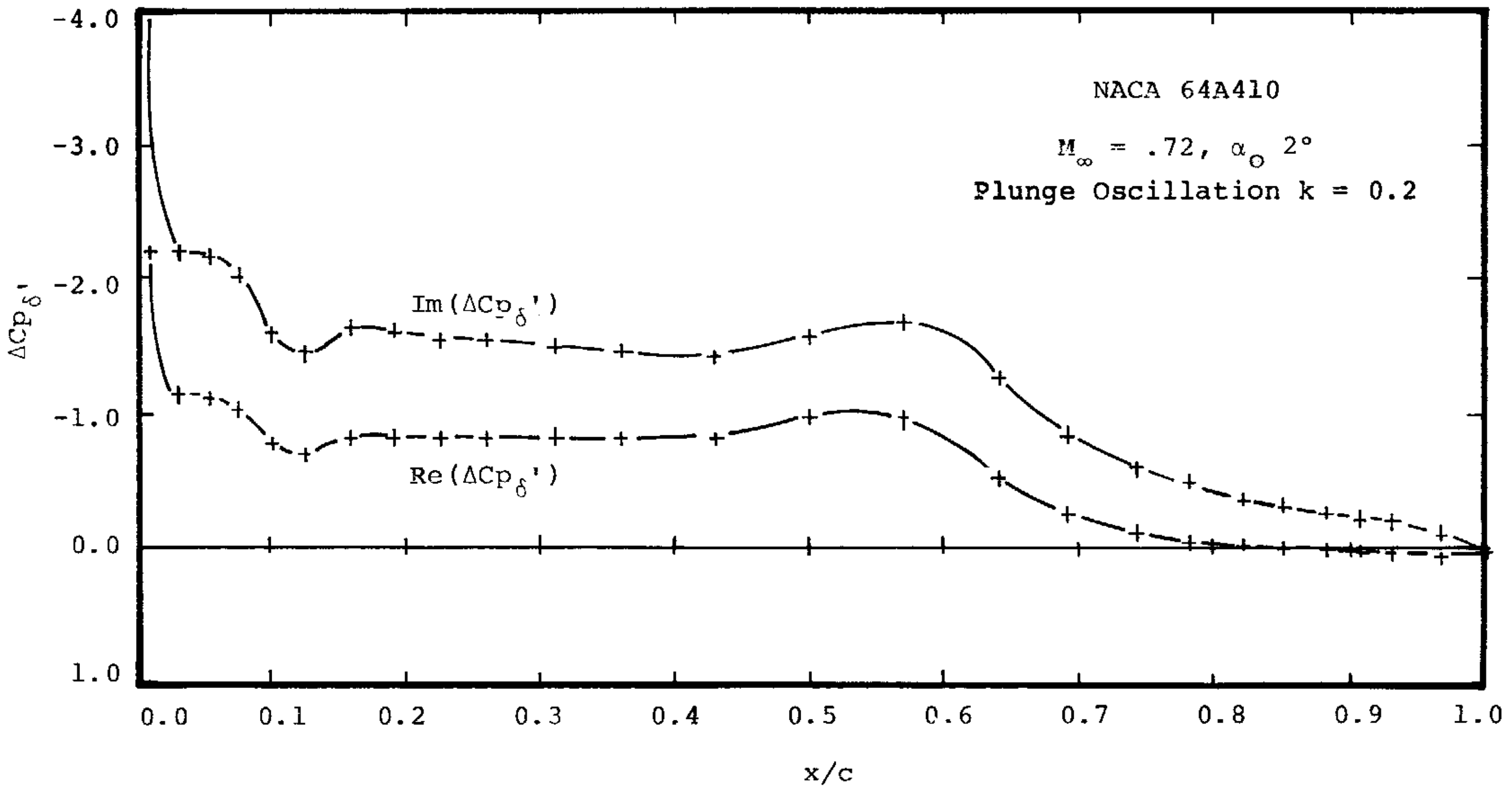

FIGURE 7. JUMP IN UNSTEADY AIRFOIL PRESSURE COEFFICIENT DUE TO OSCILLATION IN PLUNGE

3.2 Supersonic Freestream Calculations

The theory and numerical solution method described in the report applies equally well to subsonic or supersonic freestream flow. The application of the method to supersonic flows, the subject of this section, requires that certain details of the method, in particular the treatment of the farfield condition, be modified. This generalization has been accomplished for small disturbance steady flows by Murman[22,23] and his approach is followed in the present work as summarized in Section 3.2.1. Other details concerning the treatment of steady supersonic flows which were considered during the present research are also discussed in that section. The analogous treatment of unsteady supersonic flows, the prime object of this research, is discussed in Section 3.2.2.

3.2.1 Steady Flows With Supersonic Freestream

The primary generalization to the numerical solution method for treating supersonic freestream flows involves the derivation of a farfield boundary condition. The asymptotic solution available for subsonic freestream flows (Appendix A) clearly do not apply. Even if such a solution were convenient to derive for supersonic flows, the application of a Dirichlet boundary condition is not appropriate and could lead to numerical difficulties for a hyperbolic farfield flow. The method used here involves developing asymptotic approximations to the characteristic relations for the hyperbolic form of the transonic potential equation (Eq. 9), and to apply these relations as boundary conditions on the far boundary of the grid.

Letting $u = \phi_x^0$ and $v = \phi_y^0$ the characteristic directions and relations for the two dimensional steady transonic potential equation are respectively:

$$\frac{dy}{dx} = \frac{du}{dv} = \pm(u-K)^{-\frac{1}{2}} \tag{26}$$

The characteristic relations can be immediately integrated to give:

$$\frac{2}{3}(u-K)^{3/2} \mp v = R^{\pm}, \quad \text{on } \frac{dy}{dx} = \pm \ (u-K)^{-\frac{1}{2}} \tag{27}$$

where $R^{\pm}$ are the Riemann invariants. It is noted that far upstream the flow is uniform so that $u=v=\phi\equiv 0$ as $x\to-\infty$. This uniform flow condition provides the needed upstream boundary condition which is applied as a Dirichlet condition on ϕ. In the transverse direction ($y\to\pm\infty$) away from the airfoil the characteristic relations may be approximated under the assumption that $u<<-K$. Expanding equation 27 for small u gives:

$$\mp v + \left\{ \sqrt{-K}\, u + \frac{u^2}{4\sqrt{-K}} + \ldots \right\} = R^{\pm} \quad \text{on } \frac{dy}{dx} = \pm \frac{1}{\sqrt{-K}} \qquad (28)$$

It is noted that $K<0$ for supersonic freestream flow. For $y\to\pm\infty$ the assumption is made that there is no disturbance at upstream infinity ($R=0$) so that taking the first order approximation to the incoming characteristic relation gives:

$$\phi^0_y = \mp \sqrt{-K}\, \phi^0_x \quad \text{as } y\to\pm\infty \qquad (29)$$

Thus as long as the transverse boundaries of the finite difference grid are supersonic and far away from the airfoil Equations 29 provide an accurate representation of the farfield solution.

This boundary condition is incorporated into the finite difference procedure in the same manner as the airfoil boundary condition. That is, on the top and bottom of the rectangular grid $(\phi^0_{yy})_{i,j}$ is differenced as a one-sided difference using Equation 29 in the finite difference equation. For example on the top boundary ($y=y_{max}$):

$$\phi^0_{yy_{i,j}} = \frac{2}{\Delta y_{J-1}} \left\{ \phi^0_{y_{i,j}} - \frac{\phi^0_{i,j}-\phi^0_{i,j-1}}{\Delta y_{j-1}} \right\} \text{ for } j=JM \qquad (30)$$

With ϕ^0_y from equation 29 and the backward difference form for ϕ^0_x (since the flow is supersonic):

$$\phi^0_{yy_{i,j}} = \frac{2}{\Delta y_{j-1}} \left\{ \frac{-\sqrt{-K}}{2\Delta x_{i-1}} \left(\phi^0_{i,j} - \phi^0_{i-1,j}\right) - \frac{\sqrt{-K}}{2\Delta x_{i-2}} \left(\phi^0_{i-1,j} - \phi^0_{i-2,j}\right) - \frac{1}{\Delta y_{j-1}} \left(\phi^0_{i,j} - \phi^0_{i,j-1}\right) \right\} \tag{31}$$

Using this relation in the finite difference analog to the partial differential equation (Eq. 14 above) effectively closes the system of equations for a collumn of grid points and the solution proceeds as before. The downstream ($x \to +\infty$) boundary of the grid requires no special treatment, as long as the flow there is supersonic, because of the lack of upstream influence in supersonic flow.

In order to illustrate the method, fully supersonic results are presented in Figure 8 and 9 for a 6 percent thick circular arc airfoil at $M_\infty = 1.5$ and a 0.5° wedge at $M_\infty = 2.0$ respectively. The circular arc solution is compared to linear supersonic theory which would be quite accurate for this case. The calculation verifies the application of the method to supersonic freestream flows and demonstrates that the transonic theory reduces to linearized supersonic theory for $M_\infty >> 1$. The present solution shows a slight degree of nonlinearity in this case as well as demonstrating the numerical smoothing of the shock waves at the leading and trailing edge of the airfoil. The wedge solution (Figure 9) was performed to verify the accuracy of the scheme for very weak oblique shocks. Results for three grid designs with different values of Δy are shown which indicate that the sharpness of the shock is strongly dependent on grid design. The "overshoot" in the shock jumps is most likely due to the extrapolation procedure used for defining values of potential on the airfoil since it is not evident in the shock jumps away from the airfoil. The overshoot is also dependent on the strength of the shock as shown by the result for a stronger oblique shock in Figure 10. For this case with an order of magnitude stronger shock no overshoot is evident. It is also noted that the overshoot can be largely elliminated even for the weak shock case by the proper choice of Δy in the first grid point above the airfoil. This indicates that a more intelligent extrapolation method for defining the solution on the body, such as, for example, extrapolation along characterisitics (Eq. 26), would also elliminate the overshoot.

To examine the accuracy of the basic hyperbolic differencing scheme, a general higher order finite difference form has been implemented on a trial basis. The method uses an additional upstream point for the finite difference forms for ϕ^0_x and ϕ^0_{xx}:

$$(\phi^0_x)_{i,j} = \frac{2-\nu}{2}\left\{\frac{\phi^0_i-\phi^0_{i-1}}{\Delta x_{i-1}} + \frac{\phi^0_{i-1}-\phi^0_{i-2}}{\Delta x_{i-2}}\right\} - \frac{(1-\nu)}{2}\left\{\frac{\phi^0_{i-1}-\phi^0_{i-2}}{\Delta x_{i-1}} - \frac{\phi^0_{i-2}-\phi^0_{i-3}}{\Delta x_{i-3}}\right\} \tag{32}$$

$$(\phi^0_{xx})_{i,j} = \frac{2(2-\nu)}{\Delta x_{i-1}+\Delta x_{i-2}}\left\{\frac{\phi^0_i-\phi^0_{i-1}}{\Delta x_{i-1}} - \frac{\phi^0_{i-1}-\phi^0_{i-2}}{\Delta x_{i-2}}\right\} - \frac{2(1-\nu)}{\Delta x_{i-2}+\Delta x_{i-3}}\left\{\frac{\phi^0_{i-1}-\phi^0_{i-2}}{\Delta x_{i-2}} - \frac{\phi^0_{i-2}-\phi^0_{i-3}}{\Delta x_{i-3}}\right\} \tag{33}$$

For $\nu=1$ the scheme reduces to that presently used and for $\nu=0$ it is a second order accurate hyperbolic scheme after Richtmeyer and Morton[23]. Results for the 2° wedge with $M_\infty=1.25$ are shown for $\nu=0$ and $\nu=1$ in Figure 10 for comparison. Both methods give the same shock jump and differ only in the sharpness of the shock. This comparison indicates that the three point scheme used in this work is quite accurate and in fact gives sharper shock waves than higher order accurate difference schemes. Figure 10 also shows the solution away from the surface (at $\tilde{y} = .2$ and $.4$) which indicates that oblique shock waves away from the surface undergo considerable numerical smoothing. Note, however, that the shock jump condition is retained. The degree of shock smearing indicated is an attendent result of any shock capturing numerical method and can probably be elliminated only by using shock fitting; a rather complicated prospect for general transonic flows.

As described in previous work[1] and summarized in Section 2, the numerical solution method takes no special account of shock waves. As shown in the above results the procedure is adequate for oblique shocks, but as recently pointed out by Murman[24], the treatment of strong shocks (supersonic to subsonic transition) is inaccurate. The accuracy of the method can however be improved by using a special "shock point operator" (SPO) as suggested by Murman or by using shock fitting, as implemented recently by Cheng and Hafez[25]. Since strong shocks are important for transonic flows, especially low supersonic flows, it was decided to implement a form of Murman's shock point operator.

A shock point in the finite difference approximation to the transonic potential equation is defined as a point (i,j) when $(K-\phi^0_x)_{i-1,j}<0$ and $(K-\phi^0_x)_{i,j}>0$. At such a point, the finite difference equation is generalized to:

$$\alpha(K-\phi^0_x)^c_{i,j}\phi^{0\,c}_{xx_{i,j}} + \beta(K-\phi^0_x)^b_{i,j}\phi^{0\,b}_{xx_{i,j}} + \phi^{0\,c}_{yy_{i,j}} = 0 \qquad (34)$$

where superscripts b and c indicate backward and central differencing. Murman suggests $\alpha=\beta=1$ as the form which provides a "conservative" finite difference scheme. However, as can easily be seen (and as noted by Murman) this is inconsistent with the governing equation to $O(\Delta x)$. In the present work it was decided to use $\alpha=1/2$, $\beta=1/2$ which retains the consistency of the finite difference approximation to the transonic potential equation but is nonconservative by Murman's definition to $O(\Delta x)$. This form was chosen because consistency is believed to be of utmost importance and also since the conservation property of the finite difference scheme depends upon the definition of the variation of a quantity over the sides of a finite difference cell. This can clearly only be defined to first order especially near a shock. In short it is felt that the shock point differencing used is consistent with the formalism of shock capturing and could only be improved by shock fitting.

Results using the shock point formalism are shown in Figures 11,12, and 13 at the end of the section. Figure 11 presents the pressure coefficient along the axis for a circular arc airfoil at $M_\infty = 1.15$. Results calculated with and without the SPO are presented and show the important effects on the shock jump and stand-off distance. It is interesting to note that the pressure coefficient on the airfoil ($x/c>0$) is curiously unaffected by the treatment of the shock.

Results calculated with $\alpha=1$, $\beta=1$ (as per Murman) are indistinguishable from the SPO result shown in the figure. It is noted that the use of the SPO also seems to have a beneficial effect on the convergence of the iteration procedure.

Figure 12, and 13 are presented to demonstrate the application of the final developed method for supersonic freestream flows to practical airfoils of interest in the present work. The figures give the airfoil pressure distribution for a sharp leading edge, 6 percent thick circular arc airfoil at $M_\infty=1.25$ and 1.15 and a blunt leading edge NACA64A006 at $M_\infty=1.5$ and 1.2 respectively. The figures show the expected non-linear transonic results and in the case of the NACA64A006 (Figure 13) shows the development of and movement away from the airfoil of the detached bow shock as freestream Mach number approaches Mach 1.

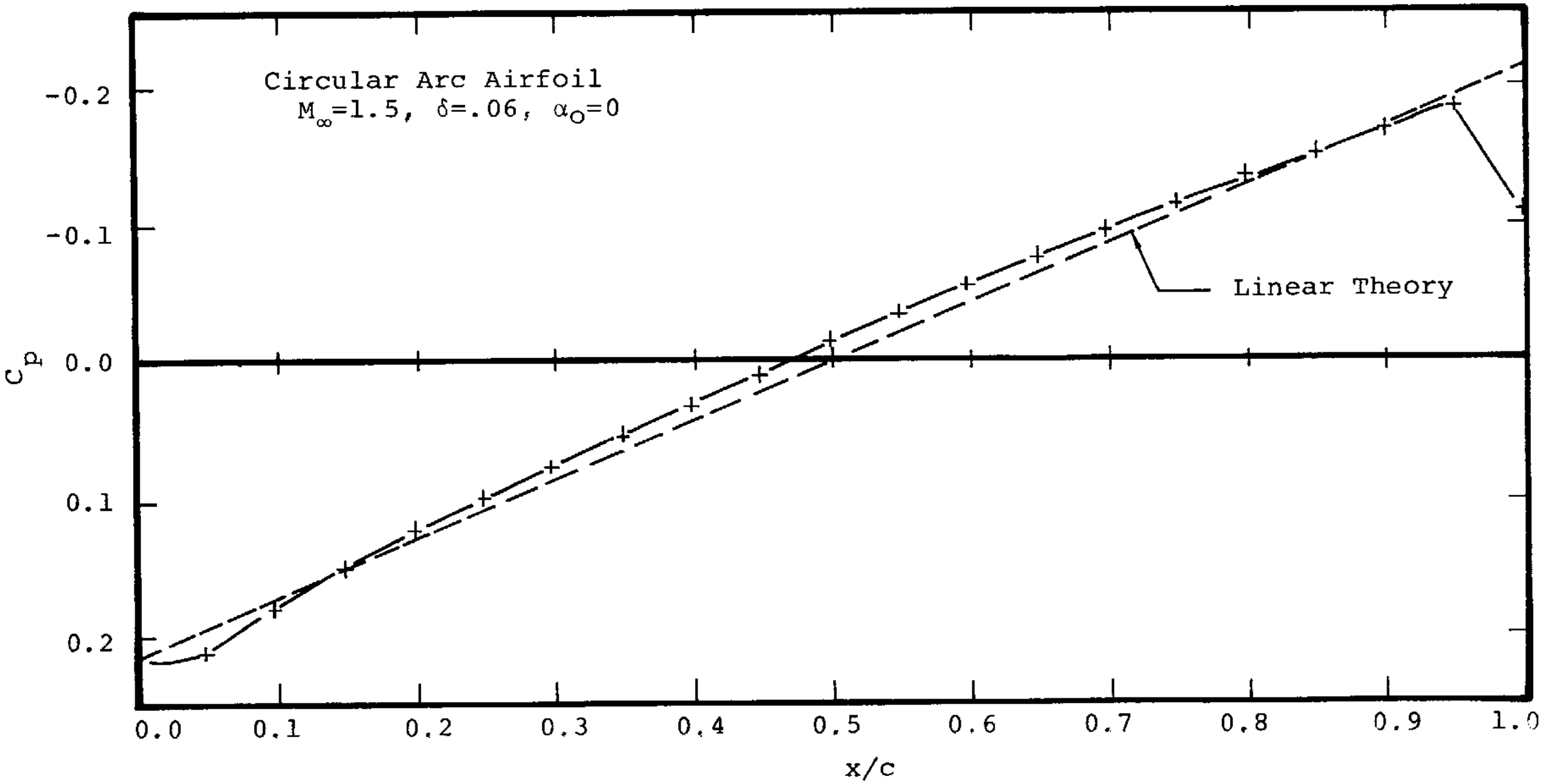

FIGURE 8. AIRFOIL PRESSURE COEFFICIENTS

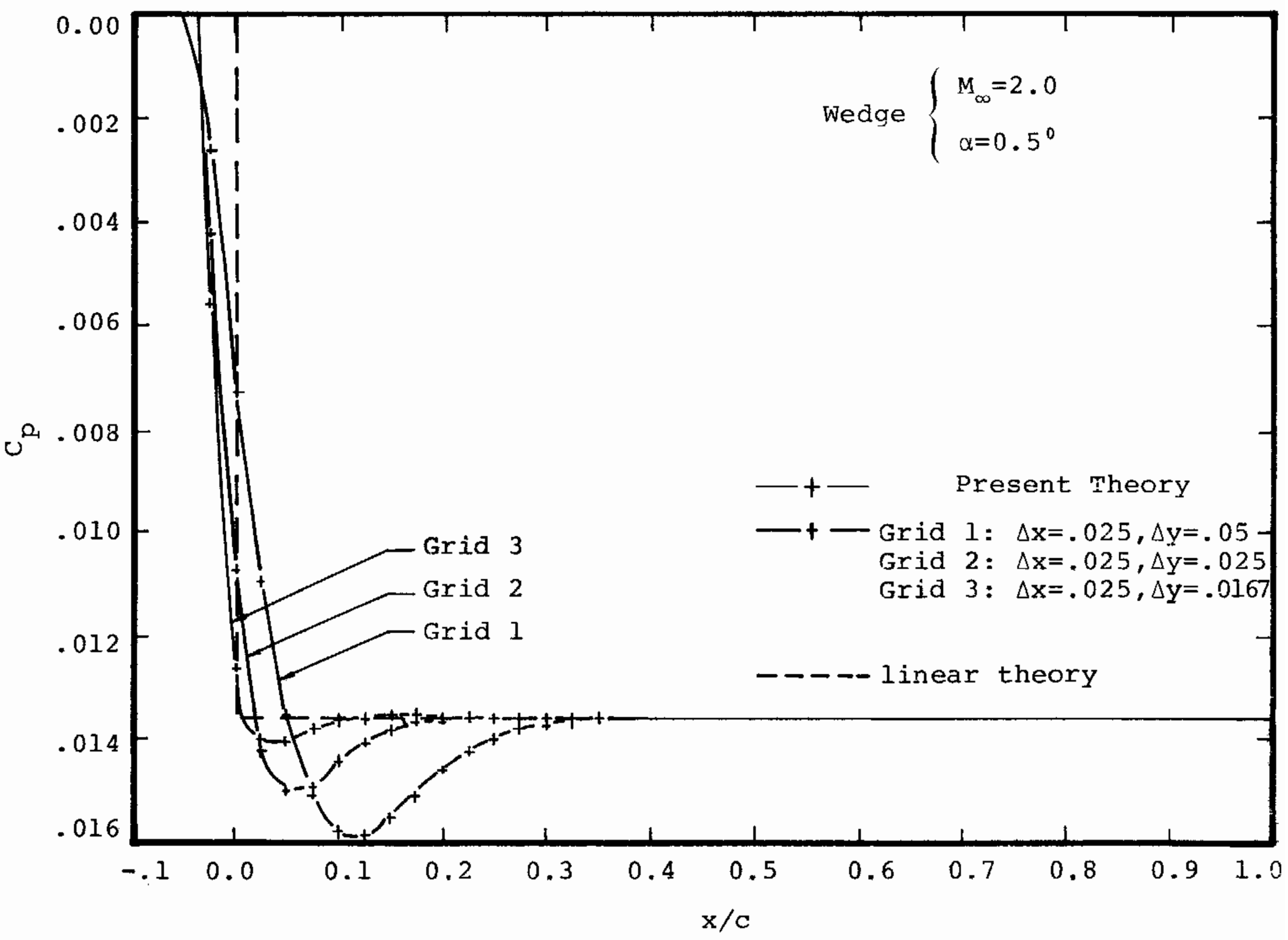

Figure 9. Pressure Coefficient for Wedge in Supersonic Flow

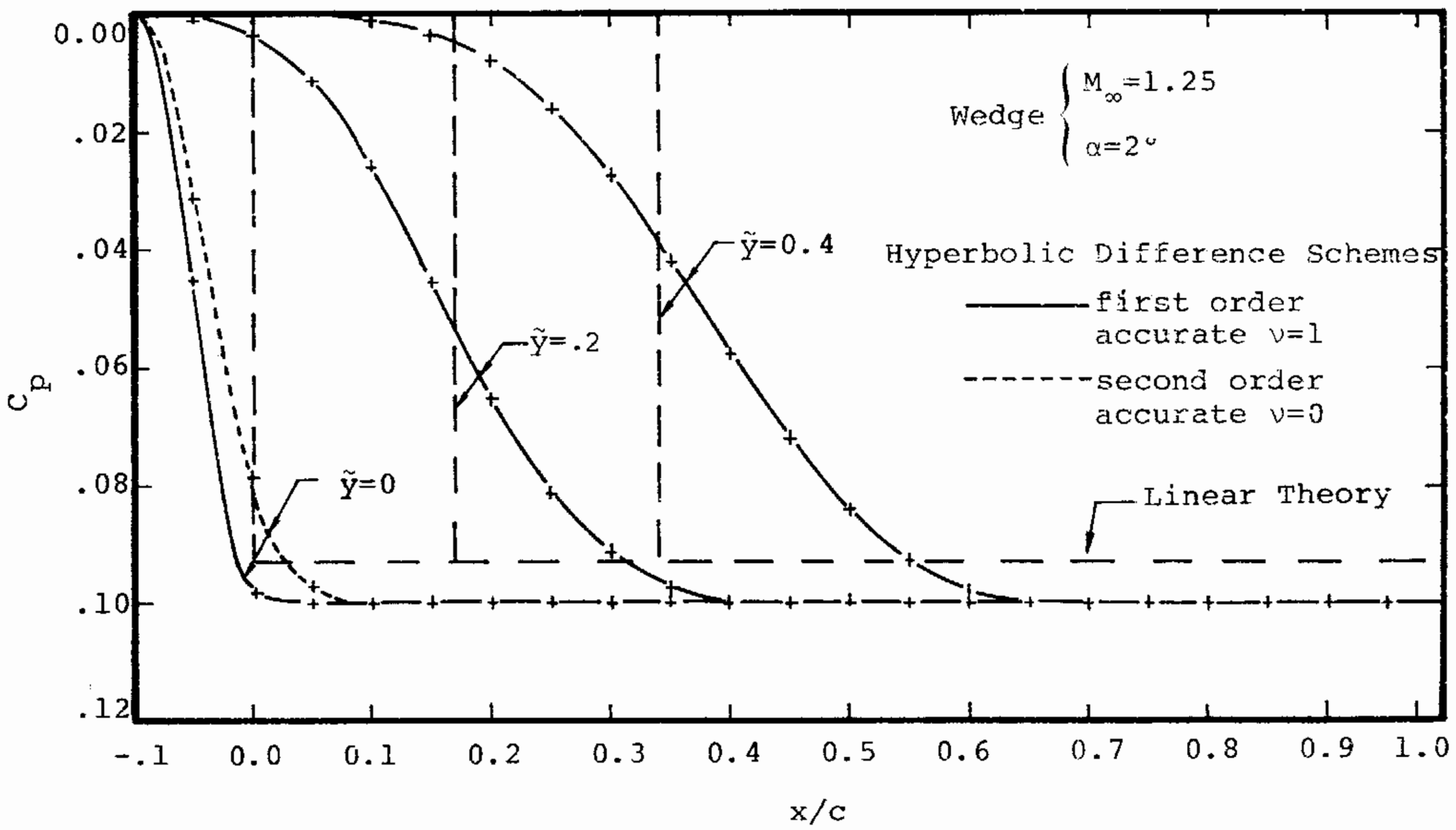

FIGURE 10. PRESSURE COEFFICIENTS FOR A WEDGE IN SUPERSONIC FLOW

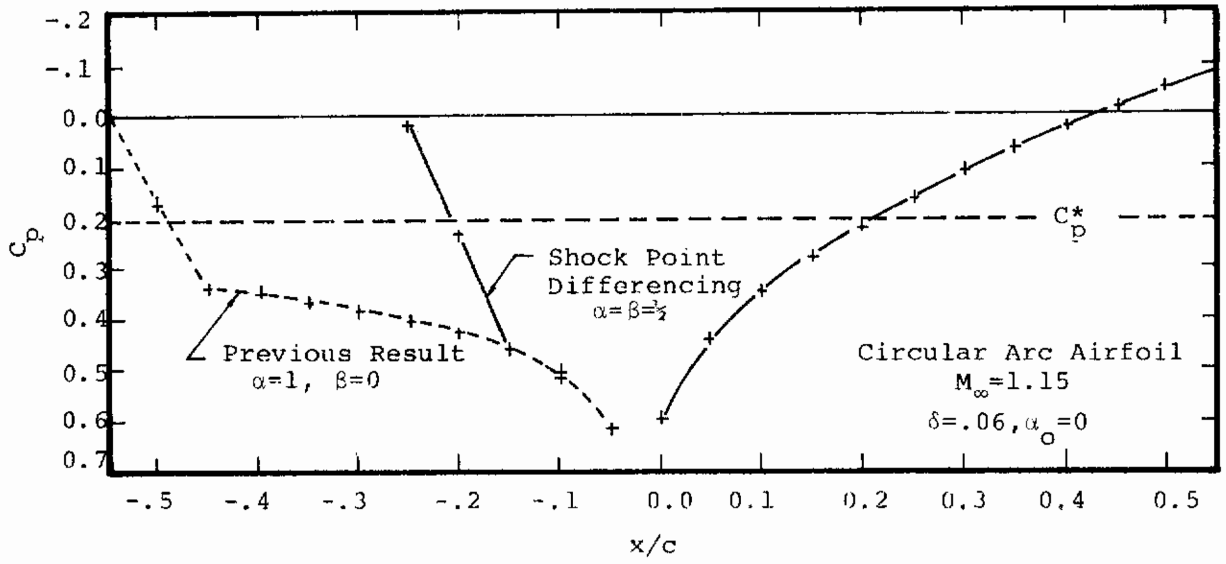

FIGURE 11. EFFECT OF SHOCK POINT DIFFERENCING ON SUPERSONIC FREESTREAM FLOW

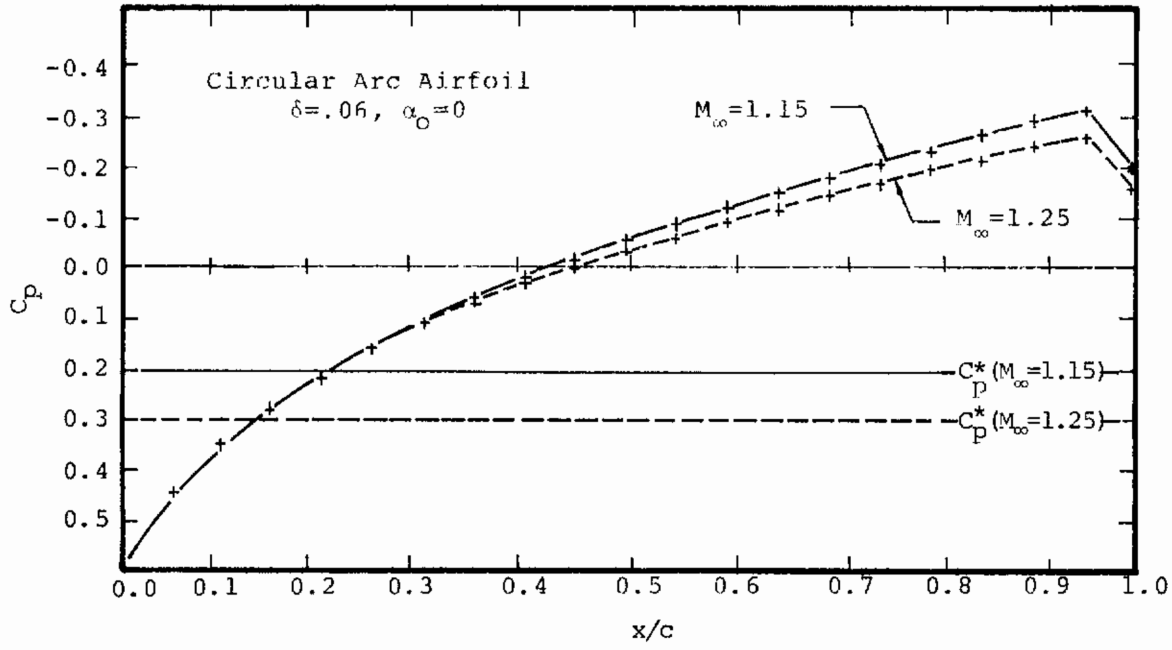

FIGURE 12. AIRFOIL PRESSURE COEFFICIENTS

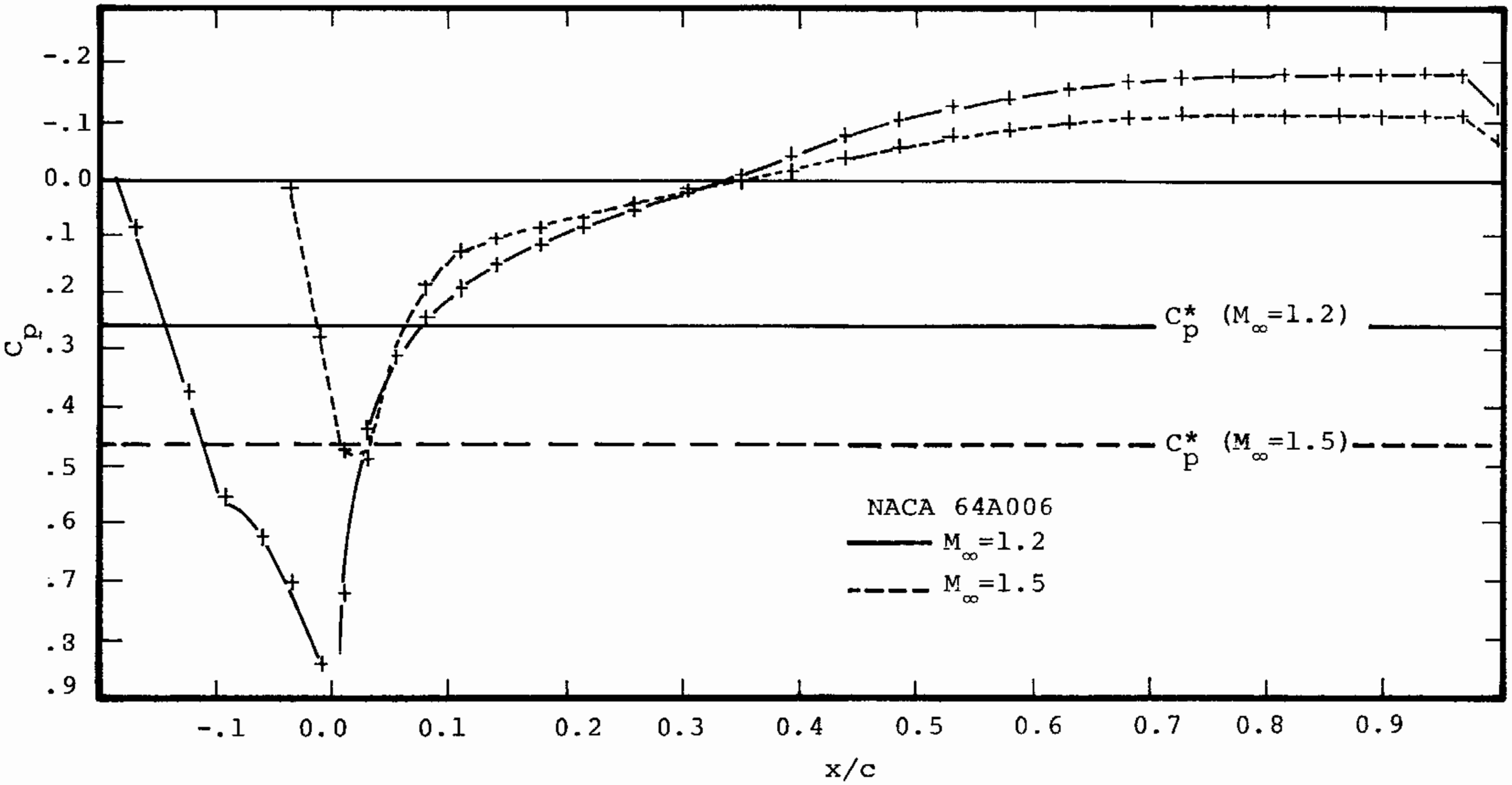

FIGURE 13. AIRFOIL PRESSURE COEFFICIENTS

3.2.2 Unsteady Flows With a Supersonic Freestream

The extension of the unsteady perturbation method to flows with supersonic freestreams proceeds in an analogous manner to the steady flow case just discussed. The main generalization involves the development and implementation of a farfield boundary condition for the numerical solution scheme. As in the steady case, a characteristic condition is developed which is valid far from the airfoil. To this end, consider the governing equation for the unsteady perturbation potential written in the following form:

$$\phi_{xx} - \frac{1}{|K|}\,\phi_{yy} = -\frac{1}{|K|}\left(2i\Omega\phi+\phi_x^0\phi_x\right)_x \tag{35}$$

where it is noted that K<0 for supersonic freestream flow. Introducing the characteristic coordinates:

$$\begin{aligned} \xi &= x + \sqrt{|K|}\;y \\ \eta &= x - \sqrt{|K|}\;y \end{aligned} \tag{36}$$

Equation (35) can be written in the following canonical form:

$$\frac{\partial^2\phi}{\partial\xi\partial\eta} = -\frac{1}{4|K|}\left\{(2i\Omega\phi+\phi_x^0\phi_x)_\xi + (2i\Omega\phi+\phi_x^0\phi_x)_\eta\right\} \tag{37}$$

Integrating along the ξ and η characteristics in turn results in the characteristic relations:

$$\begin{aligned} \frac{\partial\phi}{\partial\xi} = \frac{1}{2}\left(\phi_x + \frac{1}{\sqrt{|K|}}\,\phi_y\right) &= -\frac{1}{4|K|}\left\{(2i\Omega\phi+\phi_x^0\phi_x)\right. \\ &\qquad \left. + \int(2i\Omega\phi+\phi_x^0\phi_x)_\xi\,d\eta\right\} \\ &\text{on } \frac{dy}{dx} = -\frac{1}{\sqrt{|K|}} \end{aligned} \tag{38}$$

and

$$\frac{\partial\phi}{\partial\eta} = \frac{1}{2}\left(\phi_x - \frac{1}{\sqrt{|K|}}\phi_y\right) = -\frac{1}{4|K|}\left\{(2i\Omega\phi+\phi_x^0\phi_x)\right. \tag{39}$$

$$+\int(2i\Omega\phi+\phi_x^0\phi_x)_\eta \, d\xi$$

$$\text{on } \frac{dy}{dx} = \frac{1}{\sqrt{|K|}}$$

As before upstream infinity x→-∞ is considered a region of uniform flow so that $\phi=\phi_x\equiv 0$ and this is used to set an upstream boundary condition on ϕ. On the top and bottom of the grid the characteristic condition valid along incoming characteristics given by Equations 38 and 39 are used. Under the assumption that these boundaries are far from the airfoil and using the fact that the incoming characteristic originates in a region of uniform flow, the integrals in the characteristic equations may be neglected so that:

$$\phi_y = \mp\left\{\sqrt{|K|}\;\phi_x + \frac{1}{2\sqrt{|K|}}(2i\Omega\phi+\phi_x^0\phi_x)\right\} \tag{40}$$

$$\text{as } y\to\pm\infty$$

These boundary conditions are incorporated into the finite difference procedure by using a one sided difference form for ϕ_{yy} at the top and bottom of the grid with the required value of ϕ_y given by Equation 40. For example at the top boundary:

$$\phi_{yy_{i,j}} = \frac{2}{\Delta y_{j-1}} \left\{ -\sqrt{|K|}\,\phi^{b}_{x_{i,j}} - \frac{1}{2\sqrt{|K|}} \left(2i\Omega\phi_{i,j} + \phi^{0b}_{x_{i,j}}\phi^{b}_{x_{i,j}} \right) - \frac{1}{\Delta y_{j-1}} \left(\phi_{i,j} - \phi_{i,j-1} \right) \right\} \tag{41}$$

As before the x derivatives of ϕ^0 and ϕ are backward differenced since the boundary points are required to be supersonic for this boundary condition to apply. The use of Equation 41 and an analogous equation for the bottom boundary effectively closes the system of equations for a column of grid points.

Figures 14 and 15 below are presented to illustrate the application of the method to fully supersonic flows and low supersonic flow (mixed flow) respectively. Figure 14 presents results for change in pressure coefficient per unit quasi-steady (k=0) deflection in pitch ($f'_\epsilon=-1$) for a flat plate (uniform mean flow $\phi^0\equiv 0$) and for a circular arc airfoil both at $M_\infty=1.5$. The flat plate result should compare identically with supersonic linear theory which is also shown in the figure. As shown, the present flat plate result compares very well with linear theory with the exception of some smoothing of the centered expansion wave at the leading edge and the shock wave at the trailing edge. The present theory also shows a tendency to overexpand the flow at the leading edge which is believed due to the extrapolation procedure discussed above for the steady flow. The circular arc results (Figure 14) and results for a NACA64A006 airfoil (Figure 15) are calculated as quasi-steady (k=0) pitch perturbations to the non-uniform steady solutions presented in Section 3.2.1. The circular arc results show an appreciable non-uniform flow effect even for a fully supersonic flow of $M_\infty=1.5$. As expected, this effect is shown to be even greater in Figure 15 for the NACA airfoil at a low supersonic Mach number ($M_\infty=1.2$) In this case it is recalled that the steady flow is subsonic near the leading edge which is responsible for the leading edge singularity in the perturbation pressure coefficient shown in Figure 15.

The results presented here demonstrate the application of the present method to supersonic flow and verify that the method reduces to linear supersonic theory for $M_\infty>>1$. The method also seems to give a reasonable description of the transonic non-uniform flow effects and this is amplified upon in later sections of the report.

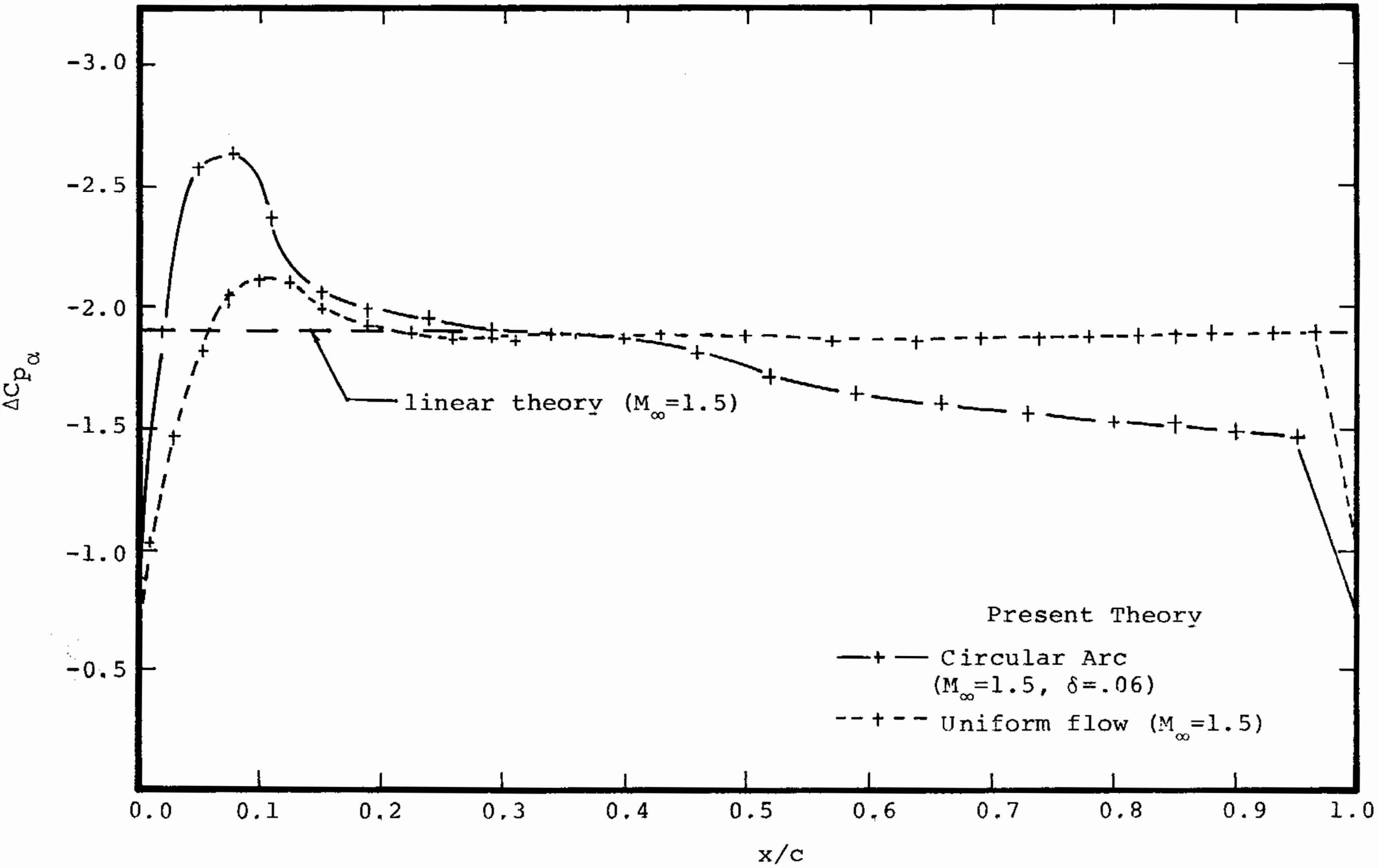

FIGURE 14. CHANGE IN PRESSURE COEFFICIENT DUE TO PITCH DEFLECTION

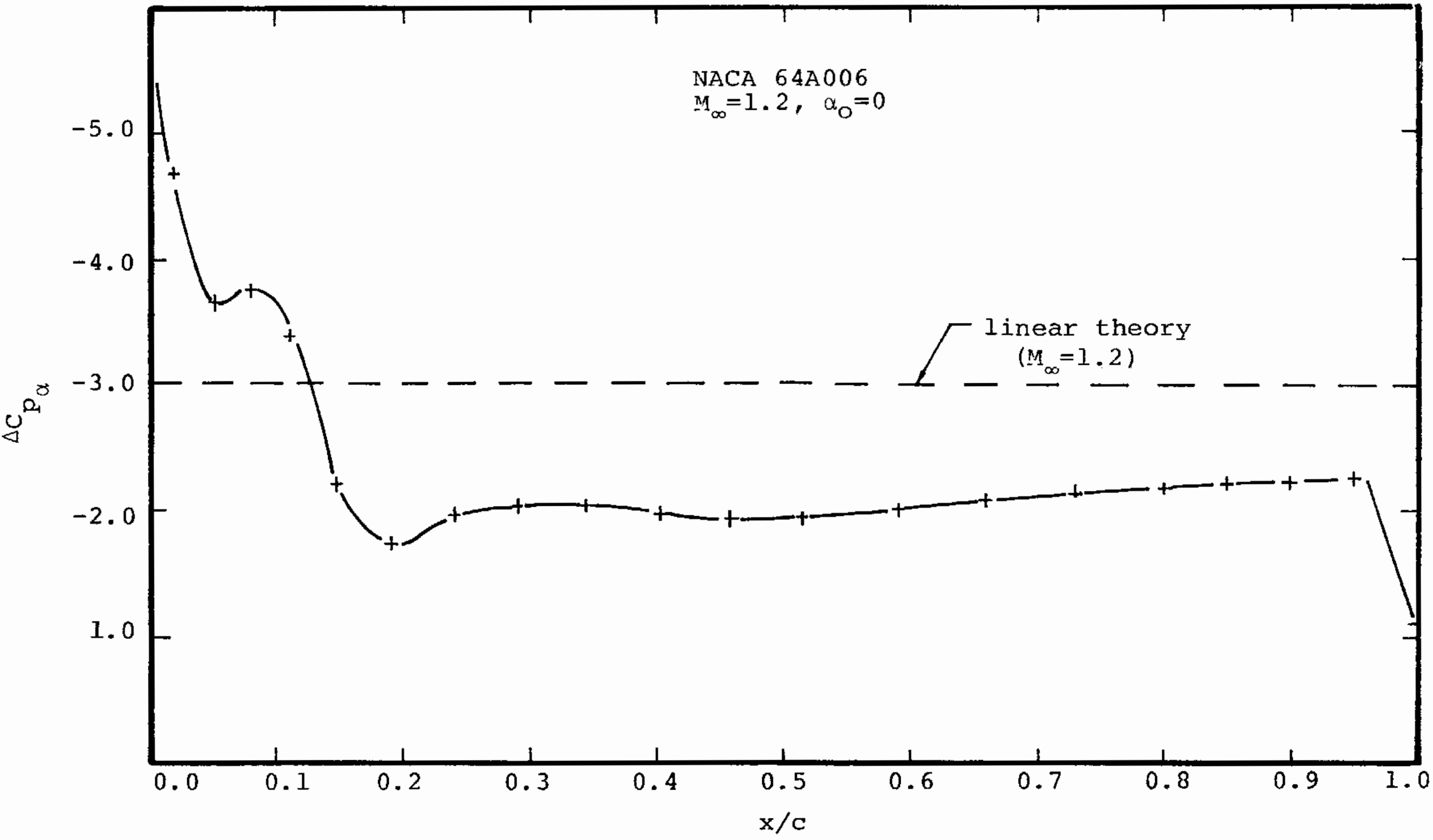

FIGURE 15. CHANGE IN PRESSURE COEFFICIENT DUE TO PITCH DEFLECTION

3.3. Wind Tunnel Wall Effects

Wind tunnel wall interference effects are extremely important for steady transonic flows and because of possible resonance effects are potentially even more important for unsteady flows. The inclusion of such effects in any theory such as the present one clearly enhances the utility of the theory for purposes of comparing with experimental data. Recent attempts have been made by Murman[26], Kacprzynski[27] and Collins and Krupp[28] to evaluate wind tunnel wall effects for steady transonic flows, and an initial attempt at including such effects in the present steady and unsteady theories is described in this section.

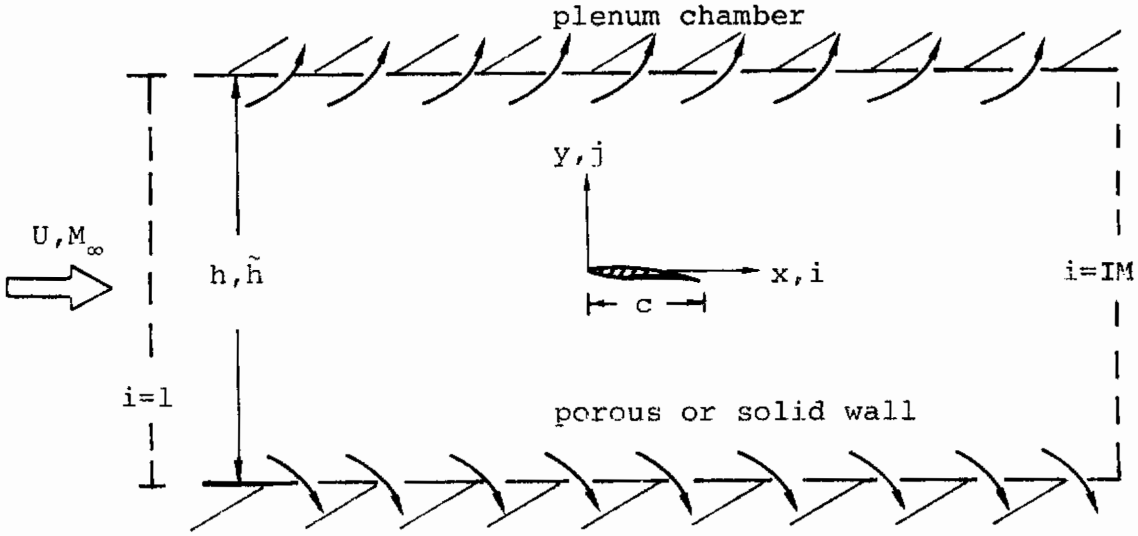

FIGURE 16. SCHEMATIC OF WIND TUNNEL CONFIGURATION

A general two-dimensional wind tunnel test configuration is sketched in Figure 16 above. It is assumed that the airfoil is on the tunnel centerline and that the solid or porous wind tunnel walls are separated by a distance h. The treatment of such a configuration by the present numerical method requires the inclusion of a proper wall boundary condition in the finite difference mesh at the scaled location of the walls and the development of a farfield solution for fixing a boundary condition on the upstream and downstream boundaries of the grid.

The treatment of upstream and downstream boundaries follows from the same general method as used for free air flows and is described in some detail in Appendix A. As summarized there, an asymptotic solution has been derived by the method of images for a general lifting airfoil in a steady subsonic flow for the solid wall case. This solution is believed to be accurate, and is also used for the case of small wall porosities. This solution is thus used to fix a Dirichlet boundary condition for ϕ^0 on the streamwise boundaries of the finite difference grid (i=1 and i=IM). No corresponding solution for the unsteady potential has been developed; however the steady solution (which applies for the unsteady perturbation potential for k=0) indicates that to leading order ϕ_x is exponentially small as $x \to \pm\infty$. Thus a zero gradient condition $\phi_x \equiv 0$ is imposed on i=1 and IM for all unsteady cases. This should be accurate for the low frequency unsteady flows considered and the adequacy of the approximation has been verified for the quasi-steady case. Supersonic wind tunnel flows can also be treated by the method and in this case the zero gradient upstream and downstream condition is imposed for both steady and unsteady solutions.

Of more immediate importance to the numerical simulation of wall interference effects is the treatment of the wall boundary condition for general porous or slotted walls. The solid wall case can be considered as a trivial special case ($\phi_y = 0$ on $y = \pm \tilde{h}/2$). Analytical modeling of ventilated wind tunnels is a subject as rich in problems and non-linear effects as the transonic flow problem itself. Kacprzynski[27] has in fact pointed out that the characteristics of porous or slotted walls can be highly dependent on flow Mach number and Reynolds number in addition to wall construction. Since the primary purpose of the present work is to demonstrate the capability of the method to treat wall effects it was decided to restrict the initial effort to the simplest possible model. As a result, the wall boundary condition is treated as the first order (linear) relation between the perturbation velocity normal to the wall and the local pressure coefficient, assuming the plenum pressure is equal to the freestream static pressure. The following equations hold for the steady and unsteady perturbations respectively:

$$\phi_y^0 = \mp \tilde{P} \phi_x^0 \quad , \quad \text{on } y = \pm \frac{\tilde{h}}{2} \tag{42}$$

$$\phi_y = \mp \tilde{P} e^{i\beta_*} \left(\phi_x + \underline{ik\phi} \right) \quad , \quad \text{on } y = \pm \frac{\tilde{h}}{2} \tag{43}$$

where the scaled tunnel height is:

$$\tilde{h} = \left[(1+\delta)\ \delta M_\infty^2 \right]^{1/3} \frac{h}{c} \tag{44}$$

and where $\tilde{P}$ is the wall porosity factor ($\tilde{P} = 0$ for solid wall) and β_* is introduced to permit a phase lag between the flow pressure and normal velocity in the unsteady case. The boundary conditions are introduced into the finite difference procedure using one sided difference forms for ϕ_{yy} on the upper and lower wall boundaries in the same manner as the body boundary condition and as described for the supersonic farfield condition above.

It is not immediately obvious how $\tilde{P}$ is to be estimated. Kacprzynski[27] points out that it could be a non-linear function of pressure (or ϕ_x) and that $\tilde{P}$ could be different for flow into or out of the plenum. In any event, one rational estimate for $\tilde{P}$ can be derived by assuming that the boundary condition is the weighted average of a free jet and a solid wall where the weighting factors are the open area ratio, S, or 1-S respectively. In scaled parameters:

$$u = \frac{\delta^{2/3}\, U}{[(1+\gamma)\delta M_\infty^2]^{1/3}}\, \phi_x = 0 \qquad \text{(free jet)} \qquad (45)$$

and

$$v = \delta\, U\, \phi_y = 0 \qquad \text{(solid wall)} \qquad (46)$$

where u and v are the streamwise and transverse perturbation velocity components. Taking the weighted average gives:

$$\phi_y = \underbrace{\frac{S}{(1-S)}\;\frac{1}{[(1+\gamma)\,\delta M_\infty^2]^{1/3}}}_{\tilde{P}}\, \phi_x \qquad (47)$$

To demonstrate the method, steady and quasi-steady (k=0) results are presented in Figures 17 and 18 respectively for the NACA 64A006 airfoil at $M_\infty = .85$. The tunnel parameters are taken to match the NLR Pilot tunnel[19] since the data presented in Sections 5.0 and 6.0 below were measured there. This tunnel has slotted wall with a 10% open area ratio so that for the test configurations at $M_\infty = .85$, $\tilde{h} = 1.44$ and $\tilde{P} = .24$ based on equations (44) and (47) respectively. The steady results for airfoil pressure distribution (Figure 17) show the main effect of the solid or porous walls to be an acceleration of the flow over the airfoil in comparison to the free air solution also shown. This results in an aft movement of and a corresponding strengthening of the shock. It is noted that the porous wall solution is not very different than the solid wall solution indicating that, for this case at least, the porosity is not sufficient to model free air conditions. Figure 18 presents the jump in pressure coefficient per unit flap angle for a quasi-steady (k=0) flap deflection calculated as linearized perturbations to the steady solutions just described. The results for the solid and porous wall are compared to the corresponding free air solution and test results from Reference 19. The results show that effect of the walls is to strengthen the perturbation through the shock and to significantly decrease the pressure perturbation on the non-deflecting forward portion of the airfoil. The comparison of the theoretical results show that the wall significantly decreases the upstream influence from the flap to the forward portion of the airfoil. Although the wall solutions do not improve the comparison with the data they do indicate that appreciable wall effects are acting for this test configuration. Additional unsteady results with wall effect are presented in Section 6.0.

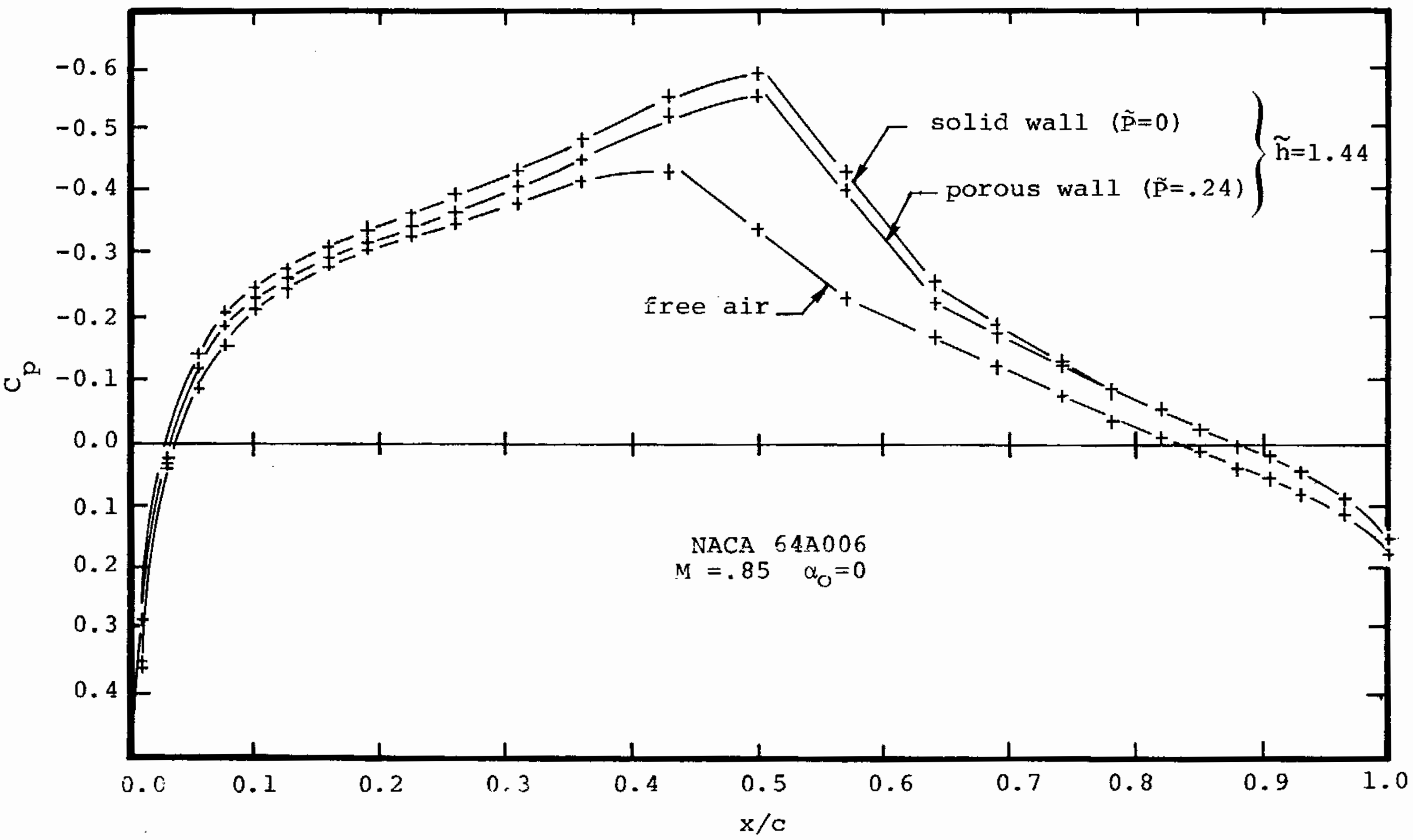

FIGURE 17. STEADY PRESSURE COEFFICIENTS

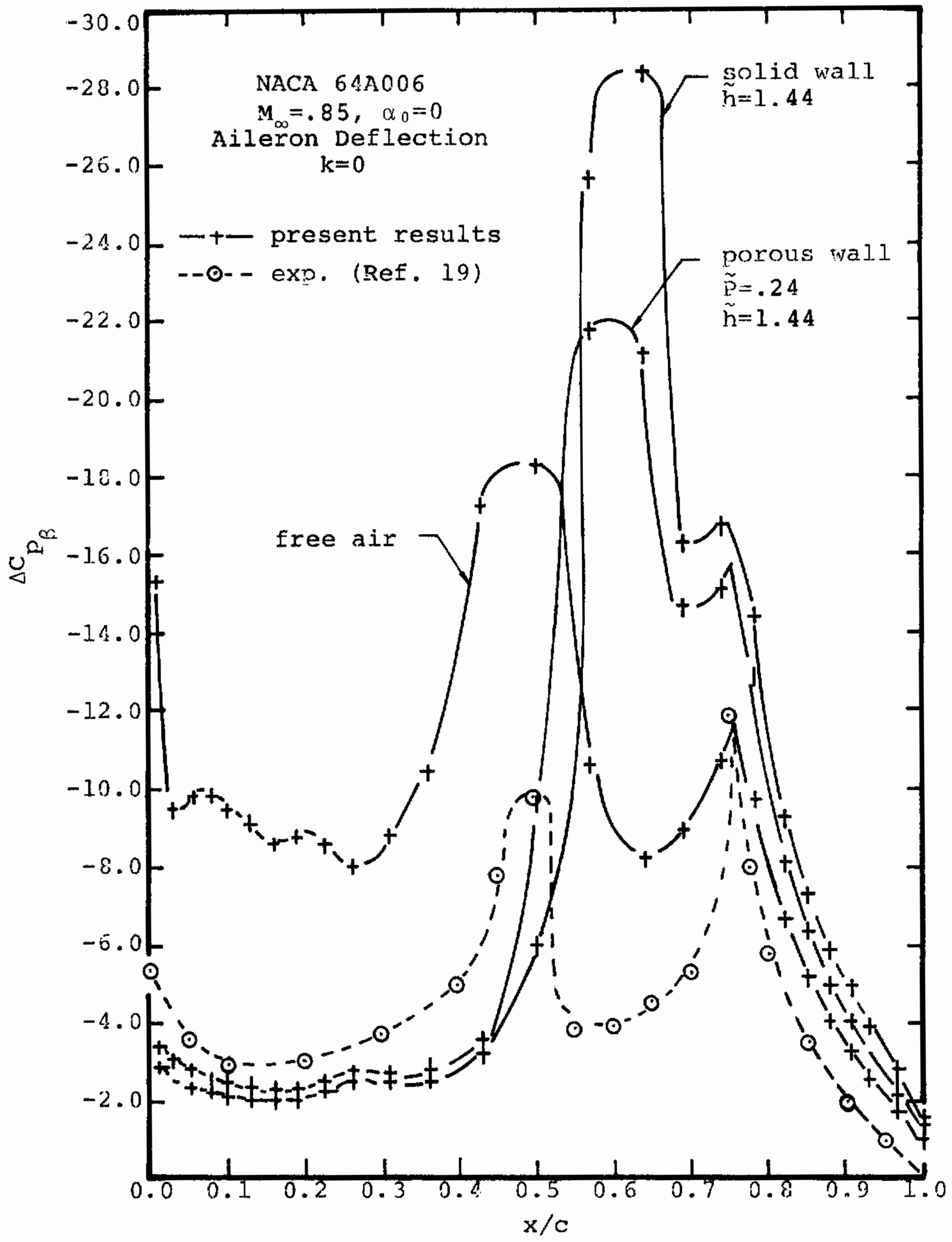

Figure 18. Effect of Wind Tunnel Walls on Airfoil Perturbation Pressures

3.4 Three Dimensional Planar Wing Calculations

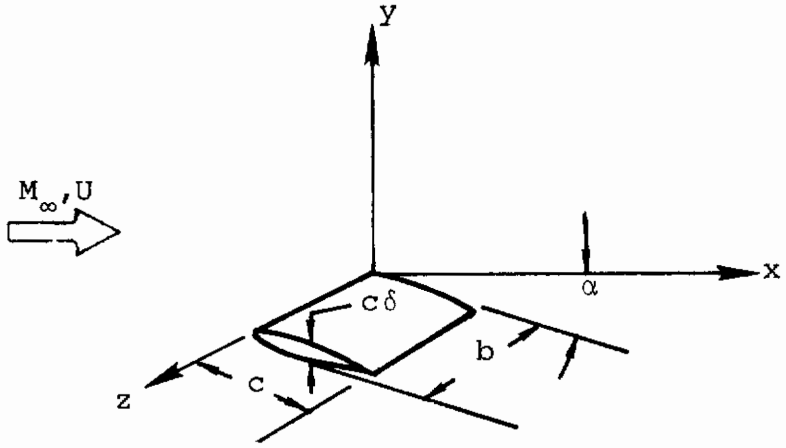

FIGURE 19. SCHEMATIC OF THREE-DIMENSIONAL PLANAR WING

The application of the theory and solution method to two-dimensional airfoil sections presented in previous work and in this report are interesting and illustrative but for practical application to dynamics or flutter problems three-dimensional effects must be considered. As with most other effects, 3-D effects are more important at transonic speeds than in the other speed ranges. The efficiency of the present scheme is such that realistic three-dimensional computations are practical on modern computers and it is the purpose of this section to describe the required generalizations and to demonstrate the method for a simple planform.

The wing parameters and coordinate definition are defined schematically in Figure 19 above. The initial development of the method is restricted to rectangular planforms undergoing oscillations symmetric with respect to the wing root ($z = 0$). The small disturbance analysis and the unsteady perturbation theory valid for three-dimensional flows were described in Section 2. As indicated there, the generalization to three dimensions requires but the addition of the ϕ_{zz} term to the governing equations for the steady and unsteady perturbation potentials. Asymptotic solutions to the governing equations have been derived for lifting wings in subsonic free-stream flow by Klunker[29], for the steady flow, and by the present authors for the unsteady perturbation. These solutions are summarized in Appendix A and used in the numerical solution method to fix farfield boundary conditions. Three dimensional solutions for steady transonic flow have been presented by

Bailey and Steger[30] and Newman and Klunker[31]; the latter work being most closely related to the method for steady flows used in this work. Extensions of the solution method for the unsteady perturbation parallel the steady method and are now described.

3.4.1 Numerical Solution Method

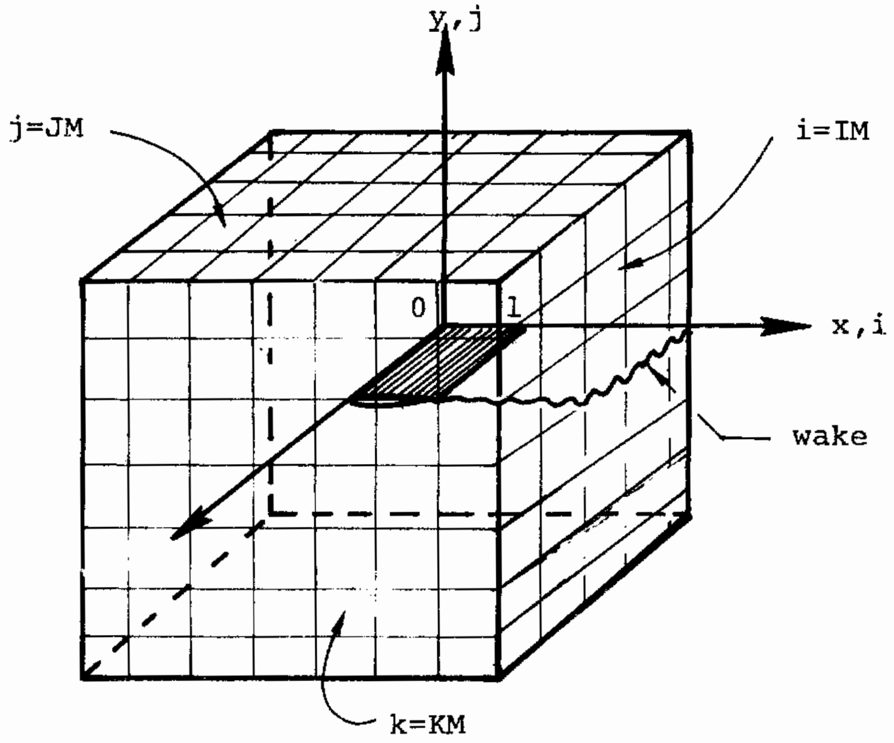

FIGURE 20. SCHEMATIC OF NUMERICAL SOLUTION DOMAIN

The three-dimensional numerical scheme constitutes the most straightforward extension of the two-dimensional method previously described in detail in Reference 1. As shown schematically in Figure 20, a cubic rectangular mesh of finite extent with uneven grid line spacing is overlayed on the 3-D solution space. The grid is concentrated near the airfoil and expanded out to the far boundaries of the grid. The finite difference equations are identical to the corresponding two-dimensional versions[1] with the addition of a centered difference form for ϕ_{zz} given by:

$$\phi_{zz_{i,j,k}} = \frac{2}{(\Delta z_k+\Delta z_{k-1})}\left\{\frac{1}{\Delta z_k}\left(\phi_{i,j,k+1}-\phi_{i,j,k}\right) - \frac{1}{\Delta z_{k-1}}\left(\phi_{i,j,k}-\phi_{i,j,k-1}\right)\right\} \tag{48}$$

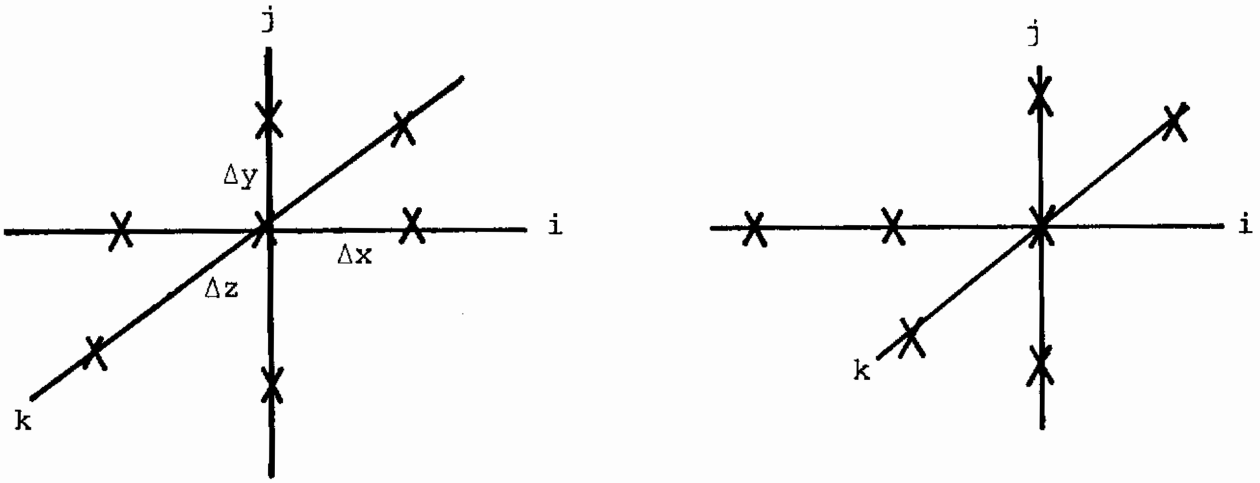

$(K-\phi^0_x)_{i,j,k} > 0$ $(K-\phi^0_x)_{i,j,k} < 0$

FIGURE 21. SCHEMATIC OF DIFFERENCE SCHEME

The computational star for the three dimensional scheme is shown schematically in Figure 21 above. The tests for the elliptic on hyperbolic nature of the equation are made on the centered difference form of $(K-\phi^0_x)_{i,j,k}$, and depending on the value of this coefficient the x derivatives of ϕ are centered or backward differenced as in the 2-D case. A parabolic point operator is used in both the steady and unsteady schemes and a shock point operator, as described for the 2-D case in Section 3.2, is used in the finite difference scheme for the steady potential.

As before, the finite difference equations are set up for each column (x,z = constants) in turn, taking account of the airfoil, wake and farfield boundary conditions. In the steady solution this results in a set of quadratic equations for the column of ϕ's which are solved by linearizing and iterating. The linearization is accomplished by using the previous iterate for the coefficient $V = K - \phi_x^0$. The resulting linear system is tri-diagonal and is solved by optimum Gaussian ellimination. The column iteration process is terminated when the difference between successive iterates is less than an arbitrary small amount (usually 10^{-5}). As in the 2-D case, convergence is usually achieved in three or four iterations. In the unsteady solution it is recalled that the equation is linear so that no column iteration is required.

After each column is solved, it is relaxed using a variable relaxation factor which depends on the local nature of the equation; $\omega \sim 1.7$ for elliptic points and $\omega \sim .7$ for hyperbolic points. The column solution process is performed for each column in turn sweeping the grid from left to right in x and from the wing root ($k = 1$) to the farfield ($k = KM$) in z. The entire grid is swept repeatedly in this manner until the change in ϕ for all grid points during one grid sweep is less than some arbitrary small amount.

The numerical treatment of airfoil and wake boundary conditions in both steady and unsteady cases is the same as the 2-D case with the exception that the airfoil shape function is now a function of z as well as x and the airfoil circulation is a function of z along the airfoil. In the subsonic freestream case considered to date, asymptotic solutions for the steady and unsteady systems described in Appendix A are used to fix a Dirichlet boundary condition on five sides of the grid. On the grid boundary containing the wing root, a symmetry boundary condition is used whereby $\phi_z \equiv 0$ on $z = 0$. The farfield solution depends on the spanwise distribution of circulation and as the solution for circulation is refined the farfield is updated periodically during the solution process.

The solution process summarized above has worked well in the few cases calculated to date. Convergence, for instance, seems to be comparable to the two-dimensional method as will be discussed in the description of the steady and unsteady demonstration calculations presented in the next section.

3.4.2 Results for Low Aspect Ratio Rectangular Planform

To demonstrate the three-dimensional applications of the method, results are presented in this section for a rectangular planform wing with a constant six percent thick circular arc section and with aspect ratio $2b/c=8$. A grid of approximately 12000 points was used with IM=30 over $-3.2 \leq x \leq 3.4$, JM=19 over $-5.4 \leq y \leq 5.4$ and KM=19 over $0 \leq z \leq 6.8$. In the x direction 16 grid lines were distributed along the airfoil with $\Delta x \simeq .06$, and in the z direction 10 grid lines were distributed over the span with $\Delta z \simeq .2$. The grid design was chosen so that the unsteady version of the program, which requires three times the grid point storage of the steady program (ϕ^0, Re ϕ and Im ϕ), would fit on small core of the CDC 7600 (∿64K storage).

Results for the steady airfoil pressure distribution at various spanwise stations are presented in Figure 22 below for the airfoil described above at a supercritical Mach number of $M_\infty=.86$ and zero angle of attack. The corresponding two-dimensional results for the same airfoil, Mach number and (x,y) grid design, are shown for comparison. It is noted that the pressure distributions for the inboard 50 percent of the semi-span are only slightly lower than the two-dimensional solution indicating very little spanwise relaxation of the flow in this region. The pressure does not begin to change significantly until the final 25 percent of the semi-span near the tip. The 75 percent station, for example, shows some weakening and forward translation of the shock but the flow does not become entirely subcritical until very near the tip station. All in all, the solution shows a lesser degree of three dimensionality than might be expected for this case.

Results for the linearized unsteady perturbations about the steady solution just described are presented in Figure 23 and 24 for a uniform pitch oscillation at k=0 and k=.1, respectively. In each case the corresponding two-dimensional solution is also shown. These results for the jump in pressure across the airfoil per unit pitch angle show the expected greater degree of three dimensional effects than the steady solution. Of particular note is the fact that the root station in each case is considerably different in magnitude than the 2-D solution. This is especially true of the quasi-steady result (Figure 23). It seems that the main effect of the three dimensionality is in depressing the peak suction through the shock, although it also has a considerable effect on the phase of the pressure distribution as indicated in the relatively large changes in $\mathrm{Im}(\Delta C_{p_\alpha})$ on the aft portion of the airfoil in the k=.1 case (Figure 24). It should be noted that the results show some residual loading on the airfoil at the tip station due to discretization which presumably could be reduced by using a finer mesh near the tip. Finally, Figure 25 gives the span-wise loading distributions for each of the 3-D cases with comparison to the corresponding two-dimensional result. A comparison of the $\mathrm{Re}(C_{\ell_\alpha})$ in each case indicates the important result that the reduced frequency effect in this low frequency regime is considerably less in the 3-D case than in the 2-D case. Such a result could have important consequences for a flutter or dynamic stability analysis for which the variation of unsteady force coefficients with reduced frequency can have a significant effect on the results.

Some comment with respect to computer run times for the cases presented here is clearly of interest. The steady computation was taken to a convergence of $\Delta\phi^0{}_{max} \sim 5.0*10^{-5}$ which required 157 full grid iterations and was performed in a total of 65 seconds on a CDC 7600. The quasi-steady perturbation required 286 grid iterations and 185 seconds of CDC 7600 time to reach a convergence of $\Delta\phi_{max}=10^{-5}$. Such a fine degree of convergence is not required for acceptable accuracy and it is noted that the same case reached $\Delta\phi_{max}=10^{-4}$ in 150 iterations and 82 seconds of 7600 time. Convergence and computer run time for the fully unsteady k=.1 case were similar to (but less than) the k=0 case.

Although somewhat greater definition (more grid points) is called for than was used in these demonstration calculations, the computer time requirements mentioned here indicate that the method is efficient enough to permit flutter aerodynamic calculations for three-dimensional planar wings. The three dimensional versions of the programs which implement the method discussed above for the steady and unsteady perturbation potentials are described in some detail in a companion users manual to this report. The method as presently programmed applies to rectangular planform wings in subsonic freestream flow but the programs could be easily generalized to treat supersonic or wind tunnel flows. The generalization to tapered and swept wings is the next major generalization which could be effected to significantly enhance the usefulness of the method.

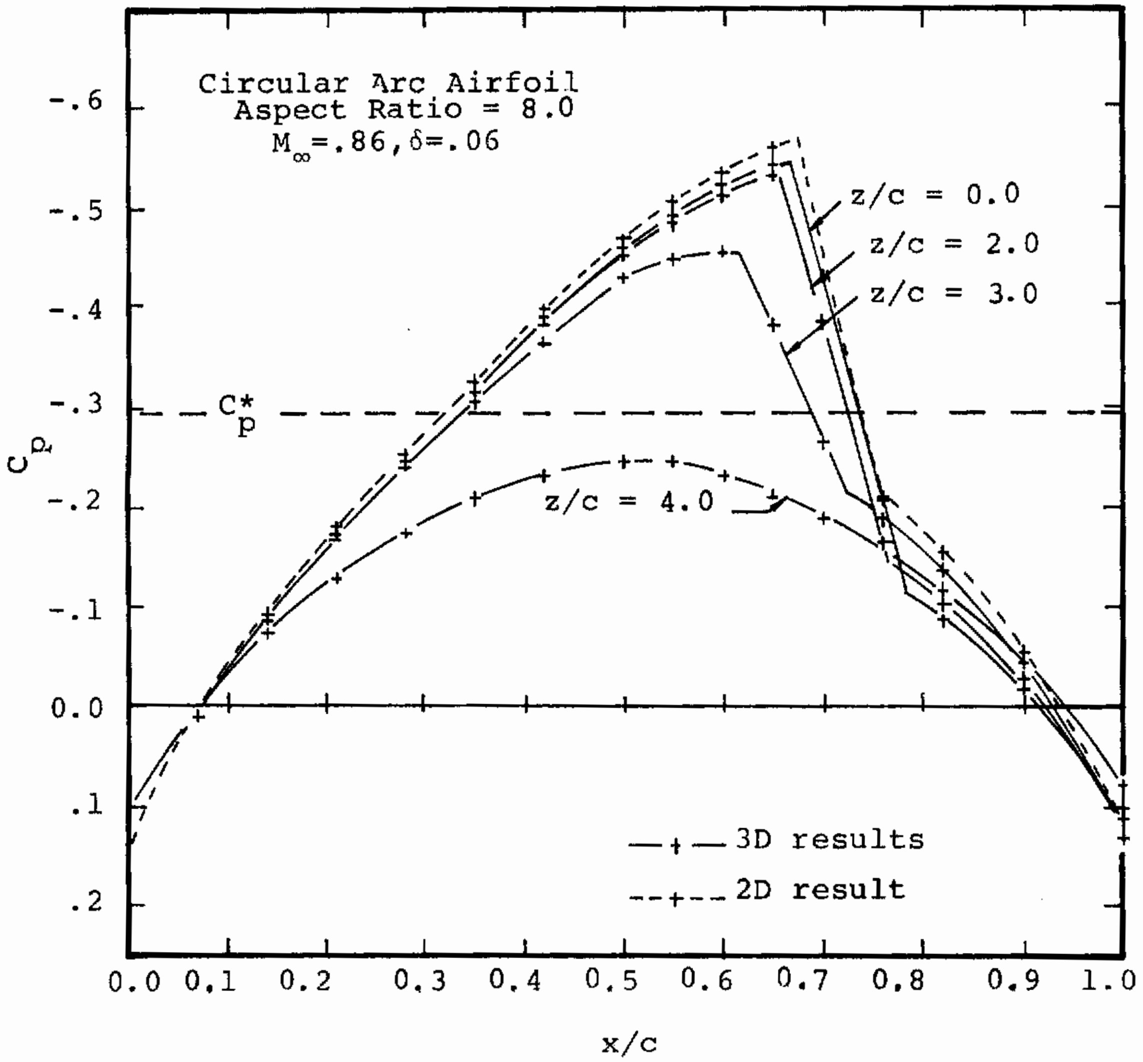

Figure 22. Steady Airfoil Pressure Coefficients

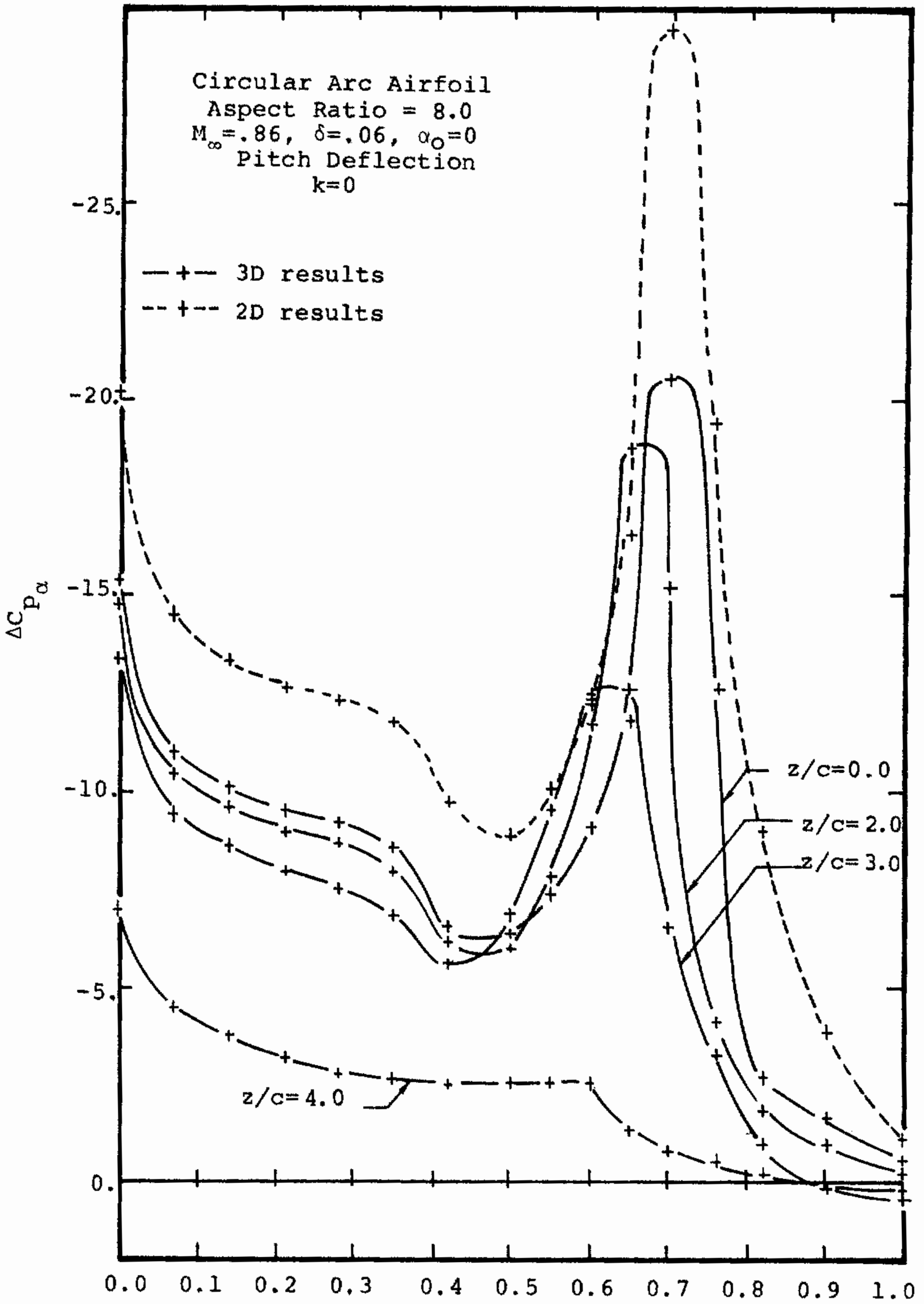

FIGURE 23. JUMP IN AIRFOIL PRESSURE COEFFICIENT DUE TO QUASI-STEADY DEFLECTION IN PITCH

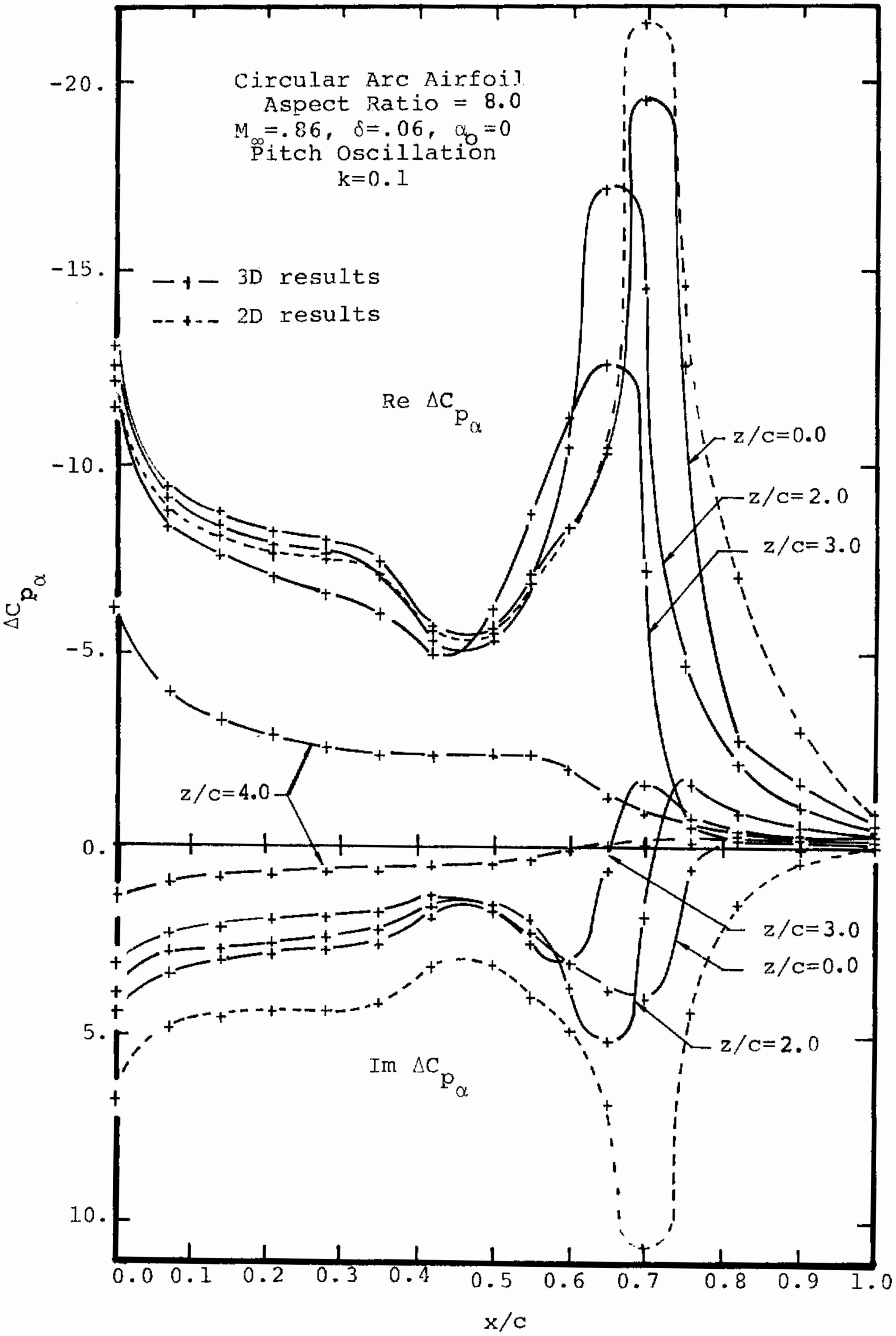

FIGURE 24. JUMP IN UNSTEADY AIRFOIL PRESSURE COEFFICIENT DUE TO OSCILLATION IN PITCH

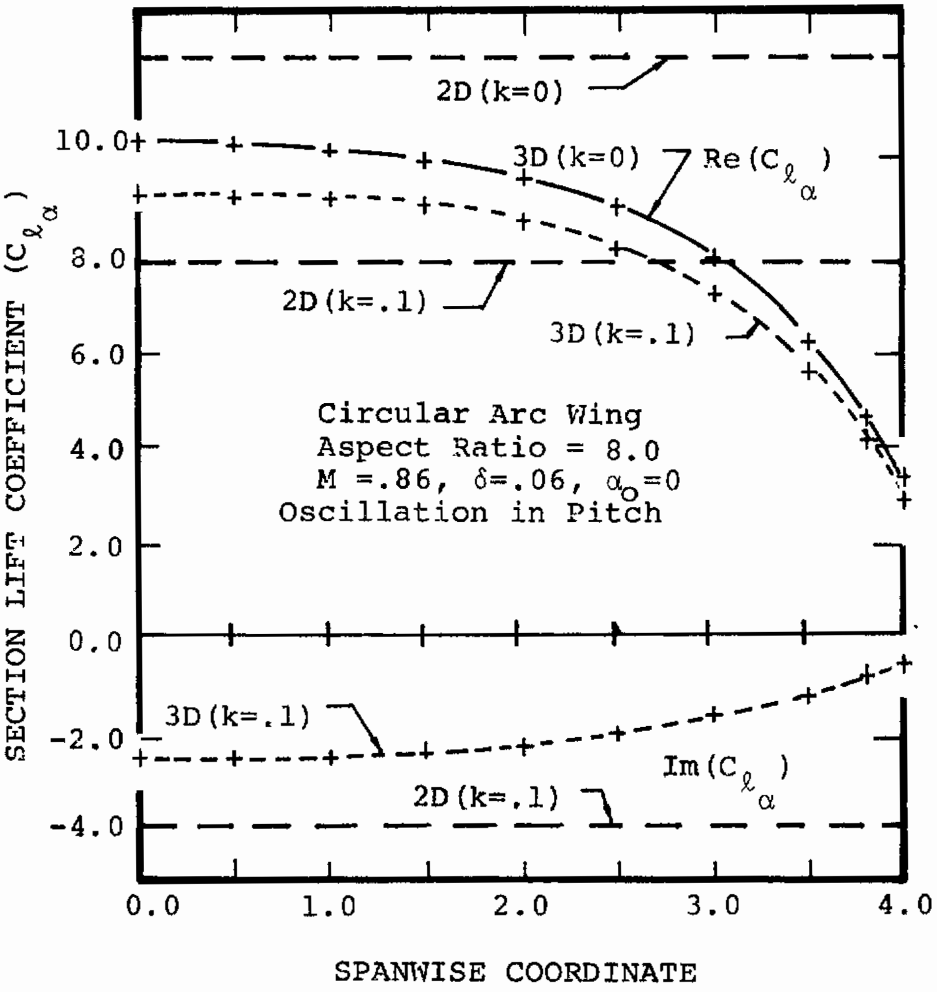

FIGURE 25. SPANWISE LOADING DISTRIBUTIONS

4.0 NUMERICAL ACCURACY, CONVERGENCE AND STABILITY CONSIDERATIONS

Before proceeding with the large number of calculations presented for verification of the method (Section 5) and for the flutter aerodynamics (Section 6) the numerical accuracy and convergence of the method was investigated in hopes of defining a grid and degree of convergence which would strike a happy medium between accuracy and efficiency. Also, attempts were made to speed convergence through the optimization of relaxation parameters and the use of standard matrix solution acceleration schemes. These studies are summarized in Sections 4.1 and 4.2. Studies of the stability of the numerical scheme have been performed throughout the research and especially upon discovering that an instability may develop for a combination of freestream Mach numbers near sonic and high reduced frequencies. Some salient results are summarized in Section 4.3.

4.1 Numerical Accuracy Considerations

In any finite difference solution technique, numerical accuracy is often as important as the accuracy of the basic theory upon which the method is based. The ultimate test of numerical accuracy is, of course, comparison with exact solutions for the same governing equations. Such comparisons have been made for the steady solution method[15,16] and these have demonstrated the accuracy of the mixed differencing line relaxation scheme for steady flows. Similar comparisons have been made for the present unsteady method in Section 4 for the special cases of linearized subsonic and supersonic flow and have indicated that the solution method is basically accurate for these relatively simple flows. It is unfortunate that no exact solutions are available for unsteady flow at supercritical Mach numbers. In this case, however, certain numerical tests can be performed which provide a measure of numerical accuracy and some results of such tests are presented here.

The accuracy of the numerical schemes for both the steady and unsteady perturbation potentials used in this work depend on many variables. Two of the most important are the degree of convergence of the iterative relaxation procedure and grid design and definition. Their effect on the accuracy of the steady and unsteady solution methods are examined in Figure 26 through 29 and Figure 30 and 31 respectively.

Figure 26 shows a typical convergence history for a supercritical steady flow calculation. The parameters plotted versus the number of iterations are the maximum change in ϕ^0 throughout the grid, ($\Delta\phi_{max}$) the change in airfoil circulation ($\Delta\gamma_{te}$) and the change in the non-uniform flow doublet distribution ($\Delta\mathcal{D}$) per iteration, where:

$$\mathcal{D} = \iint_{grid} (\phi_x^0)^2 \, d\xi d\eta \qquad (49)$$

These parameters provide a good measure of the degree to which the solution has converged. For example based on these curves the asymptotic convergence rate for each parameter can be defined and used to estimate the error, for example ($\phi_N^0-\phi_\infty^0$), which can be expected if the iteration procedure is terminated after N iterations. This has been done in this case assuming the iteration procedure was terminated when $\Delta\phi_{max}^0=10^{-4}$ (N=150) and the results are to a conservative estimate:

$$|\phi_{150}^0 - \phi_\infty^0| \leq 1.1*10^{-3}$$

$$|\gamma_{150} - \gamma_\infty| \leq .9*10^{-3}$$

$$|\mathcal{D}_{150} - \mathcal{D}_\infty| \leq 2.0*10^{-4}$$

Thus based on this result it is estimated that ϕ^0 throughout the grid has approached its limiting value to within 0.11%; likewise the airfoil lift. This is clearly more than acceptable accuracy for the calculation of unsteady aerodynamic coefficients for example; the prime purpose of the present work.

Figure 27 presents another measure of accuracy for this same case. Presented there is the distribution over the airfoil of the change in pressure coefficient due to change in the degree of convergence from $\Delta\phi_{max}=10^{-4}$ to $\Delta\phi_{max}\simeq10^{-5}$. All values shown in the figure are less than 1% of the corresponding values of pressure coefficient. This in fact is a more vigorous test of accuracy than considering the values of ϕ^0 since $C_p \sim \phi_x^0 \sim \Delta\phi/\Delta x$. Thus even though the error in $\phi^0 (\Delta\phi)$ is less than .1% the error in C_p could be larger due to the small grid size on the airfoil. This figure shows the interesting fact that the approximate error in C_p follows the same general distribution over the airfoil as the pressure distribution; with the error being greater, as might be expected, near the leading edge and at the shock.

It should be pointed out that the case considered is quite typical of all supercritical cases for which the convergence has been examined in this manner. The main result of such investigations is that a degree of convergence of $\Delta\phi_{max} \sim 10^{-4}$ should be more than sufficient to provide 1% accuracy for airfoil pressures and integrated forces.

The effect of grid size or definition on solution accuracy is indicated in Figures 28 and 29. Figure 28 presents results for the pressure distribution for a NACA64A006 airfoil at $M_\infty = .875$ using two different grid definitions: a coarse grid (25x25) with 12 grid lines on the airfoil and a more refined grid (50x50) with 26 grid lines on the airfoil. Each grid was taken to the same degree of convergence ($\Delta\phi_{max} = 10^{-4}$) and the results show a relatively large difference. The comparison with the experimental data (Tijdeman et al[19], see Section 5) is quite good, however, for the refined grid so that no further grid refinement was used in this case. The effect of an even more refined grid is shown in Figure 29 for a circular arc airfoil. As indicated there, the effect of such a highly refined grid is mainly to sharpen up the shock. The effect on the pressure distribution away from the shock is negligible. It is believed that the same sharpening of the shock could be attained by concentrating grid lines near the expected shock position rather than refining the entire grid. However, in the present work a grid which provided acceptable accuracy over a wide range of Mach numbers was required for efficiency so that such a strategy for sharpening the shock could not be used in general. Based on comparisons, such as these, it is believed that a grid with approximately 50 points in each of the x and y directions will provide acceptable accuracy.

The corresponding effect of degree of convergence on the unsteady scheme is shown in Figures 30 and 31. The case considered is the NACA64A410 airfoil at $M_\infty = .72$ with a quasi-steady pitch deflection. The convergence histories for $\Delta\phi_{max}$ and $\Delta\gamma$ in Figure 30 are of a somewhat different nature than the corresponding steady results as they show a relatively constant rate of convergence most likely due to the linearity of the governing equations. Based on the asymptotic convergence history, conservative estimates for the error in ϕ and γ if the iteration process is terminated at $\Delta\phi_{max} = 10^{-4}$ are:

$$|\phi_{360} - \phi_\infty| \leq 5.*10^{-4}$$

$$|\gamma_{360} - \gamma| \leq 10^{-3}$$

Again the error would seem to be acceptable for a degree of convergence of $\Delta\phi_{max}=10^{-4}$. The corresponding changes in perturbation pressures on the airfoil due to a change in convergence from $\Delta\phi_{max}=10^{-4}$ to $\Delta\phi_{max}=10^{-5}$ are shown in Figure 31. The distribution is shown to be somewhat erratic but in each case the change is no more than 2% of the local value of C_p with the least converged pressures being at the leading edge and in the region of the shock. The effects of grid definition on the unsteady perturbations are very similar to those shown for the steady solution. That is, the major effect of a finer grid than 50 x 50 is increased definition of perturbation pressures through the shock.

In summary, studies of numerical accuracy as briefly examined here, indicate that a 50 x 50 grid taken to a convergence level of $\Delta\phi_{max}\simeq10^{-4}$ provides approximately 1% accuracy in both steady and unsteady results for pressures on the airfoil and a corresponding level of numerical accuracy for integrated forces.

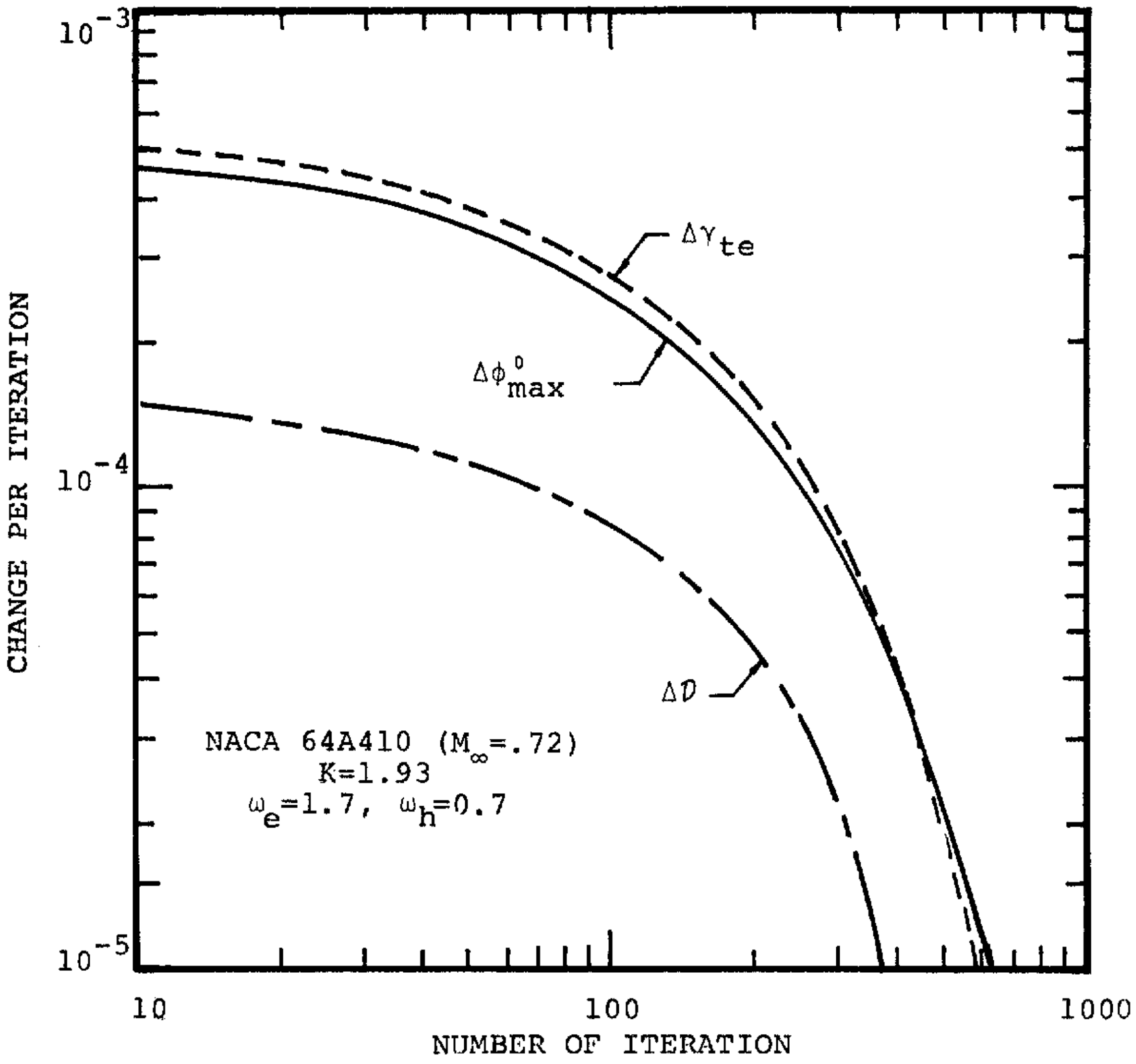

Figure 26. Typical Convergence History

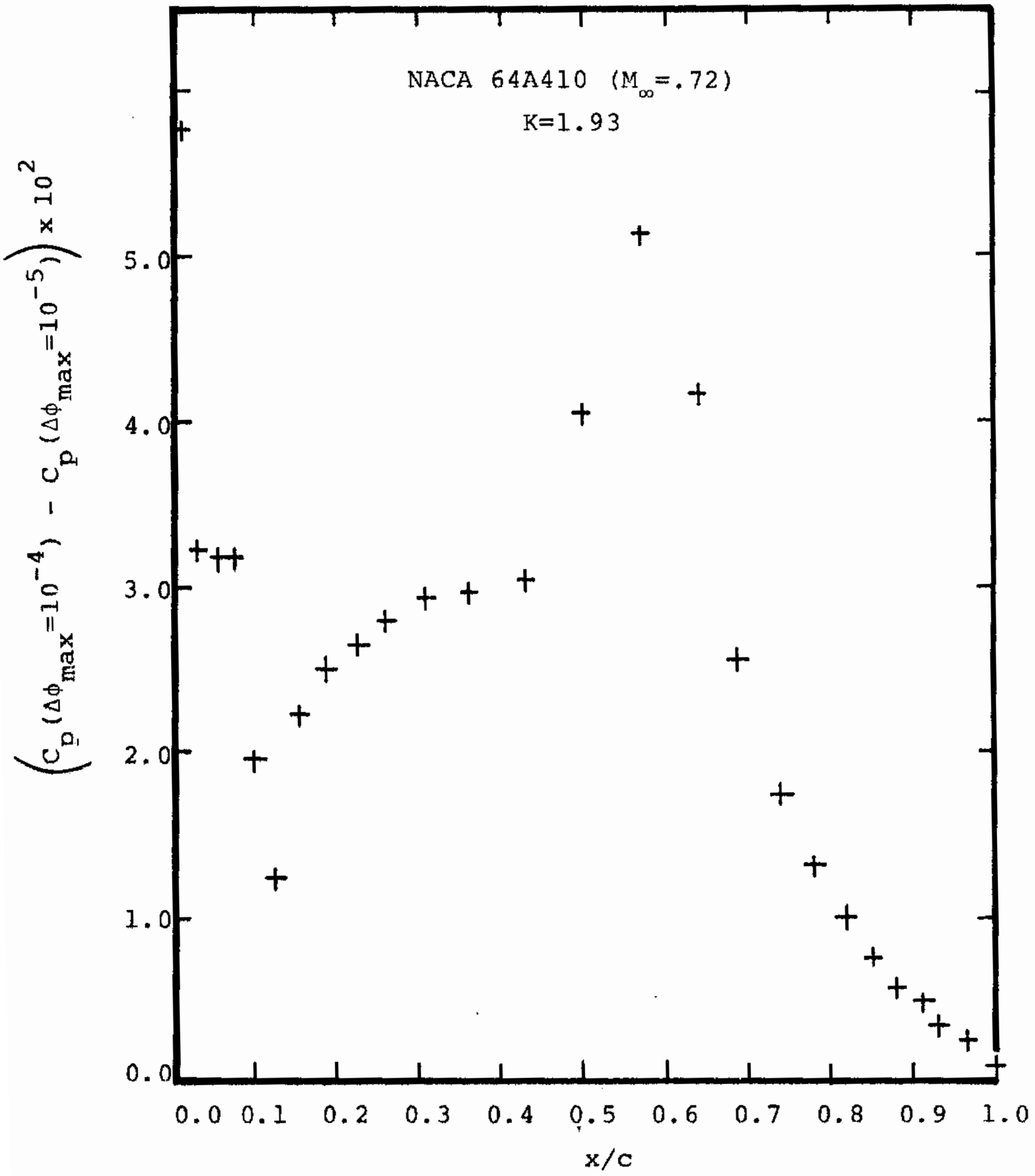

FIGURE 27. INFLUENCE OF DEGREE OF CONVERGENCE ON STEADY AIRFOIL PRESSURES

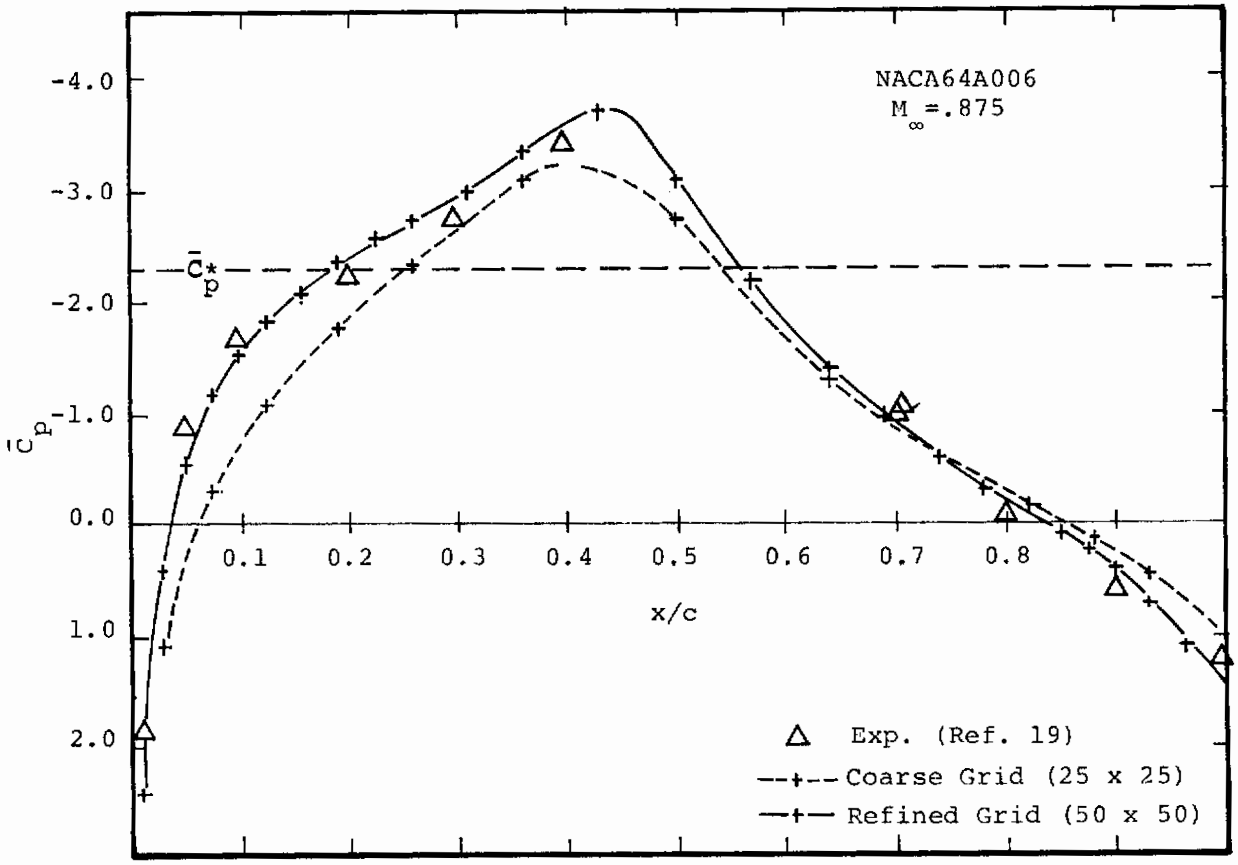

FIGURE 28. EFFECT OF GRID DEFINITION ON STEADY AIRFOIL PRESSURE

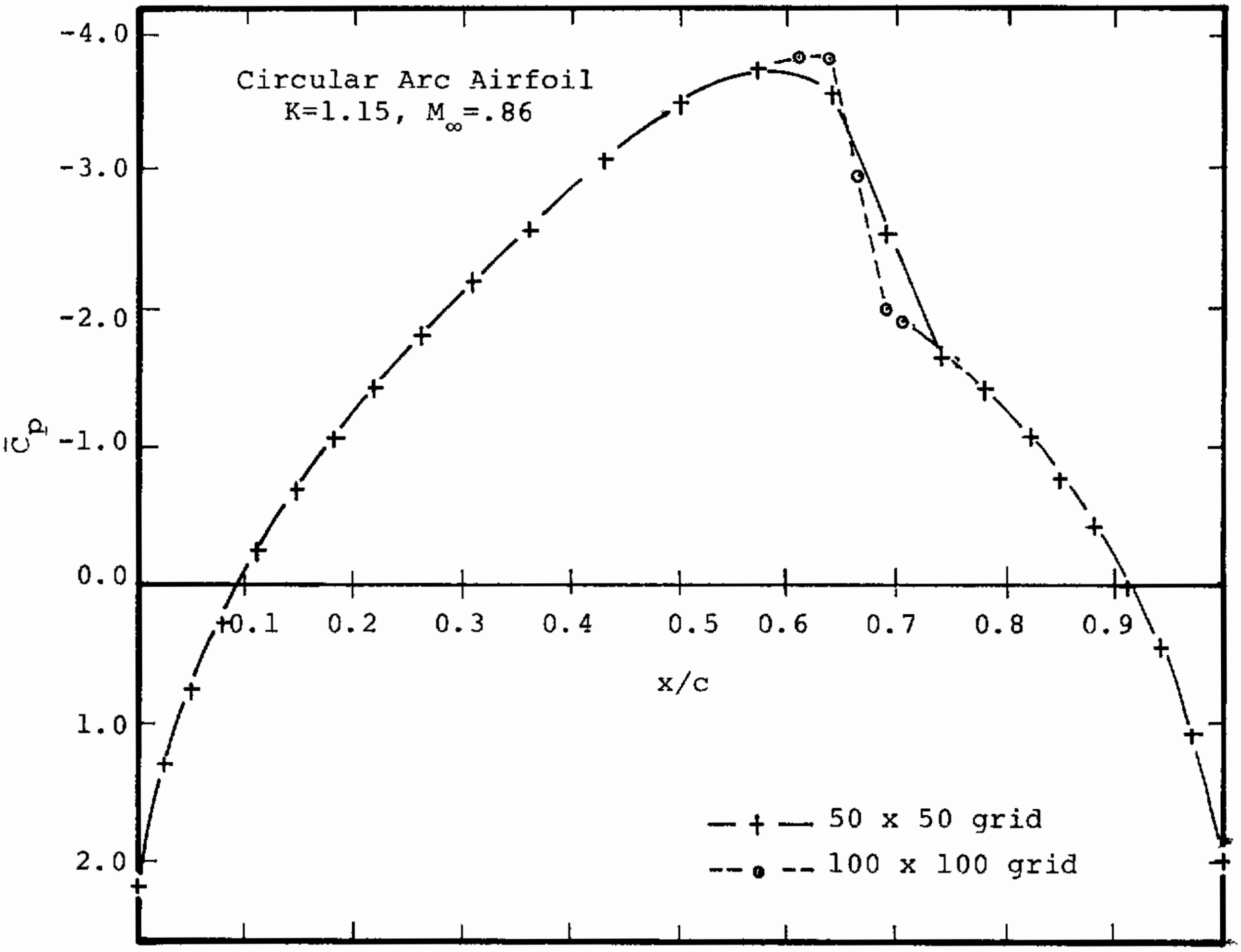

FIGURE 29. EFFECT OF GRID DEFINITION ON STEADY AIRFOIL PRESSURES

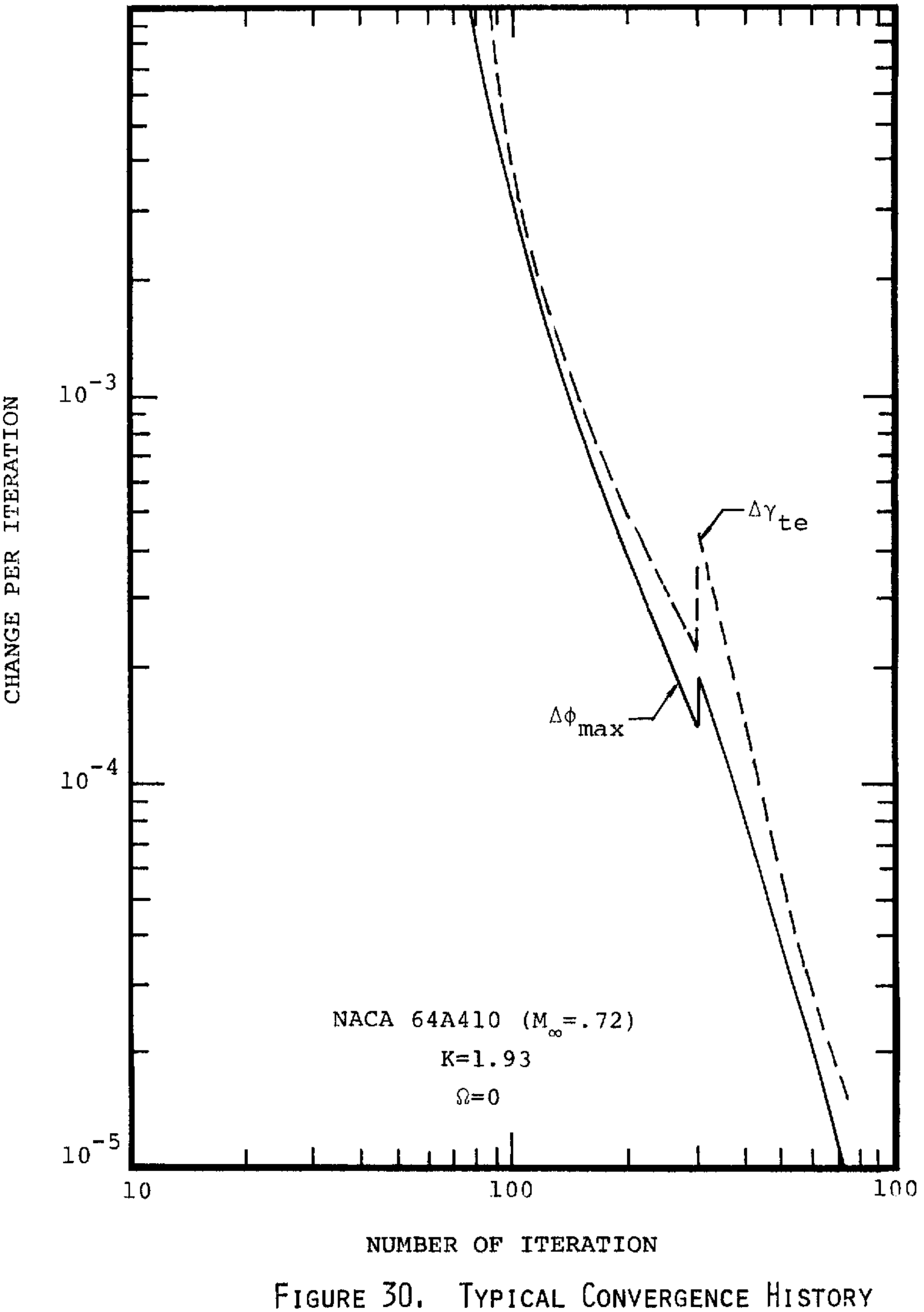

FIGURE 30. TYPICAL CONVERGENCE HISTORY

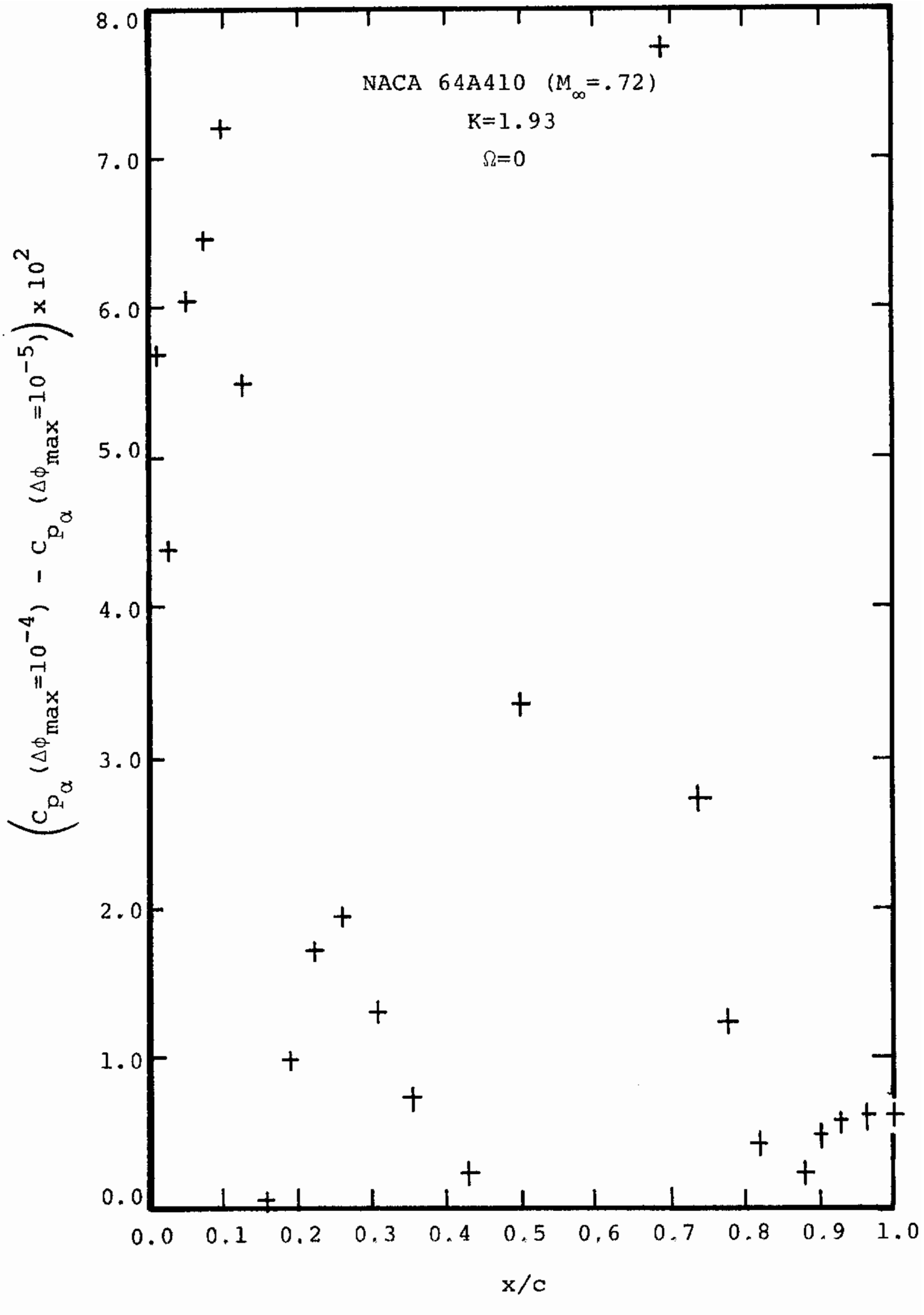

FIGURE 31. INFLUENCE OF DEGREE OF CONVERGENCE ON UNSTEADY AIRFOIL PRESSURES

4.2 Convergence of the Numerical Scheme

Convergence of the steady and unsteady solution schemes is influenced by the parameters which define the solution (similarity parameters K,Ω, airfoil shape function) and by the parameters which control the numerical solution procedure (grid design, and relaxation parameters). Based on the large number of solutions calculated for this report, using the basic 50 x 50 grid, the convergence histories presented above are typical for a wide range of supercritical Mach numbers and reduced frequencies. The relaxation parameters can have a somewhat greater effect on convergence and this effect is discussed here along with a discussion of possible convergence acceleration schemes.

As noted in previous work, a type dependent relaxation scheme is used in both the steady and unsteady solutions; that is, for locally subsonic points the solution is over-relaxed, $1 \leq \omega_e < 2$ and for locally supersonic points the solution is under-relaxed, $0 \leq \omega_h < 1$. The limits on the relaxation parameters are due to stability considerations and are common for elliptic or hyperbolic finite difference solution schemes. The values of the relaxation parameter within the above limits can affect the convergence rate and in general there exist optimum values which provide the fastest convergence. The effect of the elliptic relaxation factor, ω_e, on convergence for a typical supercritical steady case is shown in Figure 32. It shows that for a value of $\omega_e = 1.7$, $\Delta\phi_{max} = 10^{-4}$ convergence is reached in 58 iterations as compared to 78 for $\omega_e = 1.5$. Almost identical results as shown for $\omega_e = 1.7$ were obtained with $\omega_e = 1.8$ and for a value of $\omega_e = 1.9$ the convergence was somewhat faster but was oscillitory in nature. Such oscillations would indicate that $\omega_e \sim 1.7$ or 1.8 is optimum. The effect of the hyperbolic relaxation parameter in this case and for all subsonic cases considered was negligible for $\omega_h = .7$ to .9. A similar result holds for the unsteady solutions examined parametrically in this same fashion. Thus values of $\omega_e \sim 1.7$ to 1.8 and $\omega_h = .7$ to .9 seem to be close to optimum for a wide range of similarity parameters of interest. In other words, for any given case the convergence rate could probably be increased by modest amounts but the experimentation needed to determine optimum values would outweigh the increased efficiency achieved. The task of mapping out optimum values of ω_e and ω_h as functions of the similarity parameters K and Ω would be an undertaking which would not be justified due to the surprisingly small effect the parameters seem to have for values in the range given above. This is especially true since any benefits so achieved might possibly be negated by grid geometery or airfoil shape effects.

For supersonic freestream flows the importance of ω_e relative to ω_h switches. That is, ω_h becomes the more important relaxation factor. However, based on the supersonic calculations performed in this study the ranges of these parameters given above still provide close to optimum results. It should be mentioned that for fully supersonic flow the present scheme converges in one grid iteration, since in this case the scheme provides an implicit solution method for the wave equation in which x is the time like variable. This is true, however, only if $\omega_h \equiv 1$. For $\omega \neq 1$ in the fully supersonic case, the scheme may require many tens of iterations to converge.

The possibility of increasing the efficiency of the solution mehtod by using various matrix solution acceleration schemes has been investigated briefly in this study. As described in previous work,[1,20] one such method which has worked well is the so-called "grid halving" procedure in which the solution is initiated on a coarse grid, taken to a certain level of convergence, and successively refined.

Another method which was tried was the Aitken's δ^2 method[33]. This method in its most basic form assumes that a sequence of numbers $(\phi^{n-1}, \phi^n, \phi^{n+1})$ converges exponentially with respect to n and is used successfully to accelerate convergence of iterative schemes for system of equations. For use in the present scheme, on extrapolated value for the potential at any field point can be defined based on three successive iterates by:

$$\phi^{\infty} = \frac{\phi^{n+1}\phi^{n-1} - (\phi^n)^2}{\phi^{n+1} + \phi^{n-1} - 2\phi^n} \tag{50}$$

In the present work this has been applied in two ways: the first is to extrapolate all grid points and the second is to extrapolate a global quantity such as airfoil circulation.

The use of extrapolation on all grid points for the non-linear steady potential has given quite bad results in all cases tried. The non-linearity of the basic equations is a possible culprit but similarly unpleasant results were obtained when the method was applied to the linear unsteady perturbation potential. The use of extrapolation on the airfoil circulation has provided mixed results; that is it has worked well in some cases but poorly in others. However, even in the cases in which it worked, the overall convergence of the scheme was little if any better than the use of overrelaxation. A higher order extrapolation scheme after Shanks[34] which generalizes the Aitken method was also tried with similar bad results.

As a postscript, it should be mentioned that the singular lack of success with acceleration methods achieved during this study should not discourage further investigations along these lines because of the possible significant increases in computational efficiency which such schemes promise. In fact, Hafez and Cheng[25] have recently demonstrated that acceleration can be made to work even for the non-linear transonic potential equation. Their method, however, was not available in time to incorporate into the present work.

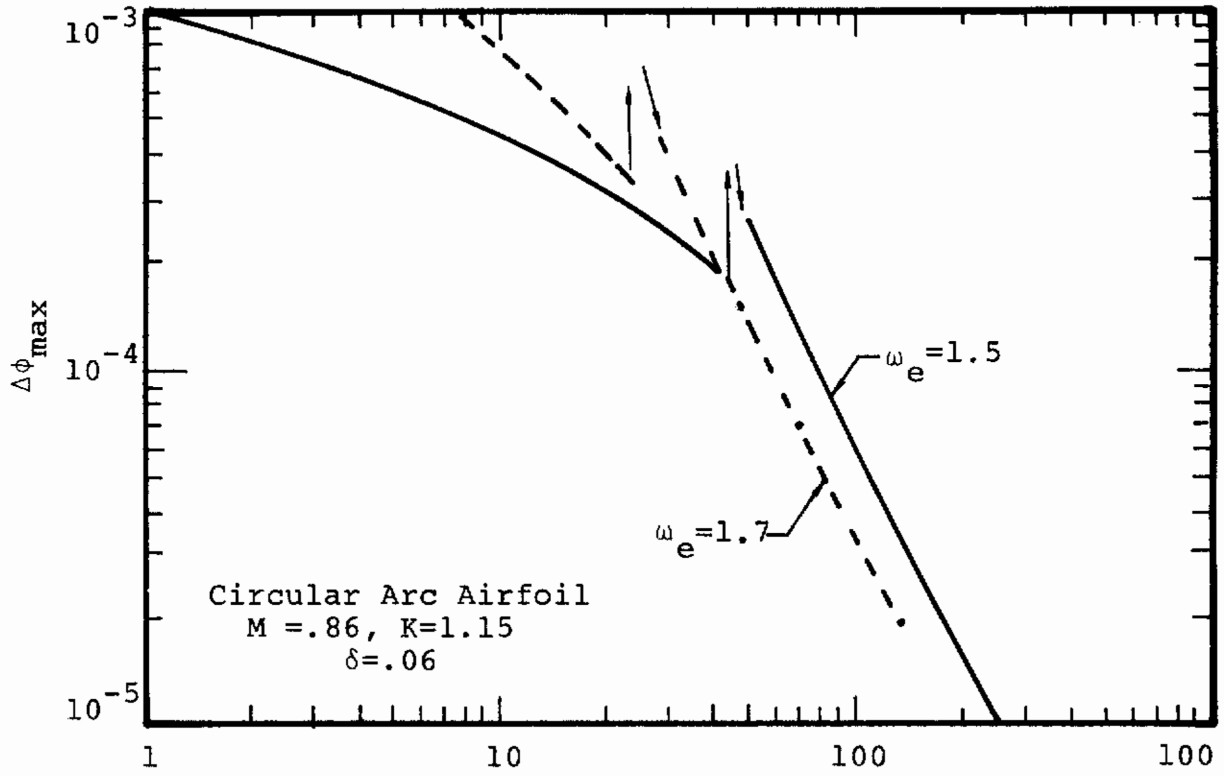

FIGURE 32. TYPICAL CONVERGENCE HISTORY

4.3 Stability Considerations

Stable, convergent steady and unsteady calculations have been performed for a wide range of Mach numbers and reduced frequencies as testified to by the numerous results presented in this report. Stability problems have however been encountered with the steady and unsteady solution schemes for near sonic freestream Mach numbers.

In the present work instabilities have developed for both steady subsonic and supersonic freestream calculations near Mach 1. Such problems have been alluded to by previous investigators[24] and Kentzer[35] has shown the potential for a long wave instability in the Murman-Cole scheme. The instability does not seem to be of practical importance, however, since many authors have applied the same basic scheme to steady flows with Mach numbers quite close to one. With respect to the problems encountered in the present work it would seem that they are more likely due to inadequate grid design. For example the scheme becomes unstable if supersonice flow regions approach the grid boundaries for subsonic freemstream flow cases and if regions of subsonic flow approach the grid boundaries for supersonic freestream flow. Such problems can usually be solved by expanding the grid farther from the airfoil. In the calculations reported here the basic grid with $-6<y<6$ could be used for the NACA64A006 up to $M_\infty=.95$ and the NACA64A410 to $M=.9$. In the supersonic flow calculations for the NACA64A410 it was necessary to expand the grid to $-12<y<12$ to perform calculations for freestream Mach number as low as $M_\infty=1.1$. A comprehensive study of these problems was beyond the scope of the present work.

The solution method for the unsteady potential was found to have a more restrictive stability problem for near sonic flows. Stability problems have been encountered for a combination of Mach numbers near 1 and/or increasing reduced frequency. For example for the NACA64A006 airfoil at $M_\infty=.95$ the method was unstable for $k\geq.1$ and for all reduced frequencies at $M_\infty=1.05$.

In previous work it was noted that the scheme could have stability problems near a compression or shock. A heuristic stability analysis indicates that the instability is related to the inability of the finite difference grid to resolve short wavelength (λ_u) upstream facing waves. That is, the requirement that $\lambda_u \simeq (1-M)/k>\Delta x$ is not satisfied as M (local Mach number) approaches 1 and k increases. If this occurs over a large enough region of the grid an instability is likely. It is noted that expansion of the grid as used here most likely compounds the problem.

A more rigorous Von Neumann stability analysis has also been performed for the present finite difference scheme. The resulting stability expression is quite complicated depending on $\Delta x, \Delta y$, k, Ω, ω_e, ω_h, ϕ_x^0, ϕ_{xx}^0 as well as the usual disturbance wavelength, and it need not be given here. For the simple case of uniform flow ($\phi_x^0 = \phi_{xx}^0 \equiv 0$), the expression indicates that the scheme is stable for all reduced frequencies with the usual restrictions on the relaxation factors. For general supercritical flows, the stability expression indicates the potential for instability for small values of $K(M_\infty \to 1)$ for large values of Ω (or k) and for long wavelength disturbances. This is similar to Kentzer's result for the steady scheme and it means that disturbances (due to round off etc.) with a wavelength long in relation to the grid size can amplify and therefore destroy the solution. A similar description of this instability has been developed by Ehlers[36] using an eigenvalue analysis of the column relaxation scheme. It is noted that this instability works at cross purposes with the requirement for a grid of ever increasing extent as flow Mach number approaches sonic. Increasing the size of the grid would in fact enhance the likelihood that this long wavelength instability would develop.

The problem can not probably be resolved by a simple change to the finite difference equations. One possible solution would be to use the results of an inner/outer expansion procedure which suggests that near the airfoil the present formulation (Equation 10) applies but away from the airfoil the high frequency equation (Equation 21) applies if $k>0(M-1)$ where M is the local flow Mach number. Thus near the airfoil where the local Mach number may be significantly different from sonic the present finite difference procedure could be used and matched to an available analytical solution for the high frequency equation away from the airfoil where local Mach number approaches freestream. The regimes of flow Mach number and reduced frequency for which this procedure is valid would be somewhat restricted but it would most surely reduce the size of the required finite difference grid for $M_\infty \sim 1$ thereby potentially elliminating the stability problems.

5.0 COMPARISONS WITH ALTERNATE THEORIES AND EXPERIMENTS

The accuracy of small disturbance theory for steady inviscid transonic flows has been well documented in recent years through comparison with exact solutions, detailed numerical calculations and experiments in which viscous effects are small. The purpose of this section is to provide some initial insight into the potential accuracy of the present small perturbation method for unsteady transonic flows. In previous work[1,17] it has been shown that the present approach matches linearized unsteady subsonic theory for subcritical Mach numbers and the results of Section 3.2 above show that the method matches linearized supersonic theory for fully supersonic flows. These trends are verified by the aerodynamic coefficients presented in this section and the next. Although no exact solutions exist for unsteady transonic flows, Magnus and Yoshihara[9] have recently presented a detailed numerical calculation and it is compared to the present theory in Section 5.1. The final verification of any theory must of course come from comparison to experimental data and such a comparison is made in Section 5.2.

Results are presented for a NACA 64A410 airfoil oscillating in pitch and a symmetric NACA 64A006 with oscillating control surface hinged at the 3/4 chord line. Before proceeding with the comparisons, some comments concerning computational details are in order.

In all of the unsteady calculations to follow, the low frequency approximation, which involves dropping underlined terms in the above formulation, was used. The effect that this approximation might have on the results has been discussed in Section 3.1 above. The form of the unsteady perturbation to the airfoil downwash for pitch, plunge, and control surface oscillations are respectively:

$$\left.\begin{array}{lll}
\text{(pitch)} & \phi_y = -1-\underline{k(x-x_p)} & 0 \le x \le 1 \\[2ex]
\text{(plunge)} & \phi_y = -ik & 0 \le x \le 1 \\[2ex]
\begin{pmatrix}\text{control}\\ \text{surface}\end{pmatrix} & \phi_y = \begin{cases} 0, & 0 \le x \le x_h \\ -i-\underline{ik(x-x_h)} & x_h \le x \le 1 \end{cases} &
\end{array}\right\} \qquad (51)$$

where x_h is the hinge point and x_p is the pitch point. In the respective cases, the magnitude of the perturbation is α/δ, β/δ or δ'/δ where α, β and δ' are the amplitudes of the oscillating component of angle of attack, flap angle or plunge displacement respectively. The amplitudes of the resulting perturbations to the airfoil pressure coefficients in unscaled (C_p) or scaled ($\bar{C}_p$) form are given by Equations 11 and 12 above. It is noted that the scaling used in Equation 11 for the pressure coefficient, commonly known as Spreiter scaling, is a natural result of the non-dimensionalization used here. No attempt has been made to modify the Mach number dependence in the scaling to provide better agreement with data or exact results as is often done elsewhere[16]. Finally, it is noted that lift, moment, and hinge moment coefficients (Ex. $C_{\ell\alpha}$, $C_{m\alpha}$, $C_{n\alpha}$) are calculated by a trapeziodal rule integration of the calculated pressure coefficient distributions.

In the calculations presented in this section and the next, the refined grid (achieved by refining a coarse grid by the "grid halving" procedure) consisted of 48 points in the x direction and 47 points in the y direction. Over half (26) of the grid columns are on the airfoil and grid rows are divided in a symmetric manner above and below the airfoil. The grid is expanded in a regular manner out to $x \approx \pm 3$ and $y \approx \pm 6$ at which point an analytic farfield expression is imposed as a boundary condition. Previous experience indicated that such a grid would provide relatively good results so that no attempt was made at optimizing the grid structure for each case. In both steady and unsteady calculations the iteration procedure was continued until the maximum change in potential, over all grid points, from one iteration to the next was less than $\sim 10^{-4}$. This is consistent with the accuracy tests described in Section 4.0 above. In each case this resulted in a convergence of the airfoil circulation to better than 10^{-4}.

5.1 NACA 64A410 Oscillating in Pitch at $M_\infty = .72$

Magnus and Yoshihara[9] (M-Y) have recently presented time-dependent calculations of the flow past a NACA 64A410 airfoil oscillating in pitch at Mach .72. Their highly refined numerical method is based on the full unsteady inviscid flow equations with kinematic boundary conditions fixed at the mean airfoil surface. These "exact" solutions provide a unique comparison for verification of the present approximate method. The nose bluntness, thickness and camber of the airfoil coupled with the mean and oscillating amplitude of angle of attack ($\alpha = 2^\circ \pm 2^\circ$) provide a severe but practical test of both the small disturbance approximation and the linearized unsteady method.

Results for the steady pressure distributions for $\alpha_o = 2^o$ are presented in Figure 33 below; pluses (+) and Δ indicate points computed by the present method and M-Y respectively. All in all the comparison is moderately good with the exception of two anomalies: the shock description and a "knee" in the small disturbance pressure distribution on the upper surface near the nose. Lift predicted by both methods compare well as do the lower surface pressure distributions. The shock calculated by the present method is farther forward, more diffuse and weaker which can be attributed to the relatively coarse grid and the use of the non-conservative differencing of the present method. It is believed that the shock description could be improved by the use of shock point differencing[24] described in Section 3.2 or shock fitting[25] as well as a denser gridwork in the region of the shock. However, it should be pointed out that the shock Mach number is about 1.3 which would indicate that the small disturbance shock description is not accurate. The other anomaly in the comparison which has some bearing on the linear perturbation results to follow is the sharp change in slope of the predicted pressure distribution near the nose. This behavior is not shown in the M-Y results. It is probably due to the approximation to the airfoil slope distribution used in the present method as well as possible inaccuracy of the small disturbance description of the rapid expansion of the flow about the nose of the airfoil. It is clear from this comparison that the present results could benefit from increased resolution as well as the use of recent developments in the treatment of shocks.

Calculations of linearized unsteady perturbations about the steady flow described above have been performed and amplitudes of perturbations to the pressure coefficents due to a 2^o pitch oscillation are shown in Figures 34 and 35 for the steady, k=0, and low frequency unsteady, k=.2, cases. The results of the present theory are again compared to results deduced from the M-Y calculations. The M-Y results for both nose up ($2^o \rightarrow 4^o$) and nose down ($2^o \rightarrow 0^o$) motion are shown to give some indication of the inherent nonlinearity. It is noted that the nonlinear behavior is surprisingly small on the supercritical upper surface and surprisingly large on the subcritical lower surface. The present results for the lower surface compare well with the M-Y results. The comparison in each case for the upper surface is consistent with the difficiencies in the present result for the steady flow being perturbed. The discrepancy at the shock is to be expected since the M-Y calculations show significant shock excursions (indicated on the graphs) which are not accounted for in the present work. The linearized results show a peak suction through the steady shock which is an attempt by the linear theory to account for the strengthening (or weakening) of the shock due to a nose up (or nose down) pitch perturbation. The present results also show an as yet unexplained decreased suction (dip) near the x=.1 station which corresponds to the "knee" in the steady pressure distribution discussed above. This behavior is not shown in the M-Y results and is an indication of possible numerical difficulties in the linear perturbation solution. This is not believed to be the case, however, since a comparison of nonlinear steady small disturbance results (not shown) for $\alpha_0=0^0$ and $\alpha_0=2^0$ show a similar dip in the distribution of $\Delta Cp_{0\to 2^0}$. This would indicate that the anomaly is due to the discrepancy in the steady solution in this same region as discussed above.

		Magnus and Yoshihara[8]	Present Results
k=0	ΔC_ℓ $0^0\to 2^0$	.3841	.338
	$2^0\to 4^0$	.3543	
	$0\to 2^0$	.129	.115
	ΔC_m $2^0\to 4^0$	.13	
k=.2	Re $\lvert\Delta C_\ell\rvert$	.2385	.243
	Im $\lvert\Delta C_\ell\rvert$	-.1003	-.096
	Re $\lvert\Delta C_m\rvert$	.08933	.0866
	IM $\lvert\Delta C_m\rvert$	-.03418	-.0304

TABLE 1. COMPARISON OF LIFT AND MOMENT PERTRUBATIONS

The results of interest for flutter applications are the perturbations to the integrated airfoil forces. The table presented above compares the increment in lift and moment coefficient in steady flow as the angle of attack increases from 0^o to 2^o and from 2^o to 4^o. Also compared are the linear parts of the oscillating coefficients for the k=.2 pitching oscillation with 2^o amplitude. The good agreement in each case would seem to indicate that the linearized perturbation method provides a useful approximation to the oscillatory forces for quasi-steady and low frequency oscillations. It may be noted that for this example the ratio of oscillatory amplitude (at 2^o) to the thickness is $\varepsilon=.35$ which is a relatively large perturbation.

The M-Y results for k=.2 shown in the table are the magnitudes of the first harmonic ($e^{i\omega t}$) coefficients which resulted from their Fourier analysis of the nonlinear time dependent results. Their analysis also shows that the higher harmonics are quite small in comparison. This is to be expected from the perturbation expansion which shows that terms involving higher harmonics are of order ε^2. This result lends some credence to the linearized approach used here. It is hoped that future improvements in both the small disturbance steady and linearized unsteady perturbation methods will improve certain details of the present results.

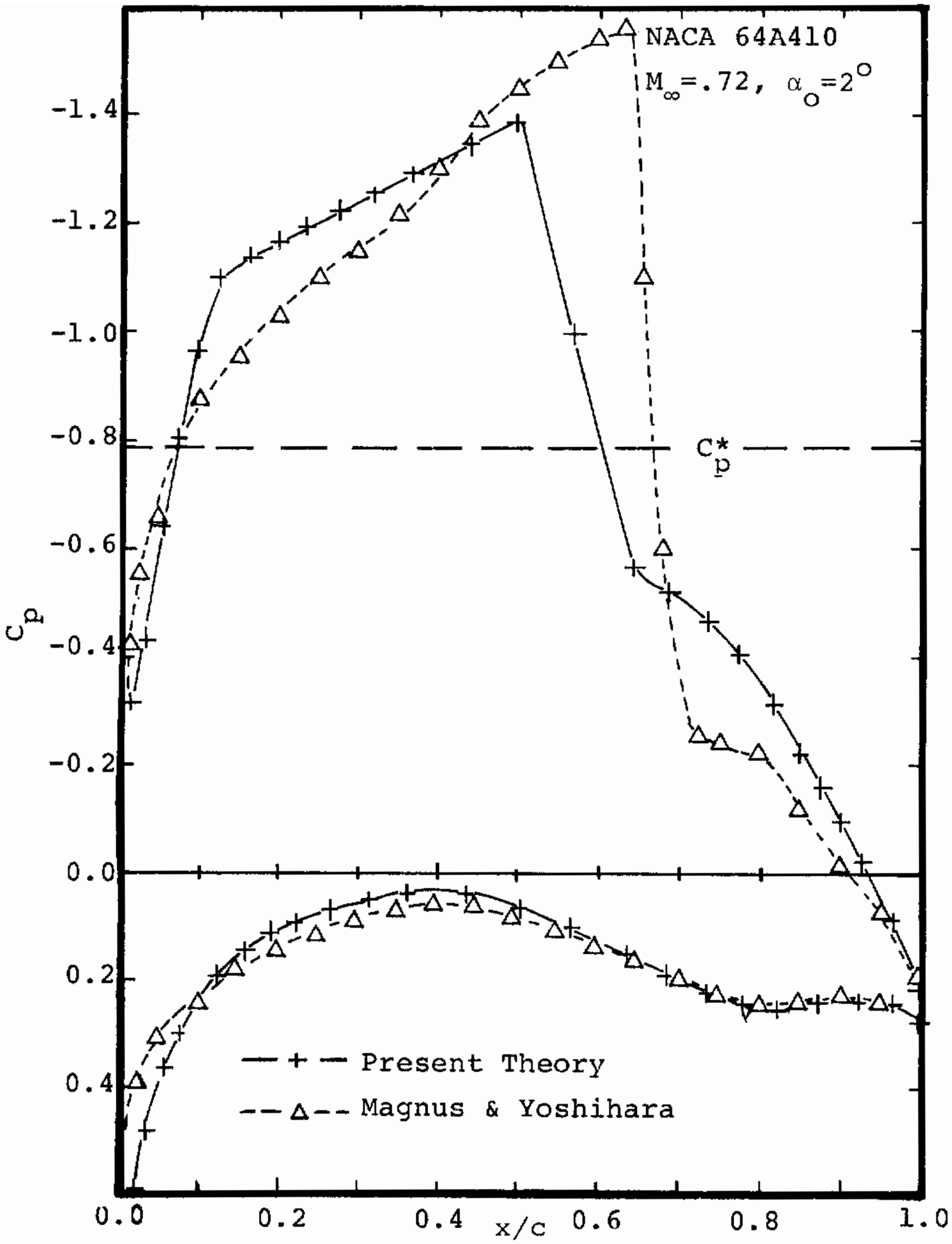

FIGURE 33. STEADY PRESSURE DISTRIBUTION (NACA64A410)

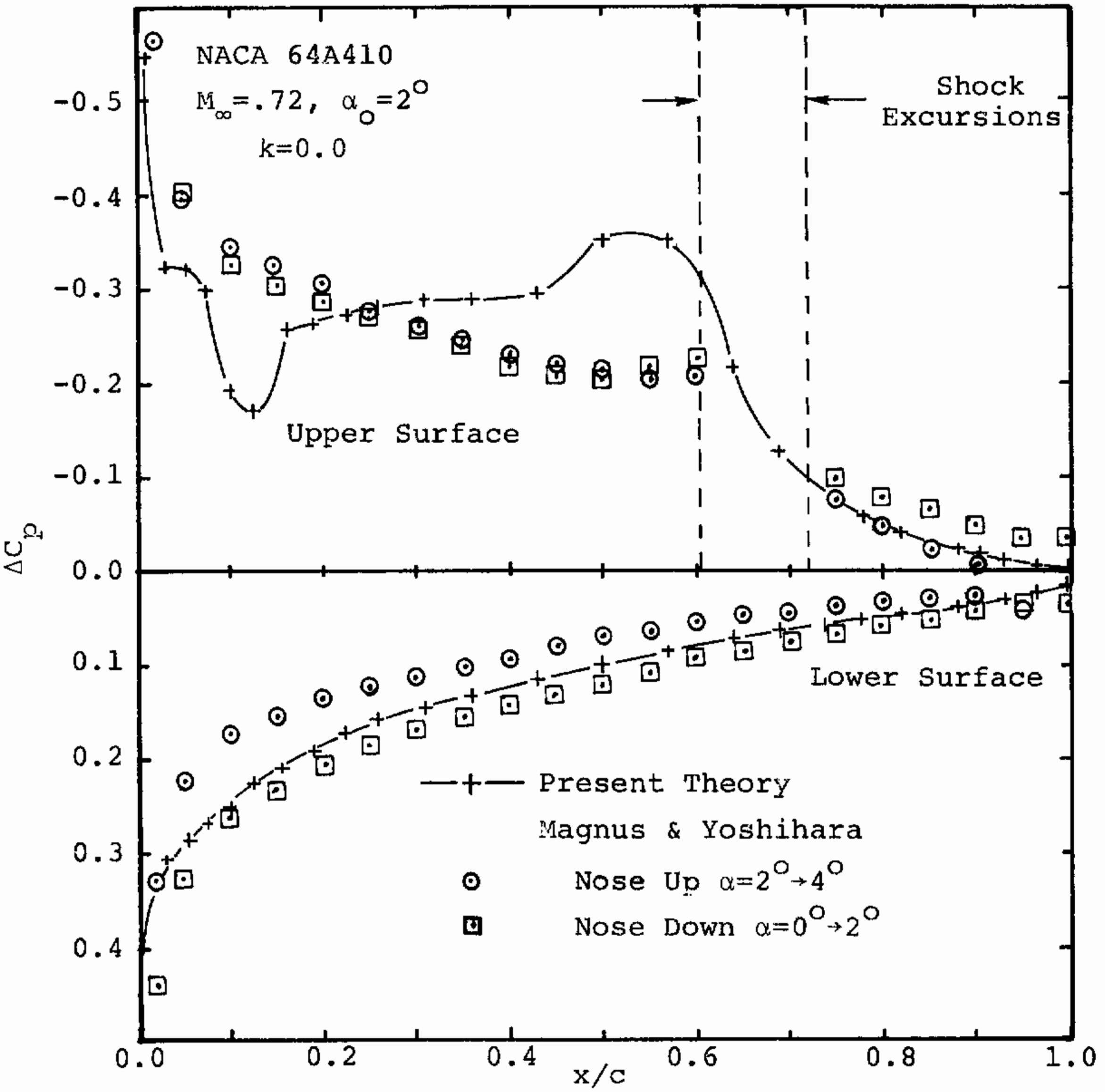

FIGURE 34. MAGNITUDE OF PRESSURE COEFFICIENT PERTURBATION DUE TO A 2^0 DEFLECTION IN PITCH

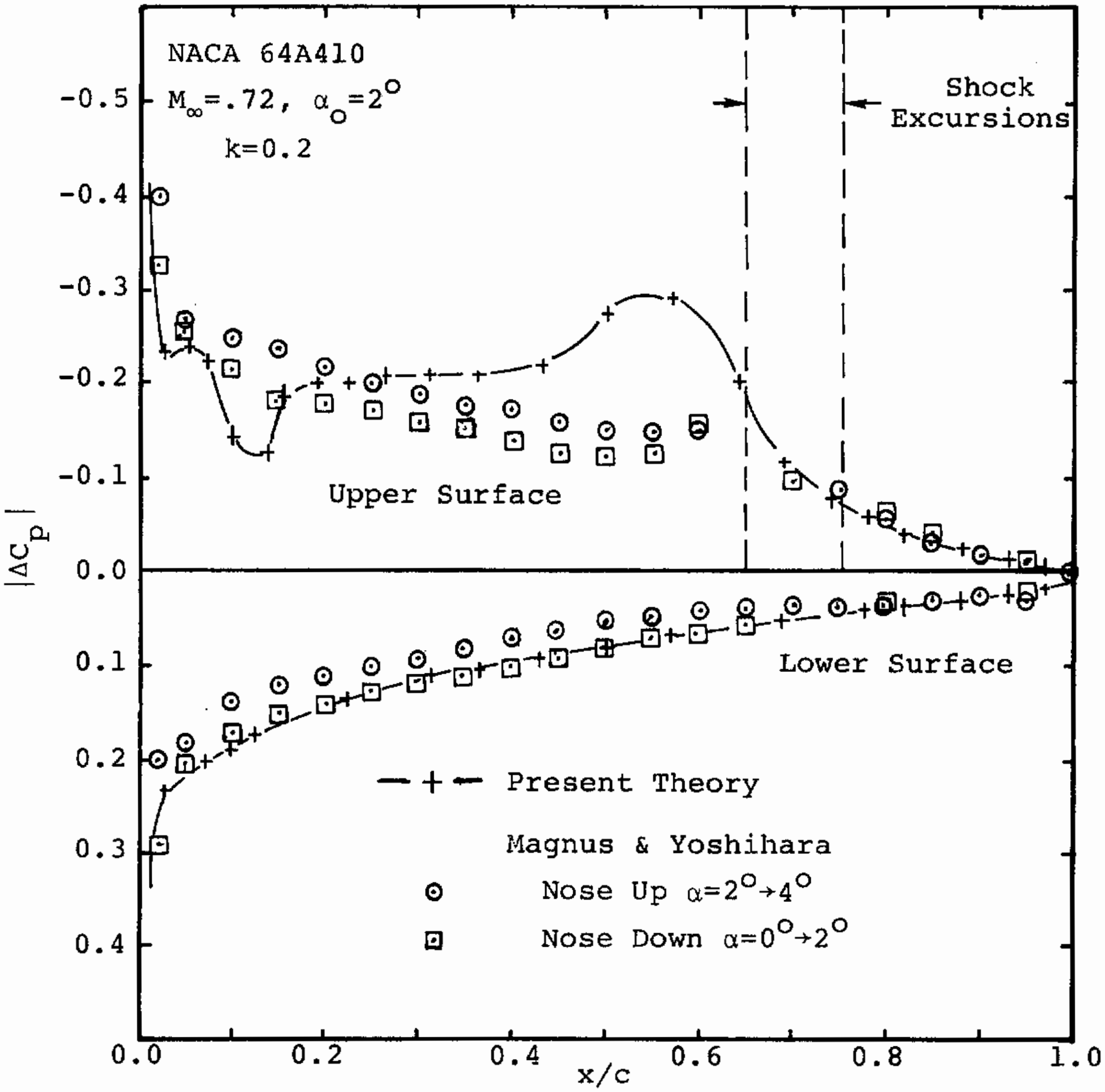

FIGURE 35. MAGNITUDE OF PRESSURE COEFFICIENT PERTURBATIONS DUE TO A 2^0 OSCILLATION IN PITCH

5.2 NACA 64A006 with Control Surface Oscillation

As mentioned in the introduction, the primary application of the method described here is the calculation of generalized unsteady forces for use in flutter studies. Such a study has been undertaken for the NACA 64A006 airfoil with three rigid body degrees of freedom: pitch, plunge and control surface oscillation, and the detailed results are presented in Section 6.0. In this section, some of the results generated for control surface oscillations are presented with comparison to the experimental data of Tijdeman, Bergh and Schippers[18,19], for the same airfoil and control surface configuration. It is noted that the experimental technique used to measure unsteady pressures was sensitive only to the first harmonic so that theory and experiment are being compared on the same bases.

Sample results for airfoil pressure coefficients (in scaled form) for the non-linear steady (Figure 36) and for linearized perturbations due to control surface deflection for k=0 (Figure 37) and k=.12 (Figure 38) are presented below. The steady results for a supercritical Mach number of .875 and zero degree angle of attack show good agreement with experiment with the exception of the region near the shock. The present small disturbance results show what must be called a rapid compression at about midchord whereas the data shows a diffuse but moderately strong shock. Refinement of the grid between x/c=.5 and .6 would most surely enhance the comparison but it is likely that the use of shock point differencing would over correct for the rearward position of the shock.

The linearized perturbation results for a steady control surface deflection and for an unsteady control surface oscillation at k=.12 (Figures 37 and 38) show good qualitative agreement with data. As shown in Figure 37, the theory overpredicts the pressure perturbation on the stationary forward portion of the airfoil in comparison to the data. This is characteristic of all cases calculated and is believed to be due in part to the reduced upstream influence resulting from wall effects in the experiment. It is recalled that the present calculations are for free air conditions. Calculations with a solid wall boundary condition, presented in Section 6.1.4, show a significant reduction in upstream influence. Other details of the pressure distribution such as peak suction at the shock (slightly forward of the experimental peak) and hinge point singularity seem to be well predicted by the theory. The unsteady k=.12 results in Figure 28 show a similar qualitative comparison with some significant quantitative differences in magnitude and phase on the forward portion of the airfoil.

Comparisons of the theoretical results for $C_{\ell\beta}$ with experimental data and with linear subosnic/supersonic theory are made in Figures 39 and 40 for k=0 and 0.1 respectively. As shown, the present theory reduces to linear theory away from Mach 1. In each case the present results are significantly greater than the data although a qualitative agreement is apparent. The peak in the theoretical results at M=.85 seems to result from a lift augmentation effect due to coalescence at the shock of upstream traveling control surface perturbations. This effect does not occur in linear, uniform flow theory for obvious reasons and is not in evidence in the data perhaps because of the reduced upstream influence mentioned above. One final comment with respect to these comparisons is in order. It is noted that the data is in considerable disagreement with subsonic linear theory (and the present theory) for a fully subcritical Mach number of .7. Nonuniform flow or wind tunnel wall effects could not be the culprits because they both have an effect which would tend to enhance the discrepancy. It seems highly probable that the reasons for the discrepancy is the existence of a strong viscous effect in the data. The estimated chord Reynold's number of less than 200,000 for the experiments adds further weight to this conclusion. Such effects could only be magnified in the transonic speed range.

Further comparisons with the data are presented in the next section along with some results for mean angle of attack and wall effects.

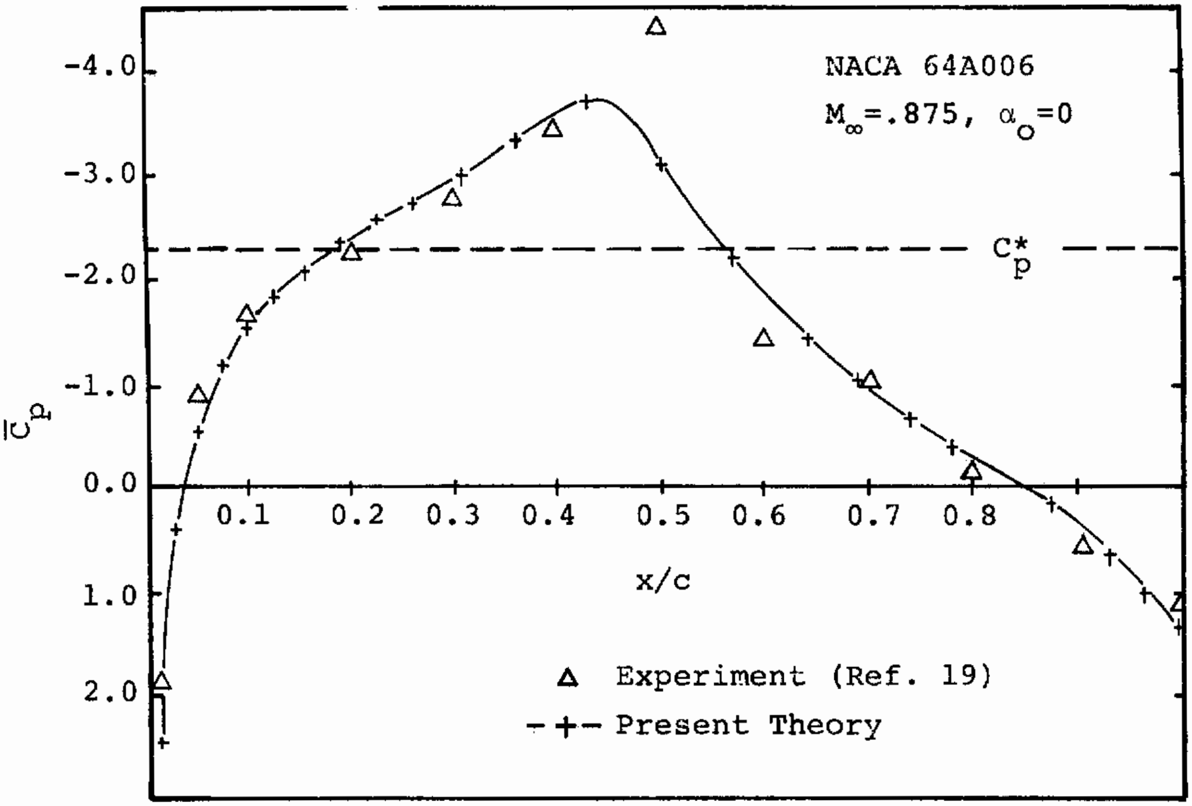

FIGURE 36. STEADY PRESSURE DISTRIBUTION (NACA64A006)

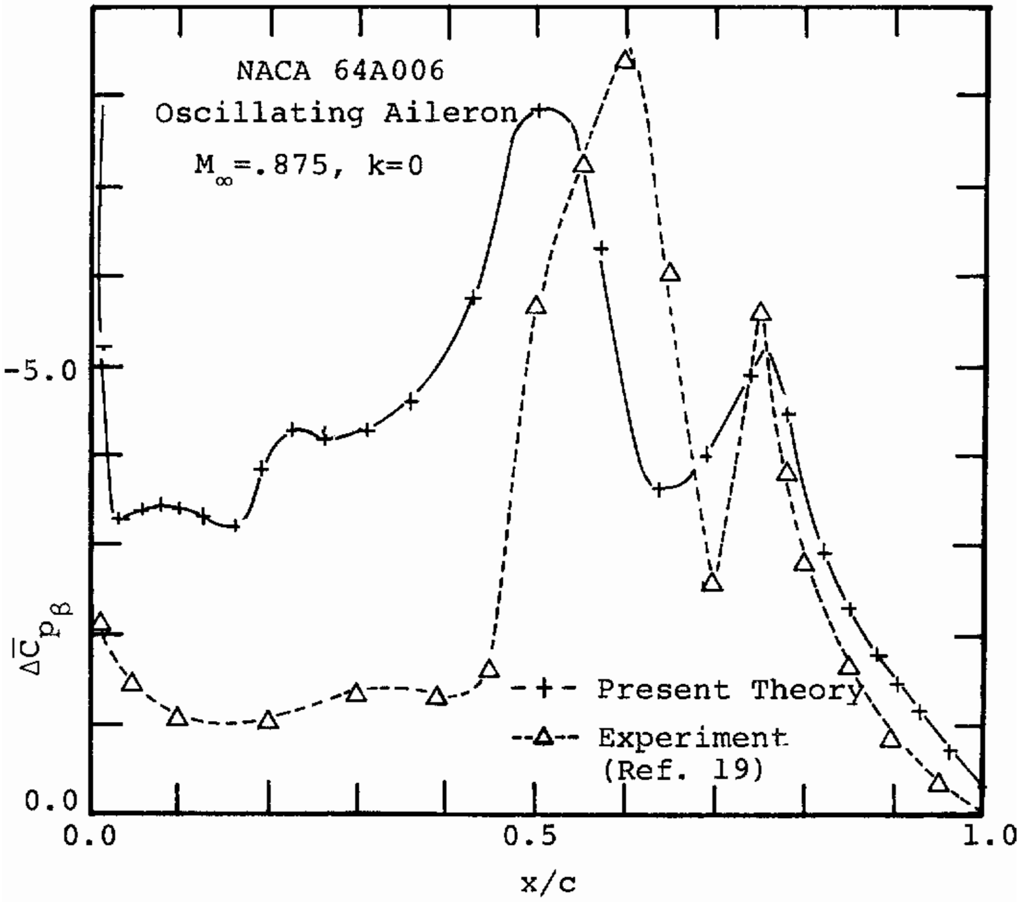

FIGURE 37. SCALED PRESSURE PERTURBATION DUE TO AILERON DEFLECTION

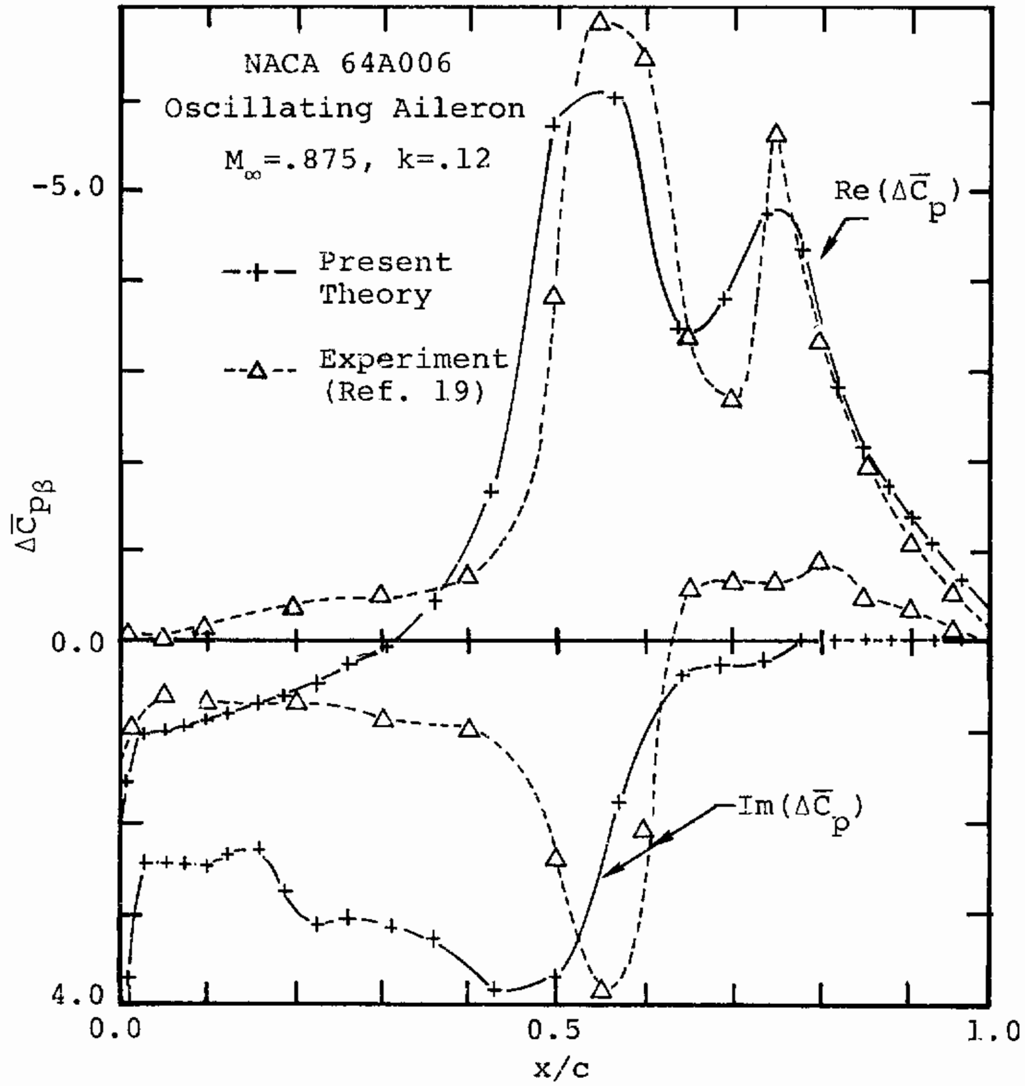

FIGURE 38. SCALED PRESSURE PERTURBATION DUE TO AILERON OSCILLATION

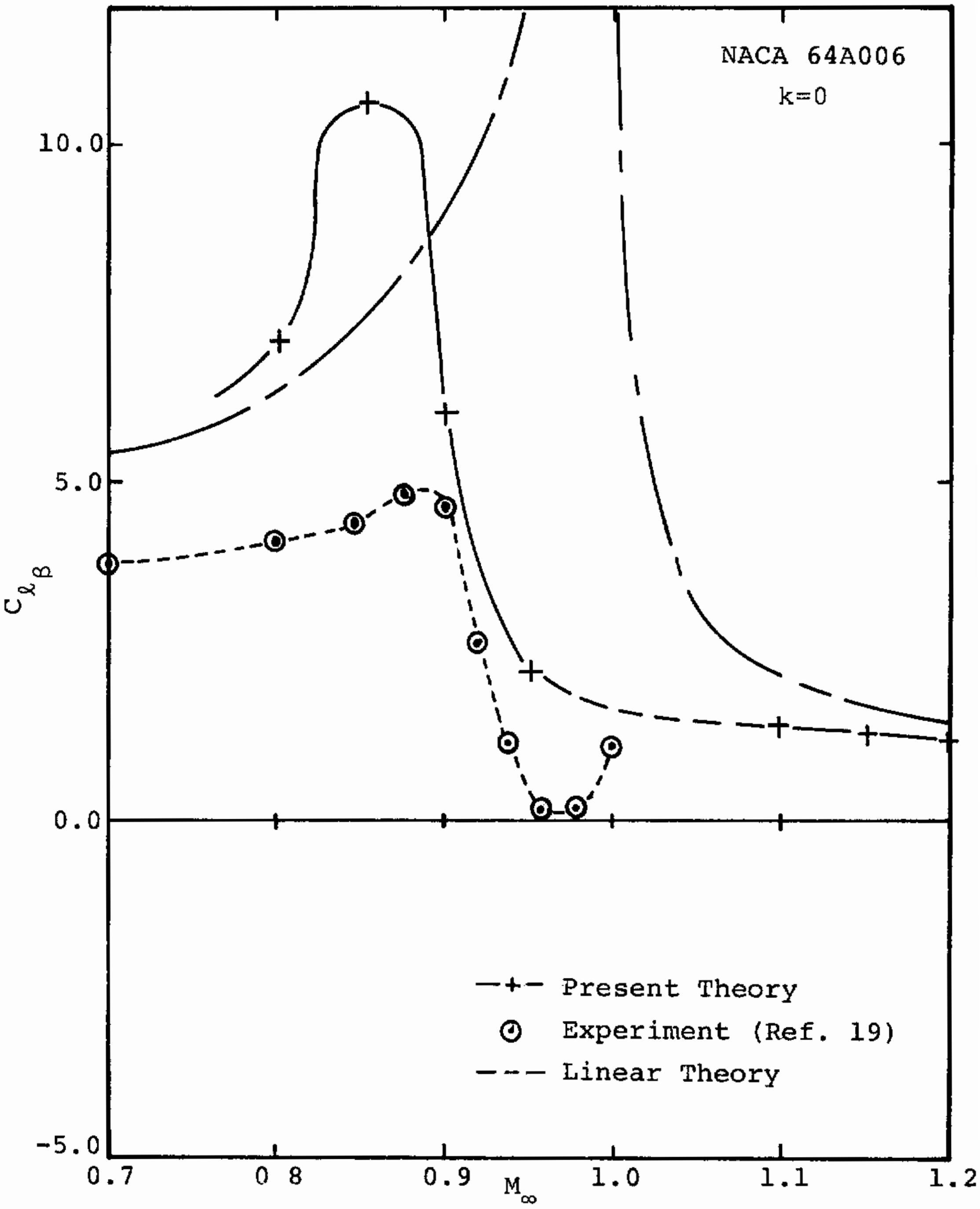

FIGURE 39. LIFT DUE TO AILERON DEFLECTION

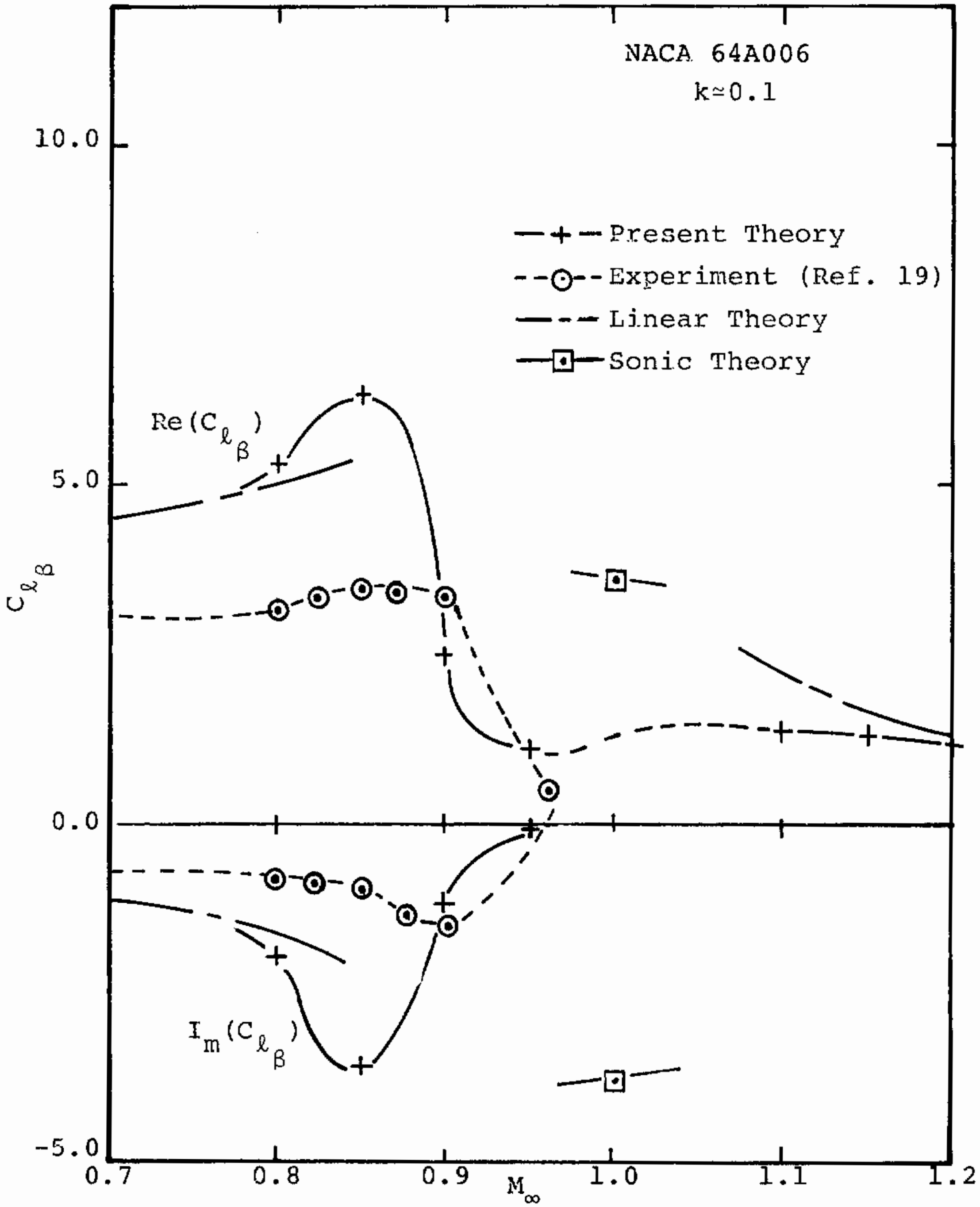

FIGURE 40. LIFT DUE TO AILERON OSCILLATION

6.0 CALCULATED RESULTS

Using the method described in this report, a wide range of steady and unsteady results have been calculated to provide the necessary aerodynamic coefficient data for the flutter studies to be presented in Section 7. These results, described in this section, are for two practical airfoil: a NACA64A006 oscillating in pitch, plunge and control surface rotation and a NACA64A410 oscillating in pitch and plunge. The ranges of Mach number (M_∞=.75 to 1.2) and reduced frequency (k=0 to 0.2) considered serve to demonstrate the efficiency and utility of the method for treating unsteady transonic flows.

The same basic grid as just described in Section 5 ($IM=JM\simeq50, -3<x<3, -6<y<6$) was used in all cases with but slight variations for some special cases. Also, as is the usual practice with the method, convergence in each case was taken to $\max_{i,j} \Delta\phi \simeq 10^{-4}$, which resulted in the convergence of airfoil circulation to better that 10^{-4}. It is reiterated that this grid design and degree of convergence represents a reasonable compromise between numerical accuracy and computer run time.

6.1 Results for a NACA 64A006 Airfoil

Results are presented in this section for a NACA64A006 airfoil with a 25% trailing edge flap. Detailed steady and unsteady pressure distributions are presented in Section 6.1.1 and the calculated unsteady aerodynamic coefficients for pitch, plunge and control surface oscillations are summarized in Section 6.1.2. Mean angle of attack and wall interference effects on the aerodynamic coefficients are briefly examined in Section 6.1.3 and 6.1.4 respectively. It is noted that the unsteady results for pitch and control surface oscillations were calculated using the low frequency approximation since the high frequency generalizations to the method, required and used for the plunge results, were not inplemented at the time these calculations were performed. The effect of the approximation on the results has been discussed in Section 3.1.

6.1.1 Free Air Results of Steady and Unsteady Pressures

Steady pressure distributions for the NACA64A006 at zero angle of attack for subsonic freestream Mach numbers,

M_∞=.8, .85, .9, .95, and for supersonic freestream Mach numbers, M_∞=1.1, 1.15, 1.2, are presented in Figure 41 and 42 respectively. The various curves show the progression of airfoil pressures from subcritical through the supercritical regime to low supersonic and points out the large non-linear effect in the transonic regime. The airfoil first becomes supercritical at a Mach number between .8 and .85 and by M_∞= .85 a weak shock has formed which strengthens and moves aft on the airfoil as M_∞ increases. At M_∞=.9 the shock is about at the aileron hinge point (x/c=.75) and at M_∞=.95 the present inviscid calculations indicate the shock is at the airfoil trailing edge. It should be noted that the experimental data of Tijdeman et al[18,19] indicate that at M_∞=.9 the shock is between 5 and 10 percent chord forward of the aileron hinge point and that the shock does not reach the trailing edge until very close to M_∞=1. This tendency of the inviscid small disturbance result to overpredict the shock strength and its aft location is typical and is most likely due to viscous effects neglected in the theory. It is recalled that the comparison of the present results with the data (Figure 36 of Section 5.3) is very good for a fully supercritical Mach number of M_∞=.875.

It is noted that the M_∞=.95 pressure distribution is very similar in shape to the low supersonic results shown in Figure 42. In fact, the distributions of $C_p-C_p^*$ for, M_∞= .95, 1.1, 1.15, 1.2, compare to within 10% in each case. This result is the so called "Mach freeze" phenomena for flows near Mach 1 and in fact indicates that, although the magnitudes of the pressures differ considerably, the local flow Mach number over and in the near field of the airfoil most likely varies by no more than 10% in the freestream Mach number range M_∞= .95 to 1.2. Since the nature of unsteady perturbations to the mean flow are determined largely by the flow Mach number field about the airfoil the "Mach freeze" phenomena has important consequences with respect to the unsteady perturbation results. It is expected, for example, that the unsteady results for M_∞ between .95 and 1.2 will not vary a great deal. This expectation is substantiated somewhat by the unsteady aerodynamic coefficients presented in the next section.

Results for unsteady pressures due to control surface perturbations of the subsonic mean flow solutions are presented in Figures 43 through 49. The results in each case are compared to the data of Tijdeman et al[18,19] Results for the jump in pressure coefficient across the airfoil per unit flap angle due to a quasi-steady (k=0) control surface deflection are given in Figures 43,44,45, and 46 for freestream Mach numbers of M_∞=.8, .85, .9, .95 respectively. The results demonstrate the strong non-uniform flow effect for transonic Mach numbers. In each case the comparison with the data is qualitatively good but quantitatively in error. As discussed above in Section 5.2, the most probable reason for the discrepancy is viscous effects. Of some note are the supercritical results for M_∞=.85 and above. The results for M_∞=.85 (Figure 44) for example shows that the theory predicts the location of the peak pressure perturbation through the weak shock but overpredicts its magnitude. This overprediction of the perturbation over the non-deflecting forward portion of the airfoil is shown in this case as well as the higher Mach number cases M_∞=.9 (Figure 45) and M_∞=.95 (Figure 46). This indicates that in addition to viscous effects wall interference effects could be reducing the upstream influence in the experiment as compared to the present free air results. The wind tunnel wall results of Section 6.1.4 add some weight to this possibility.

One final comment with respect to the quasi-steady results concerns the significant effect that the mean flow results can have on the unsteady perturbations. A large part of the discrepancy between the theory and experiment in the M_∞=.9 and .95 cases can be attributed to the fact that the present steady theory predicts a shock location aft of the experimental data. For example at M_∞=.9 the theory predicts the shock at the hinge point which results in a peak in the perturbation pressure at the hinge point whereas the data shows the shock location to be at about x/c=.7 hence the experimental peak in perturbation pressure at that location. Also at M_∞=.95 the present results for perturbation pressure (Figure 46) compare very well to the experimental results at $M_\infty \simeq 1.0$. It is recalled that the theoretical steady solution at M =.95 compared more closely (as far as shock location) to the experimental result at M_∞=1.0 than the M_∞=.96 data (shown in the figure) for example.

Results for the perturbation pressure for fully unsteady, k=.1, aileron oscillations are presented in Figures 47,48, and 49 for M =.8, .85, and .9 respectively. The comparison to the data, shown in the figures, is similar to the comparison for the k=0 results just discussed in detail. As discussed there the results are qualitatively good but quantitatively in error.

The results presented in this section indicate that the most likely cause for the discrepancy between the present unsteady perturbation theory and the data is the effect of viscosity. Viscosity can have a direct effect on the unsteady perturbations but for small perturbations has a more likely indirect effect by way of its modification to the mean flow. In other words, it is believed that the present unsteady results would be in somewhat better agreement with the data if the steady results for example for shock strength and location agreed with the data. This brings up the interesting possibility of improving the overall theory by performing viscous modifications to the steady solution by coupling the present inviscid theory to a boundary layer analysis. Although this would be a significant undertaking it would be considerably easier than performing an unsteady boundary layer analysis coupled to the fully unsteady theory.

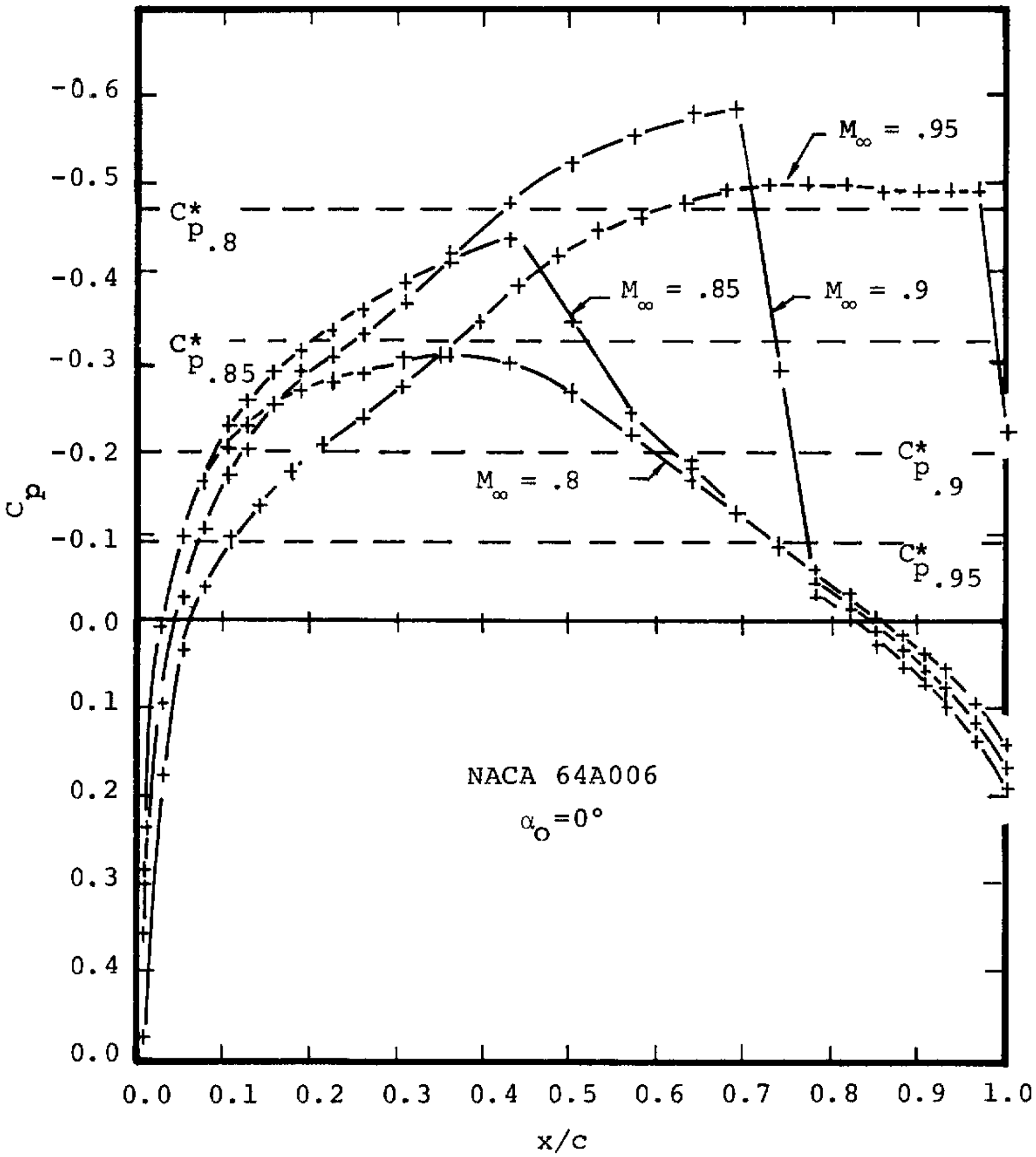

FIGURE 41. STEADY PRESSURE COEFFICIENTS

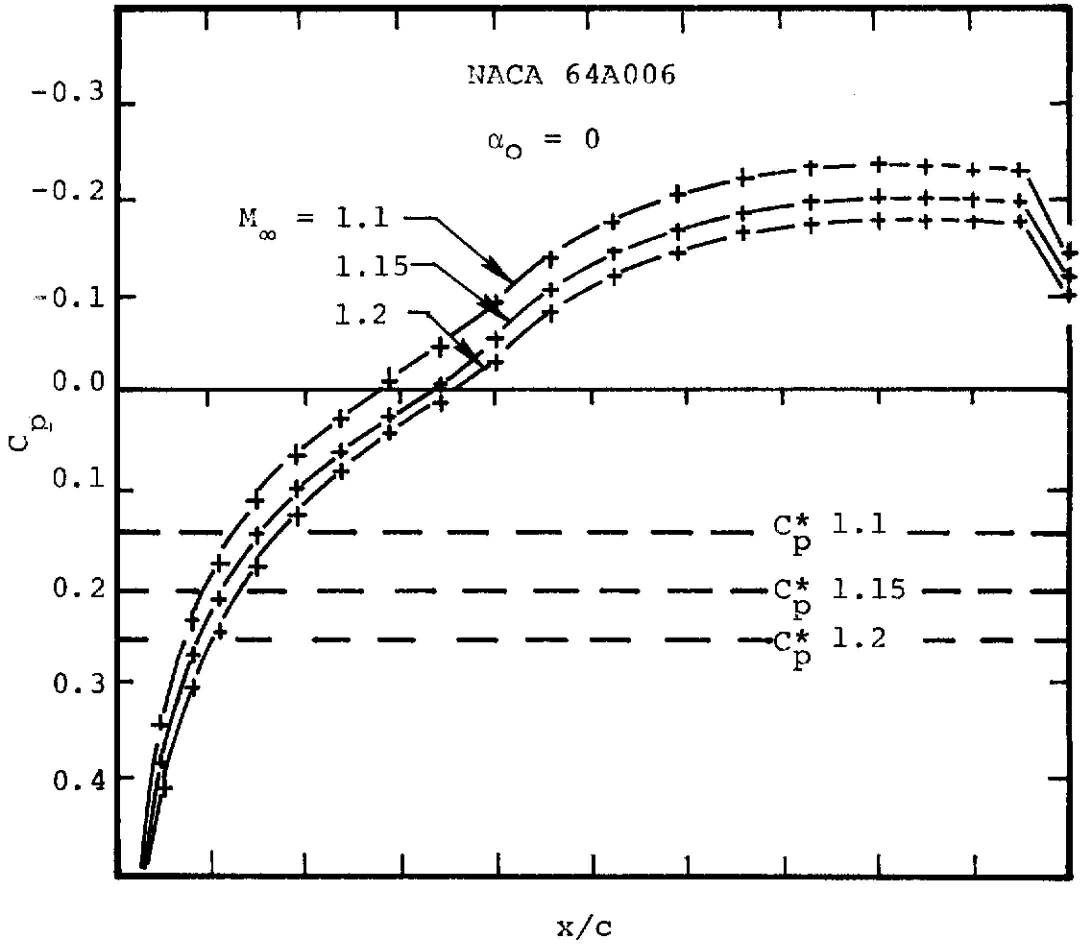

Figure 42. Steady Pressure Coefficients

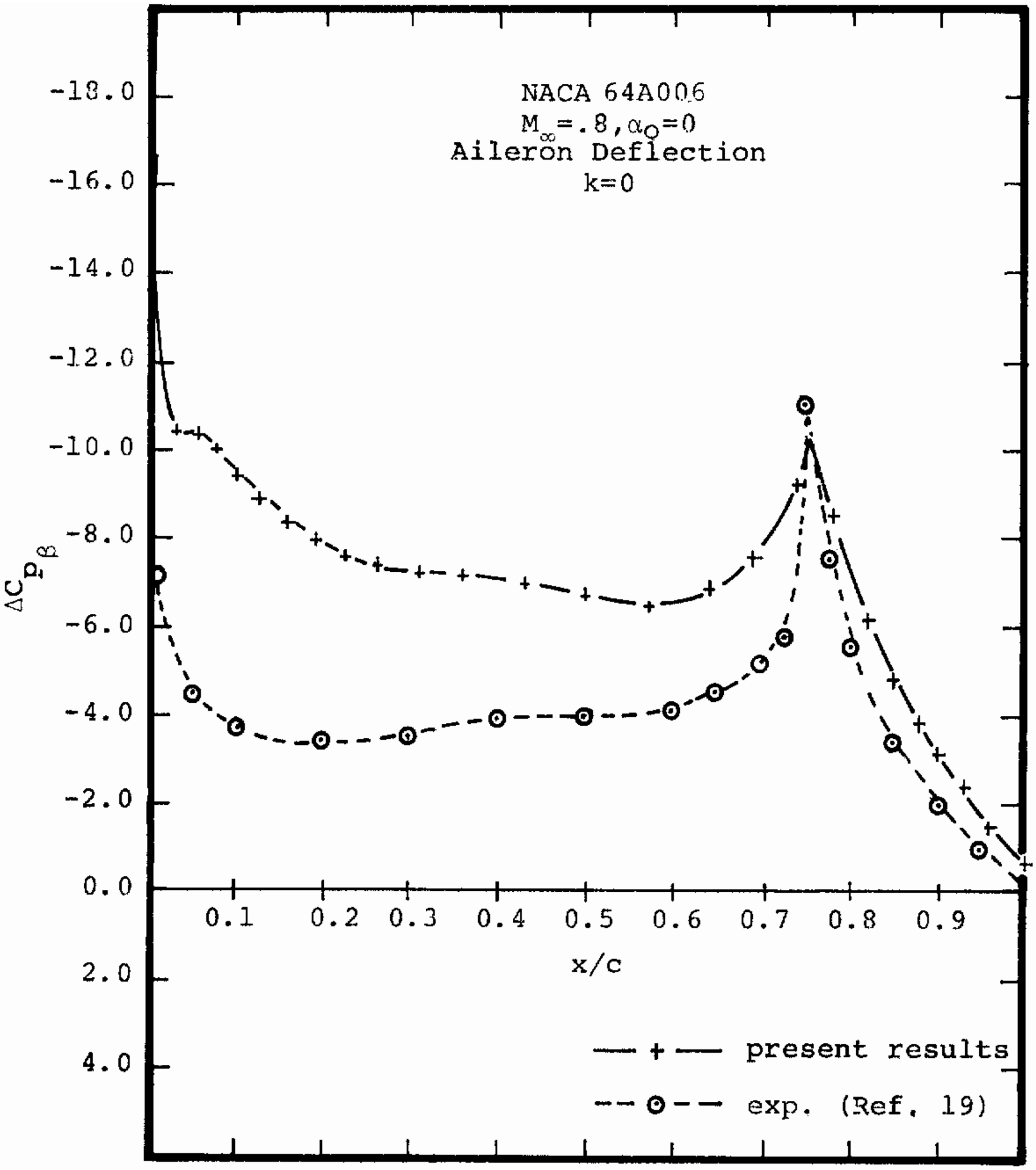

FIGURE 43. AIRFOIL PRESSURE PERTURBATION DUE TO AILERON DEFLECTION

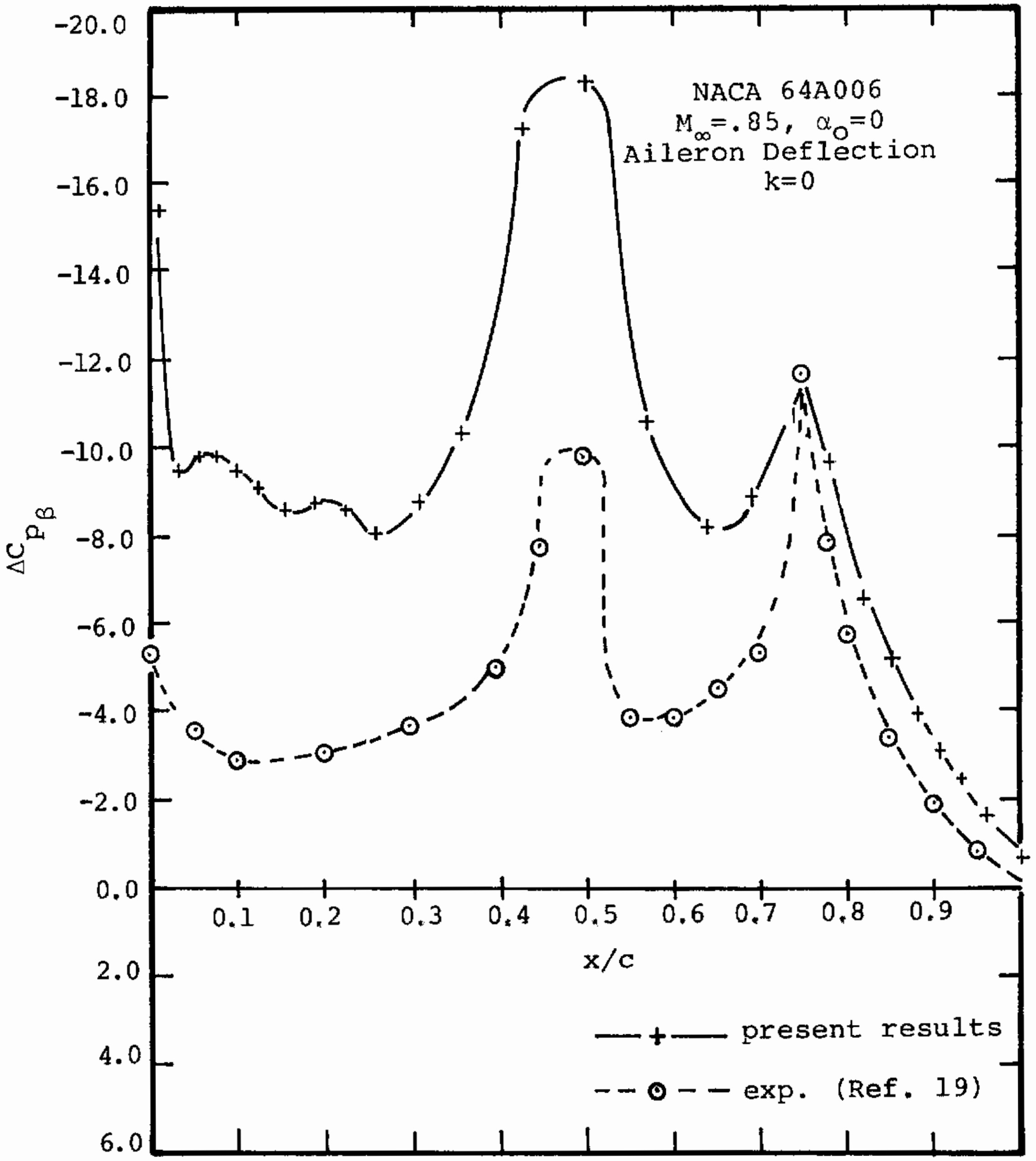

FIGURE 44. AIRFOIL PRESSURE PERTURBATION DUE TO AILERON DEFLECTION

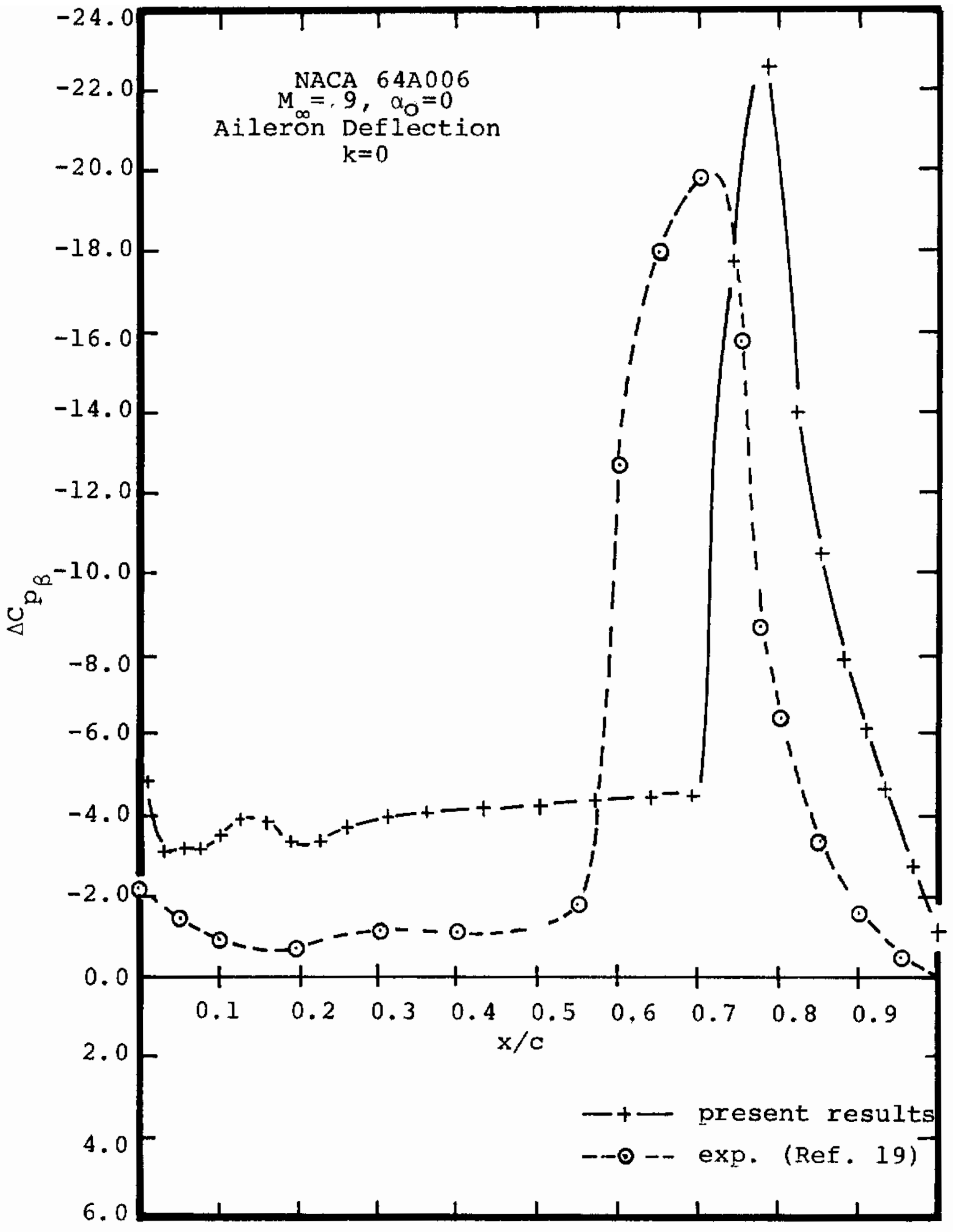

FIGURE 45. AIRFOIL PRESSURE PERTURBATION DUE TO AILERON DISTRIBUTION

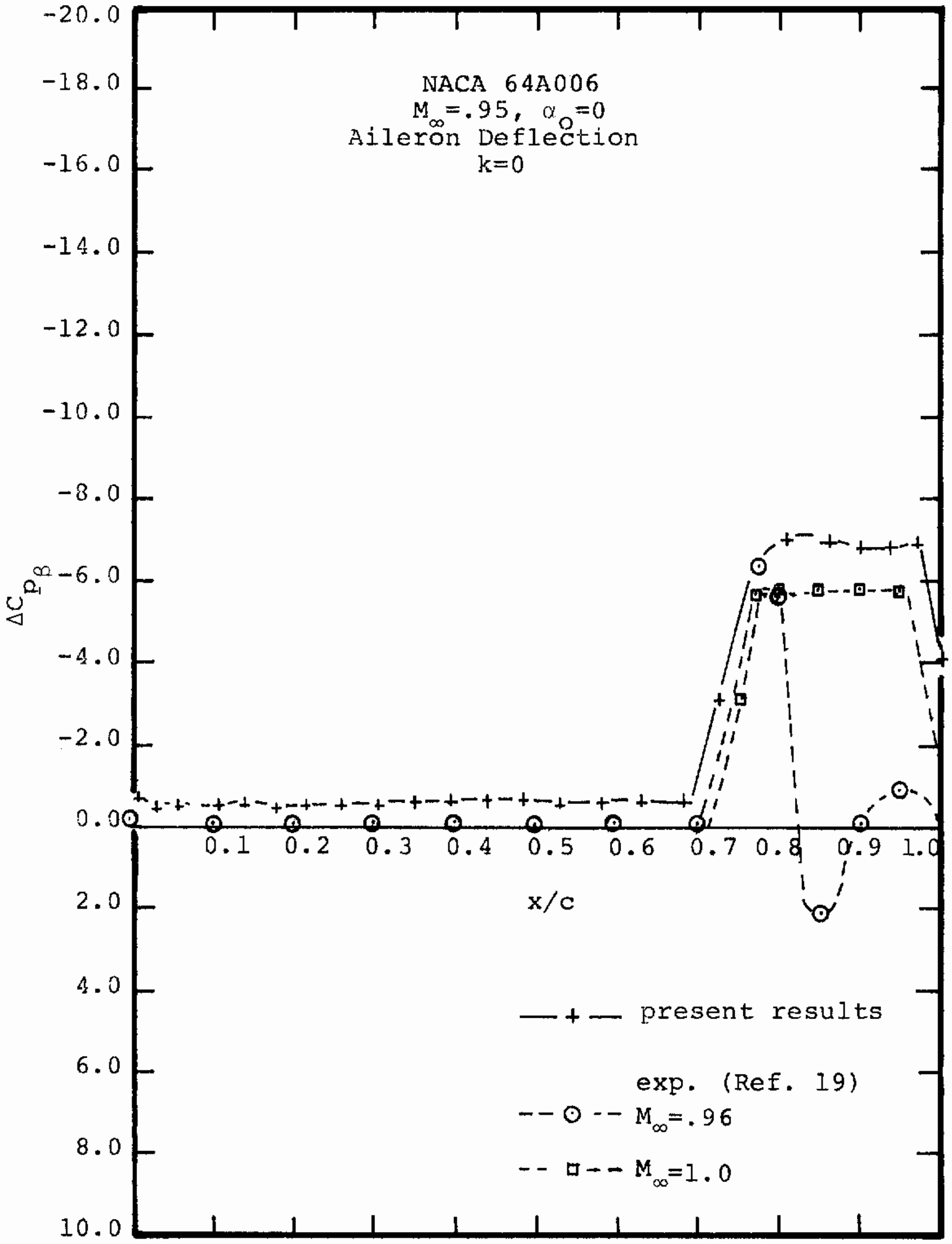

FIGURE 46. AIRFOIL PRESSURE DISTRIBUTION DUE TO AILERON DEFLECTION

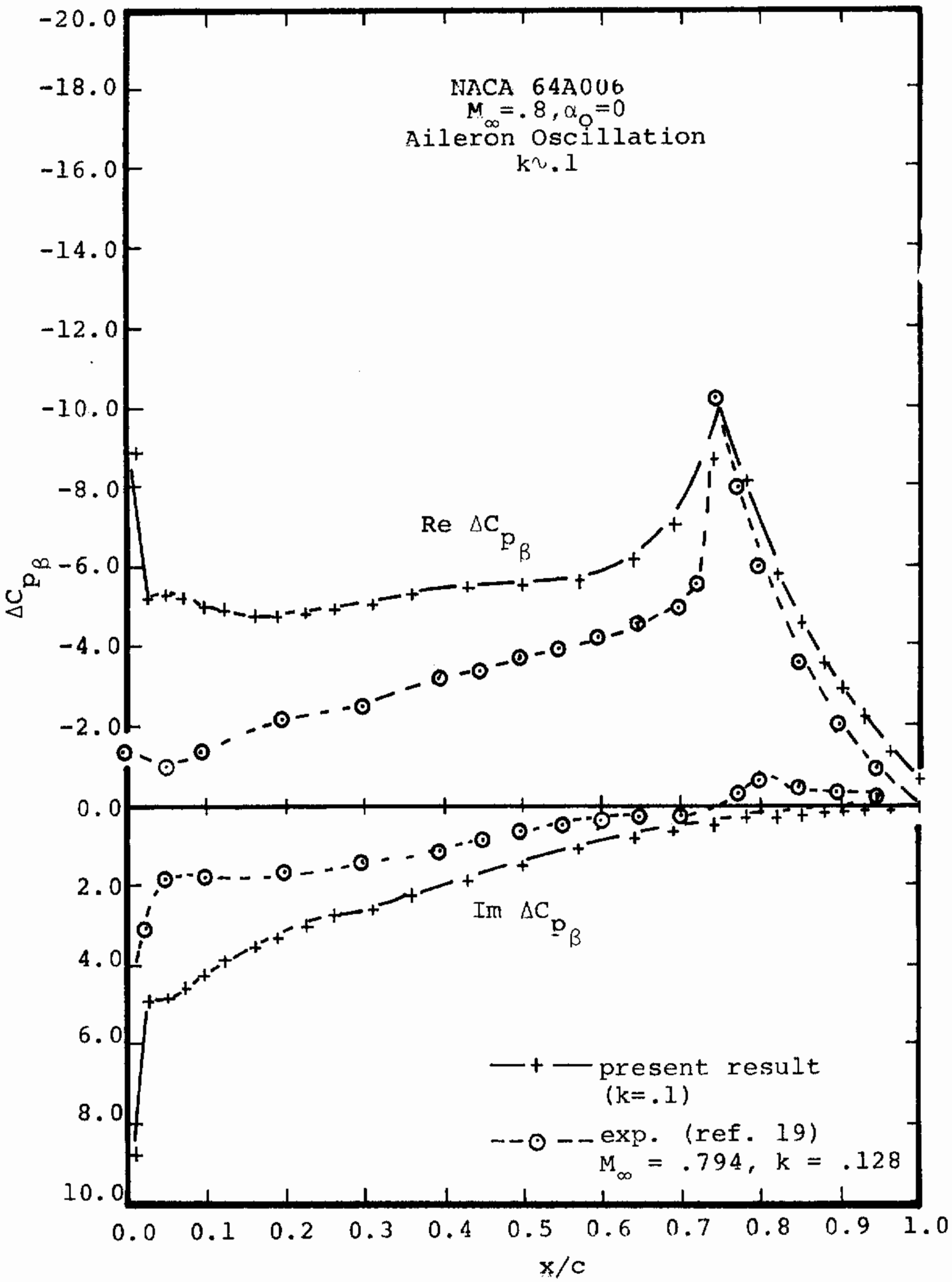

FIGURE 47. AIRFOIL PRESSURE PERTURBATION DUE TO AILERON OSCILLATION

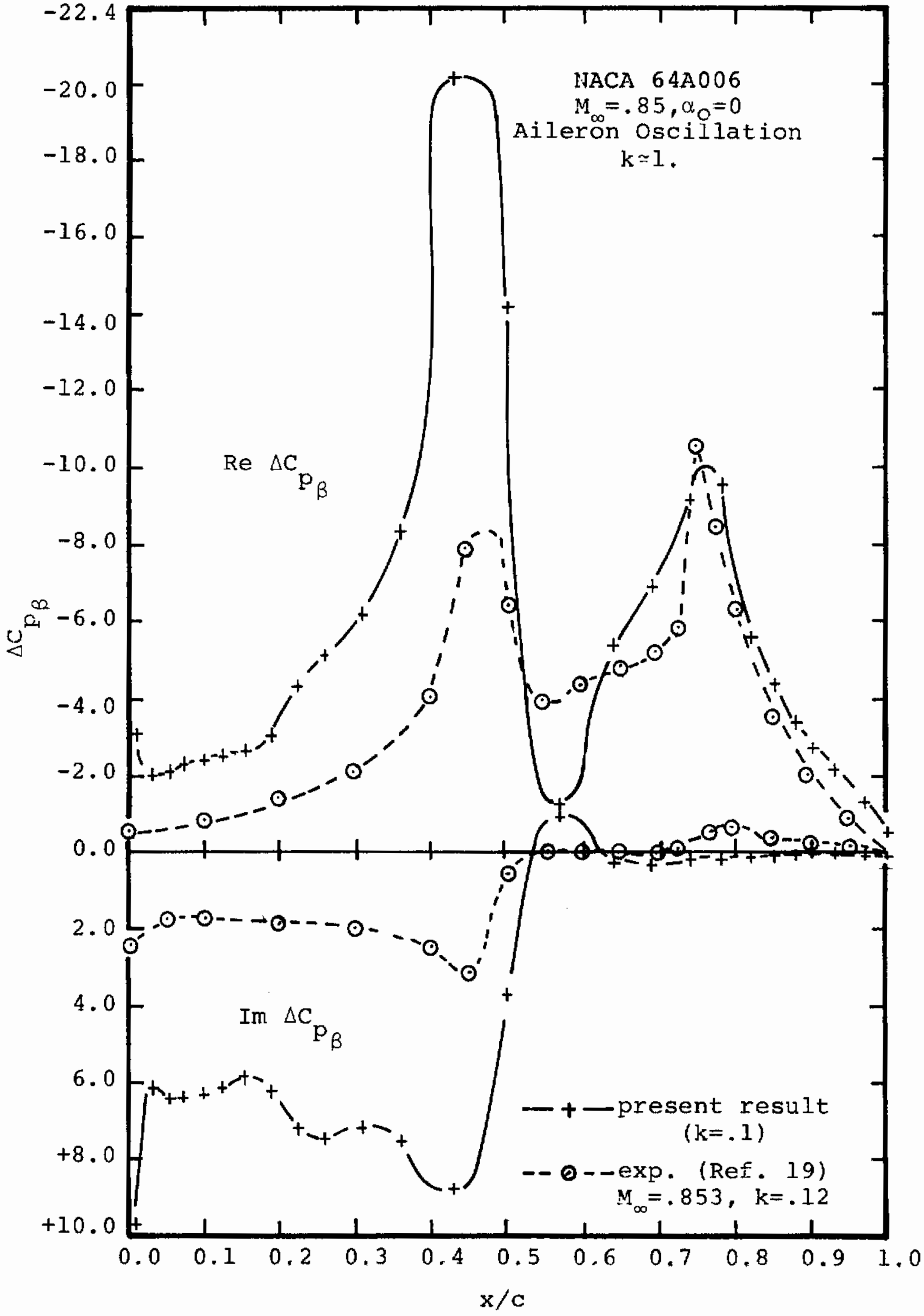

FIGURE 48. AIRFOIL PRESSURE PERTURBATION DUE TO AILERON OSCILLATION

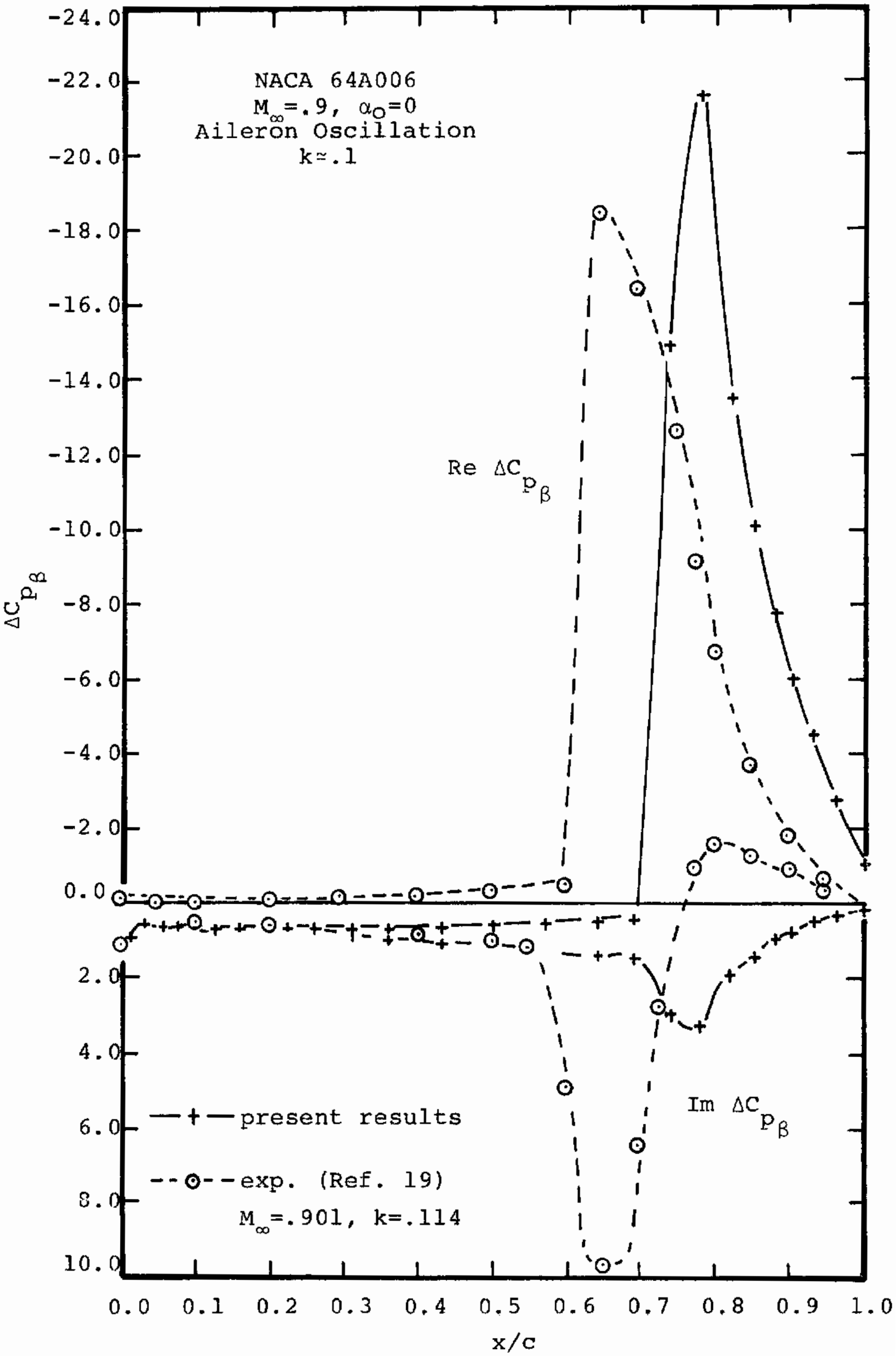

FIGURE 49. AIRFOIL PRESSURE PERTURBATION DUE TO AILERON OSCILLATION

6.1.2 Summary of Unsteady Aerodynamic Coefficients

To perform the transonic flutter analysis of Section 7.0, unsteady aerodynamic coefficients for pitch, plunge and control surface oscillations have had to be generated for the Mach number range $M_\infty = .8$ to 1.2 and low reduced frequency range ($k = 0.0$ to 0.2). The results were calculated as unsteady perturbations to the zero angle of attack steady solutions presented above. The resulting unsteady aerodynamic coefficients for each degree of freedom are presented in this section in graphical form as functions of freestream Mach number for each reduced frequency considered. The definitions used for the coefficients are believed consistent with the American literature and are defined in detail in Appendix B, which also contains tables of the numerical results.

The entire matrix of cases for this airfoil involved approximately 110 separate and distinct steady and unsteady calculations. This matrix of calculations required, by conservative estimate, approximately 1.25 hours of CDC 7600 time. This is a better measure of the efficiency and utility of the method than quoting the often widely varying run time for an individual case. It also indicates that transonic flutter analyses for two-dimensional airfoils are possible with relatively modest expenditures of computer time.

Figures 50 through 59 present a summary of the results for real and imaginary parts of the lift, moment and hinge moment coefficients per unit flap angle, pitch angle, or plunge deflection for the three rigid body degrees of freedom. The figures are presented for completeness and the the readers perusal in total as they point out the important transonic effects on all coefficients. Figure 50, for example, presents the lift coefficient due to control surface oscillation and demonstrates the expected strong nonlinear effects in the transonic regime as well as the large phase shifts in unsteady forces. Portions of the curves between $M_\infty = .95$ and 1.1 are extrapolated due to the inability to perform stable unsteady calculations in this region. For example at $M_\infty = .95$ the numerical method was unstable for $k \geq .1$ and for all reduced frequencies at $M_\infty = 1.05$. The required extrapolations are made with some degree of confidence however because of the "Mach freeze" effect in this region. As discussed just above, the steady calculations for $M_\infty = .95$ and 1.05 show only slight differences in the flow Mach number in the solution field on or near the airfoil so that unsteady perturbations are expected to vary only slightly from the $M_\infty = .95$ or 1.1 results. This should be expecially true for the control surface perturbations as in fact is verified by Figures 50, 51 and 52. Figures 53 through 59 show that the variation in the coefficients between $M_\infty = .95$ and 1.01 for the pitch and plunge modes is, as might be expected, somewhat greater

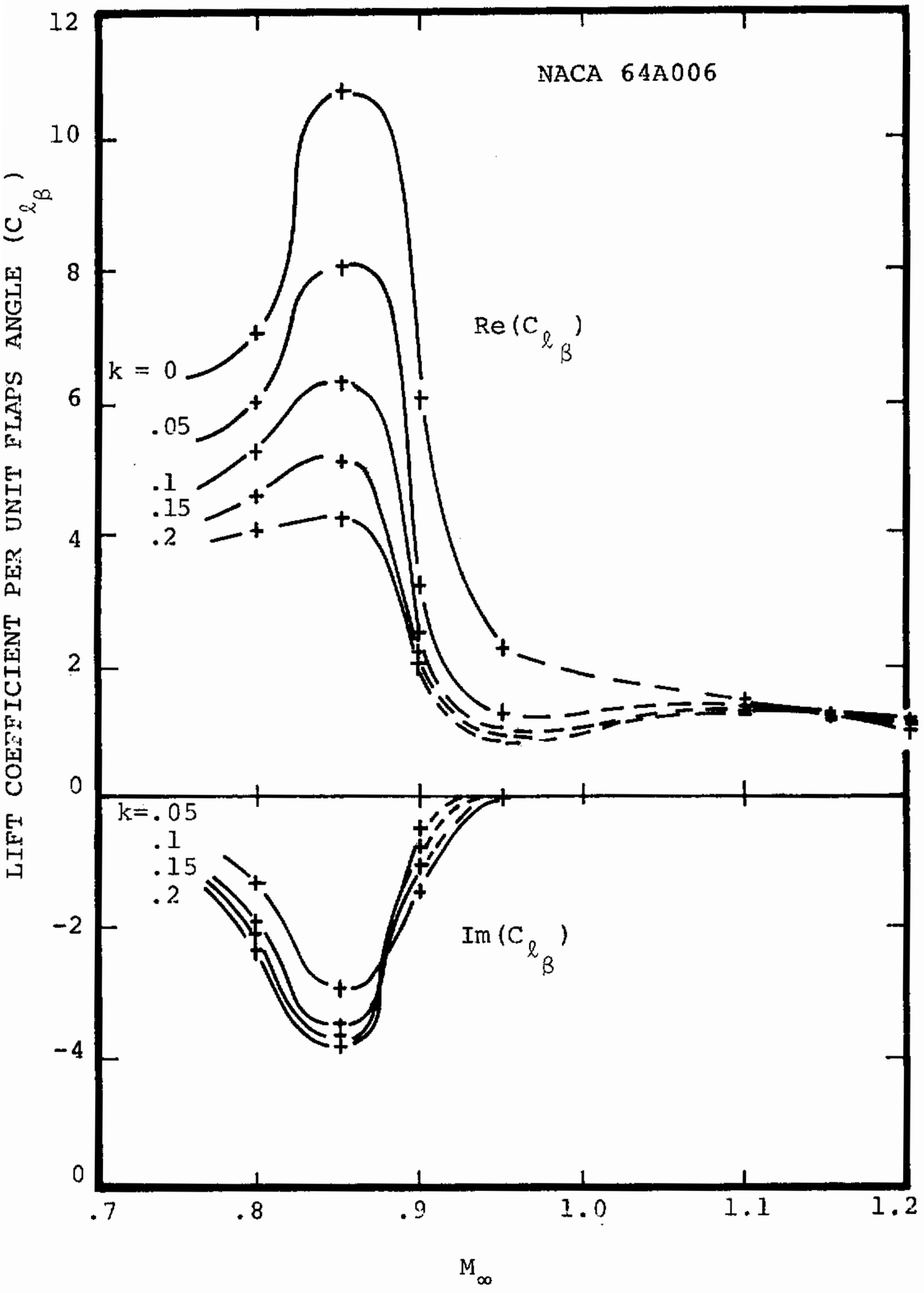

FIGURE 50. LIFT COEFFICIENT DUE TO AILERON OSCILLATION

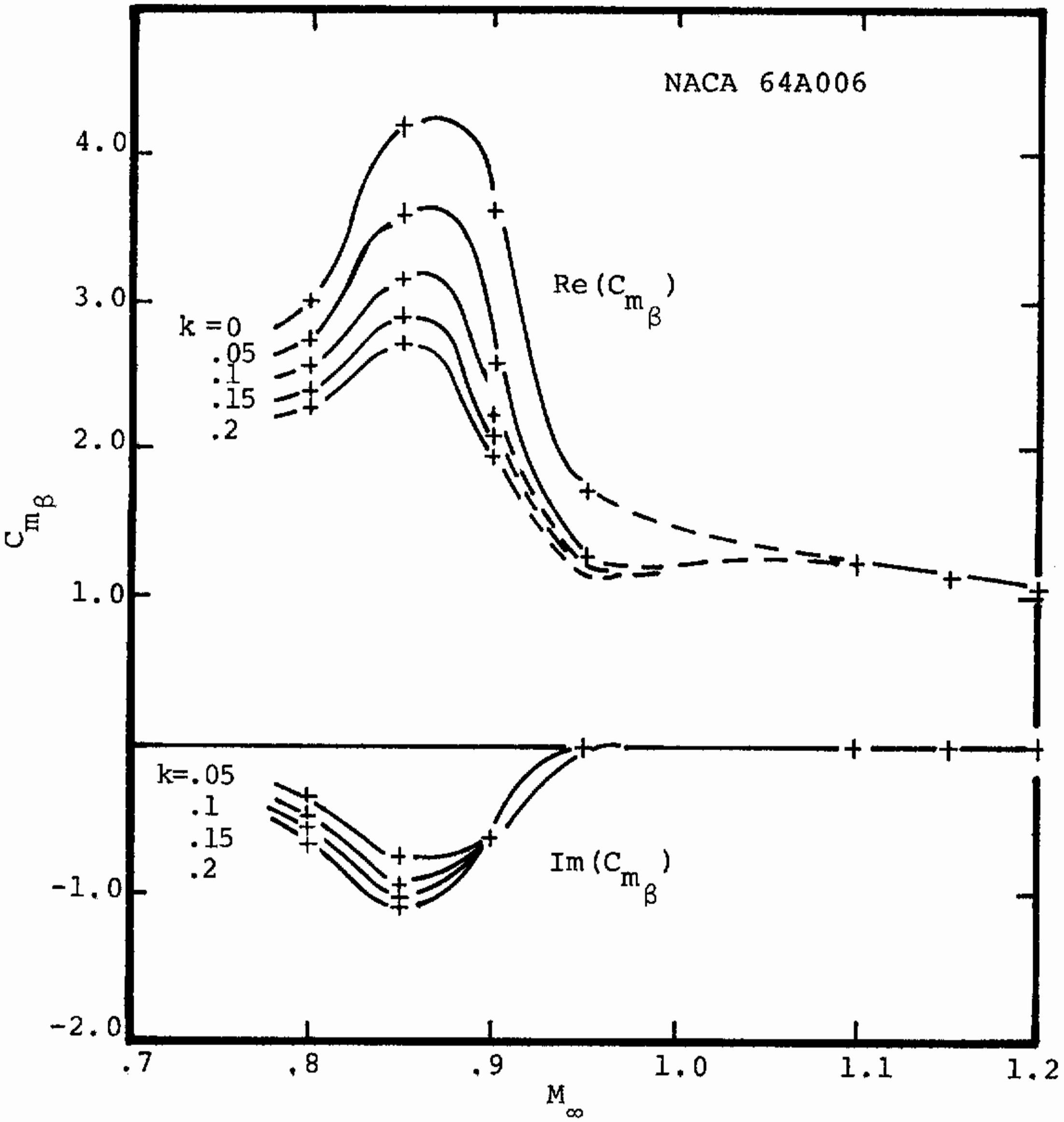

FIGURE 51. MOMENT COEFFICIENT (ABOUT LEADING EDGE) DUE TO AILERON OSCILLATION

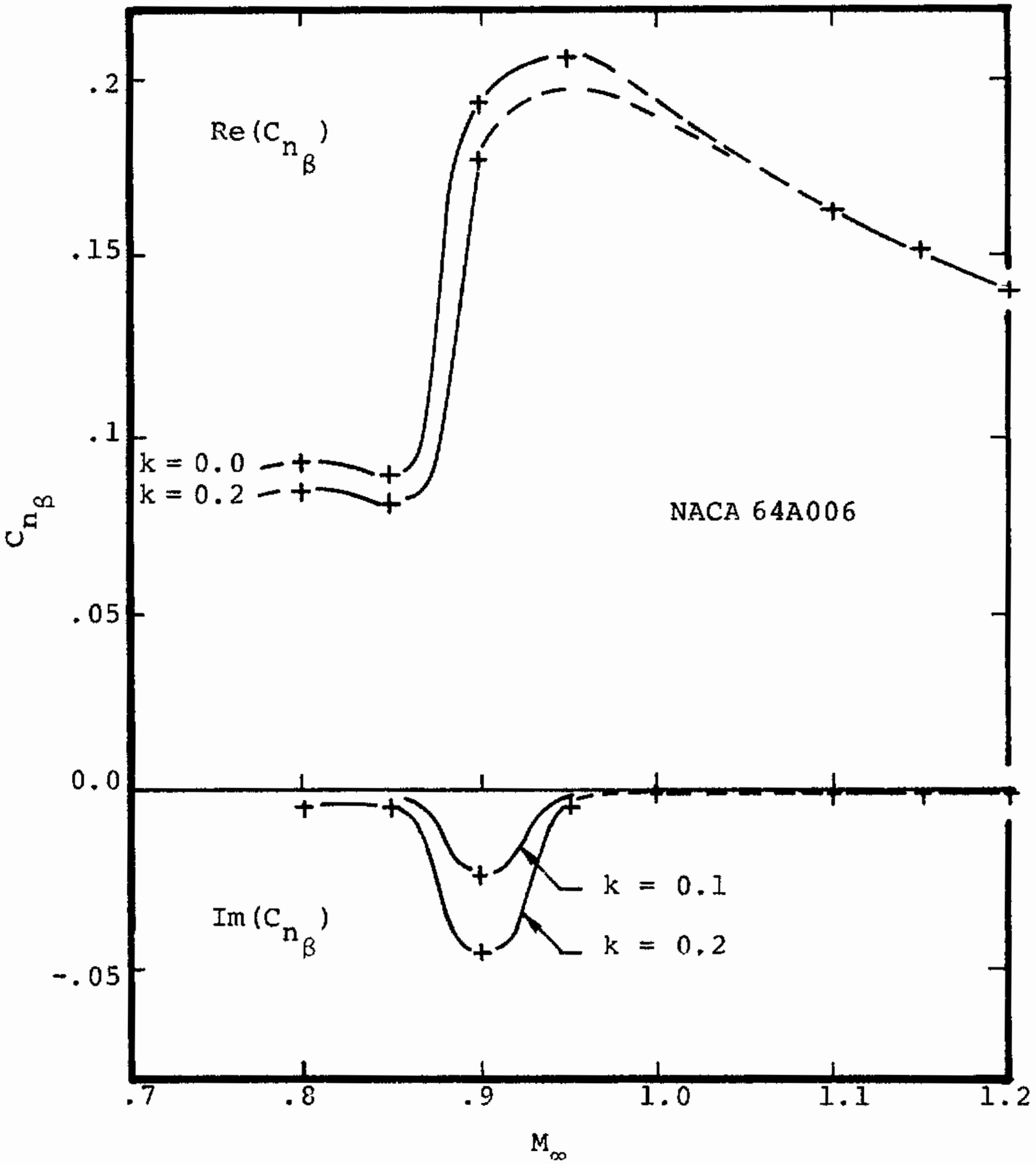

FIGURE 52. HINGE MOMENT COEFFICIENT DUE TO AILERON OSCILLATION

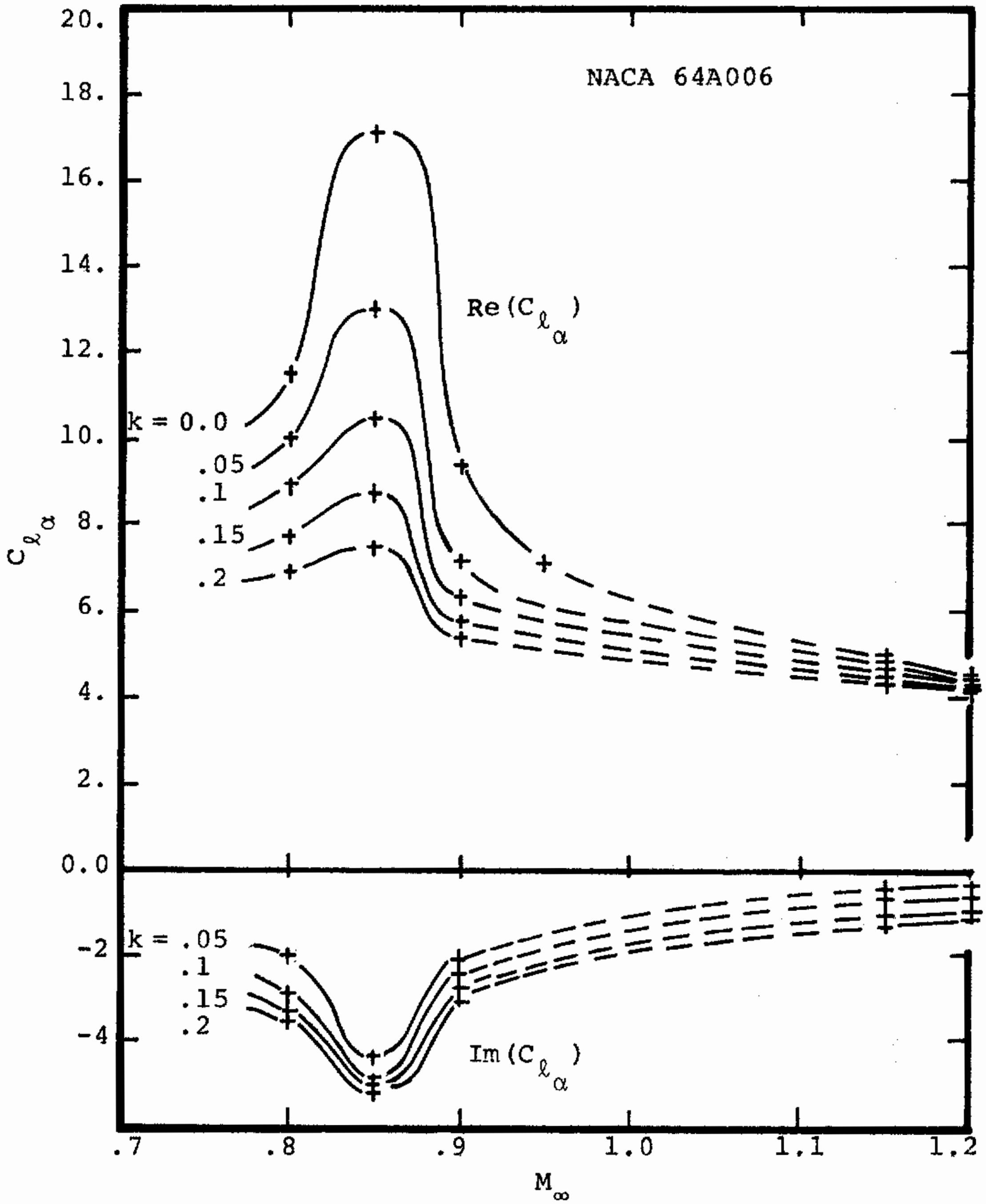

Figure 53. Lift Coefficient Due to Pitching Oscillation

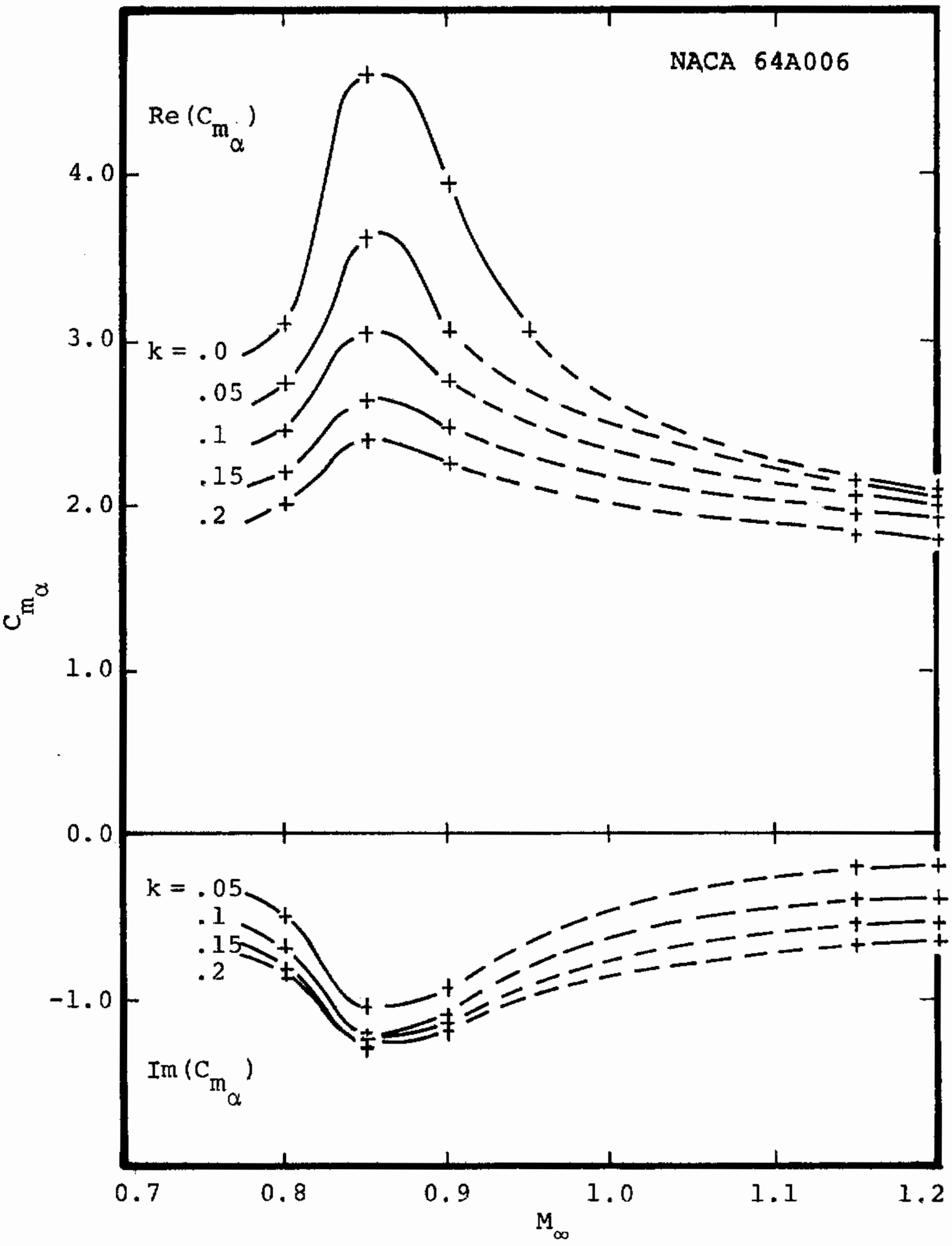

FIGURE 54. MOMENT COEFFICIENT (ABOUT LEADING EDGE) DUE TO PITCHING OSCILLATION

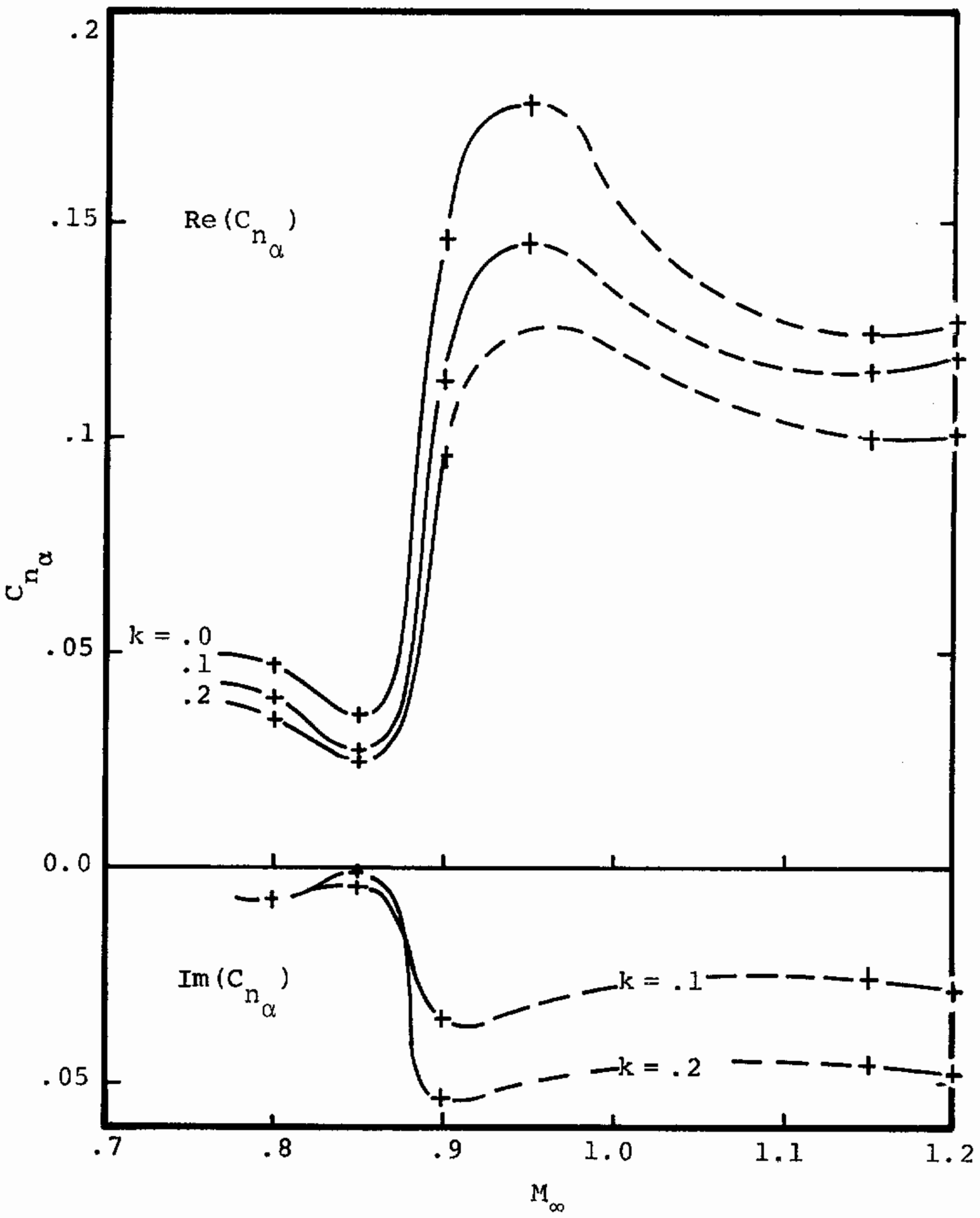

FIGURE 55. HINGE MOMENT COEFFICIENT DUE TO PITCHING OSCILLATION

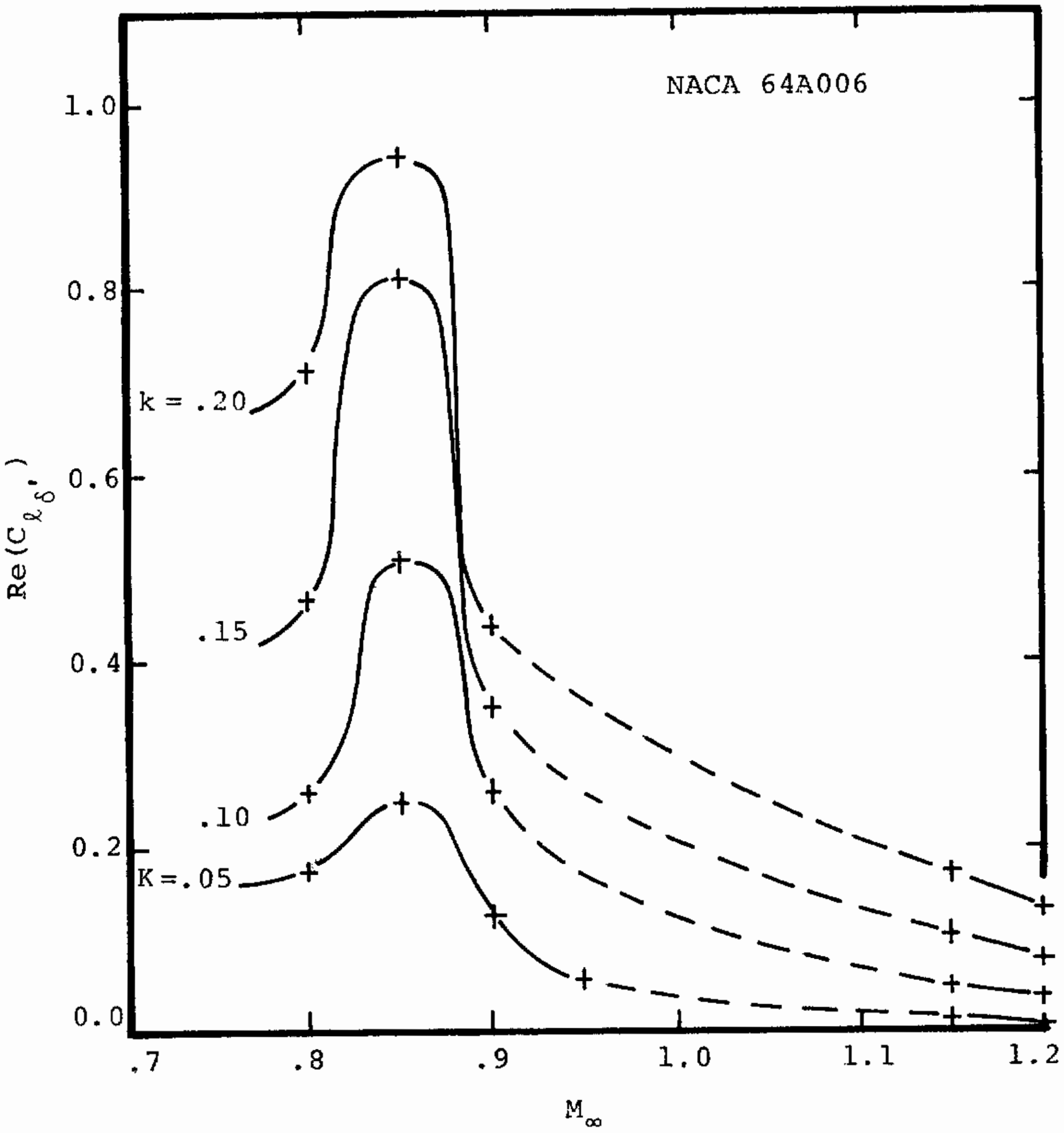

FIGURE 56. LIFT COEFFICIENT DUE TO PLUNGING OSCILLATION

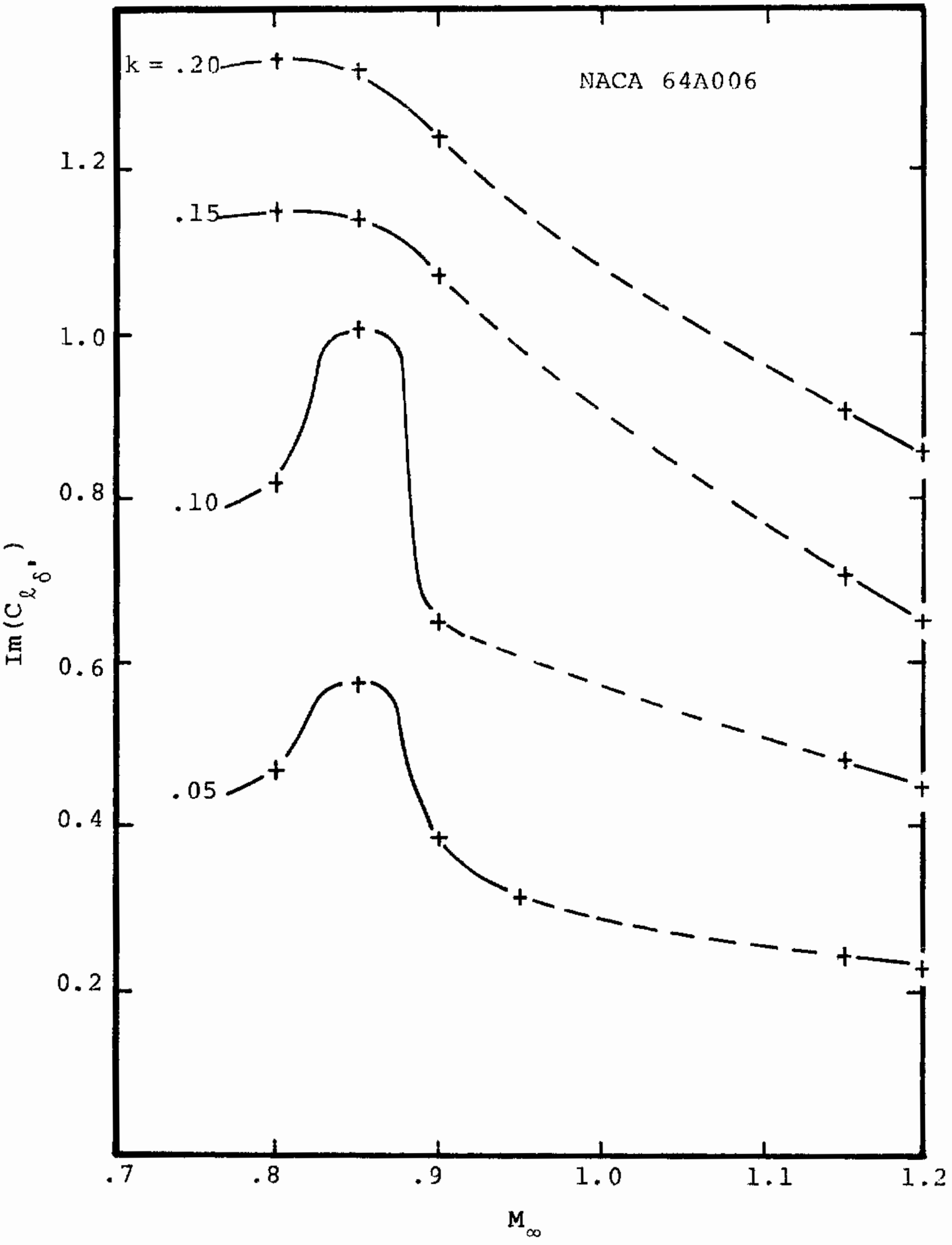

FIGURE 57. LIFT COEFFICIENT DUE TO PLUNGING OSCILLATION

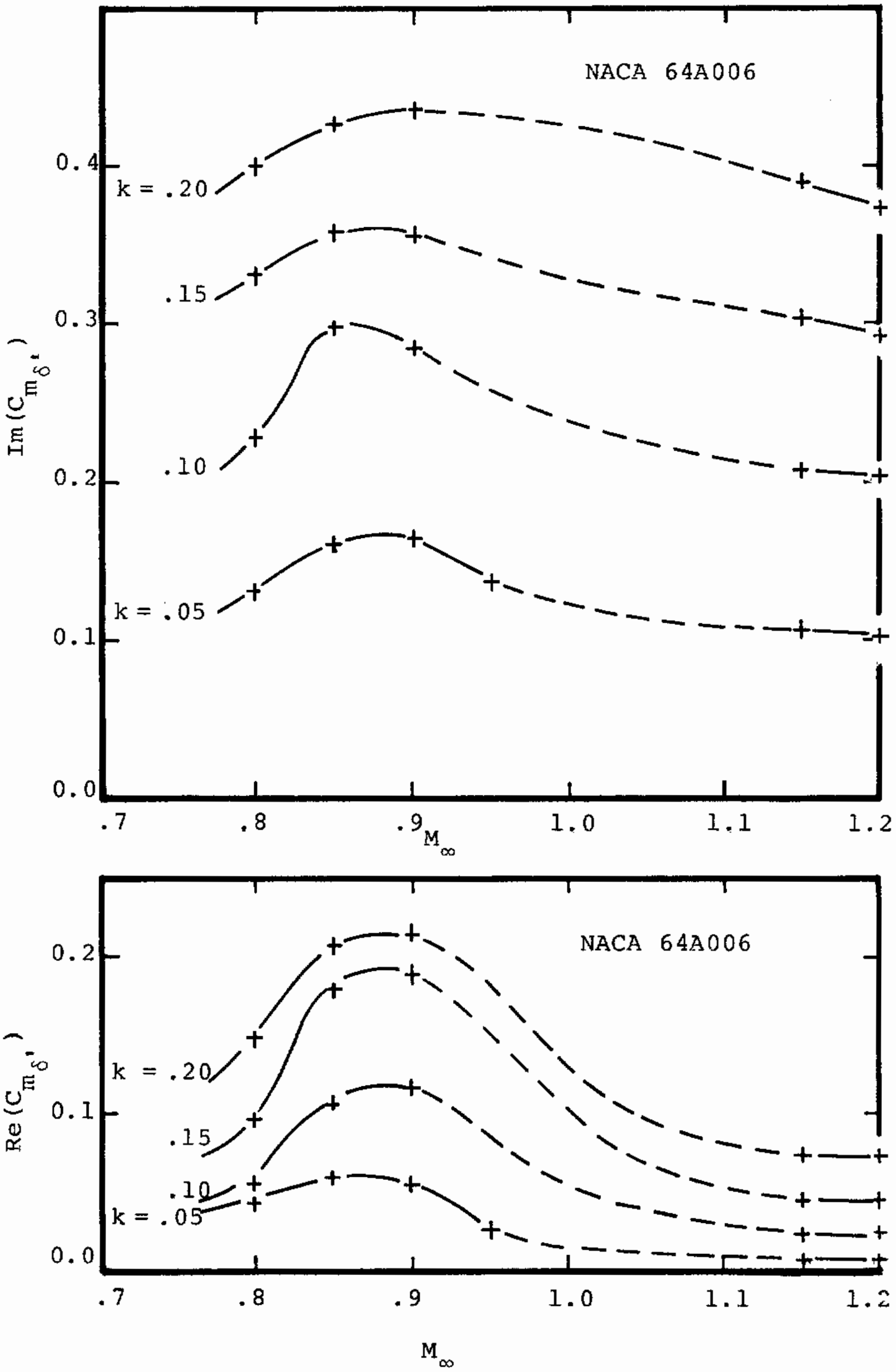

FIGURE 58. MOMENT COEFFICIENT (ABOUT LEADING EDGE) DUE TO PLUNGING OSCILLATION

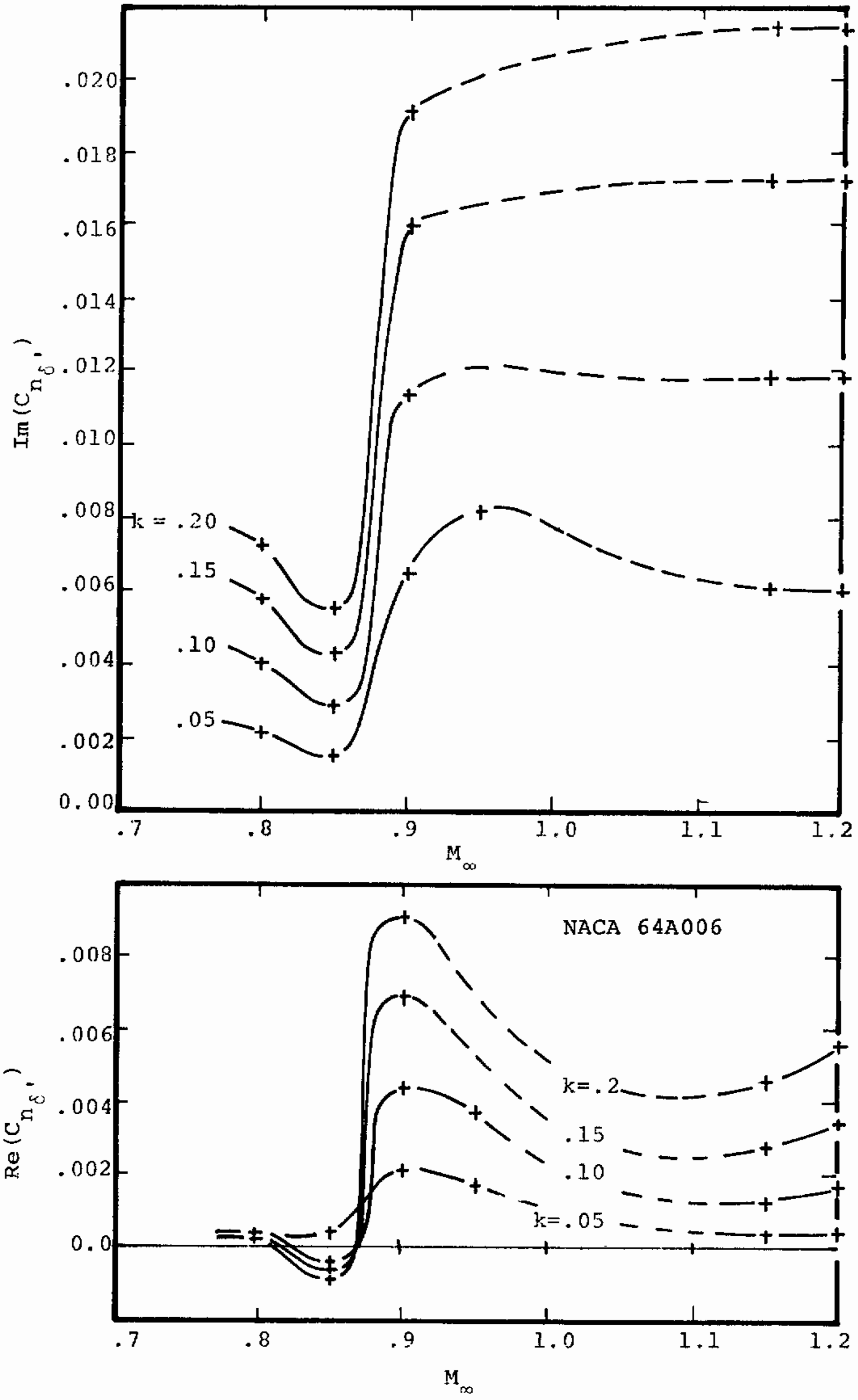

FIGURE 59. HINGE MOMENT COEFFICIENT DUE TO PLUNGING OSCILLATION

6.1.3 Mean Angle of Attack Effects on Unsteady Aerodynamic Coefficients

The basic theory and all of the unsteady results presented in this report indicate and demonstrate that non-uniform mean flow effects dominate the development of the unsteady flow at transonic speeds even in the limit of small unsteady perturbations. This is in contradistinction to the usual experience for subsonic and supersonic flows for which the first order unsteady flow uncouples and is therefore independent of the mean flow. One manifestation of the non-uniform flow effects is the effect of mean airfoil angle of attack (or mean flap angle) which since it may significantly affect the mean flow can therefore influence the resulting unsteady perturbation. This effect is briefly demonstrated here for the NACA 64A006 at a supercritical Mach number of $M_\infty = .85$.

Figure 60 below presents the calculated pressure distribution for this airfoil at $M_\infty = .85$ for mean angles of attack $\alpha_o = 0$, 1^o and 2^o. The figure shows that the upper and lower surface pressure distributions which are identical for $\alpha_o = 0$ (symmetric airfoil) are significantly altered for angles of attack of 1^o and 2^o. As shown, as angle of attack increases, the lower surface becomes subcritical and the upper surface becomes more and more supercritical. Also the relatively weak shock at $\alpha_o = 0$ becomes stronger and moves aft on the upper surface much as it would if the freestream Mach number were increased. It seems clear that this relatively large change in the mean flow will significantly affect the unsteady flow perturbation.

This is indeed shown to be the case in Figure 61, 62, and 63 which present the variation with reduced frequency of the lift, moment and hinge moment coefficients, respectively, due to the oscillating aileron. Results are presented there for 0, 1^o and 2^o mean angle of attack and limited experimental data at zero angle of attack are presented for comparison. The strong reduced frequency effect shown for $C_{\ell\beta}$ and $C_{m\beta}$ and weak dependence for $C_{n\beta}$ are consistent with subsonic linear theory. The primary result of note is the prediction of a substantial mean angle of attack effect. Of some considerable interest to the flutter problem is the change in sign of the imaginary (out of phase) part of the hinge moment due to mean angle of attack. This indicates a potential for one degree of freedom flutter (control surface buzz) due solely to mean airfoil angle of attack; an important result not predicted by linear theory.

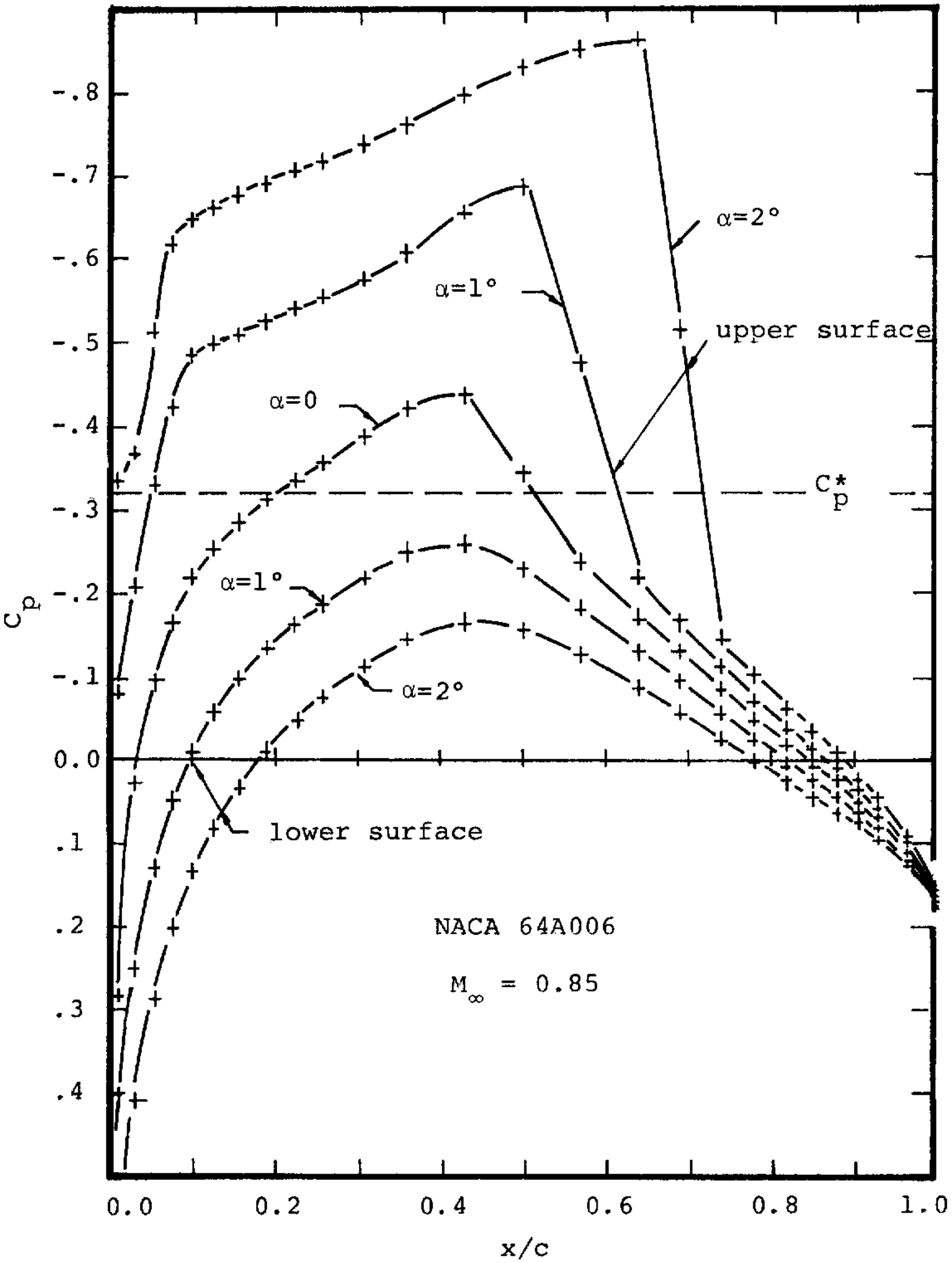

FIGURE 60. STEADY PRESSURE COEFFICIENTS

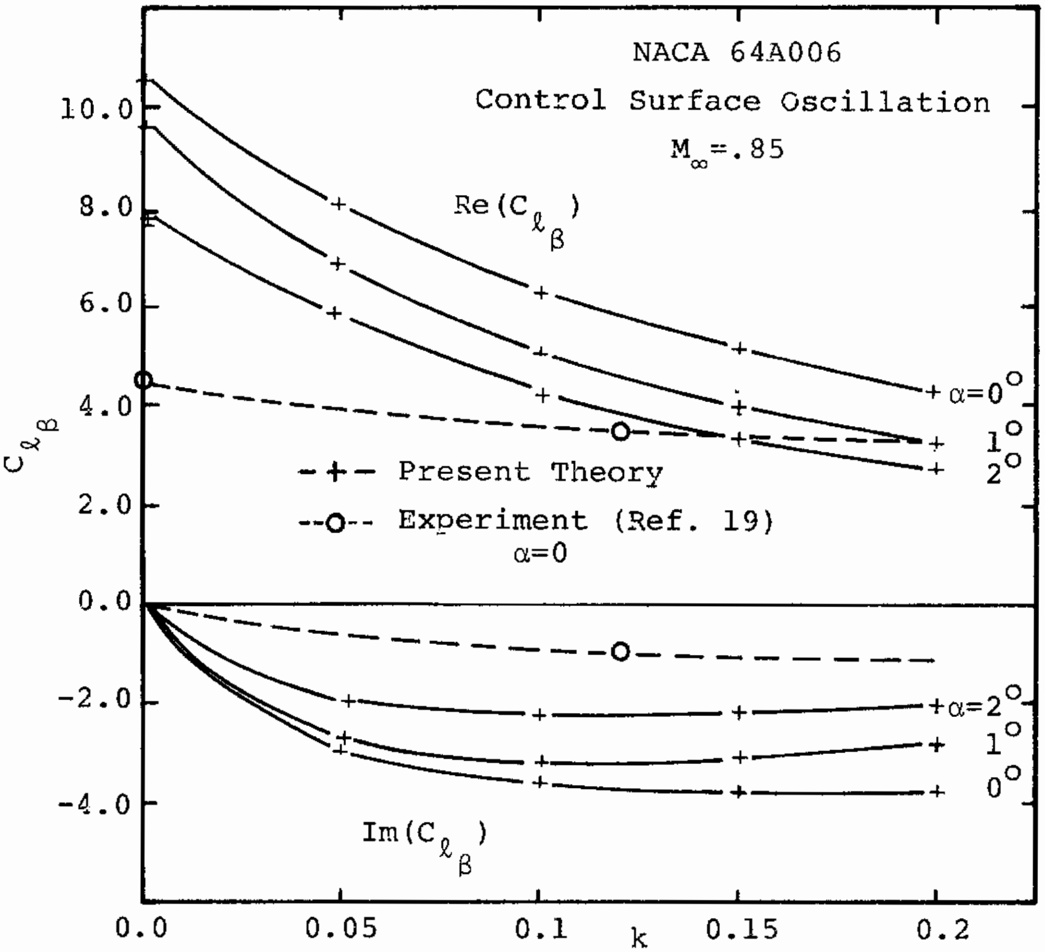

FIGURE 61. MEAN ANGLE OF ATTACK AND REDUCED FREQUENCY EFFECT ON LIFT COEFFICIENT

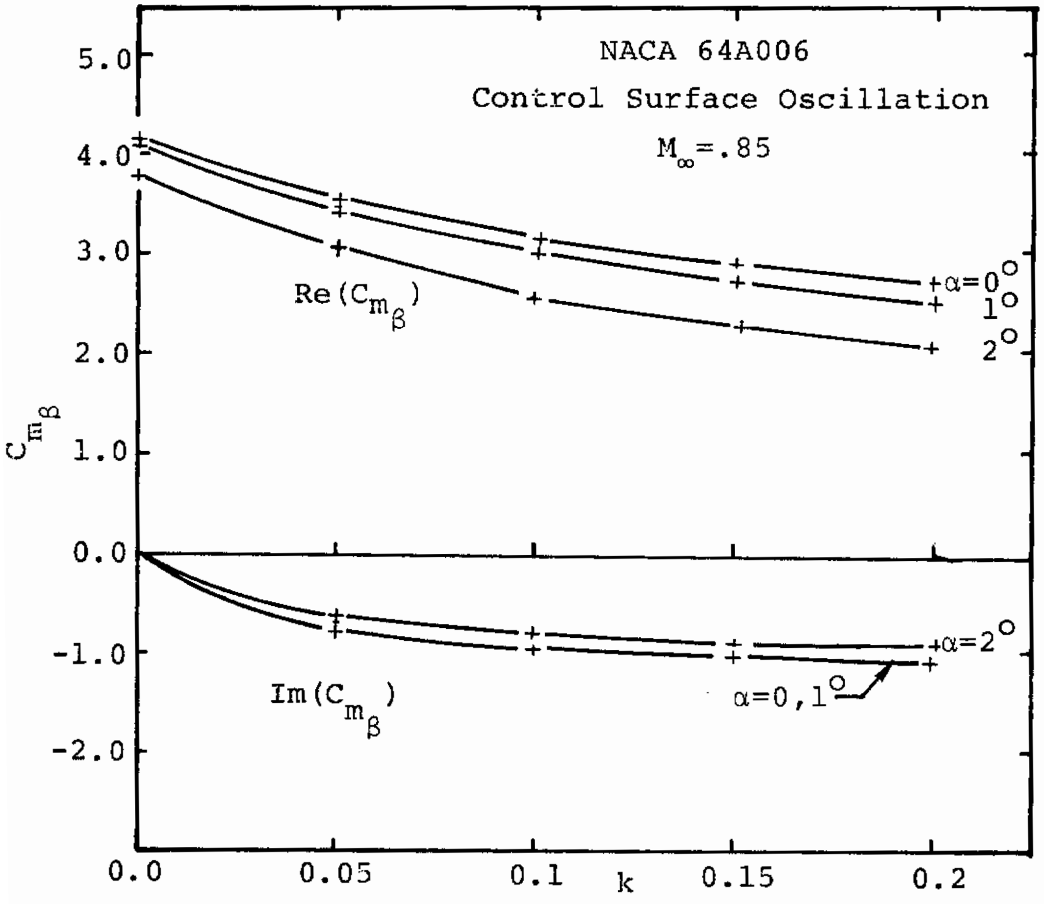

FIGURE 62. MEAN ANGLE OF ATTACK AND REDUCED FREQUENCY EFFECT ON MOMENT COEFFICIENT (ABOUT LEADING EDGE)

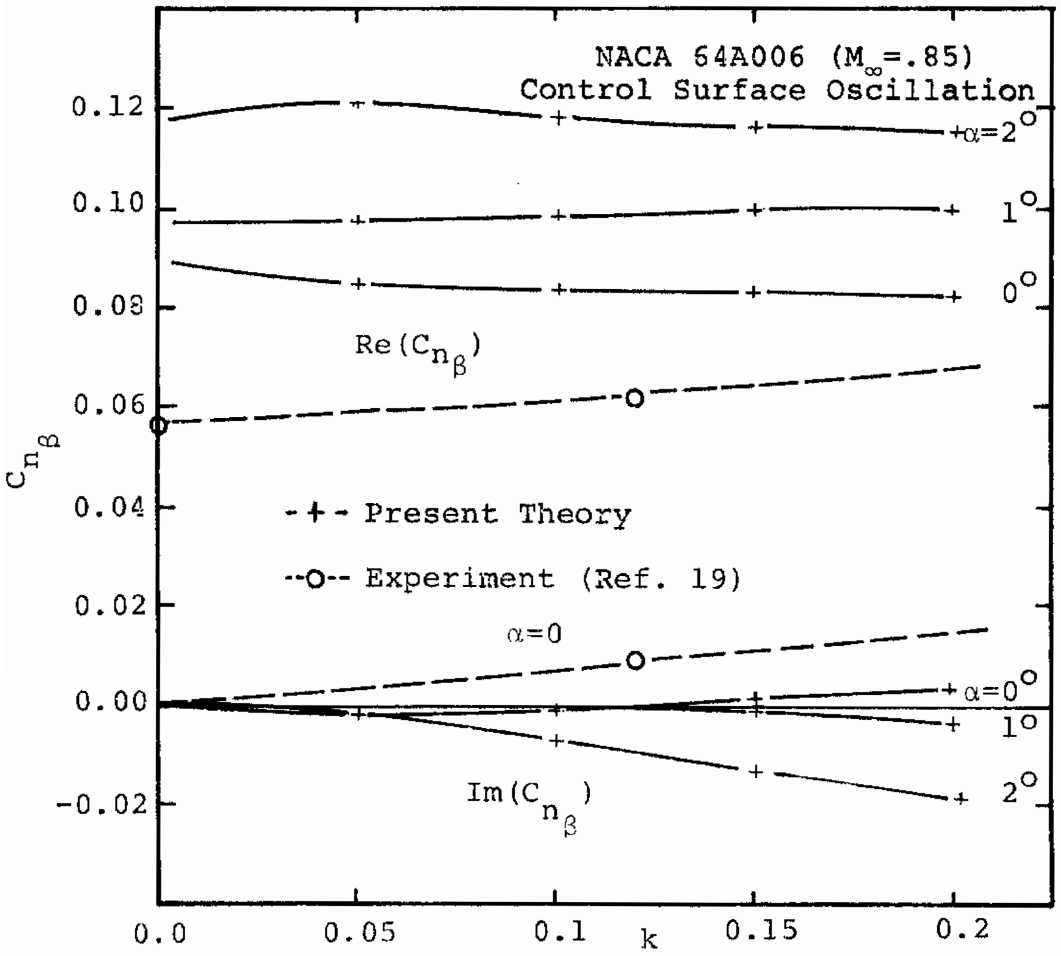

FIGURE 63. MEAN ANGLE OF ATTACK AND REDUCED FREQUENCY EFFECT ON HINGE MOMENT COEFFICIENT

6.1.4 Wall Interference Effects on Unsteady Aerodynamic Coefficients

The extentions of the steady and unsteady flow solution method to include wall effects were described above in Section 3.3. In this section the capability is used to briefly examine the potential effect of the wind tunnel configuration used in the Tijdeman et al. experiments on their results.

The approximate modeling of the wall boundary condition was discussed in the earlier section and steady and quasi-steady perturbation results for the NACA 64A006 were presented there. These results indicated that although the effect of the walls was appreciable there was little difference between solid and the slotted wall results. Also as shown there the inclusion of wall effects seemed in fact to increase the discrepancy with experiment with respect to the important peak pressure perturbation through the shock (re: Figure 18). This is shown in Figure 64 below which essentially repeats Figure 18 with the addition of experimental data for the same airfoil and a quasi-steady aileron deflection at $M_\infty = .875$. As shown in Figure 64 the addition of the slotted walls reduces the agreement with the data with respect to location and magnitude of the peak pressure through the shock but enhances the agreement with respect to the depressed pressure perturbation forward of the peak. The reasons for the difference between the free air and the wall solution can be explained almost entirely by the effect of the walls on the corresponding steady solution. That is, the effect of the wall is to strengthen the shock and move it aft on the airfoil hence the enhanced perturbation pressure through the shock and the aft location with respect to the free air result. The depressed perturbation forward of the peak is due to the stronger shock and larger supersonic region in the steady wall solution, both of which have the effect of decreasing the signal which reaches the forward part of the airfoil from the control surface.

The data at $M_\infty = .875$ is added to present a possible explanation for the discrepancy between the present results and the data. Although it may be fortuitous, the comparison of the present porous wall results at $M_\infty = .85$ and the data at $M_\infty=.875$ is very good with the exception of an overprediction of the magnitude of the perturbation through and just aft of the shock. As discussed earlier, the inviscid small disturbance steady results are almost without exception more supercritical than the corresponding experimental results. This is usually attributed to the effect of viscosity, neglected in the theory, which has the effect of weakening and moving the inviscid shock forward on the airfoil. If this one comparison is to be believed, a possible alternative to the viscous coupling suggested above would be to include wall effects in the inviscid theory and to account for viscosity as an effective "shift" in the Mach number for comparison to experimental data. This could clearly only be done apriori and of course would reduce the practical utility of the method.

Figures 65, 66, and 67 are presented to show the effect of solid or ventilated walls on the lift coefficient due to control surface, pitch and plunge oscillations respectively. As shown, the effect is quite appreciable in the low reduced frequency regime. Of some particular note is the fact that the trend with respect to reduced frequency is different for the wall cases as compared to the free air case. This could be due to the fact that the wall cases are effectively for a higher Mach number due to the influence of the walls on the steady flow.

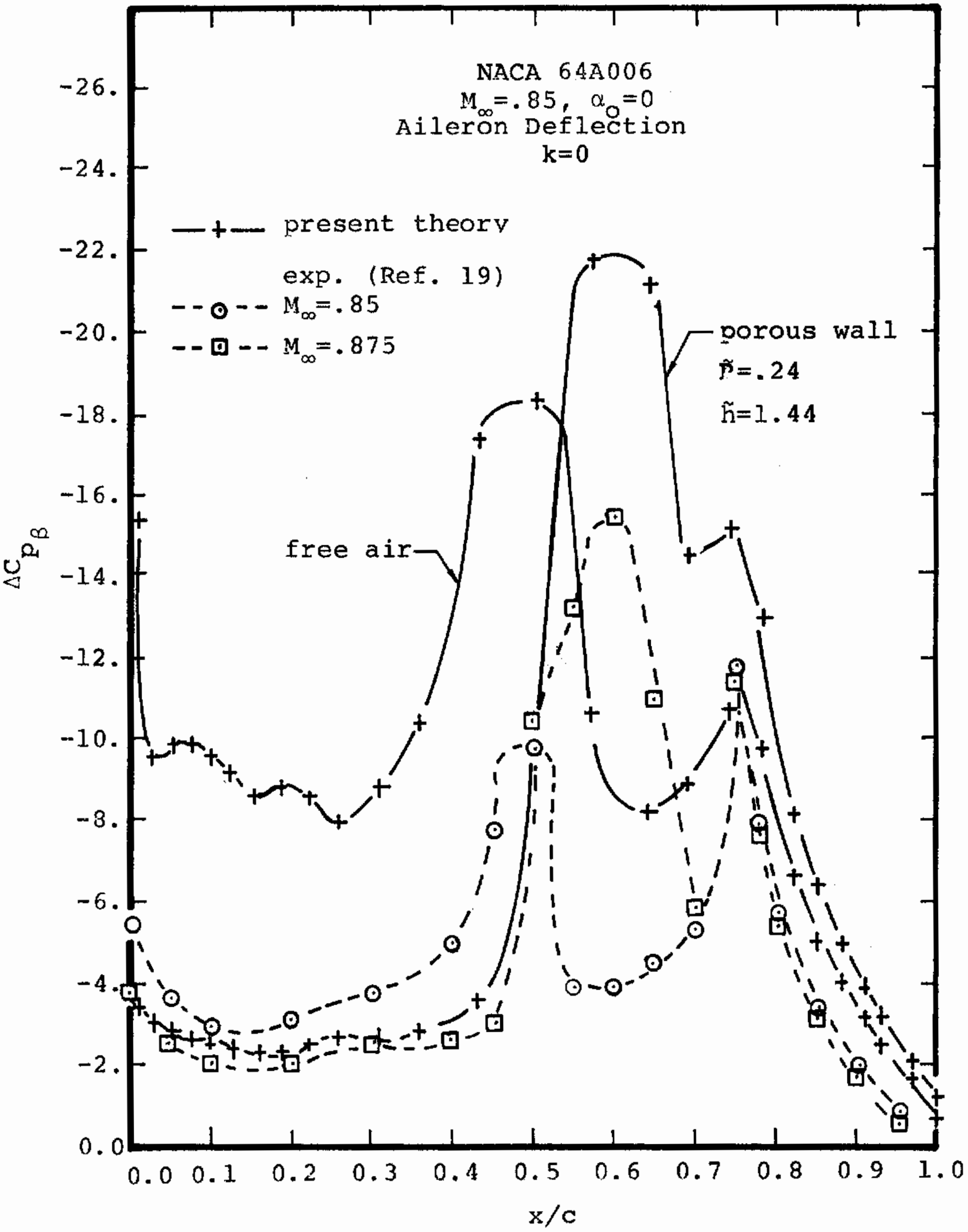

FIGURE 64. EFFECT OF WIND TUNNEL WALLS ON AIRFOIL PERTURBATION PRESSURE

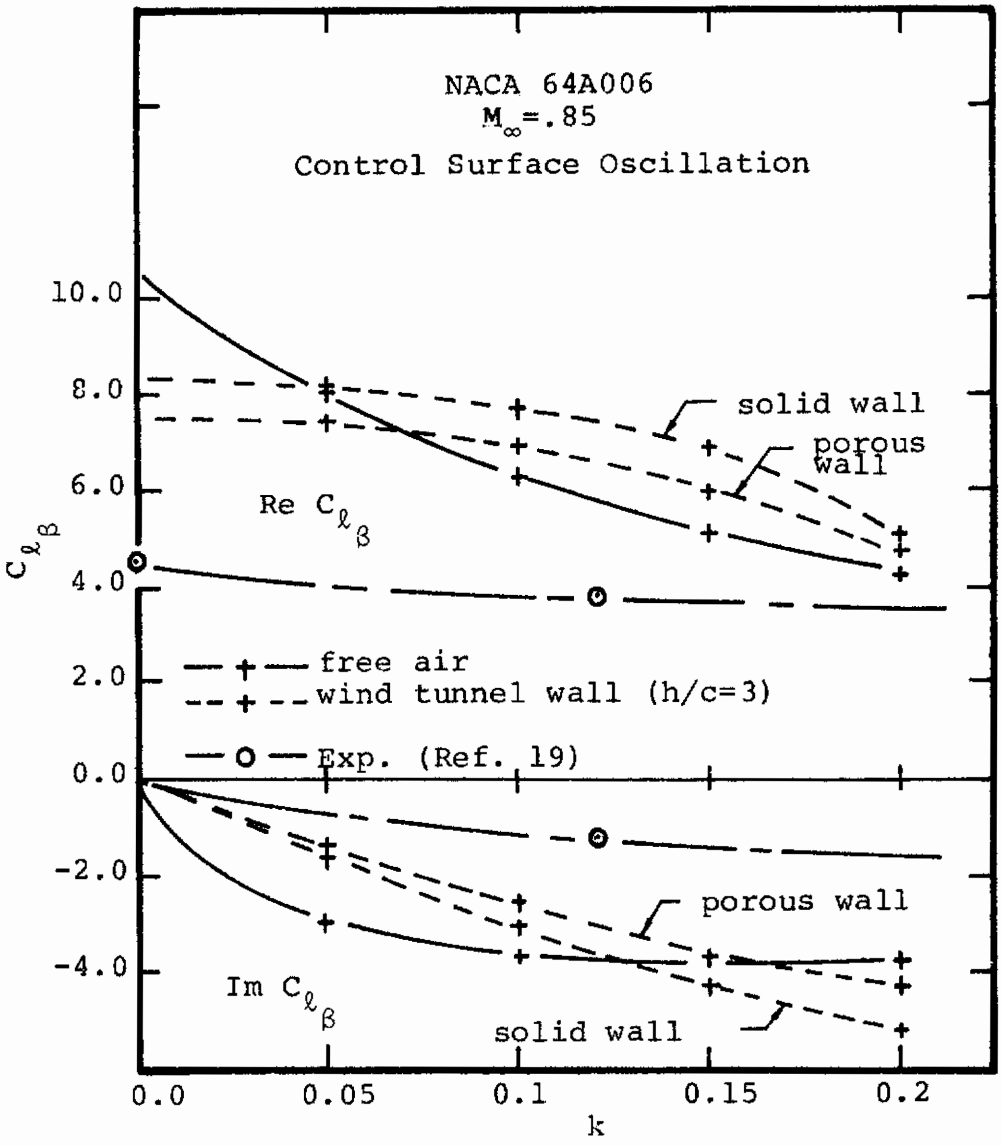

FIGURE 65. WIND TUNNEL WALL AND REDUCED FREQUENCY EFFECT ON LIFT COEFFICIENT DUE TO CONTROL SURFACE ROTATION

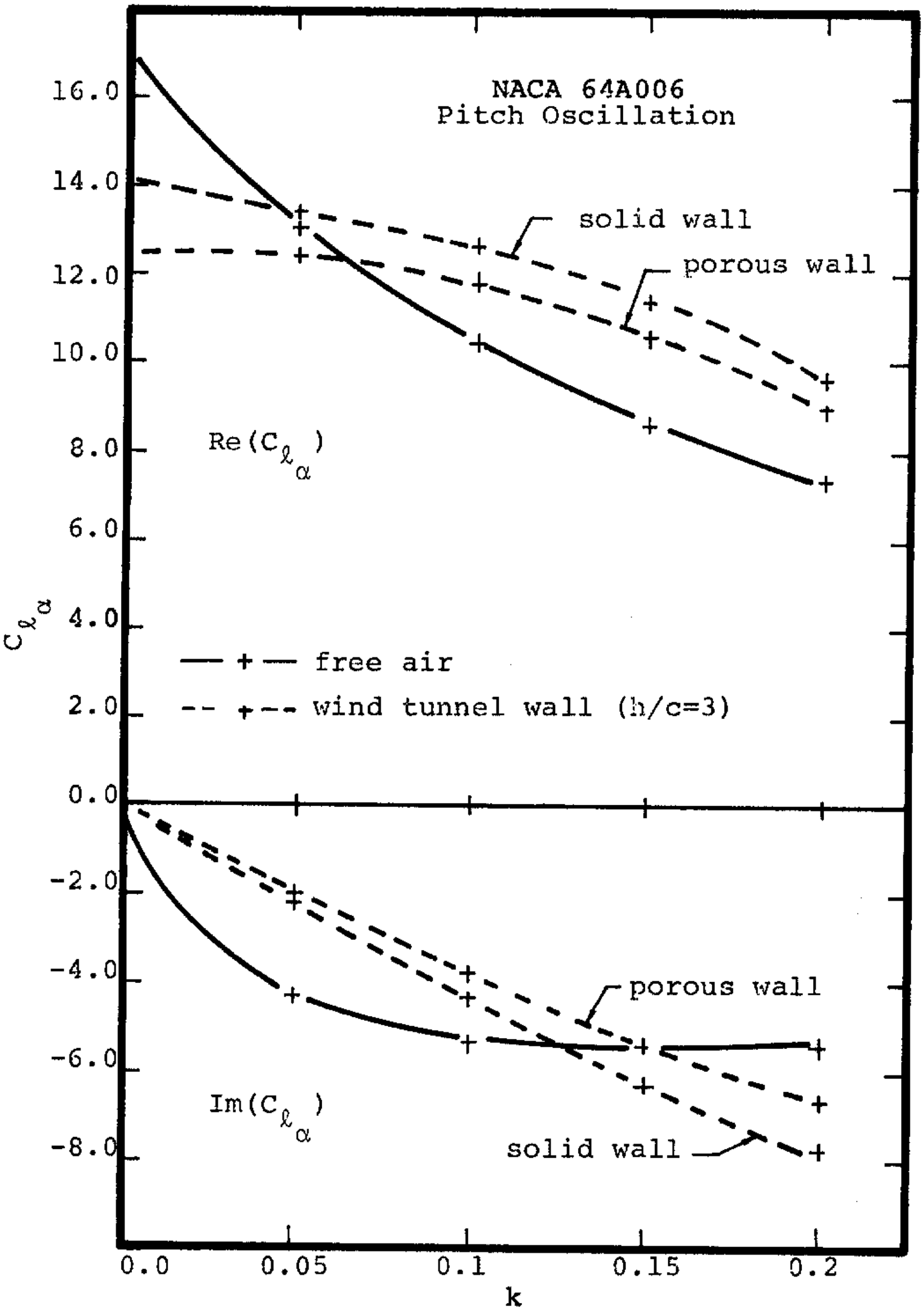

FIGURE 66. WIND TUNNEL WALL AND REDUCED FREQUENCY EFFECT ON LIFT COEFFICIENT DUE TO PITCH

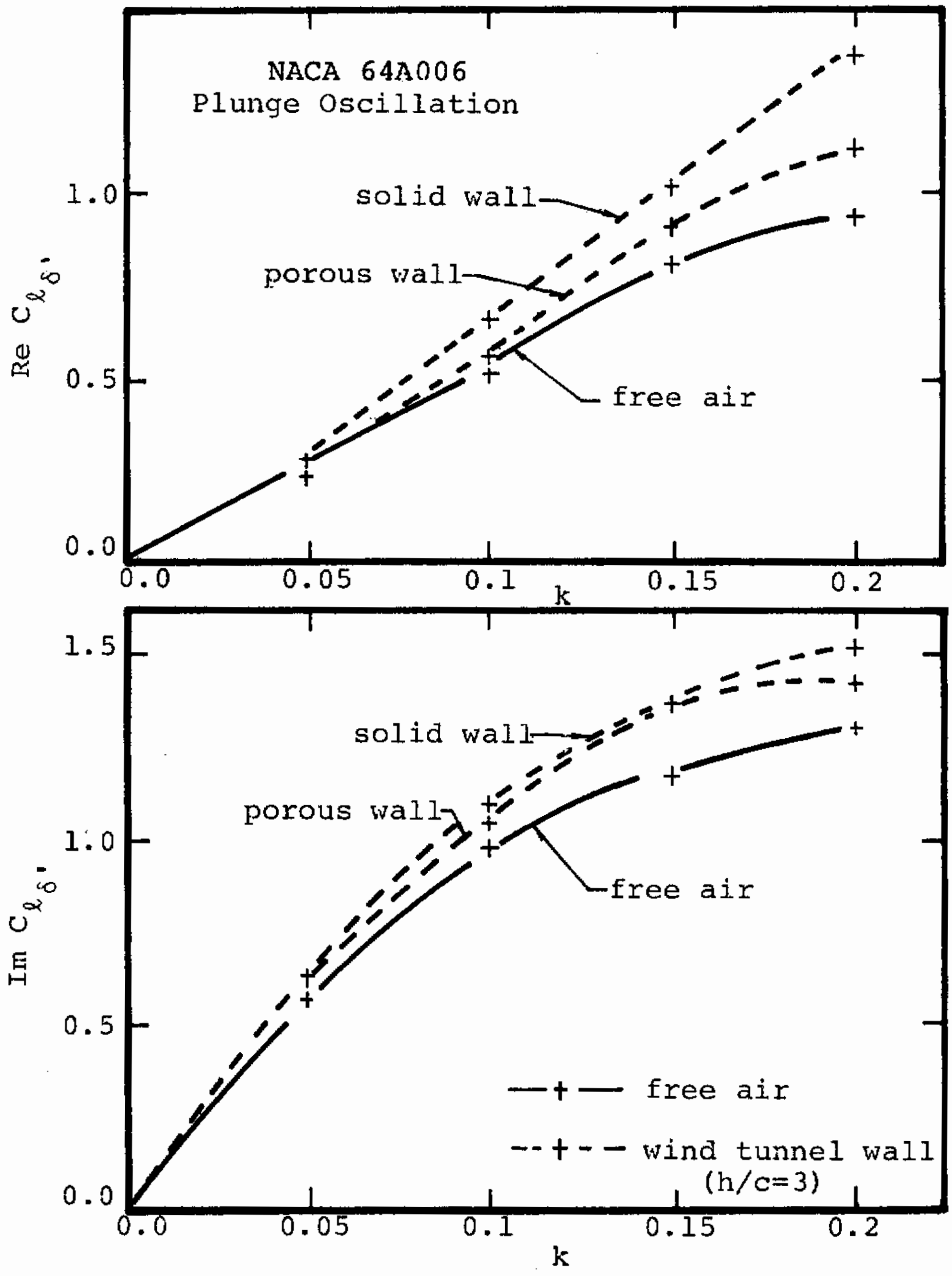

FIGURE 67. WIND TUNNEL WALL AND REDUCED FREQUENCY EFFECT ON LIFT COEFFICIENT DUE TO PLUNGE

6.2 Results for a NACA64A410 Airfoil

Steady and unsteady results are presented in this section for a NACA64A410 airfoil for supercritical Mach numbers. Calculations have been performed for pitch and plunge oscillations at reduced frequencies of k=0 to 0.2 for free air Mach numbers of M_∞=.75, .8 and .9 at zero mean angle of attack and additionally at 1° and 2° angles of attack at M_∞=.8. The solutions for this airfoil follow the same general trends as those already discussed in detail for the NACA64A006 so that the results are presented for completeness with minimal additional comment.

The NACA64A410 airfoil has a 10% thickness and adds the additional variable of a 4% camber, both of which significantly increase the non-uniform flow effects in comparison to the 64A006 which is of the same family of airfoils. The steady results are shown in Figures 68 and 69 below and demonstrate the large supercritical region even at a relatively low Mach number of M_∞=.75. Due to the airfoils non-symetrical shape, there is a relatively large difference between the upper and lower surfaces at zero angle of attack as shown in Figure 68. The results for progressively higher Mach numbers show the strengthening and aft movement of the shock and it is noted that the shock is already at the airfoil trailing edge at M_∞=.85. The results for different angles of attack, given in Figure 69, indicate that at least for small angles of attack the variation of the steady solution is also small due presumably to the fact that the airfoil is already at a relatively large "effective" angle of attack because of its camber. Based on these comparisons it is expected that the unsteady perturbations to these mean flows would show a large Mach number variation but perhaps a small effect of angle of attack. A table of the calculated steady lift coefficients is presented below for all the cases calculated. The values demonstrate the large transonic flow effect on lift. In particular the zero angle of attack lift is shown to peak at about M_∞=.85 and to decrease significantly at M_∞=.9.

	FREESTREAM MACH NUMBER					
	.75	.80			.85	.9
	$\alpha_0=0$	$\alpha_0=0$	$\alpha_0=1^0$	$\alpha_0=2^0$	$\alpha_0=0$	$\alpha_0=0$
C_ℓ	.625	.715	.918	1.047	.773	.305

Table 2. Lift Coefficients for NACA 64A410

The results for unsteady lift and moment coefficients due to pitch and plunge perturbations to the above steady solutions are presented in Figures 70 through 73. The reduced frequency variation of the various coefficients as shown in the figures, is typical of those shown previously and again demonstrates the large reduced frequency effect in the low frequency regime. Also of considerable note is the large non-linear effect of mean flow Mach number. Another result not shown is that the efffect of mean angle of attack at M_∞=.8 is quite small. In fact the aerodynamic coefficients vary by only a few precent for angles of attack between 0 and 2^o.

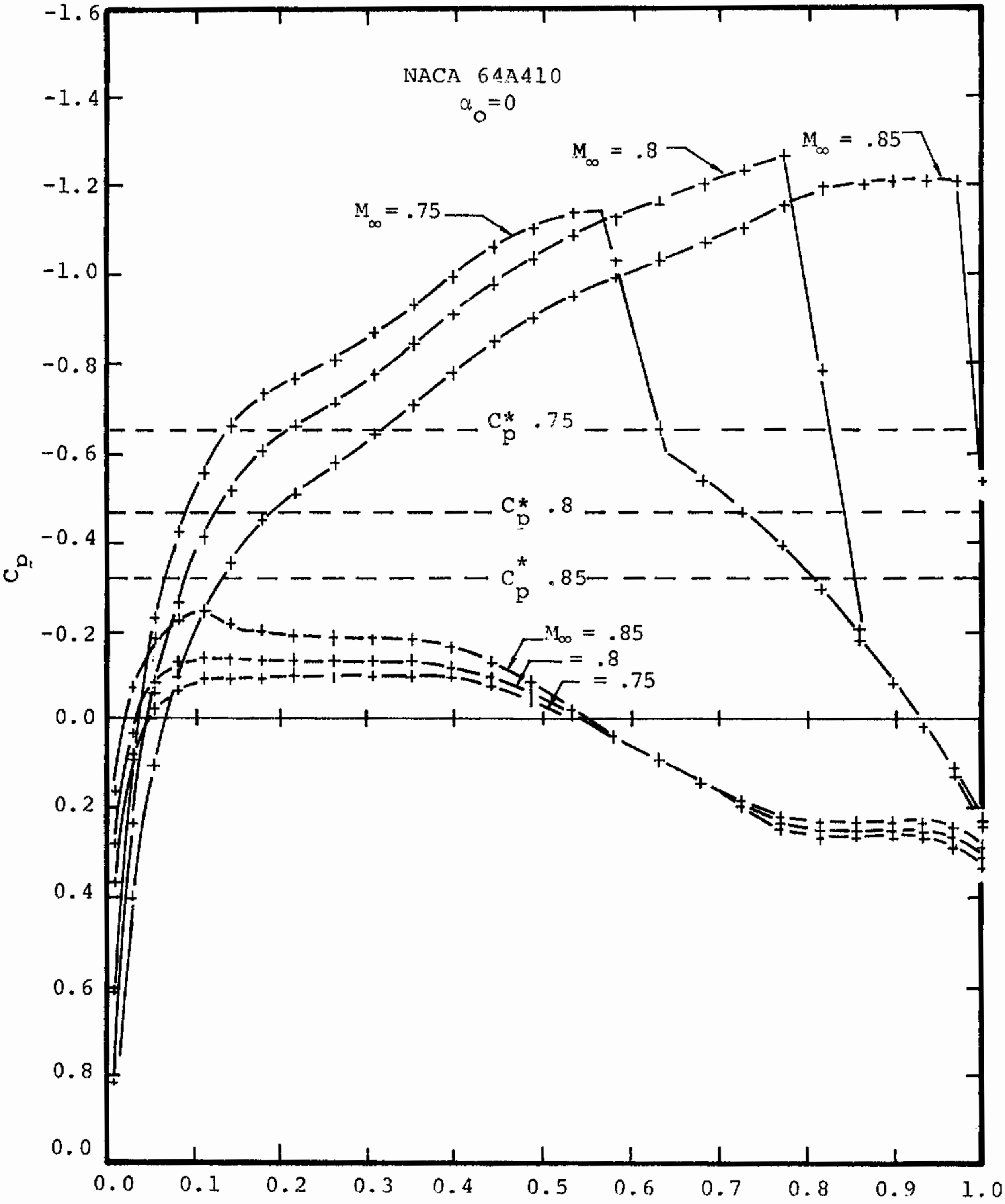

FIGURE 68. STEADY PRESSURE DISTRIBUTIONS

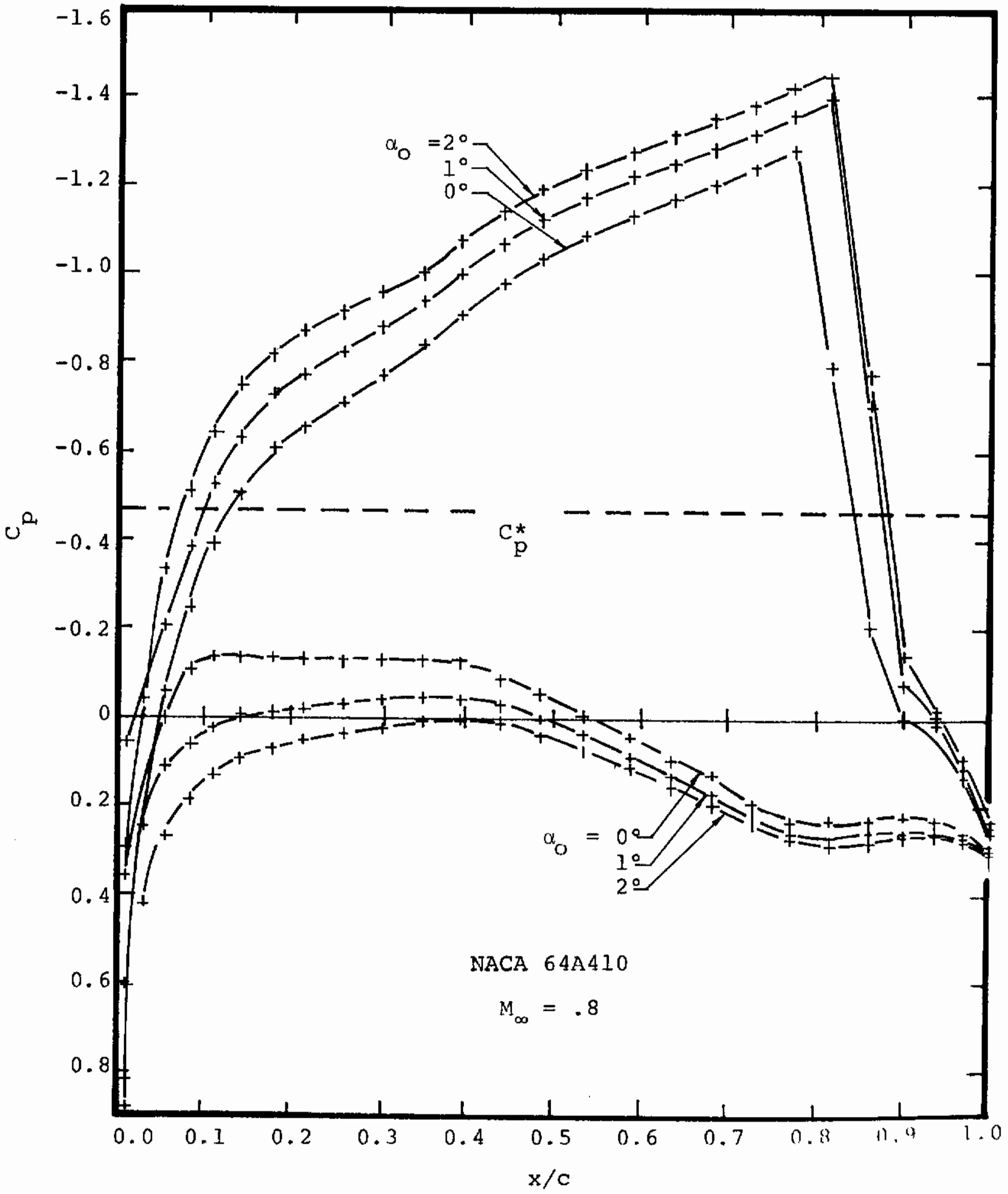

FIGURE 69. STEADY PRESSURE DISTRIBUTIONS

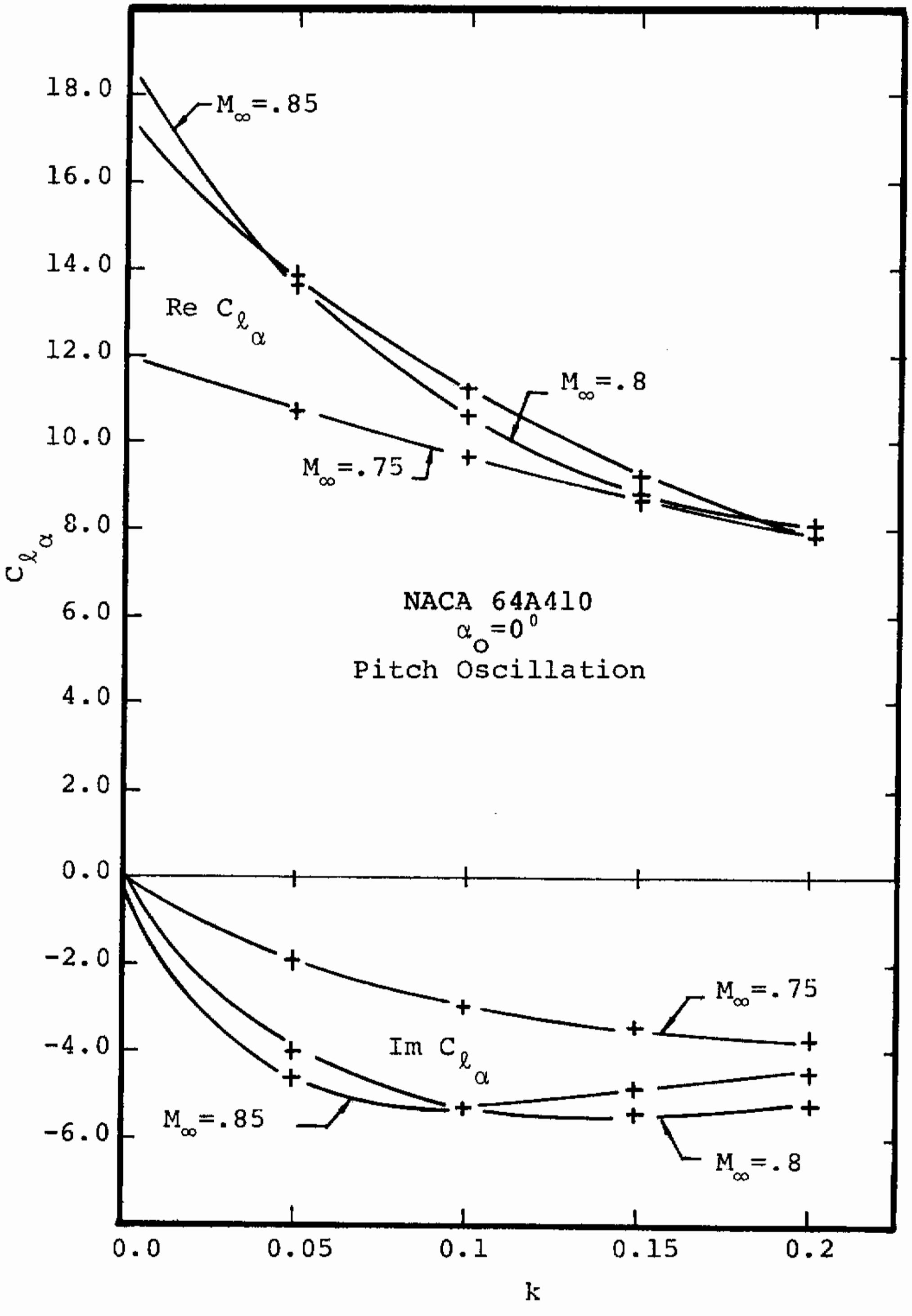

FIGURE 70. MACH NUMBER AND REDUCED FREQUENCY

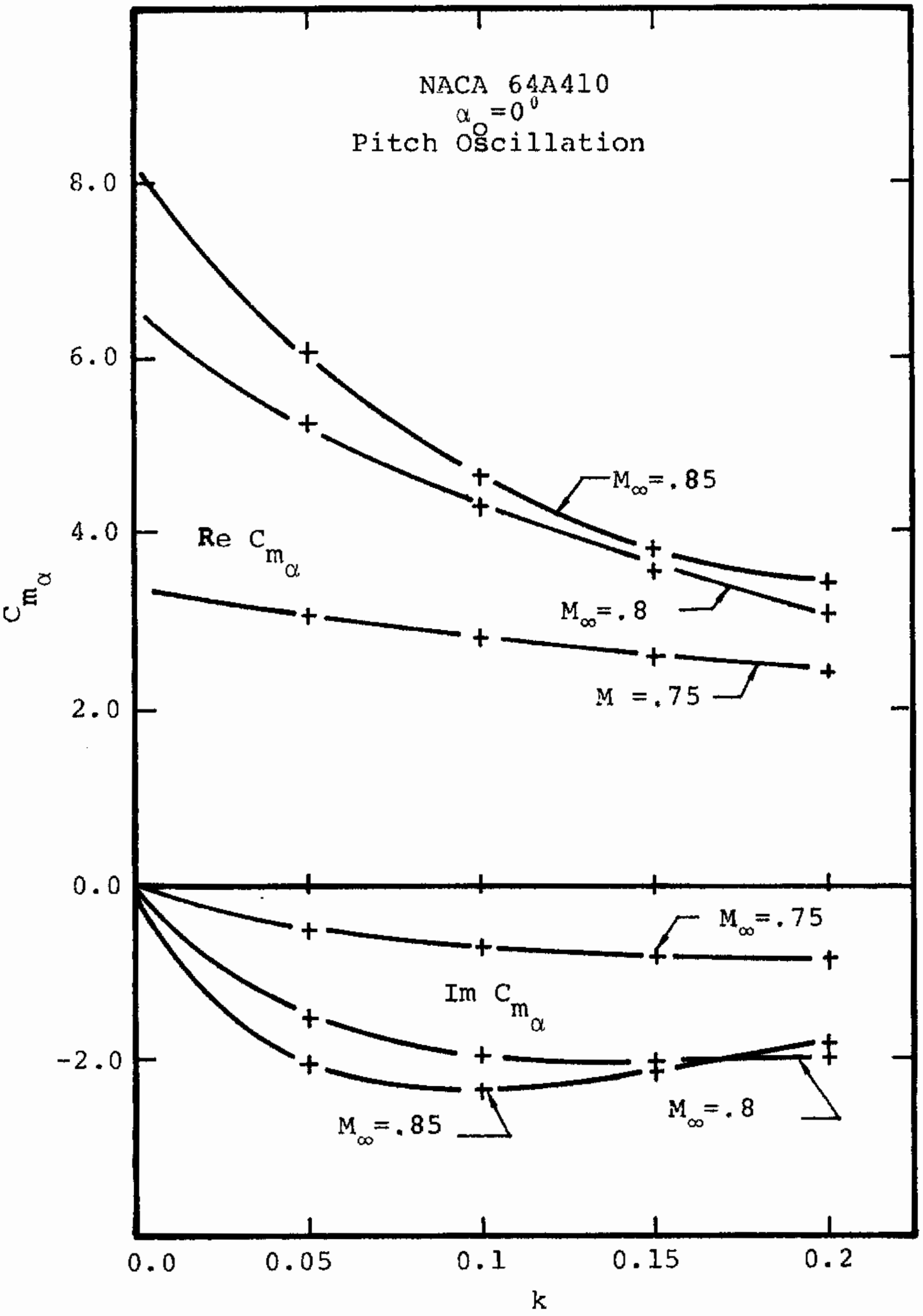

FIGURE 71. MACH NUMBER AND REDUCED FREQUENCY EFFECT ON MOMENT COEFFICIENT (ABOUT X=0) DUE TO PITCH

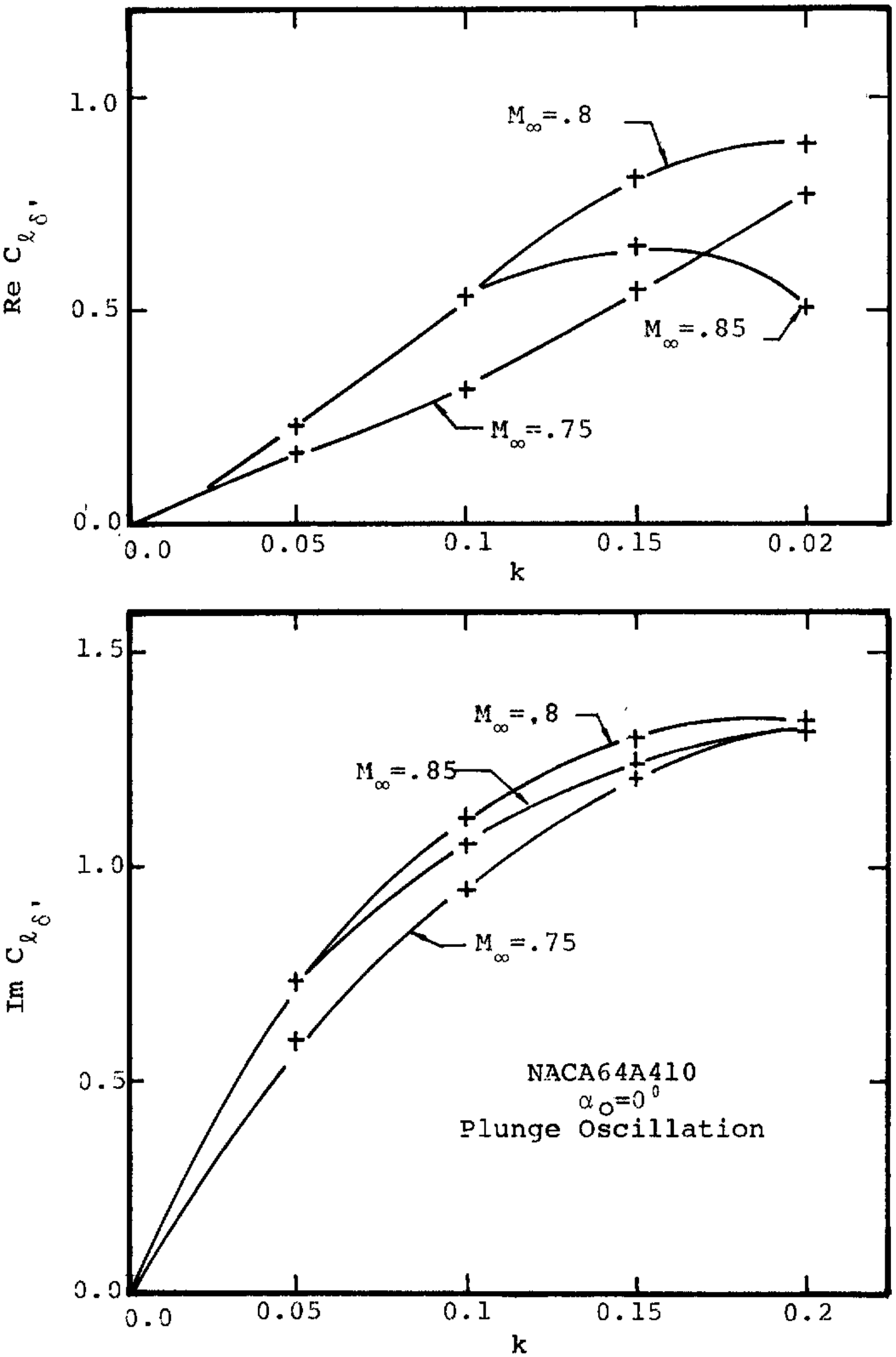

FIGURE 72. MACH NUMBER AND REDUCED FREQUENCY EFFECT ON LIFT COEFFICIENT DUE TO PLUNGE

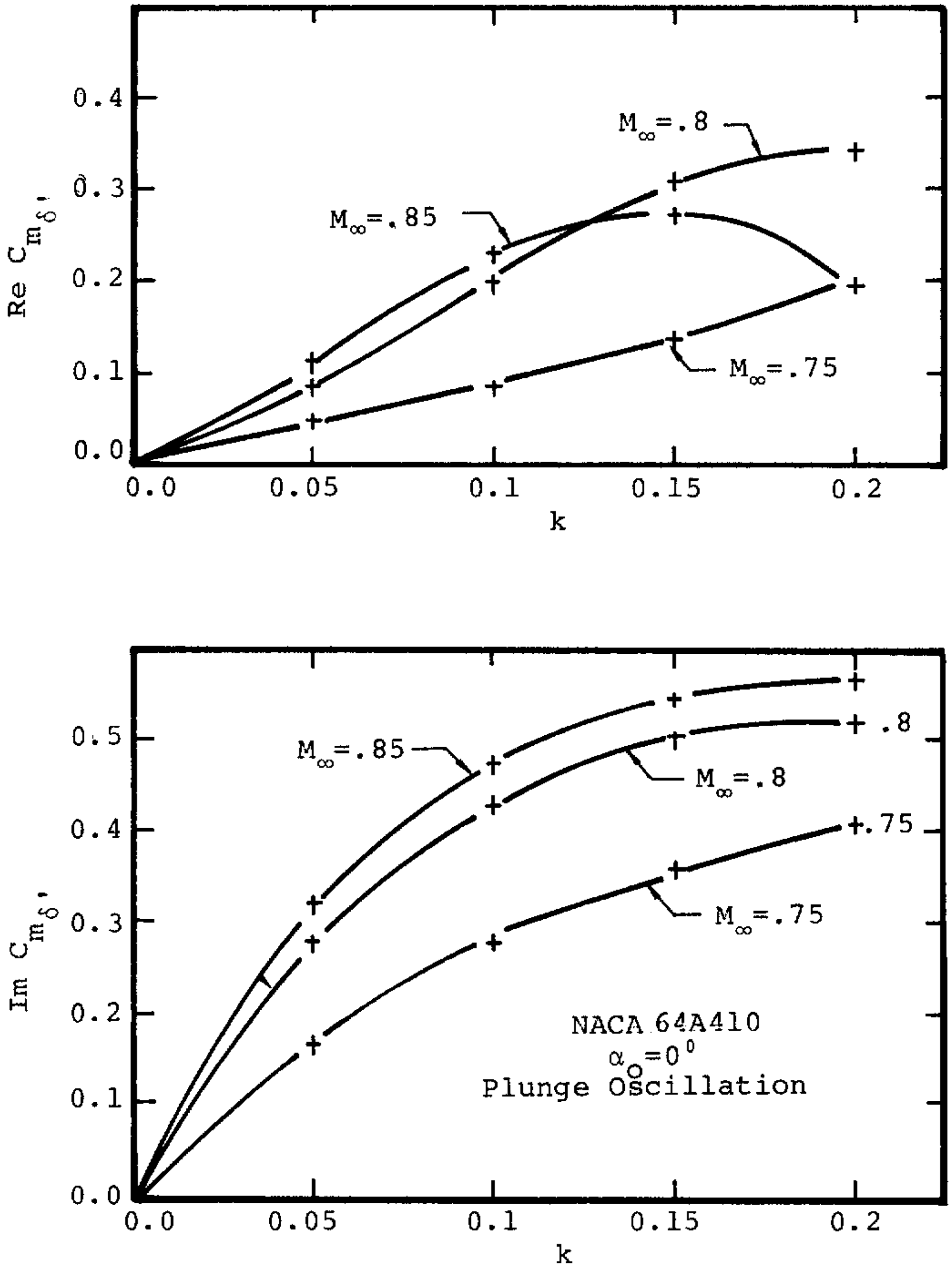

FIGURE 73. MACH NUMBER AND REDUCED FREQUENCY EFFECT ON MOMENT COEFFICIENT (ABOUT X=0) DUE TO PLUNGE

7.0 TRANSONIC AIRFOIL FLUTTER ANALYSIS

The primary purpose of the research reported here was to develop a method for calculating unsteady aerodynamic coefficients for use in transonic flutter analyses. These analyses were carried out for two representative airfoils to illustrate the practical effects of transonic unsteady aerodynamics on flutter computations. The flutter analysis method and results are summarized in this section

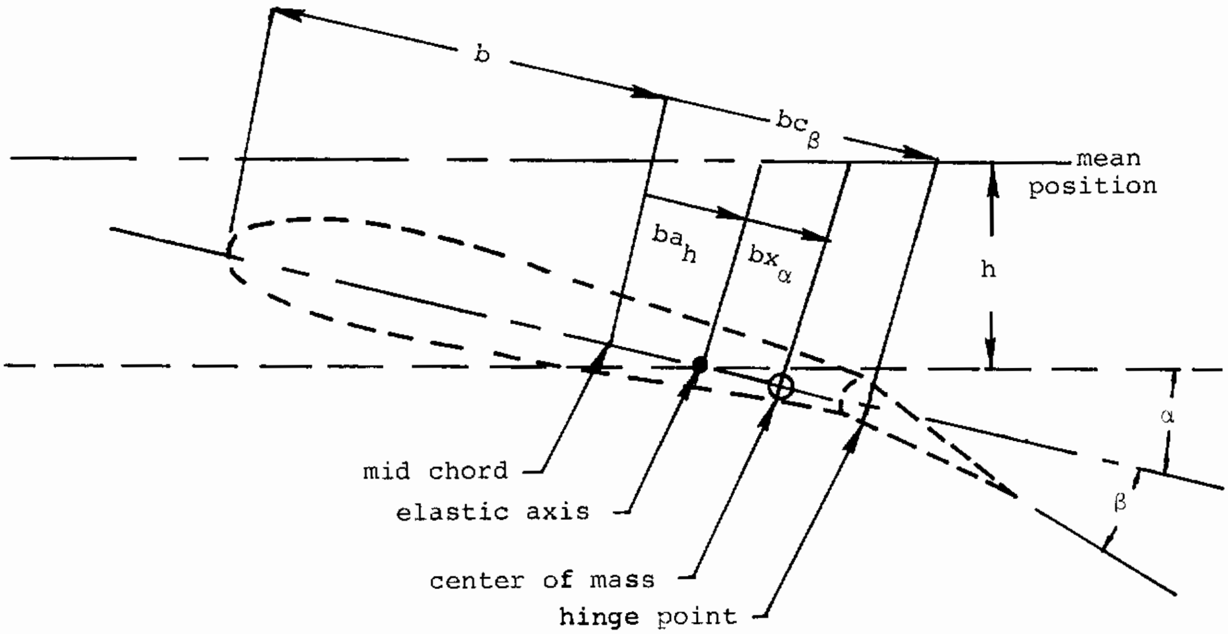

FIGURE 74. NOTATION FOR FLUTTER ANALYSIS

The flutter analysis follows the method of Fung[37] and is the so-called V-g method which is commonly used in current practice. A two-dimensional airfoil with semi-chord, b, and of unit length in the spanwise direction is considered free to oscillate in three degrees of freedom (plunge, pitch, and control surface oscillation) as shown schematically in Figure 74 where:

h = plunge deflection of the elastic axis, positive downward

α = pitch about the elastic axis, positive nose up

β = angular deflection of aileron about the aileron hinge point relative to the wing chord, positive tail down.

The notation used in the analysis, some of which is defined in the figure, is consistent with that used by Fung. It is noted that all dimensions are non-dimensionalized with respect to the semi-chord and distances are measured with the mid-chord point as the origin.

It is assumed that each degree of freedom is restrained by a linear elastic restraint with zero structural damping. The three equations of motion are determined by summing the inertia, elastic and aerodynamic forces; and assuming harmonic oscillations these equations at the flutter point can be written in the following matrix form:

$$\left(\mu\ k^2[M] - [A]\right)\begin{Bmatrix} h \\ \alpha \\ \beta \end{Bmatrix} = \lambda[K]\begin{Bmatrix} h \\ \alpha \\ \beta \end{Bmatrix} \tag{52}$$

where the flutter eigenvalue is:

$$\lambda = \mu\ (1+ig)\omega_r^2\ b^2/U^2 \tag{53}$$

with flow velocity and density, U and ρ respectively, reference frequency, ω_r, wing mass per unit span, m and mass ratio $\mu = m/\pi\ \rho\ b^2$. Also, the artificial structural damping required to maintain simple harmonic motion is denoted by g in the flutter eigenvalue. The reduced frequency of oscillation is defined in the section using the usual American definition, namely:

$$k = \frac{\omega b}{U} \tag{54}$$

where it is noted that the semi-chord, b, is used in the expression rather than the chord, c, used in other sections of this report. It is hoped that this change of definitions for k does not cause undue confusion. The mass matrix [M] and stiffness matrix [K] are written in terms of the airfoil inertial and stiffness parameters as follows:

$$[M] = \begin{bmatrix} 1 & x_\alpha & x_\beta \\ (\ ) & r_\alpha^2 & r_\beta^2 + (C_\beta - a_h)x_\beta \\ (\ ) & (\ ) & r_\beta^2 \end{bmatrix} \tag{55}$$

and

$$[K] = \text{diag}\left\langle \left(\frac{\omega_h}{\omega_r}\right)^2,\ r_\alpha^2\left(\frac{\omega_\alpha}{\omega_r}\right)^2,\ r_\beta^2\left(\frac{\omega_\beta}{\omega_r}\right)^2 \right\rangle \tag{57}$$

where many parameters have been defined in Figure 74 and where x_β is the distance from the aileron hinge point to its center of mass and r_α and r_β are the radii of gyration for the mass moment of inertia of the airfoil about the elastic axis and for the aileron about its hinge. The frequencies, ω_h, ω_α, ω_β are the uncoupled natural frequencies for the airfoil in plunge, pitch and control surface oscillation respectively. Finally, the aerodynamic coefficient matrix is given by:

$$[A] = \frac{2}{\pi} \begin{bmatrix} 1 & 0 & 0 \\ -(1+a_h) & 1 & 0 \\ 0 & 0 & 1 \end{bmatrix} \begin{bmatrix} \frac{1}{4} C_{\ell_\delta}, & \frac{1}{2} C_{\ell_\alpha} & \frac{1}{2} C_{\ell_\beta} \\ \frac{1}{2} C_{m_\delta}, & C_{m_\alpha} & C_{m_\beta} \\ \frac{1}{2} C_{n_\delta}, & C_{n_\alpha} & C_{n_\beta} \end{bmatrix} \qquad (57)$$

which transforms the unsteady aerodynamic coefficients as defined in this report (see Appendix B) to account for the nondimensionalization with respect to b used in this section (rather than c used elsewhere in the report). The transformation also accounts for the shift in the definition of airfoil moments from the leading edge (as used in the definition of C_{m_α}, etc.) to the elastic axis, a_h, required in this analysis.

Performing a standard eigenvalue analysis of the above system (Eq. 52), provides the formalism for determining the so-called flutter point. For a given airfoil, the flutter point at fixed Mach number and air density is determined by finding the lowest value of flow velocity for which the artificial damping parameter, g (imaginary part of λ) is zero. This is found by solving for the eigenvalues of Eq. 52 for various reduced frequencies and cutting and trying until the flutter velocity is determined within acceptable accuracy.

The results of this analysis are presented here in the form of a dimensionless flutter speed, u^*, and flutter frequency, ω^*, where

$$u^* = \frac{U}{b\ \omega_\alpha} \quad , \quad \omega^* = \frac{\omega}{\omega_\alpha} \qquad (58)$$

Representative values for the airfoil geometry, inertia and stiffness parameters were used as follows:

$\mu = 20, \quad r_\alpha = 0.6, \quad r_\beta = 0.1$

$c_\beta = 0.5, \quad x_\alpha = -.025, \quad x_\beta = .03$

$a_h = -.46048$

$\omega_h = .2, \quad \omega_\alpha = 1.0, \quad \omega_\beta = 50$

Variations from these values were used to illustrate special trends as will be discussed.

The primary results of the analysis are for the two degree of freedom (2 d.o.f.) case for the NACA 64A006 and these results are presented in Figure 75 through 77. In the 2 d.o.f. case the aileron is assumed fixed with respect to the airfoil so that the motion is restricted to pitch and plunge oscillations. Figures 75 and 76 present results for flutter velocity and frequency respectively, as functions of freestream Mach number. The figures demonstrate the crucial importance of the transonic Mach number range by way of the dip in flutter velocity at $M_\infty = .85$ and the corresponding large variation in flutter frequency in this range. The results for flutter velocity are presented for two values of the center of mass location; x , which indicate the importance of this parameter on flutter speed. It is noted that the airfoil is statically stable (divergence free) for Mach numbers greater than $M_\infty = .85$ due to the shift in the aerodynamic center aft of the elastic axis for $M_\infty > .85$. Also note that the normal flutter mode for all cases given in the figures was dominated by motion in plunge for $\omega_h/\omega_\alpha = .2$. It would be expected that the coupling between the pitch and plunge mode would increase as ω_h approaches ω_α and that therefore the critical flutter velocity would be decreased. This effect is shown in Figure 77 for ω_h/ω_α up to 0.5.

	u^*	ω^*
$\alpha_o = 0$ free air	10.25	.473
$\alpha_o = 2^\circ$	11.0	.175
porous wall	8.12	.075

TABLE 3. ANGLE OF ATTACK AND WALL EFFECT ON FLUTTER PARAMETER (NACA64A006, M_∞=.85)

The effect of mean angle of attack and wind tunnel wall interference on the critical flutter parameters was also examined for the limited cases for which the aerodynamic coefficients have been calculated. The results are summarized in Table 3 for the NACA64A006 at M_∞=.85 and indicate a modest beneficial effect of mean angle of attack on flutter velocity and a somewhat greater detrimental effect of wall interference. Both, however, have a considerably greater effect on the flutter frequency which is decreased from $\omega^* = .473$ for the free air case to $\omega^* = .075$ for the wall case.

Fully three degree of freedom flutter calculations have also been performed for the NACA 64A006 with not altogether complete results. Due to the rather restricted reduced frequency range ($0 \leq k \leq .1$) of the present aerodynamic data, it was impossible to determine the true flutter velocity because an aileron dominated normal mode (aileron buzz) was fluttering at a frequency which was out of the range of the data. It was determined, however, that the aileron significantly damped the plunge dominated normal mode which fluttered in the 2 d.o.f. case. This happened even for unrealistically high values of $\omega_\beta/\omega_\alpha \sim 50$ and for values of $\omega_\beta/\omega_\alpha \gtrsim 30$ the plunge dominated mode was completely damped and therefore did not flutter. This curious coupling of the aileron and plunge modes and the high frequency aileron buzz phenomena would seem to be peculiar to the present unsteady aerodynamic data and merits further investigation. Time constraints on the present study did not permit a comprehensive study of the 3 d.o.f. flutter case.

Finally, it is noted that 2 d.o.f. flutter calculations have been performed for the NACA 64A410. However, the restricted Mach number range of the aerodynamic data did not permit an in-depth examination of the transonic flow effects. For example, at $M_\infty = .75$ the airfoil flutter velocity was 25.1 and flutter frequency of .19. Mean angle of attack had the expected negligible effect on the flutter parameters as did the data at $M_\infty = .8$ and .85.

In summary, the two degree of freedom flutter results for the NACA 64A006 airfoil, presented here, demonstrate the crucial importance of the transonic speed range with respect to airfoil flutter. A thorough examination of three degree of freedom flutter would require the generation of unsteady aerodynamic coefficients over a more extended range of reduced frequencies than were considered in the present work.

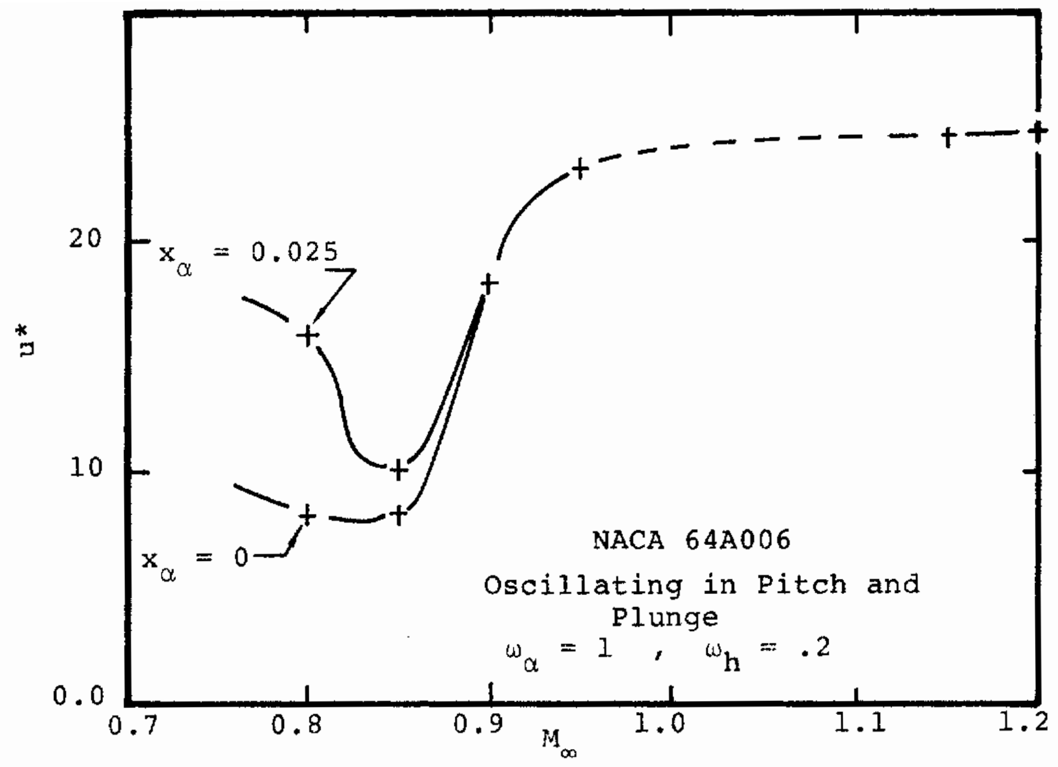

FIGURE 75. FLUTTER VELOCITY VERSUS MACH NUMBER

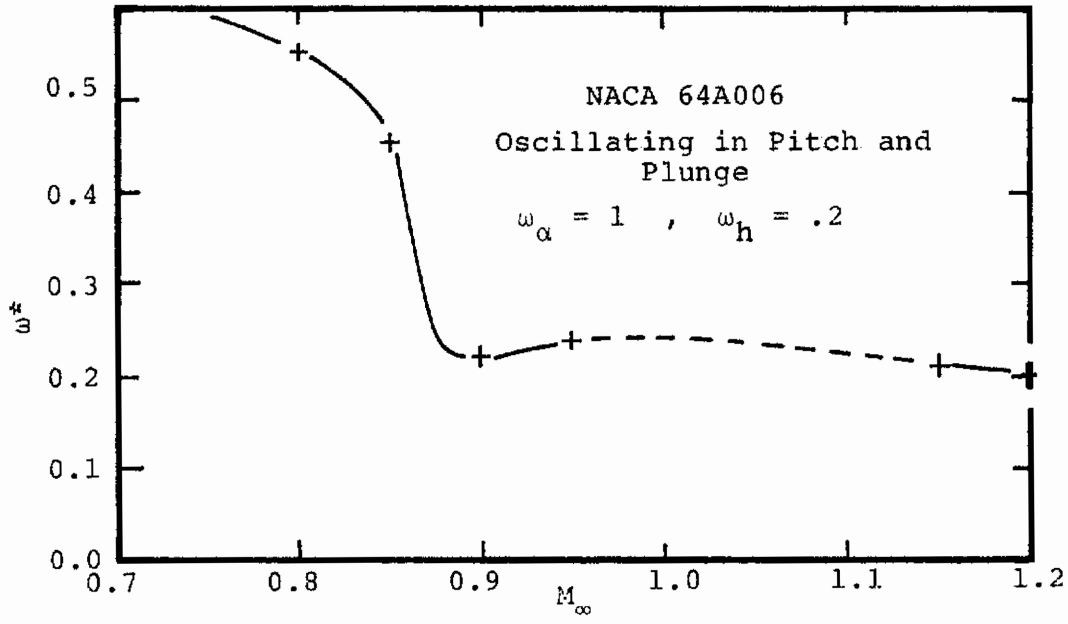

FIGURE 76. FLUTTER FREQUENCIES VERSUS MACH NUMBER

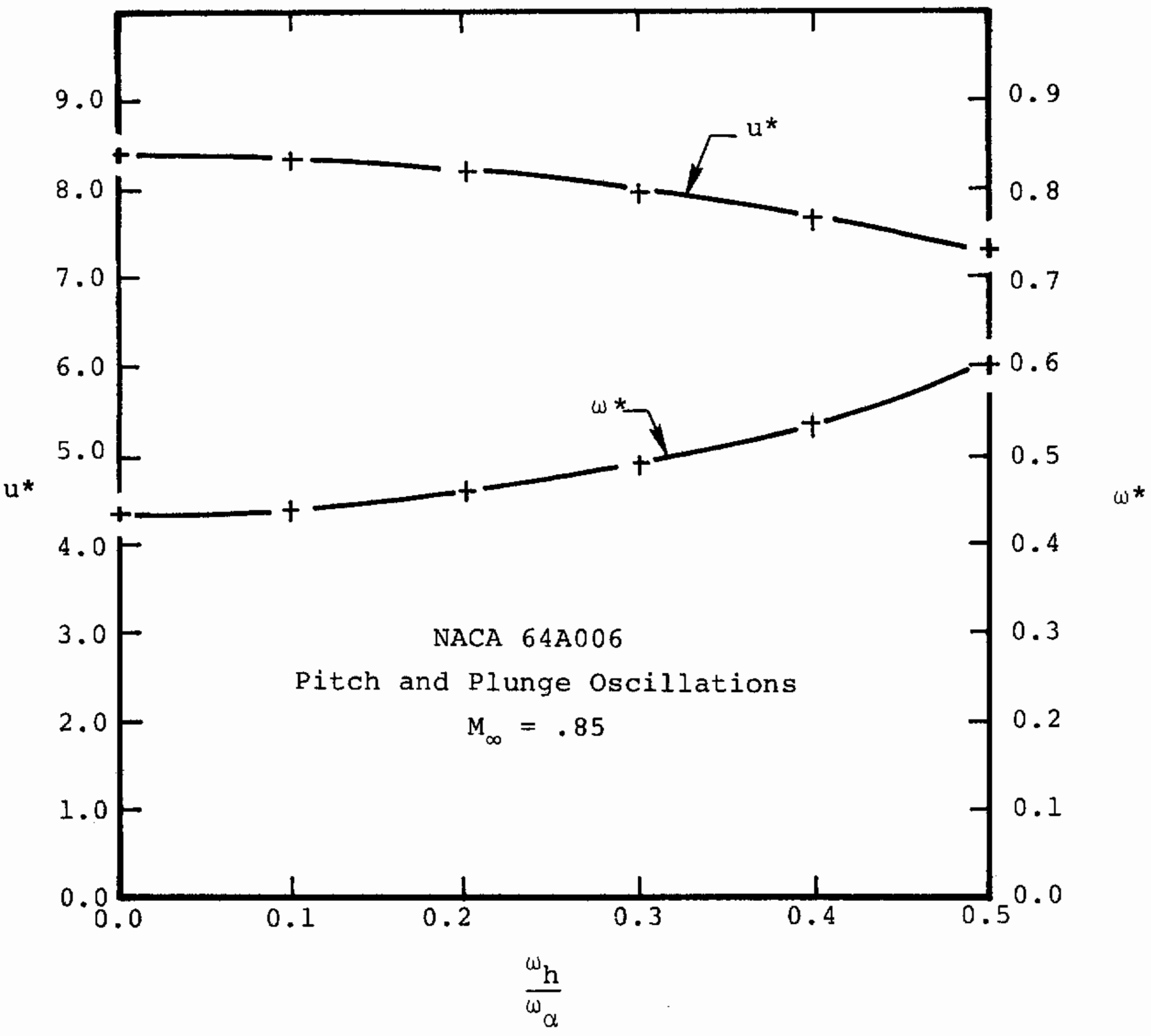

FIGURE 77. EFFECT OF PLUNGE/PITCH NATURAL FREQUENCY RATIO ON TRANSONIC FLUTTER

8.0 CONCLUSIONS

In this report, a treatment of unsteady transonic flow as a small perturbation about the nonlinear small disturbance steady flow is presented. The technique has been applied to representative airfoils oscillating at subsonic, through transonic to supersonic Mach numbers. It is shown that the present theory matches linearized unsteady subsonic or supersonic theory as Mach number decreases or increases away from sonic respectively. The theory includes the effects of thickness and angle of attack which are ignored in linear theories but which, as the results presented here demonstrate, are significant in the low frequency unsteady transonic speed regime. A measure of the efficiency of the computational scheme is given by the fact that the matrix of calculations required to generate unsteady aerodynamic coefficients for a transonic flutter study of a three degree of freedom, two dimensional airfoil can be completed in about 1 and 1/4 hours of CDC 7600 time.

As a result of the research reported here, the method has been generalized to treat higher frequency effects, supersonic freestream flows, wind tunnel walls and to perform three dimensional planar wing calculations. The method is currently in a state of development that the study of such effects is routine using computer programs developed during the study. The method is somewhat limited by a numerical instability which develops for freestream Mach numbers very near Mach 1, but a wide range of supercritical flows may be successfully calculated. A possible resolution to this instability has been postulated based on an inner/outer expansion analysis for near sonic Mach numbers but its implementation would require further development effort.

The results presented here indicate that the theory and numerical solution method provide a meaningful representation of inviscid transonic flows about practical airfoils for reasonable amplitudes of unsteady motion. The results are shown to compare adequately with the "exact" numerical calculations or Magnus and Yoshihara for low frequency unsteady supercritical flows, for an expenditure of over two orders of magnitude less computer time. Although these comparisons show some qualitative differences in unsteady airfoil pressure perturbations, unsteady aerodynamic forces compare very well in both amplitude and phase. Detailed comparisons of the present results to limited available two dimensional experimental data shows good qualitative agreement. Quantitative discrepancies would seem to be related mainly to viscous effects, not accounted for in the model, and to possible wind tunnel wall or three dimensional flow effects in the data.

A brief study of such effects indicates that, as expected, they can be quite significant in the transonic speed range.

The need for an accurate and efficient method for calculating unsteady aerodynamic coefficients at transonic speeds is pointed out by the flutter dynamics study presented in this report. Aerodynamic coefficients were calculated using the present method and used in a flutter analysis of a NACA 64A006 with three rigid body degrees of freedom (pitch, plunge, control surface rotation) and of a NACA 64A410 with two rigid body degrees of freedom (pitch, plunge) The results show the expected critical effect of the transonic regime on flutter speed.

It seems clear that viscous effects are quite important for unsteady flows in the transonic speed regime. The comparison of the present inviscid results to data, given above, indicate that the inclusion of viscous effects is crucial to the practical accuracy of an unsteady transonic theory. The modest computer time requirements of the present small disturbance theory make it a potential candidate for the introduction of such effects and it is recommended that this be the next area for further development of the method.

9.0 REFERENCES

1. Traci, R. M., Albano, E. D., Farr, J. L., and Cheng, H. K., "Small Disturbance Transonic Flows about Oscillating Airfoils," AFFDL-TR-74-37, June 1974.

2. Landahl, M. T., Unsteady Transonic Flow, International Series of Monographs in Aeronautics and Astronautics, Pergamon Press, London, 1961.

3. Rott, N., "Flugelschwingungsformen in Ebener Kompressibler Potential-Stromung," Z. Angev. Math. Phys., Vol. 1, Fasc. 6, 1950.

4. Landahl, M. T., "Linearized Theory for Unsteady Transonic Flow," In Symposium Transsonicum (ed. by K. Oswatitsch), Springer-Verlag, Berlin.

5. Nelson, H. C. and Berman, J. H., "Calculations on the Forces and Moments for an Oscillating Wing-Aileron Combination in a Two-Dimensional Potential Flow at Sonic Speeds," NACA Rept. 1128, 1953.

6. Stahara, S. S. and Spreiter, J. R., "Development of a Nonlinear Unsteady Transonic Flow Theory," NASA CR-2258, June 1973.

7. Isogai, K., "Unsteady Transonic Flow Over Oscillating Circular-Arc Airfoils," AIAA Paper 74-360, April 1974.

8. Magnus, R. and Yoshihara, H., "Inviscid Transonic Flow Over Airfoils," AIAA Paper 70-47, June 1970.

9. Magnus, R. and Yoshihara, H., "Calculations of Transonic Flow Over an Oscillating Airfoil," AIAA Paper No. 75-98, January 1975.

10. Beam, R. M. and Warming, R. F., "Numerical Calculations of Two Dimensional, Unsteady Transonic Flows with Circulation," NASA TN D-7605, February 1974.

11. Ballhaus, W. F., and Lomax, H., "The Numerical Simulation of Low Frequency Unsteady Transonic Flow Fields," 4th International Conf. on Num. Meth. in Fluid Dynamics, Denver, Colorado.

12. Ballhaus, W. F., Magnus, R. and Yoshihara, H., "Some Finite Difference Examples of Unsteady Planar Flows," Symposium on Unsteady Aerodynamics, Tucson, Arizona, March 1975.

13. Bratanow, T. and Ecer, A., "Computational Considerations in Application of the Finite Element Method for Analysis of Unsteady Flow around Airfoils," AIAA Computational Fluid Dynamics Conference, Palm Springs, California, July 1973.

14. Chan, S. T. K. and Brashears, M. R., "Finite Element Analysis of Transonic Flow," AFFDL-TR-74-1I, March 1974.

15. Murman, E. M. and Cole, J. D., "Calculation of Plane Steady Transonic Flows," AIAA Paper 70-188, June 1970.

16. Murman, E. M. and Krupp, J. A., "The Numerical Calculations of Steady Transonic Flows Past Thin Lifting Airfoils and Slender Bodies," AIAA Paper No. 71-566, June 1971.

17. Ehlers, F. E., "A Finite Difference Method for the Solution of the Transonic Flow around Harmonically Oscillating Wings," NASA CR-2257, January 1974.

18. Tijdeman, H. and Bergh, H., "Analysis of Pressure Distributions Measured on a Wing with Oscillating Control Surface in Two-Dimensional High Subsonic and Transonic Flow," NLR-TR F.253, 1967.

19. Tijdeman, H. and Schippers, P., "Results of Pressure Measurements on an Airfoil with Oscillating Flap in Two-Dimensional High Subsonic and Transonic Flow," Provisional Issue, NLR TR 730-78 U, August 1973.

20. Farr, J. L., Traci, R. M., Albano, E. D., "Computer Programs for Calculating Small Disturbance Transonic Flows about Oscillating Airfoils," AFFDL-TR-73-135, November 1974.

21. Albano, E. and Rodden, W. P., "A Doublet-Lattice Method for Calculating Lift Distributions on Oscillating Surfaces in Subsonic Flows," AIAA Journal, Vol. 7, No. 2, February 1969.

22. Murman, E. M., "A Relaxation Method for Calculating Transonic Flows with Detached Bow Shocks," Proceedings 3rd International Conference on Computational Fluid Mechanics, 1971.

24. Murman, E. M., "Analysis of Embedded Shock Waves Calculated by Relaxation Methods," AIAA Journal, Vol. 12, No. 5, pp. 626-633.

25. Hafez, M. M. and Cheng, H. K., "Convergence Acceleration and Shock Fitting for Transonic Aerodynamics Computation," AIAA Paper No. 75-51, January 1975.

26. Murman, E. M., "Computations of Wall Effects in Ventilated Transonic Wind Tunnels," AIAA Paper No. 72-1007, 1972.

27. Kacprzynski, J. J., "Transonic Flow Field Past 2-D Airfoils Between Porous Wind Tunnel Walls with Nonlinear Characteristics," AIAA Paper No. 75-81, 1975.

28. Collins, D. J. and Krupp, J. A., "Experimental and Theoretical Investigations in Two-Dimensional Transonic Flow," AIAA Journal, Vol. 12, No. 6, June 1974.

29. Klunker, E. B., "Contributions to Methods for Calculating the Flow about Thin Lifting Wings at Transonic Speeds," NASA TN D-6530, November 1971.

30. Bailey, F. R. and Steger, J. L., "Relaxation Techniques for Three Dimensional Transonic Flow About Wings," AIAA Paper 72-189, San Diego, California, 1972.

31. Newman, P. A. and Klunker, E. B., "Computation of Transonic Flow About Finite Lifting Wings," AIAA Journal, Vol. 10, No. 7, p. 971, July 1972.

32. Cole, J. D., "Twenty Years of Transonic Flow," Boeing Scientific Research Laboratories Document D1-82-0878, July, 1969.

33. Isaacson, E. and Keller, H. G., Analysis of Numerical Methods, John Wiley and Sons, New York.

34. Shanks, D., "Nonlinear Transformation of Divergent and Slowly Convergent Sequences," J. of Math. and Physics, Vol. 34, p. 1-42, 1955.

35. Kentzer, C. P., "Relaxation Factors for Supercritical Flows," Proceedings AIAA Comp. Fluid. Dynamics Conf., p. 41, Palm Springs, California, 1973.

36. Ehlers, F. E., Private Communication, Mary 1975.

37. Fung, Y. C., Theory of Aeroelasticity, Dover Publication, New York, 1969.

APPENDIX A

FARFIELD BOUNDARY PRESCRIPTIONS

In the solution technique presented in this report, a solution field of finite extent is defined. The completion of the finite difference analogs to the steady and unsteady transonic flow problems, require that boundary conditions be fixed in some manner on the farfield boundary. In this report, calculations are performed for two dimensional airfoil sections in subsonic or supersonic free air or constrained by solid or porous wind tunnel walls and for three dimensional planar wings in subsonic free air flows. In each case a different farfield prescription is required and the purpose of this appendix is to summarize, for completeness sake, the asymptotic solutions used to fix these farfield boundary conditions.

A.1 Two-Dimensional Airfoil in Free Air

The basic method used to develop asymptotic solutions for the steady or unsteady perturbation potentials involves the integral representation which results from applying Green's theorem to the appropriate partial differential equation. Suitable approximations are made to the integral expressions valid far from the airfoil and a farfield solution results. Results for steady and unsteady free air flows are presented below.

A.1.1 Steady Free Air Flows

The farfield for the non-linear steady potential was examined in the manner mentioned above initially by Cole[32] and most extensively by Klunker[29], whose result is used. The farfield representation describes thickness and lift effects to leading order and is given by:

$$\phi^{0}_{ff}(x,y) = \frac{1}{\pi\sqrt{K}} \; \frac{x}{x^{2}+Ky^{2}} \left\{ \int_{0}^{1} t(\xi)ds + \iint_{-\infty}^{\infty} (\phi^{0}_{x})^{2} d\xi d\eta \right\}$$

$$+ \gamma \left\{ \arctan \frac{x}{\sqrt{K}\, y} + \frac{\pi}{2} \operatorname{sgn} y \right\}_{x^{2}+Ky^{2}\to\infty} \qquad \text{(A.1)}$$

where $t(\xi)$ is the airfoil thickness distribution. The doublet strength due to the nonuniform flow is given by the integral of $(\phi^{0}_{x})^{2}$ over the solution field. This is evaluated periodically as the iterative solution proceeds using a trapezoidal rule integration scheme. Similarly, in calculations with lift, the airfoil circulation, γ, is updated. As the doublet strength and circulation are refined, Eq. A.1 is used to update ϕ^{0} on the boundaries of the finite difference grid. Thus the farfield boundary condition depends on the numerical solution and is treated as a Dirichlet boundary condition.

For supersonic freestream Mach numbers, an approximate characteristic relation can be developed from either the integral equation or the governing partial differential equation. This was done for steady flows by Murman[22] and for unsteady flows by the present authors(20). This characteristic condition is thus used to define a boundary condition on the farfield boundaries. It is assumed that the disturbance from the body is weak so that the characteristic relation on the incoming characteristic applies. The first order approximation to the relation is given and the farfield boundaries are treated as follows:

$$\left.\begin{array}{lll} \phi^{0}_{y} = \mp \sqrt{-K}\, \phi^{0}_{x} & & \text{on } y = \pm\infty \\ \phi^{0} \equiv \phi^{0}_{x} \equiv 0 & & \text{as } x \to -\infty \\ \phi^{0}_{x} \equiv 0 & & \text{as } x \to +\infty \end{array}\right\} \qquad \text{(A.2)}$$

The upstream boundary ($x \to -\infty$) is taken ahead of the bow shock so that the flow is uniform. Because of the backward differencing used for supersonic grid points, no prescription is required on the downstream boundary ($x \to +\infty$) as long as the boundary is completely supersonic. If during the iteration procedure a grid point on the boundary becomes subsonic, a zero gradient ($\phi_x^0 = 0$) condition is used. The above conditions are incorporated in the finite difference procedure as a Dirichlet condition on the upstream boundary and using one sided finite difference equations for the gradient conditions on the top and downstream boundaries.

A.1.2 Unsteady Free Air Flows

In the same manner as the steady flow, the farfield boundary conditions for the unsteady perturbation potential in the low frequency regime are defined from an asymptotic expression for subsonic freestream flow and an approximation to the unsteady characteristic relation for supersonic freestream flows. For subsonic flow the asymptotic expression is used to fix values of ϕ in the Dirichlet sense on all four boundaries of the grid. The expression was derived in Reference 1 and is given by:

$$\frac{4\sqrt{K}\ \phi_{ff}(x,y)}{\Omega\gamma y} = -\left\{ i\hat{k}\int_0^1 e^{-i\hat{k}\xi}\ \Delta\phi(\xi)\,d\xi + e^{-i\hat{k}} \right\} e^{i\hat{k}x}\ \frac{H_1^2(R_1)}{R_1} \tag{A.3}$$

$$+ I_1 + I_2 \qquad \text{for } R_1 >> 1$$

where I_1 is given by:

$$I_1 \sim \frac{2}{\sqrt{\pi}}\ e^{i\left(\frac{\pi}{4} - S(R_1)\right)} \sum_{n=0}^{\infty} \frac{a_n}{(2i)^n} \left\{ \sum_{\nu=0}^{\infty} (-i)^{\nu}\ \frac{d^{\nu}g}{dS^{\nu}}\bigg|_{S(R_1)} \right\} \tag{A.4}$$

where

$$S(R) = \sqrt{R^2 - K\hat{k}^2 y^2} + R$$

$$g(S) = \frac{S^{n-\frac{1}{2}}(S^2-K\hat{k}^2y^2)}{(S^2+K\hat{k}^2y^2)^{n+3/2}}$$

$$a_n = \frac{(16-1)(16-3^2)\ldots\ [16-(2n-1)^2]}{n!\ 2^{2n}}$$

and I_2 is:

$$I_2 = \begin{cases} 0 & \text{for } x \le 1 \\ -2i\displaystyle\int_{\hat{k}\sqrt{K}\,y}^{R_1} \sin\sqrt{R^2-K\hat{k}^2y^2}\ \frac{H_2^2(R)}{R}\,dR & \text{for } x > 1 \end{cases} \tag{A.5}$$

where $\hat{k} = \Omega/K$, $R_1 = \hat{k}\sqrt{(x-1)^2+Ky^2}$ and H_i^2 is the Hankel function of the second kind of ith order. The integral cannot be evaluated in closed form but, since it is over a finite range, it can be integrated numerically with little difficulty. It is noted that the farfield approximation depends on the solution through the airfoil circulation γ and also through the "airfoil integral". Thus as the airfoil circulation and potential distributions are refined, the farfield is periodically updated using equation A.3-A.5.

Supersonic freestream flows are treated in a analagous manner to the steady flow. A low frequency unsteady characteristic condition has been developed[20] and is used along with upstream and downstream conditions as farfield boundary conditions. The relations are:

$$\left.\begin{aligned} \phi_y &= \mp\left\{\left(\sqrt{-K}+\frac{\phi_x^0}{\sqrt{-K}}\right)\phi_x + i\,\frac{\Omega}{\sqrt{-K}}\,\phi\right\} && \text{on } y = \pm\infty \\ \phi &\equiv \phi_x \equiv 0 && \text{as } x \to -\infty \\ \phi_x &\equiv 0 && \text{as } x \to +\infty \end{aligned}\right\} \tag{A.6}$$

A.2 Two-Dimensional Airfoil Between Wind Tunnel Walls

The effect of wind tunnel walls in the steady and unsteady flow is of considerable concern especially for transonic flows and the effect can be modeled by treating the appropriate boundary conditions at the wall and far upstream and downstream.

A linearized boundary condition which relates the normal velocity at the wall to the local pressure is used in the present study for general porous walls (solid walls are considered as a special case). Also asymptotic expressions valid for upstream and downstream have been developed for subsonic upstream flow. In the present work a farfield expression for solid walls has been developed and is used in the general case. The expression results from the superposition of a infinite sequence of doublets and vortices (of alternating signs) each separated by the scaled distance between the walls, $\tilde{h}$. This solution is used to fix a Dirichlet boundary condition on the upstream and downstream boundaries of the finite difference grid. The resulting set of boundary conditions for subsonic steady flow are:

$$\phi^0_y = \mp \tilde{P}\, \phi^0_x \quad \text{on } y = \pm \tilde{h}/2$$

$$\phi^0_{ff}(x,y) = \frac{\mathcal{D}}{\tilde{h}K} \, \mathrm{Re} \left\{ \coth \left[\frac{\pi(x+i\sqrt{K}\,y)}{\tilde{h}\sqrt{K}} \right] \right\} + \frac{\gamma}{2\pi} \left\{ \pi - \arctan \left[\frac{\sin \frac{\pi y}{\tilde{h}}}{\sinh \frac{\pi x}{\sqrt{K}\tilde{h}}} \right] \right\} \text{ as } x \to \pm\infty \qquad \text{(A.7)}$$

where

$$\mathcal{D} = \int_0^1 t(\xi)\,d\xi + \int_{-\infty}^{\infty} \int_{-\tilde{h}/2}^{\tilde{h}/2} (\tilde{\phi}^0_x)^2 \, d\eta\, d\xi$$

and where $\tilde{P}$ is the wall porosity coefficient. As before, the doublet strength, $\mathcal{D}$, and the airfoil circulation γ are refined as the solution proceeds and used to update the farfield. As stated above, the wall boundary condition is treated as the first order (linear) relation between the perturbation velocity normal to the wall and the local pressure coefficient ($C_p = -2\phi_x^0$), assuming the plenum pressure is equal to the freestream static pressure. For solid wall note that $\tilde{P}=0$ so that $\phi_y^0=0$ at the wall. An Approximation for $\tilde{P}$ for general porous or slotted walls can be developed by assuming the boundary condition is the weighted average of a free jet ($\phi_x^0=0$) and a solid wall ($\phi_y^0=0$) where the weighting factors are the open area ratio, S, or 1-S respectively. The resulting expression for $\tilde{P}$ is:

$$\tilde{P} = \frac{S}{1-S} \; \frac{1}{[(1+\gamma)\delta M_\infty^2]^{1/3}} \qquad \text{(A.8)}$$

The boundary conditions for the wall case with supersonic upstream flow can be treated in a simple manner as long as the upstream and downstream boundaries are defined far enough from the airfoil. In this case the wall condition is the same as given in Equation A.8 and the upstream condition is taken as uniform flow. No downstream condition is required due to the absence of upstream influence. Thus the boundary conditions became:

$$\begin{aligned} \phi_y^0 &= \pm \tilde{P}\ \phi_x && \text{on } y = \pm \frac{\tilde{h}}{2} \\ \phi^0 &= \phi_x^0 \equiv 0 && \text{as } x \to -\infty \end{aligned} \qquad \text{(A.9)}$$

In each of the above cases, the gradient boundary condition is treated by using a one sided finite difference approximation.

In the present work, the farfield boundary conditions for the unsteady perturbation potential are treated in the same manner as the supersonic steady case. The wall condition is modified to allow phase changes between the unsteady perturbation velocity normal to the wall and the unsteady pressure At upstream and downstream infinity a zero gradient condition is assumed to apply. This is believed to be accurate for the low frequency unsteady conditions considered, and the adequacy of the approximation has in fact been verified for the quasi-steady (k=0) case for which a asymptotic solution exists (Equation A.7). Thus the boundary conditions for both supersonic and subsonic upstream flows are:

$$\phi_y = \mp \tilde{P}\, e^{i\beta_*} (\phi_x + \underline{ik\phi}) \quad \text{on } y = \pm \tilde{h}/2$$

$$\phi_x \equiv 0 \qquad ,\text{as } x \to \pm \infty \tag{A.10}$$

where β_* is the phase relationship between the unsteady velocity normal to the wall and the unsteady pressure $(-2(\phi_x+ik\phi))$. It is recalled that the $ik\phi$ term in the above expression is reglected in the low frequency approximation.

A.3 Three-Dimensional Planar Wing in Free Air

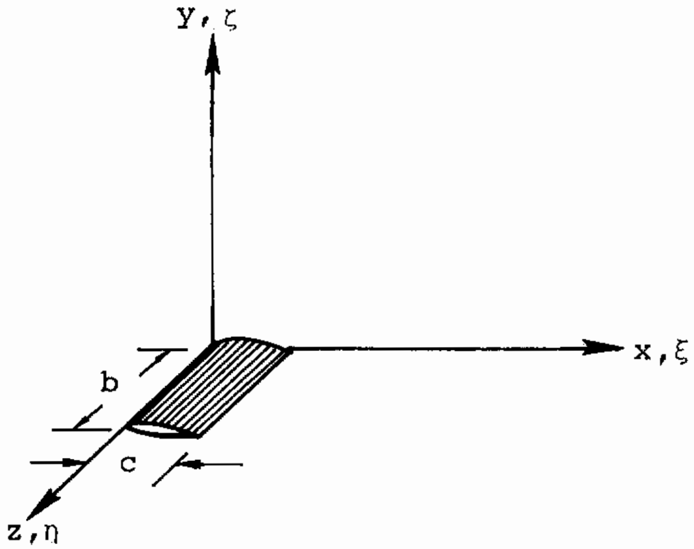

FIGURE A.1 THREE DIMENSIONAL WING COORDINATE SYSTEM

The development of three dimensional subsonic farfield approximations for the steady and unsteady perturbation potentials proceeds in the same manner as described above for the two dimensional flow. As before the method involves the approximation of various integrals over the wing and wake which result from the application of Green's theorem to the appropriate partial differential equation. Again, Klunker has used the method to develop asymptotic solutions for the three dimensional steady flow and his result in the following form is used:

$$\phi^{0}_{ff}(x,y,z) = -\frac{x}{2\pi R^{3}}\left\{\int_{-b}^{b}\int_{0}^{1} t(\xi,\eta)\,d\xi\,d\eta\right\}$$

$$+\begin{cases} \dfrac{y}{4\pi(y^{2}+z^{2})}\left(1+\dfrac{x}{R}\right)\displaystyle\int_{-b}^{b}\gamma(\eta)\,d\eta & \text{for } \begin{cases} y^{2}+z^{2}\to\infty \\ x\to-\infty \end{cases} \\[2ex] \dfrac{y}{2\pi}\displaystyle\int_{-b}^{b}\frac{\gamma(\eta)}{(z-\eta)^{2}+y^{2}}\,d\eta & \text{for } x\to+\infty \end{cases} \qquad \text{(A.11)}$$

where $R = [(x^{2}+K(y^{2}+z^{2}))]^{\frac{1}{2}}$, $t(\xi,\eta)$ is the wing thickness distribution and $\gamma(\eta)$ is the spanwise distribution of circulation.

The development of an asymptotic solution for the unsteady perturbation potential follows the method of Klunker and is now described in some detail. The field equation for the unsteady perturbation potential (Equation A.10) is written as:

$$L[\phi] \equiv K\phi_{xx} + \phi_{yy} + \phi_{zz} - 2i\Omega\phi_{x} + k\Omega\phi$$

$$= (\phi^{0}_{x}\ \phi_{x})_{x} \qquad \text{(A.12)}$$

The application of Green's theorem to the linear operator L and the use of wing and wake boundary conditions and weak shock conditions results in the following integral equation for ϕ:

$$\phi(x,y,z) = \iint\limits_{\text{wing}} \Delta\phi(\xi,\eta)\ \psi_\zeta\ d\xi d\eta$$

$$\underbrace{+\int\limits_{\text{span}} \gamma(\eta) \int_1^\infty \psi_\zeta\ e^{-ik(\xi-1)}\ d\xi d\eta}_{\text{wake integral}} \qquad (A.13)$$

$$+\iiint_{-\infty}^{\infty} (\phi_\xi^0 \phi_\xi)\ \psi_\zeta\ d\xi d\eta d\zeta$$

where ψ is the source solution to $L[\phi] = 0$:

$$\psi(x,y,z;\xi,\zeta,\eta) = \frac{1}{4\pi R}\, e^{i\left(\frac{\Omega}{K}(x-\xi) - \frac{\mu}{\sqrt{K}} R\right)} \qquad (A.14)$$

where

$$\mu = \sqrt{\Omega\left(\frac{\Omega}{K} + k\right)}$$

$$R = \sqrt{(x-\xi)^2 + K[(y-\zeta)^2 + (z-\eta)^2}$$

The use of the source function ψ in A.13, neglecting the volume integral as a higher order term, and after considerable manipulation and approximation (as $x^2+y^2+z^2 \to \infty$) of the various integrals results in the following farfield solution:

$$\phi_{ff}(x,y,z) = \frac{Ky}{4}\ \frac{(1+i\frac{\mu}{\sqrt{K}}R)}{R^{3}}\ e^{i\left(\frac{\Omega}{k}x - \frac{\mu}{\sqrt{K}}R\right)}\int_{-b}^{b}\int_{0}^{1}\Delta\phi(\xi,\eta)e^{-i\frac{\Omega}{K}\xi}\ d\xi d\eta$$

$$+ \frac{y}{4\pi}\ e^{-ik(x-1)}\cdot\begin{cases}\left[G_{1}(x,y,z;\eta)+G_{2}(x,y,z;\eta)\right]_{\eta=0}\displaystyle\int_{-b}^{b}\gamma(\eta)d\eta & \text{for } \begin{cases} y^{2}+z^{2}\to\infty \\ x\to-\infty\end{cases} \\ \displaystyle\int_{-b}^{b}G_{1}\left[(x,y,z;\eta)+G\ (x,y,z;\eta)\right]\ \gamma(\eta)d\eta & \text{for } x\to+\infty\end{cases} \qquad (A.15)$$

where

$$G_{1} = \frac{KM_{\infty}\ e^{-ikt_{1}}}{R[R-M_{\infty}(x-1)]}$$

$$G_{2} = \frac{I_{1}}{r^{2}}$$

and where

$$r = \sqrt{K[y^{2}+(z-\eta)^{2}]}$$

$$R = \sqrt{(x-1)^{2}+K[y^{2}+(z-\eta)^{2}]}$$

$$t_{1} = \frac{M_{\infty}R-(x-1)}{1-M_{\infty}^{2}}$$

I_1 in the equation, is an integral that can be evaluated using a rational approximation to its integrand and is presented at the end of the appendix.

It is noted that both the steady and unsteady farfield solutions involve integrals over the wing and span which depend on the solution $(\Delta\phi,\gamma)$. These integrals are evaluated numerically as the numerical solution proceeds and the respective equations are used to update the values of the steady or unsteady potential on the farfield boundaries.

The use of a rational approximation to evaluate the portion of the wake integral given as I_1 above, results in the following function:

$$I_1 = \frac{-|u_1|}{\sqrt{1+u_1^2}}\, e^{-ik\hat{r}|u_1|} + ik\hat{r}\sum_{\nu=0}^{11} \frac{b_\nu}{c\nu+ik\hat{r}}\, e^{-(c\nu+ik\hat{r})|u_1|}$$

$$+\left(1-\frac{u_1}{|u_1|}\right)\cdot \mathrm{Re}\left\{ \frac{u}{\sqrt{1+u^2}}\, e^{-ik\hat{r}u}\Bigg|_0^{|u_1|} \right. \tag{A.16}$$

$$\left. - ik\hat{r}\sum_{\nu=0}^{11} \frac{b_\nu}{c\nu+ik\hat{r}}\, e^{-(c\nu+ik\hat{r})u}\Bigg|_0^{|u_1|} \right\}$$

where

$$\hat{r} = \frac{r}{[(1+\gamma)\delta M_\infty^2]^{1/3}}$$

$$u_1 = \frac{t_1}{\hat{r}}$$

and $c = 0.372$ with b_ν defined in the table.

ν	b_ν
0	1.0
1	-0.2418 6198
2	2.7918 027
3	-24.9910 79
4	111.5919 6
5	-271.4354 9
6	305.7528 8
7	41.1836 30
8	-545.9853 7
9	-644.7815 5
10	-328.7275 5
11	64.2795 11

APPENDIX B

SUMMARY TABLE OF UNSTEADY AERODYNAMIC FORCE COEFFICIENTS

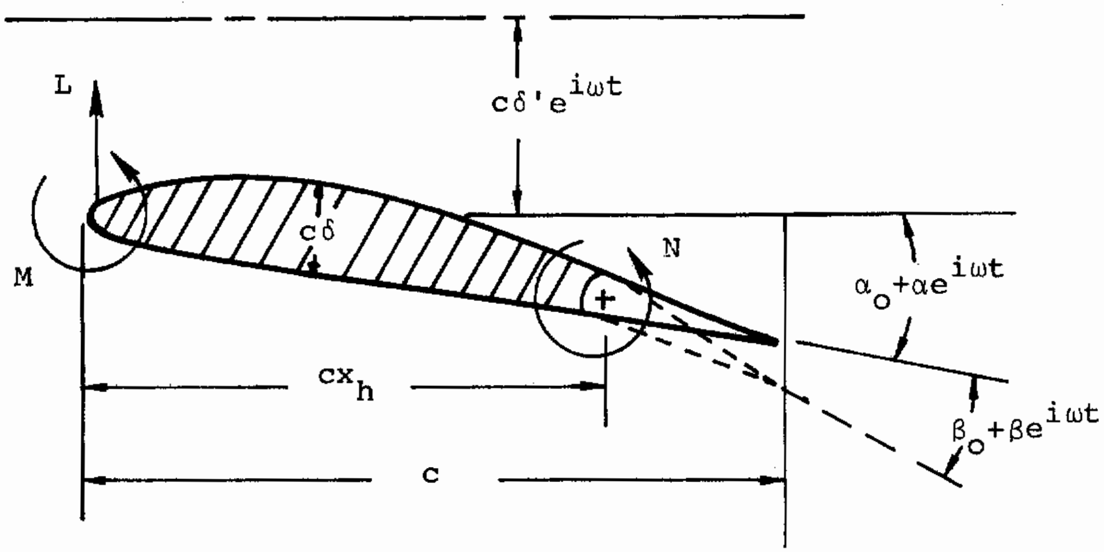

FIGURE B.1 DEFINITION OF AIRFOIL FORCES

The unsteady aerodynamic force coefficients calculated by the method of this report are defined and tabulated in this appendix. Results are presented for two airfoils, a NACA 64A006 and NACA 64A410 undergoing low frequency oscillations ($k=0\rightarrow0.2$) in pitch, plunge and control surface rotation in the transonic speed range ($M_\infty=.75\rightarrow1.2$).

Figure B.1 above defines the airfoil section geometric and force parameters. The definition of aerodynamic forces are defined positive for tail down pitch and control surface oscillations and positive for vertical translation down. The forces are given by:

$$L = q_\infty c \left\{ C_\ell^0 + \left(\alpha C_{\ell_\alpha} + \beta C_{\ell_\beta} + \delta' C_{\ell_{\delta'}} \right) e^{i\omega t} \right\} \qquad (A.1)$$

$$M = q_\infty c^2 \left\{ C_m^0 + \left(\alpha C_{m_\alpha} + \beta C_{m_\beta} + \delta' C_{m_{\delta'}}\right) e^{i\omega t} \right\} \qquad (A.2)$$

$$N = q_\infty c^2 \left\{ C_n^0 + \left(\alpha C_{n_\alpha} + \beta C_{n_\beta} + \delta' C_{n_{\delta'}}\right) e^{i\omega t} \right\} \qquad (A.3)$$

where q_∞ is freestream dynamic pressure and α, β, δ' are the magnitudes of the unsteady oscillations in pitch, control surface and plunge. Also, ω is the frequency of oscillation and the corresponding reduced frequency is defined by $k=\omega c/U$ It is noted that the reduced frequency and magnitude of plunging oscillation are based on airfoil chord.

Tables of unsteady aerodynamic coefficients, so defined, now follow for k=0.0, 0.05, 0.1, 0.15, 0.2 for:

- <u>NACA 64A006</u> (pitch, plunge, control surface modes)
  - $\left\{ \begin{array}{l} M_\infty = .8, .85, .9, .95, 1.1, 1.15, 1.2 \\ \alpha_0 = 0° \end{array} \right.$
  - $\left\{ \begin{array}{l} M_\infty = .85 \\ \alpha_0 = 0°, 1°, 2° \end{array} \right.$
- <u>NACA 64A410</u> (pitch, plunge)
  - $\left\{ \begin{array}{l} M_\infty = .75, .8, .85 \\ \alpha_0 = 0° \end{array} \right.$
  - $\left\{ \begin{array}{l} M = .8 \\ \alpha = 0°, 1°, 2° \end{array} \right.$

NACA 64A006 (x_H = .75)

M_∞, α_o		Reduced Frequency (k)									
		0.0		0.05		0.1		0.15		0.2	
		Re	Im	Re	Im	Re	Im	Re	Im	Re	Im
.80 α_o = 0°	C_{ℓ_α}	11.5	0.0	10.0	-2.08	8.84	-2.99	7.76	-3.43	6.94	-3.55
	C_{ℓ_β}	7.10		6.07	-1.31	5.31	-1.91	4.66	-2.20	4.13	-2.35
	$C_{\ell_{\delta'}}$	.175		.175	.47	.259	.817	.471	1.15	.708	1.34
	C_{m_α}	0.0		2.75	-.50	2.46	-.70	2.21	-.79	2.02	-.81
	C_{m_β}	2.99		2.74	-.33	2.56	-.49	2.41	-.57	2.29	-.63
	$C_{m_{\delta'}}$	0.0		4.3 E-2	.130	5.5 E-2	.229	9.6 E-2	.332	.147	.401
	C_{n_α}	4.8 E-2		4.3 E-2	-5.8 E-3	3.9 E-2	-7.4 E-3	3.7 E-2	-7.5 E-3	3.5 E-2	-7.2 E-3
	C_{n_β}	9.2 E-2		8.9 E-2	-3.4 E-3	8.7 E-2	-4.3 E-3	8.5 E-2	-4.3 E-3	8.4 E-2	-4.0 E-3
	$C_{n_{\delta'}}$	0.0	0.0	2.6 E-4	2.13 E-3	3.3 E-4	4.0 E-3	3.3 E-4	5.7 E-3	1.6 E-4	7.2 E-3
.85 α_o = 0	C_{ℓ_α}	17.1	0.0	13.1	-4.36	10.5	-5.30	8.74	-5.38	7.52	-5.34
	C_{ℓ_β}	10.6		8.04	-2.96	6.29	-3.59	5.14	-3.77	4.27	-3.82
	$C_{\ell_{\delta'}}$	0.0		.246	.575	.512	1.04	.816	1.15	.941	1.32
	C_{m_α}	4.59		3.62	-1.04	3.03	-1.23	2.63	-1.23	2.39	-1.21
	C_{m_β}	4.19		3.57	-.750	3.15	-.930	2.91	-1.01	2.73	-1.08
	$C_{m_{\delta'}}$	0.0	0.0	6.0 E-2	.160	.112	.303	.186	.356	.206	.428

NACA 64A006 (x_H = .75) (CONTD)

M_∞, α_o		Reduced Frequency (k)									
		0.0		0.05		0.1		0.15		0.2	
		Re	Im	Re	Im	Re	Im	Re	Im	Re	Im
.85 α_o = 0° (Contd)	C_{n_α}	3.6 E-2	0.0	3.0 E-2	-4.7 E-3	2.7 E-2	-4.2 E-3	2.5 E-3	-3.1 E-3	2.4 E-2	-1.7 E-3
	C_{n_β}	8.9 E-2		8.6 E-2	-1.9 E-3	8.4 E-2	-6.5 E-4	8.3 E-2	1.2 E-3	8.2 E-2	3.3 E-3
	$C_{n_{\delta'}}$	0.0	0.0	4.6 E-5	1.6 E-3	-4.7 E-5	2.8 E-3	-5.7 E-4	4.3 E-3	-9.6 E-4	5.5 E-3
.85 α_o = 1°	C_{ℓ_α}	21.7	0.0	15.0	-5.72	11.5	-6.73	9.14	-6.55	7.56	-6.14
	C_{ℓ_β}	9.85		6.84	-2.79	5.06	-3.19	3.96	-3.06	3.25	-2.81
	$C_{\ell_{\delta'}}$	0.0		.260	.708	.676	1.11	.914	1.29	1.10	1.39
	C_{m_α}	5.77		4.20	-1.34	3.42	-1.58	2.92	-1.59	2.58	-1.58
	C_{m_β}	4.18		3.48	-.765	3.05	-.97	2.76	-1.06	2.54	-1.12
	$C_{m_{\delta'}}$	0.0		6.0 E-2	.196	.158	.334	.218	.409	.278	.469
	C_{n_α}	1.45 E-2		1.74 E-2	2.97 E-3	2.0 E-2	5.3 E-3	2.3 E-2	5.8 E-3	2.6 E-2	5.07 E-3
	C_{n_β}	9.7 E-2		9.8 E-2	1.8 E-4	9.9 E-2	-2.1 E-4	.100	-1.5 E-3	.101	-3.5 E-3
	$C_{n_{\delta'}}$	0.0	0.0	-2.2 E-4	9.4 E-4	-8.9 E-4	2.1 E-3	-1.4 E-3	3.7 E-3	-1.8 E-3	5.3 E-3
.85 α_o = 2°	C_{ℓ_α}	21.7	0.0	14.6	-5.62	11.1	-6.19	9.15	-5.70	7.80	-5.17
	C_{ℓ_β}	7.9		5.94	-1.93	3.87	-2.08	3.37	-2.19	2.80	-2.01
	$C_{\ell_{\delta'}}$	0.0		.283	.7514	.470	1.19	.804	1.51	1.08	1.62
	C_{m_α}	7.26		5.02	-1.84	3.87	-2.04	3.25	-1.90	2.80	-1.77
	C_{m_β}	3.78	0.0	3.19	-.663	2.47	-.781	2.31	-.878	2.08	-.883

NACA 64A006 (x_H = .75) (CONTD)

M_∞, α_o		Reduced Frequency (k)									
		0.0		0.05		0.1		0.15		0.2	
		Re	Im	Re	Im	Re	Im	Re	Im	Re	Im
.85 α_o = 2° (Contd)	$C_{m_{\delta'}}$	0.0	0.0	.093	.260	.141	.414	.253	.545	.365	.598
	C_{n_α}	.022		.026	1.7 E-4	.028	-2.1 E-4	.029	-1.8 E-3	.031	-5.2 E-3
	C_{n_β}	.118		.122	-2.3 E-3	.118	-7.9 E-3	.119	-.0131	.116	-.0199
	$C_{n_{\delta'}}$	0.0	0.0	-2.4 E-5	1.39 E-3	-1.13 E-3	2.56 E-3	-1.22 E-3	5.05 E-3	3.35 E-4	7.31 E-3
.90 α_o = 0°	C_{ℓ_α}	9.36	0.0	7.1	-2.01	6.34	-2.47	5.8	-2.8	5.4	-2.95
	C_{ℓ_β}	6.031		3.3	-1.45	2.5	-1.16	2.21	-.876	2.08	-.652
	$C_{\ell_{\delta'}}$	0.0		.125	.388	.259	.651	.35	1.07	.44	1.24
	C_{m_α}	3.95		3.05	-.94	2.75	-1.08	2.47	-1.13	2.25	-1.16
	C_{m_β}	3.63		2.58	-.661	2.24	-.642	2.09	-.625	1.96	-.622
	$C_{m_{\delta'}}$	0.0		.056	.167	.118	.283	.186	.356	.216	.435
	C_{n_α}	.147		.128	-.024	.113	-.035	.104	-.046	.099	-.054
	C_{n_β}	.194		.191	-.0125	.188	-.0231	.184	-.0341	.177	-.0457
	$C_{n_{\delta'}}$	0.0	0.0	.0021	.0065	.0044	.0114	.0068	.0161	.0090	.0192

NACA 64A006 (x_H = .75) (CONTD)

M_∞, α_o		Reduced Frequency (k)									
		0.0		0.05		0.1		0.15		0.2	
		Re	Im	Re	Im	Re	Im	Re	Im	Re	Im
.95 $\alpha_o = 0°$	C_{ℓ_α}	7.095	0.0	6.10	-1.5	-	-	-	-	-	-
	C_{ℓ_β}	2.26		1.39	-.0105	-	-	-	-	-	-
	$C_{\ell_{\delta'}}$	0.0		.0574	.315	-	-	-	-	-	-
	C_{m_α}	3.05		2.7	-.64	-	-	-	-	-	-
	C_{m_β}	1.73		1.28	-7.86 E-3	-	-	-	-	-	-
	$C_{m_{\delta'}}$	0.0		.0257	.137	-	-	-	-	-	-
	C_{n_α}	.178		.156	-.025	-	-	-	-	-	-
	C_{n_β}	.206		.177	-8.57 E-4	-	-	-	-	-	-
	$C_{n_{\delta'}}$	0.0	0.0	.0017	.0082	-	-	-	-	-	-
1.1 $\alpha_o = 0°$	C_{ℓ_α}	-	-	-	-	-	-	-	-	-	-
	C_{ℓ_β}	1.24	0.0	1.24	-3.92 E-3	1.24	-7.84 E-3	1.24	-1.18 E-2	1.24	-1.57 E-2
	$C_{\ell_{\delta'}}$	-	-	-	-	-	-	-	-	-	-
	C_{m_α}	-	-	-	-	-	-	-	-	-	-
	C_{m_β}	1.07	0.0	1.07	-3.34 E-3	1.07	-6.68 E-3	1.07	-1.00 E-2	1.07	-1.34 E-2
	$C_{m_{\delta'}}$	-	-	-	-	-	-	-	-	-	-
	C_{n_α}	-	-	-	-	-	-	-	-	-	-
	C_{n_β}	.140	0.0	.140	-4.04 E-4	.140	-8.08 E-4	.140	-1.21 E-3	.140	-1.62 E-3
	$C_{n_{\delta'}}$	-	-	-	-	-	-	-	-	-	-

NACA 64A006 (x_H = .75)(CONCLUDED)

M_∞, α_0		Reduced Frequency (k)									
		0.0		0.05		0.1		0.15		0.2	
		Re	Im	Re	Im	Re	Im	Re	Im	Re	Im
1.15 $\alpha_0 = 0°$	C_{ℓ_α}	4.95	0.0	4.91	-.396	4.79	-.765	4.60	-1.08	4.37	-1.34
	C_{ℓ_β}	1.34		1.34	-4.59 E-3	1.34	-9.18 E-3	1.34	-1.38 E-2	1.34	-1.84 E-2
	$C_{\ell_{\delta'}}$	0.0		.0127	.246	.0491	.484	.1047	.708	.173	.912
	C_{m_α}	2.15		2.12	-.199	2.06	-.384	1.96	-.543	1.84	-.668
	C_{m_β}	1.16		1.16	-3.91 E-3	1.16	-7.83 E-3	1.16	-1.12 E-2	1.16	-1.57 E-2
	$C_{m_{\delta'}}$	0.0		5.6 E-3	.107	.0214	.209	.0454	.305	.0745	.392
	C_{n_α}	.123		.121	-.0136	.116	-.0261	.109	-.037	.100	-.0447
	C_{n_β}	.152		.152	-4.75 E-4	.152	-9.49 E-4	.152	-1.42 E-3	.152	-1.90 E-3
	$C_{n_{\delta'}}$	0.0	0.0	3.5 E-4	6.1 E-3	1.3 E-3	.0119	2.8 E-3	.0173	4.6 E-3	.022
1.20 $\alpha_0 = 0°$	C_{ℓ_α}	4.54	0.0	4.51	-.323	4.43	-.629	4.29	-.903	4.12	-1.14
	C_{ℓ_β}	1.45		1.45	-5.26 E-3	1.45	-1.05 E-2	1.45	-1.58 E-2	1.45	-2.10 E-2
	$C_{\ell_{\delta'}}$	0.0		9.85 E-3	.226	.0383	.447	.0823	.656	.137	.852
	C_{m_α}	2.08		2.06	-.188	1.99	-.365	1.91	-.519	1.80	-.645
	C_{m_β}	1.25		1.25	-4.48 E-3	1.25	-8.97 E-3	1.25	-1.35 E-2	1.25	-1.79 E-2
	$C_{m_{\delta'}}$	0.0		5.5 E-3	.103	.0211	.202	.0447	.295	.0732	.378
	C_{n_α}	.126		.124	-.015	.119	-.0287	.110	-.040	.101	-.049
	C_{n_β}	0.163		0.163	-5.46 E-4	0.163	-1.09 E-3	0.163	-1.64 E-3	0.163	-2.18 E-3
	$C_{n_{\delta'}}$	0.0	0.0	4.5 E-4	6.2 E-3	1.7 E-3	.0121	3.5 E-3	.0173	5.7 E-3	.0217

NACA 64A410

M_∞, α_o		Reduced Frequency (k)									
		0.0		0.05		0.1		0.15		0.2	
		Re	Im	Re	Im	Re	Im	Re	Im	Re	Im
.75 $\alpha_o = 0°$	C_{ℓ_α}	12.02	0.0	10.79	-1.96	9.74	-2.94	8.72	-3.44	7.92	-3.72
	C_{ℓ_β}	-	-	-	-	-	-	-	-	-	-
	$C_{\ell_{\delta'}}$	0.0	0.0	.167	.586	.318	.945	.556	1.21	.779	1.34
	C_{m_α}	3.41	0.0	3.09	-.485	2.84	-.713	2.60	-.825	2.42	-.89
	C_{m_β}	-	-	-	-	-	-	-	-	-	-
	$C_{m_{\delta'}}$	0.0	0.0	.044	.169	.078	.275	.136	.359	.194	.406
	C_{n_α}	-	-	-	-	-	-	-	-	-	-
	C_{n_β}	-	-	-	-	-	-	-	-	-	-
	$C_{n_{\delta'}}$	-	-	-	-	-	-	-	-	-	-
.80 $\alpha_o = 0°$	C_{ℓ_α}	17.45	0.0	13.8	-4.06	11.25	-5.3	9.29	-5.4	7.88	-5.22
	C_{ℓ_β}	-	-	-	-	-	-	-	-	-	-
	$C_{\ell_{\delta'}}$	0.0	0.0	.232	.733	.532	1.11	.820	1.29	.894	1.34
	C_{m_α}	6.6	0.0	5.26	-1.50	4.33	-1.96	3.61	-2.02	3.09	-1.98
	C_{m_β}	-	-	-	-	-	-	-	-	-	-
	$C_{m_{\delta'}}$	0.0	0.0	.085	.279	.195	.428	.304	.504	.338	.516
	C_{n_α}	-	-	-	-	-	-	-	-	-	-
	C_{n_β}	-	-	-	-	-	-	-	-	-	-
	$C_{n_{\delta'}}$	-	-	-	-	-	-	-	-	-	-

NACA 64A410 (CONTD)

M_∞, α_o		Reduced Frequency (k)									
		0.0		0.05		0.1		0.15		0.2	
		Re	Im	Re	Im	Re	Im	Re	Im	Re	Im
.80 $\alpha_o = 1°$	C_{ℓ_α}	17.8	0.0	14.05	-4.30	11.27	-5.37	9.55	-5.34	8.00	-5.10
	C_{ℓ_β}	-	-	-	-	-	-	-	-	-	-
	$C_{\ell_{\delta'}}$	0.0	0.0	.203	.696	.521	1.12	.804	1.32	.903	1.42
	C_{m_α}	7.19	0.0	5.71	-1.73	4.59	-2.16	3.91	-2.16	3.39	-2.09
	C_{m_β}	-	-	-	-	-	-	-	-	-	-
	$C_{m_{\delta'}}$	0.0	0.0	.080	.281	.206	.461	.321	.546	.364	.579
	C_{n_α}	-	-	-	-	-	-	-	-	-	-
	C_{n_β}	-	-	-	-	-	-	-	-	-	-
	$C_{n_{\delta'}}$	-	-	-	-	-	-	-	-	-	-
.80 $\alpha_o = 2°$	C_{ℓ_α}	17.58	0.0	13.87	-3.95	11.35	-5.07	9.47	-5.14	8.14	-4.89
	C_{ℓ_β}	-	-	-	-	-	-	-	-	-	-
	$C_{\ell_{\delta'}}$	0.0	0.0	.196	.687	.493	1.13	.767	1.35	.834	1.43
	C_{m_α}	7.03	0.0	5.57	-1.57	4.58	-2.02	3.84	-2.06	3.30	-1.99
	C_{m_β}	-	-	-	-	-	-	--	-	-	-
	$C_{m_{\delta'}}$	0.0	0.0	.076	.275	.193	.457	.304	.548	.335	.574
	C_{n_α}	-	-	-	-	-	-	-	-	-	-
	C_{n_β}	-	-	-	-	-	-	-	-	-	-
	$C_{n_{\delta'}}$	-	-	-	-	-	-	-	-	-	-

NACA 64A410 (CONCLUDED)

M_∞, α_o		Reduced Frequency (k)									
		0.0		0.05		0.1		0.15		0.2	
		Re	Im	Re	Im	Re	Im	Re	Im	Re	Im
.85 α_o = 0°	C_{ℓ_α}	18.72	0.0	13.7	-4.66	10.7	-5.27	8.77	-4.81	8.16	-4.48
	C_{ℓ_β}	-	-	-	-	-	-	-	-	-	-
	$C_{\ell_{\delta'}}$	0.0	0.0	.233	.73	.529	1.06	.647	1.24	.510	1.32
	C_{m_α}	8.25	0.0	6.04	-2.06	4.67	-2.34	3.79	-2.13	3.48	-1.82
	C_{m_β}	-	-	-	-	-	-	-	-	-	-
	$C_{m_{\delta'}}$	0.0	0.0	.099	.322	.226	.473	.270	.545	.196	.562
	C_{n_α}	-	-	-	-	-	-	-	-	-	-
	C_{n_β}	-	-	-	-	-	-	-	-	-	-
	$C_{n_{\delta'}}$	-	-	-	-	-	-	-	-	-	-

☆ U. S. GOVERNMENT PRINTING OFFICE: 1975 — 657-630/189